

**STUDY OF COMPRESSIBILITY AND PERMEABILITY CHARACTERISTICS OF
STATICALLY AND DYNAMICALLY COMPACTED SOILS**



A dissertation submitted in

Partial Fulfillment of the Requirements for the Award of the Degree of

MASTER OF TECHNOLOGY

In

CIVIL ENGINEERING

(With specialization in Geotechnical Engineering)

Of

Assam Science & Technology University

Session: 2021-2023



By

PRIYANKA DAS

Roll No: PG-C-013

ASTU Registration No: 124202116

Under the guidance of

DR. (MRS.) BINU SHARMA

PROFESSOR, ASSAM ENGINEERING COLLEGE

DEPARTMENT OF CIVIL ENGINEERING

**ASSAM ENGINEERING COLLEGE
JALUKBARI, GUWAHATI-13, ASSAM.**

DECLARATION

I hereby declare that the work presented in this report entitled “**STUDY OF COMPRESSIBILITY AND PERMEABILITY CHARACTERISTICS OF STATICALLY AND DYNAMICALLY COMPACTED SOILS**” in partial fulfilment of the requirement for the award of the degree of Master of Technology in Civil Engineering with specialization in Geotechnical engineering submitted to the Department of Civil Engineering, Assam Engineering College, Jalukbari, Guwahati-13 under Assam Science and Technology University, is an authentic record of my own work carried out in the said college for twelve months under the supervision and guidance of Dr. Binu Sharma, Professor, Department of Civil Engineering, Assam Engineering College, Jalukbari, Guwahati-13, Assam.

Do hereby declare that this project report is solemnly done by me and is my effort and that no part of it has been plagiarized without citation.

Date:

PRIYANKA DAS

Place: Guwahati

M.Tech 4th Semester

Roll No: PG-C-013

ASTU Registration No: 124202116

Department of Civil Engineering

Assam Engineering College

Jalukbari, Guwahati-781013

CERTIFICATE

This is to certify that the work presented in the dissertation report entitled “**STUDY OF COMPRESSIBILITY AND PERMEABILITY CHARACTERISTICS OF STATICALLY AND DYNAMICALLY COMPACTED SOILS**” is submitted by Priyanka Das, Roll No: PG-C-013, a student of M.Tech 4th semester, Department of Civil Engineering, Assam Engineering College, under my supervision and guidance and submitted in partial fulfillment of the requirement for the award of the Degree of Master of Technology in Civil Engineering with specialization in Geotechnical Engineering under Assam Science and Technology University

Date:

Place: Guwahati

DR. (MRS.) BINU SHARMA

B.E. (Gau), M.E. (U.O.R), Ph.D. (Gau)

Professor

Department Of Civil Engineering

Assam Engineering College

Jalukbari, Guwahati-781013

CERTIFICATE FROM THE HEAD OF THE DEPARTMENT

This is to certify that the dissertation entitled “**STUDY OF COMPRESSIBILITY AND PERMEABILITY CHARACTERISTICS OF STATICALLY AND DYNAMICALLY COMPACTED SOILS**” has been submitted by PRIYANKA DAS, bearing Roll No: PG-C-013, a student of M.Tech 4th Semester, Department of Civil Engineering, Assam Engineering College, in partial fulfilment of the requirement for the award of the Degree of Master of Technology in Civil Engineering with specialization in Geotechnical Engineering under the Assam Science and Technology University

Date:

Place: Guwahati

DR. JAYANTA PATHAK

Professor & Head of the Department

Department of Civil Engineering

Assam Engineering College

Guwahati-781013

ACKNOWLEDGEMENT

I would like to extend my sincere appreciation to Dr. (Mrs.) Binu Sharma, Professor in the Department of Civil Engineering at Assam Engineering College, for her extensive support and encouragement throughout the project. Her guidance, constant supervision and provision of necessary information were invaluable to me. Working under her was an inspiring and great experience, and I am highly indebted to her.

This project would not have been possible without the help of my seniors, Trideep Kalita and Rituraj Bhuyan; laboratory assistants and staffs, for their guidance in various ways. Without their guidance and support it would have not been possible for me to prepare and complete this study.

I am also grateful to Dr. Jayanta Pathak, Professor and Head of the Department of Civil Engineering at Assam Engineering College as well as the entire community of the Department of Civil Engineering at Assam Engineering College for providing us with the necessary infrastructure and comfort throughout the course, particularly during my project.

Date:

Place: Guwahati

PRIYANKA DAS

M.Tech 4th Semester

Department of Civil Engineering

Assam Engineering College

Jalukbari, Guwahati-781013

ABSTRACT

This study investigates the compressibility and permeability characteristics of five different soils which were statically and dynamically compacted. These characteristics were studied at dry of the optimum moisture content, at optimum moisture content and at wet of optimum moisture content. Dynamic compaction was performed by the Standard Proctor compaction test while static compaction was carried out using the Proctor mould and a static compaction apparatus.

Consolidation behaviours were explored when the water content is kept at three different levels: OMC-3%, OMC, and OMC+3%, using the corresponding dry unit weights for each moisture level.

The results indicated that for the dry side of optimum moisture content, statically compacted curves exhibited a slightly greater compressibility compared to the dynamic curves across all samples. In contrast, at both OMC and the wet side of optimum, dynamically compacted curves demonstrated a slightly higher compressibility compared to statically compacted curves for all samples.

When consolidation curves of dynamically compacted soil samples were superimposed, a distinct sequence of the consolidation curves emerged from highest void ratio to lowest as follows: dry side, wet side, and OMC. A similar pattern was observed for statically compacted soil samples.

Permeability characteristics between statically and dynamically compacted soil samples were also examined. The permeability values on the dry side of optimum indicated slightly higher values for static compaction, but both methods fell within a similar range. At OMC and the wet side of optimum, permeability variations were minimal between the two compaction methods.

Permeability values for dry, OMC, and wet conditions exhibited slight variations but closely aligned on semi-logarithmic graphs for dynamic compaction. A similar pattern was observed for static compaction.

The relationship between permeability and molding water content revealed consistent patterns across moisture levels for both compaction methods. Permeability values followed a sequence: highest on the dry side, decreasing at OMC, and reaching the lowest on the wet side of the optimum spectrum. Some samples exhibited slightly elevated permeability values on the wet side compared to OMC, while dry side values remained the highest.

LIST OF TABLES

| Table No. | Description | Page No. |
|------------------|--|-----------------|
| 2.1. | Compaction data of specimens from soils 1 and 2 | 10 |
| 3.1. | Physical properties of soil | 31 |
| 3.2. | Particle Size distribution results of the soil samples | 31 |
| 3.3. | Optimum moisture content and maximum dry unit weight by Standard Proctor compaction test | 34 |
| 3.4. | Equivalent static pressures of all the five soil samples | 50 |
| 3.5. | Specimen height and void ratio calculation for sample 1 (dynamic at dry of optimum) | 144 |
| 3.6. | Specimen height and void ratio calculation for sample 1 (dynamic at optimum moisture content) | 144 |
| 3.7. | Specimen height and void ratio calculation for sample 1 (dynamic at wet of optimum) | 144 |
| 3.8. | Specimen height and void ratio calculation for sample 1 (static at dry of optimum) | 145 |
| 3.9. | Specimen height and void ratio calculation for sample 1 (static at optimum moisture content) | 145 |
| 3.10. | Specimen height and void ratio calculation for sample 1 (static at wet of optimum) | 145 |
| 3.11. | Specimen height and void ratio calculation for sample 2 (dynamic at dry of optimum) | 146 |
| 3.12. | Specimen height and void ratio calculation for sample 2 (dynamic at optimum moisture content) | 146 |
| 3.13. | Specimen height and void ratio calculation for sample 2 (dynamic at wet of optimum) | 146 |
| 3.14. | Specimen height and void ratio calculation for sample 2 (static at dry of optimum) | 147 |
| 3.15. | Specimen height and void ratio calculation for sample 2 (static at optimum moisture content) | 147 |

| | | |
|-------|---|-----|
| 3.16. | Specimen height and void ratio calculation for sample 2 (static at wet of optimum) | 147 |
| 3.17. | Specimen height and void ratio calculation for sample 3 (dynamic at dry of optimum) | 148 |
| 3.18. | Specimen height and void ratio calculation for sample 3 (dynamic at optimum moisture content) | 148 |
| 3.19. | Specimen height and void ratio calculation for sample 3 (dynamic at wet of optimum) | 148 |
| 3.20. | Specimen height and void ratio calculation for sample 3 (static at dry of optimum) | 149 |
| 3.21. | Specimen height and void ratio calculation for sample 3 (static at optimum moisture content) | 149 |
| 3.22. | Specimen height and void ratio calculation for sample 3 (static at wet of optimum) | 149 |
| 3.23. | Specimen height and void ratio calculation for sample 4 (dynamic at dry of optimum) | 150 |
| 3.24. | Specimen height and void ratio calculation for sample 4 (dynamic at optimum moisture content) | 150 |
| 3.25. | Specimen height and void ratio calculation for sample 4 (dynamic at wet of optimum) | 150 |
| 3.26. | Specimen height and void ratio calculation for sample 4 (static at dry of optimum) | 151 |
| 3.27. | Specimen height and void ratio calculation for sample 4 (static at optimum moisture content) | 151 |
| 3.28. | Specimen height and void ratio calculation for sample 4 (static at wet of optimum) | 151 |
| 3.29. | Specimen height and void ratio calculation for sample 5 (dynamic at dry of optimum) | 152 |
| 3.30. | Specimen height and void ratio calculation for sample 5 (dynamic at optimum moisture content) | 152 |
| 3.31. | Specimen height and void ratio calculation for sample 5 (dynamic at wet of optimum) | 152 |
| 3.32. | Specimen height and void ratio calculation for sample 5 (static at dry of optimum) | 153 |
| 3.33. | Specimen height and void ratio calculation for sample 5 (static at optimum moisture content) | 153 |
| 3.34. | Specimen height and void ratio calculation for sample 5 (static at wet of optimum) | 153 |
| 3.35. | Consolidation and permeability properties of sample 1(dynamic at dry of optimum) | 73 |
| 3.36. | Consolidation and permeability properties of sample 1(dynamic at OMC) | 73 |

| | | |
|-------|--|-----|
| 3.37. | Consolidation and permeability properties of sample 1(dynamic at wet of optimum) | 74 |
| 3.38. | Consolidation and permeability properties of sample 1(static at dry of optimum) | 74 |
| 3.39. | Consolidation and permeability properties of sample 1(static at OMC) | 74 |
| 3.40. | Consolidation and permeability properties of sample 1(static at wet of optimum) | 75 |
| 3.41. | Consolidation and permeability properties of sample 2(dynamic at dry of optimum) | 223 |
| 3.42. | Consolidation and permeability properties of sample 2(dynamic at optimum moisture content) | 223 |
| 3.43. | Consolidation and permeability properties of sample 2(dynamic at wet of optimum) | 223 |
| 3.44. | Consolidation and permeability properties of sample 2(static at dry of optimum) | 224 |
| 3.45. | Consolidation and permeability properties of sample 2(static at optimum moisture content) | 224 |
| 3.46. | Consolidation and permeability properties of sample 2(static at wet of optimum) | 224 |
| 3.47. | Consolidation and permeability properties of sample 3(dynamic at dry of optimum) | 225 |
| 3.48. | Consolidation and permeability properties of sample 3(dynamic at optimum moisture content) | 225 |
| 3.49. | Consolidation and permeability properties of sample 3(dynamic at wet of optimum) | 225 |
| 3.50. | Consolidation and permeability properties of sample 3(static at dry of optimum) | 226 |
| 3.51. | Consolidation and permeability properties of sample 3(static at optimum moisture content) | 226 |
| 3.52. | Consolidation and permeability properties of sample 3(static at wet of optimum) | 226 |

| | | |
|-------|---|-----|
| 3.53. | Consolidation and permeability properties of sample 4(dynamic at dry of optimum) | 227 |
| 3.54. | Consolidation and permeability properties of sample 4(dynamic at optimum moisture content) | 227 |
| 3.55. | Consolidation and permeability properties of sample 4(dynamic at wet of optimum) | 227 |
| 3.56. | Consolidation and permeability properties of sample 4(static at dry of optimum) | 228 |
| 3.57. | Consolidation and permeability properties of sample 4(static at optimum moisture content) | 228 |
| 3.58. | Consolidation and permeability properties of sample 4(static at wet of optimum) | 228 |
| 3.59. | Consolidation and permeability properties of sample 5 (dynamic at dry of optimum) | 229 |
| 3.60. | Consolidation and permeability properties of sample 5 (dynamic at optimum moisture content) | 229 |
| 3.61. | Consolidation and permeability properties of sample 5 (dynamic at wet of optimum) | 229 |
| 3.62. | Consolidation and permeability properties of sample 5(static at dry of optimum) | 230 |
| 3.63. | Consolidation and permeability properties of sample 5(static at optimum moisture content) | 230 |
| 3.64. | Consolidation and permeability properties of sample 5(static at wet of optimum) | 230 |
| 4.1. | Compression Index (C_c) values for static and dynamic compaction at dry of optimum | 82 |
| 4.2. | Compression Index (C_c) values for static and dynamic compaction at OMC | 85 |
| 4.3. | Compression Index (C_c) values for static and dynamic compaction at wet of optimum | 89 |

LIST OF FIGURES

| Figure No. | Title | Page No. |
|------------|--|----------|
| 2.1. | Comparison between static compaction method by Reddy and Jagadish (1993) and the Standard Proctor compaction method | 6 |
| 2.2. | Static Packing Pressure Equipment by Hafez et al. 2010 | 8 |
| 2.3. | Comparison between static compaction method by Hafez et al. (2010) and the dynamic compaction method | 9 |
| 2.4. | Compaction curves and unconfined compressive strength (UCS) of soils 1 and 2 (Dario et al. 2011) | 10 |
| 2.5. | Relative differences between mean values of the parameters γ_d and RCNC of soils 1 and 2, adopting the dynamic compaction data as reference. (Dario et al.) | 11 |
| 2.6. | Photomicrographs taken from thin section obtained from specimens of soils 1 and 2 statically and dynamically compacted at the water contents w_{ot} and $w_{ot}-3\%$ (Dario et al. 2011) | 12 |
| 2.7. | Porosity data obtained from photomicrographs taken from thin sections of specimens of soils 1 and 2 (Dario et al. 2011) | 13 |
| 2.8. | Permeability as a function of moulding water content for samples silty clay prepared to constant density by kneading compaction | 17 |
| 2.9. | Permeability vs molding water content relationship for silty clay kneading compaction | 18 |
| 2.10. | Permeability vs molding water content relationship for AASHO road test soil kneading compaction | 19 |
| 2.11. | Contours of equal permeability for samples of silty clay prepared by kneading compaction | 20 |
| 2.12. | Influence of method of compaction of strength and shrinkage of silty clay | 20 |
| 2.13. | Influence of method of compaction on the permeability | 21 |
| 3.1. | Static Compaction Test Set up | 26 |
| 3.2. | Dynamically Compacted soil at Dry of Optimum | 28 |
| 3.3. | Insertion of consolidation ring in compacted soil mass | 28 |

| | | |
|-------|--|----|
| 3.4. | Recovered soil sample from the Proctor mould | 29 |
| 3.5. | Upper surface of consolidation sample | 29 |
| 3.6. | Lower surface of consolidation sample | 29 |
| 3.7. | Consolidation cell under the loading frame | 30 |
| 3.8. | The whole consolidation setup | 30 |
| 3.9. | Gradation curve for sample 1 | 32 |
| 3.10. | Gradation curve for sample 2 | 32 |
| 3.11. | Gradation curve for sample 3 | 32 |
| 3.12. | Gradation curve for sample 4 | 33 |
| 3.13. | Gradation curve for sample 5 | 33 |
| 3.14. | Standard Proctor Curve for sample 1 | 34 |
| 3.15. | Standard Proctor Curve for sample 2 | 35 |
| 3.16. | Standard Proctor Curve for sample 3 | 35 |
| 3.17. | Standard Proctor Curve for sample 4 | 36 |
| 3.18. | Standard Proctor Curve for sample 5 | 36 |
| 3.19. | Dry unit weight vs Static Pressure curve of sample 1 at 9.03% water content | 37 |
| 3.20. | Dry unit weight vs Static Pressure curve of sample 1 at 11.10% water content | 37 |
| 3.21. | Dry unit weight vs Static Pressure curve of sample 1 at 14% water content | 38 |
| 3.22. | Dry unit weight vs Static Pressure curve of sample 1 at 17.60% water content | 38 |
| 3.23. | Dry unit weight vs Static Pressure curve of sample 1 at 20.61% water content | 39 |
| 3.24. | Dry unit weight vs Static Pressure curve of sample 1 at 22.49% water content | 39 |
| 3.25. | Dry unit weight vs Static Pressure curve of sample 2 at 15.74% water content | 40 |

| | | |
|-------|---|-----|
| 3.26. | Dry unit weight vs Static Pressure curve of sample 2 at 19.54% water content | 40 |
| 3.27. | Dry unit weight vs Static Pressure curve for sample 2 at 22.64% water content | 41 |
| 3.28. | Dry unit weight vs Static Pressure curve for sample 2 at 25.50% water content | 41 |
| 3.29. | Dry unit weight vs Static Pressure curve for sample 3 at 19.64% water content | 137 |
| 3.30. | Dry unit weight vs Static Pressure curve for sample 3 at 21.95% water content | 137 |
| 3.31. | Dry unit weight vs Static Pressure curve for sample 3 at 24.43% water content | 138 |
| 3.32. | Dry unit weight vs Static Pressure curve for sample 3 at 28.16% water content | 138 |
| 3.33. | Dry unit weight vs Static Pressure curve for sample 4 at 12.28% water content | 139 |
| 3.34. | Dry unit weight vs Static Pressure curve for sample 4 at 15.09% water content | 139 |
| 3.35. | Dry unit weight vs Static Pressure curve for sample 4 at 17.77% water content | 140 |
| 3.36. | Dry unit weight vs Static Pressure curve for sample 4 at 19.43% water content | 140 |
| 3.37. | Dry unit weight vs Static Pressure curve for sample 4 at 21.36% water content | 141 |
| 3.38. | Dry unit weight vs Static Pressure curve for sample 5 at 10.09% water content | 141 |
| 3.39. | Dry unit weight vs Static Pressure curve for sample 5 at 12.80% water content | 142 |

| | | |
|-------|--|-----|
| 3.40. | Dry unit weight vs Static Pressure curve for sample 5 at 14.94% water content | 142 |
| 3.41. | Dry unit weight vs Static Pressure curve for sample 5 at 16.82% water content | 143 |
| 3.42. | Dry unit weight vs Static Pressure curve for sample 5 at 20.93% water content | 143 |
| 3.43. | Static and dynamic compaction curve for sample 1 | 42 |
| 3.44. | Static and dynamic compaction curve for sample 2 | 43 |
| 3.45. | Static and dynamic compaction curve for sample 3 | 44 |
| 3.46. | Static and dynamic compaction curve for sample 4 | 45 |
| 3.47. | Static and dynamic compaction curve for sample 5 | 46 |
| 3.48. | Determination of equivalent static pressure of sample 1 | 47 |
| 3.49. | Determination of equivalent static pressure of sample 2 | 48 |
| 3.50. | Determination of equivalent static pressure of sample 3 | 48 |
| 3.51. | Determination of equivalent static pressure of sample 4 | 49 |
| 3.52. | Determination of equivalent static pressure of sample 5 | 49 |
| 3.53. | Consolidation pressure-void ratio curve of sample 1(dynamic at dry of optimum) | 51 |
| 3.54. | Consolidation pressure-void ratio curve of sample 2(dynamic at dry of optimum) | 51 |
| 3.55. | Consolidation pressure-void ratio curve of sample 3(dynamic at dry of optimum) | 52 |
| 3.56. | Consolidation pressure-void ratio curve of sample 4(dynamic at dry of optimum) | 52 |
| 3.57. | Consolidation pressure-void ratio curve of sample 5(dynamic at dry of optimum) | 53 |
| 3.58. | Consolidation pressure-void ratio curve of sample 1(dynamic at OMC) | 53 |
| 3.59. | Consolidation pressure-void ratio curve of sample 2(dynamic at OMC) | 54 |
| 3.60. | Consolidation pressure-void ratio curve of sample 3(dynamic at OMC) | 54 |

| | | |
|-------|--|----|
| 3.61. | Consolidation pressure-void ratio curve of sample 4(dynamic at OMC) | 55 |
| 3.62. | Consolidation pressure-void ratio curve of sample 5(dynamic at OMC) | 55 |
| 3.63. | Consolidation pressure-void ratio curve of sample 1(dynamic at wet of optimum) | 56 |
| 3.64. | Consolidation pressure-void ratio curve of sample 2(dynamic at wet of optimum) | 56 |
| 3.65. | Consolidation pressure-void ratio curve of sample 3(dynamic at wet of optimum) | 57 |
| 3.66. | Consolidation pressure-void ratio curve of sample 4(dynamic at wet of optimum) | 57 |
| 3.67. | Consolidation pressure-void ratio curve of sample 5(dynamic at wet of optimum) | 58 |
| 3.68. | Consolidation pressure-void ratio curve of sample 1(static at dry of optimum) | 59 |
| 3.69. | Consolidation pressure-void ratio curve of sample 2(static at dry of optimum) | 59 |
| 3.70. | Consolidation pressure-void ratio curve of sample 3(static at dry of optimum) | 60 |
| 3.71. | Consolidation pressure-void ratio curve of sample 4(static at dry of optimum) | 60 |
| 3.72. | Consolidation pressure-void ratio curve of sample 5(static at dry of optimum) | 61 |
| 3.73. | Consolidation pressure-void ratio curve of sample 1(static at OMC) | 61 |
| 3.74. | Consolidation pressure-void ratio curve of sample 2(static at OMC) | 62 |
| 3.75. | Consolidation pressure-void ratio curve of sample 3(static at OMC) | 62 |
| 3.76. | Consolidation pressure-void ratio curve of sample 4(static at OMC) | 63 |
| 3.77. | Consolidation pressure-void ratio curve of sample 5(static at OMC) | 63 |
| 3.78. | Consolidation pressure-void ratio curve of sample 1(static at wet of optimum) | 64 |

| | | |
|-------|---|----|
| 3.79. | Consolidation pressure-void ratio curve of sample 2(static at wet of optimum) | 64 |
| 3.80. | Consolidation pressure-void ratio curve of sample 3(static at wet of optimum) | 65 |
| 3.81. | Consolidation pressure-void ratio curve of sample 4(static at wet of optimum) | 65 |
| 3.82. | Consolidation pressure-void ratio curve of sample 5(static at wet of optimum) | 66 |
| 3.83. | Time-consolidation curve of sample 1 (dynamic at dry of optimum) at 80-160kPa | 67 |
| 3.84. | Time-consolidation curve of sample 1 (dynamic at OMC) at 80-160kPa | 67 |
| 3.85. | Time-consolidation curve of sample 1 (dynamic at wet of optimum) at 80-160kPa | 68 |
| 3.86. | Time-consolidation curve of sample 1 (static at dry of optimum) at 80-160kPa | 68 |
| 3.87. | Time-consolidation curve of sample 1 (static at OMC) at 80-160kPa | 69 |
| 3.88. | Time-consolidation curve of sample 1 (static at wet of optimum) at 80-160kPa | 69 |
| 3.89. | Time-consolidation curve of sample 2 (dynamic at dry of optimum) at 80-160kPa | 70 |
| 3.90. | Time-consolidation curve of sample 2 (dynamic at OMC) at 80-160kPa | 70 |
| 3.91. | Time-consolidation curve of sample 2 (dynamic at wet of optimum) at 80-160kPa | 71 |
| 3.92. | Time-consolidation curve of sample 2 (static at dry of optimum) at 80-160kPa | 71 |
| 3.93. | Time-consolidation curve of sample 2 (static at OMC) at 80-160kPa | 72 |
| 3.94. | Time-consolidation curve of sample 2 (static at wet of optimum) at 80-160kPa | 72 |

| | | |
|--------|--|-----|
| 3.95. | Time-consolidation curve of sample 1 (dynamic at dry of optimum) at 20-40kPa | 154 |
| 3.96. | Time-consolidation curve of sample 1 (dynamic at dry of optimum) at 40-80kPa | 154 |
| 3.97. | Time-consolidation curve of sample 1 (dynamic at dry of optimum) at 160-320kPa | 155 |
| 3.98. | Time-consolidation curve of sample 1 (dynamic at dry of optimum) at 320-640kPa | 155 |
| 3.99. | Time-consolidation curve of sample 1 (dynamic at optimum moisture content) at 20-40kPa | 156 |
| 3.100. | Time-consolidation curve of sample 1 (dynamic at optimum moisture content) at 40-80kPa | 156 |
| 3.101. | Time-consolidation curve of sample 1 (dynamic at optimum moisture content) at 160-320kPa | 157 |
| 3.102. | Time-consolidation curve of sample 1 (dynamic at optimum moisture content) at 320-640kPa | 157 |
| 3.103. | Time-consolidation curve of sample 1 (dynamic at wet of optimum) at 20-40kPa | 158 |
| 3.104. | Time-consolidation curve of sample 1 (dynamic at wet of optimum) at 40-80kPa | 158 |
| 3.105. | Time-consolidation curve of sample 1 (dynamic at wet of optimum) at 160- 320kPa | 159 |
| 3.106. | Time-consolidation curve of sample 1 (dynamic at wet of optimum) at 320-640kPa | 159 |
| 3.107. | Time-consolidation curve of sample 1 (static at dry of optimum) at 20-40kPa | 160 |
| 3.108. | Time-consolidation curve of sample 1 (static at dry of optimum) at 40-80kPa | 160 |
| 3.109. | Time-consolidation curve of sample 1 (static at dry of optimum) at 160-320kPa | 161 |
| 3.110. | Time-consolidation curve of sample 1 (static at dry of optimum) at 320-640kPa | 161 |
| 3.111. | Time-consolidation curve of sample 1 (static at optimum moisture content) at 20-40kPa | 162 |
| 3.112. | Time-consolidation curve of sample 1 (static at optimum moisture content) at 40-80kPa | 162 |

| | | |
|--------|--|-----|
| 3.113. | Time-consolidation curve of sample 1 (static at optimum moisture content) at 160-320kPa | 163 |
| 3.114. | Time-consolidation curve of sample 1 (static at optimum moisture content) at 320-640kPa | 163 |
| 3.115. | Time-consolidation curve of sample 1 (static at wet of optimum) at 20-40kPa | 164 |
| 3.116. | Time-consolidation curve of sample 1 (static at wet of optimum) at 40-80kPa | 164 |
| 3.117. | Time-consolidation curve of sample 1 (static at wet of optimum) at 160-320kPa | 165 |
| 3.118. | Time-consolidation curve of sample 1 (static at wet of optimum) at 320-640kPa | 165 |
| 3.119. | Time-consolidation curve of sample 2 (dynamic at dry of optimum) at 20-40kPa | 166 |
| 3.120. | Time-consolidation curve of sample 2 (dynamic at dry of optimum) at 40-80kPa | 166 |
| 3.121. | Time-consolidation curve of sample 2 (dynamic at dry of optimum) at 160-320kPa | 167 |
| 3.122. | Time-consolidation curve of sample 2 (dynamic at dry of optimum) at 320-640kPa | 167 |
| 3.123. | Time-consolidation curve of sample 2 (dynamic at optimum moisture content) at 20-40kPa | 168 |
| 3.124. | Time-consolidation curve of sample 2 (dynamic at optimum moisture content) at 40-80kPa | 168 |
| 3.125. | Time-consolidation curve of sample 2 (dynamic at optimum moisture content) at 160-320kPa | 169 |
| 3.126. | Time-consolidation curve of sample 2 (dynamic at optimum moisture content) at 320-640kPa | 169 |
| 3.127. | Time-consolidation curve of sample 2 (dynamic at wet of optimum) at 20-40kPa | 170 |
| 3.128. | Time-consolidation curve of sample 2 (dynamic at wet of optimum) at 40-80kPa | 170 |
| 3.129. | Time-consolidation curve of sample 2 (dynamic at wet of optimum) at 160-320kPa | 171 |
| 3.130. | Time-consolidation curve of sample 2 (dynamic at wet of optimum) at 320-640kPa | 171 |
| 3.131. | Time-consolidation curve of sample 2(static at dry of optimum) at 20-40kPa | 172 |
| 3.132. | Time-consolidation curve of sample 2(static at dry of optimum) at 40-80kPa | 172 |
| 3.133. | Time-consolidation curve of sample 2(static at dry of optimum) at 160-320kPa | 173 |
| 3.134. | Time-consolidation curve of sample 2(static at dry of optimum) at 320-640kPa | 173 |

| | | |
|--------|---|-----|
| 3.135. | Time-consolidation curve of sample 2(static at optimum moisture content) at 20-40kPa | 174 |
| 3.136. | Time-consolidation curve of sample 2(static at optimum moisture content) at 40-80kPa | 174 |
| 3.137. | Time-consolidation curve of sample 2(static at optimum moisture content) at 160-320kPa | 175 |
| 3.138. | Time-consolidation curve of sample 2(static at optimum moisture content) at 320-640kPa | 175 |
| 3.139. | Time-consolidation curve of sample 2(static at wet of optimum) at 20-40kPa | 176 |
| 3.140. | Time-consolidation curve of sample 2(static at wet of optimum) at 40-80kPa | 176 |
| 3.141. | Time-consolidation curve of sample 2(static at wet of optimum) at 160-320kPa | 177 |
| 3.142. | Time-consolidation curve of sample 2(static at wet of optimum) at 320-640kPa | 177 |
| 3.143. | Time-consolidation curve of sample 3(dynamic at dry of optimum) at 20-40kPa | 178 |
| 3.144. | Time-consolidation curve of sample 3(dynamic at dry of optimum) at 40-80kPa | 178 |
| 3.145. | Time-consolidation curve of sample 3(dynamic at dry of optimum) at 80-160kPa | 179 |
| 3.146. | Time-consolidation curve of sample 3(dynamic at dry of optimum) at 160-320kPa | 179 |
| 3.147. | Time-consolidation curve of sample 3(dynamic at dry of optimum) at 320-640kPa | 180 |
| 3.148. | Time-consolidation curve of sample 3(dynamic at optimum moisture content) at 20-40kPa | 180 |
| 3.149. | Time-consolidation curve of sample 3(dynamic at optimum moisture content) at 40-80kPa | 181 |
| 3.150. | Time-consolidation curve of sample 3(dynamic at optimum moisture content) at 80-160kPa | 181 |
| 3.151. | Time-consolidation curve of sample 3(dynamic at optimum moisture content) at 160-320kPa | 182 |
| 3.152. | Time-consolidation curve of sample 3(dynamic at optimum moisture content) at 320-640kPa | 182 |
| 3.153. | Time-consolidation curve of sample 3(dynamic at wet of optimum) at 20-40kPa | 183 |
| 3.154. | Time-consolidation curve of sample 3(dynamic at wet of optimum) at 40-80kPa | 183 |
| 3.155. | Time-consolidation curve of sample 3(dynamic at wet of optimum) at 80-160kPa | 184 |
| 3.156. | Time-consolidation curve of sample 3(dynamic at wet of optimum) at 160-320kPa | 184 |

| | | |
|--------|--|-----|
| 3.157. | Time-consolidation curve of sample 3(dynamic at wet of optimum) at 320-640kPa | 185 |
| 3.158. | Time-consolidation curve of sample 3(static at dry of optimum) at 20-40kPa | 185 |
| 3.159. | Time-consolidation curve of sample 3(static at dry of optimum) at 40-80kPa | 186 |
| 3.160. | Time-consolidation curve of sample 3(static at dry of optimum) at 80-160kPa | 186 |
| 3.161. | Time-consolidation curve of sample 3(static at dry of optimum) at 160-320kPa | 187 |
| 3.162. | Time-consolidation curve of sample 3(static at dry of optimum) at 320-640kPa | 187 |
| 3.163. | Time-consolidation curve of sample 3(static at optimum moisture content) at 20-40kPa | 188 |
| 3.164. | Time-consolidation curve of sample 3(static at optimum moisture content) at 40-80kPa | 188 |
| 3.165. | Time-consolidation curve of sample 3(static at optimum moisture content) at 80-160kPa | 189 |
| 3.166. | Time-consolidation curve of sample 3(static at optimum moisture content) at 160-320kPa | 189 |
| 3.167. | Time-consolidation curve of sample 3(static at optimum moisture content) at 320-640kPa | 190 |
| 3.168. | Time-consolidation curve of sample 3(static at wet of optimum) at 20-40kPa | 190 |
| 3.169. | Time-consolidation curve of sample 3(static at wet of optimum) at 40-80kPa | 191 |
| 3.170. | Time-consolidation curve of sample 3(static at wet of optimum) at 80-160kPa | 191 |
| 3.171. | Time-consolidation curve of sample 3(static at wet of optimum) at 160-320kPa | 192 |
| 3.172. | Time-consolidation curve of sample 3(static at wet of optimum) at 320-640kPa | 192 |
| 3.173. | Time-consolidation curve of sample 4(dynamic at dry of optimum) at 20-40kPa | 193 |
| 3.174. | Time-consolidation curve of sample 4(dynamic at dry of optimum) at 40-80kPa | 193 |
| 3.175. | Time-consolidation curve of sample 4(dynamic at dry of optimum) at 80-160kPa | 194 |
| 3.176. | Time-consolidation curve of sample 4(dynamic at dry of optimum) at 160-320kPa | 194 |
| 3.177. | Time-consolidation curve of sample 4(dynamic at dry of optimum) at 320-640kPa | 195 |
| 3.178. | Time-consolidation curve of sample 4(dynamic at optimum moisture content) at 20-40kPa | 195 |

| | | |
|--------|---|-----|
| 3.179. | Time-consolidation curve of sample 4(dynamic at optimum moisture content) at 40-80kPa | 196 |
| 3.180. | Time-consolidation curve of sample 4(dynamic at optimum moisture content) at 80-160kPa | 196 |
| 3.181. | Time-consolidation curve of sample 4(dynamic at optimum moisture content) at 160-320kPa | 197 |
| 3.182. | Time-consolidation curve of sample 4(dynamic at optimum moisture content) at 320-640kPa | 197 |
| 3.183. | Time-consolidation curve of sample 4(dynamic at wet of optimum) at 20-40kPa | 198 |
| 3.184. | Time-consolidation curve of sample 4(dynamic at wet of optimum) at 40-80kPa | 198 |
| 3.185. | Time-consolidation curve of sample 4(dynamic at wet of optimum) at 80-160kPa | 199 |
| 3.186. | Time-consolidation curve of sample 4(dynamic at wet of optimum) at 160-320kPa | 199 |
| 3.187. | Time-consolidation curve of sample 4(dynamic at wet of optimum) at 320-640kPa | 200 |
| 3.188. | Time-consolidation curve of sample 4(static at dry of optimum) at 20-40kPa | 200 |
| 3.189. | Time-consolidation curve of sample 4(static at dry of optimum) at 40-80kPa | 201 |
| 3.190. | Time-consolidation curve of sample 4(static at dry of optimum) at 80-160kPa | 201 |
| 3.191. | Time-consolidation curve of sample 4(static at dry of optimum) at 160-320kPa | 202 |
| 3.192. | Time-consolidation curve of sample 4(static at dry of optimum) at 320-640kPa | 202 |
| 3.193. | Time-consolidation curve of sample 4(static at optimum moisture content) at 20-40kPa | 203 |
| 3.194. | Time-consolidation curve of sample 4(static at optimum moisture content) at 40-80kPa | 203 |
| 3.195. | Time-consolidation curve of sample 4(static at optimum moisture content) at 80-160kPa | 204 |
| 3.196. | Time-consolidation curve of sample 4(static at optimum moisture content) at 160-320kPa | 204 |
| 3.197. | Time-consolidation curve of sample 4(static at optimum moisture content) at 320-640kPa | 205 |
| 3.198. | Time-consolidation curve of sample 4(static at wet of optimum) at 20-40kPa | 205 |
| 3.199. | Time-consolidation curve of sample 4(static at wet of optimum) at 40-80kPa | 206 |
| 3.200. | Time-consolidation curve of sample 4(static at wet of optimum) at 80-160kPa | 206 |
| 3.201. | Time-consolidation curve of sample 4(static at wet of optimum) at | 207 |

| | | |
|--------|--|--|
| | 160-320kPa | |
| 3.202. | Time-consolidation curve of sample 4(static at wet of optimum) at 207 320-640kPa | |
| 3.203. | Time-consolidation curve of sample 5(dynamic at dry of optimum) at 208 20-40kPa | |
| 3.204. | Time-consolidation curve of sample 5(dynamic at dry of optimum) at 208 40-80kPa | |
| 3.205. | Time-consolidation curve of sample 5(dynamic at dry of optimum) at 209 80-160kPa | |
| 3.206. | Time-consolidation curve of sample 5(dynamic at dry of optimum) at 209 160-320kPa | |
| 3.207. | Time-consolidation curve of sample 5(dynamic at dry of optimum) at 210 320-640kPa | |
| 3.208. | Time-consolidation curve of sample 5(dynamic at optimum moisture 210 content) at 20-40kPa | |
| 3.209. | Time-consolidation curve of sample 5(dynamic at optimum moisture 211 content) at 40-80kPa | |
| 3.210. | Time-consolidation curve of sample 5(dynamic at optimum moisture 211 content) at 80-160kPa | |
| 3.211. | Time-consolidation curve of sample 5(dynamic at optimum moisture 212 content) at 160-320kPa | |
| 3.212. | Time-consolidation curve of sample 5(dynamic at optimum moisture 212 content) at 320-640kPa | |
| 3.213. | Time-consolidation curve of sample 5(dynamic at wet of optimum) at 213 20-40kPa | |
| 3.214. | Time-consolidation curve of sample 5(dynamic at wet of optimum) at 213 40-80kPa | |
| 3.215. | Time-consolidation curve of sample 5(dynamic at wet of optimum) at 214 80-160kPa | |
| 3.216. | Time-consolidation curve of sample 5(dynamic at wet of optimum) at 214 160-320kPa | |
| 3.217. | Time-consolidation curve of sample 5(dynamic at wet of optimum) at 215 320-640kPa | |
| 3.218. | Time-consolidation curve of sample 5(static at dry of optimum) at 20- 215 40kPa | |
| 3.219. | Time-consolidation curve of sample 5(static at dry of optimum) at 40- 216 80kPa | |
| 3.220. | Time-consolidation curve of sample 5(static at dry of optimum) at 80- 216 160kPa | |
| 3.221. | Time-consolidation curve of sample 5(static at dry of optimum) at 160 217 -320kPa | |
| 3.222. | Time-consolidation curve of sample 5(static at dry of optimum) at 320 217 -640kPa | |
| 3.223. | Time-consolidation curve of sample 5(static at optimum moisture 218 content) at 20-40kPa | |

| | | |
|--------|---|-----|
| 3.224. | Time-consolidation curve of sample 5(static at optimum moisture content) at 40-80kPa | 218 |
| 3.225. | Time-consolidation curve of sample 5(static at optimum moisture content) at 80-160kPa | 219 |
| 3.226. | Time-consolidation curve of sample 5(static at optimum moisture content) at 160-320kPa | 219 |
| 3.227. | Time-consolidation curve of sample 5(static at optimum moisture content) at 320-640kPa | 220 |
| 3.228. | Time-consolidation curve of sample 5(static at wet of optimum) at 20-40kPa | 220 |
| 3.229. | Time-consolidation curve of sample 5(static at wet of optimum) at 40-80kPa | 221 |
| 3.230. | Time-consolidation curve of sample 5(static at wet of optimum) at 80-160kPa | 221 |
| 3.231. | Time-consolidation curve of sample 5(static at wet of optimum) at 160-320kPa | 222 |
| 3.232. | Time-consolidation curve of sample 5(static at wet of optimum) at 320-640kPa | 222 |
| 3.233. | Void ratio vs. Coefficient of permeability for sample 1 (dynamic at dry of optimum) | 75 |
| 3.234. | Void ratio vs. Coefficient of permeability for sample 1 (dynamic at optimum moisture content) | 76 |
| 3.235. | Void ratio vs. Coefficient of permeability for sample 1 (dynamic at wet of optimum) | 76 |
| 3.236. | Void ratio vs. Coefficient of permeability for sample 1 (static at dry of optimum) | 77 |
| 3.237. | Void ratio vs. Coefficient of permeability for sample 1 (static at optimum moisture content) | 77 |
| 3.238. | Void ratio vs. Coefficient of permeability for sample 1 (static at wet of optimum) | 78 |
| 3.239. | Void ratio vs. Coefficient of permeability for sample 2 (dynamic at dry of optimum) | 231 |
| 3.240. | Void ratio vs. Coefficient of permeability for sample 2 (dynamic at optimum moisture content) | 231 |
| 3.241. | Void ratio vs. Coefficient of permeability for sample 2 (dynamic at wet of optimum) | 232 |
| 3.242. | Void ratio vs. Coefficient of permeability for sample 2 (static at dry of optimum) | 232 |
| 3.243. | Void ratio vs. Coefficient of permeability for sample 2 (static at optimum moisture content) | 233 |
| 3.244. | Void ratio vs. Coefficient of permeability for sample 2 (static at wet of optimum) | 233 |
| 3.245. | Void ratio vs. Coefficient of permeability for sample 3 (dynamic at dry of optimum) | 234 |
| 3.246. | Void ratio vs. Coefficient of permeability for sample 3 (dynamic at | 234 |

| | | |
|--------|---|-----|
| | optimum moisture content) | |
| 3.247. | Void ratio vs. Coefficient of permeability for sample 3 (dynamic at wet of optimum) | 235 |
| 3.248. | Void ratio vs. Coefficient of permeability for sample 3 (static at dry of optimum) | 235 |
| 3.249. | Void ratio vs. Coefficient of permeability for sample 3 (static at optimum moisture content) | 236 |
| 3.250. | Void ratio vs. Coefficient of permeability for sample 3 (static at wet of optimum) | 236 |
| 3.251. | Void ratio vs. Coefficient of permeability for sample 4 (dynamic at dry of optimum) | 237 |
| 3.252. | Void ratio vs. Coefficient of permeability for sample 4 (dynamic at optimum moisture content) | 237 |
| 3.253. | Void ratio vs. Coefficient of permeability for sample 4 (dynamic at wet of optimum) | 238 |
| 3.254. | Void ratio vs. Coefficient of permeability for sample 4 (static at dry of optimum) | 238 |
| 3.255. | Void ratio vs. Coefficient of permeability for sample 4 (static at optimum moisture content) | 239 |
| 3.256. | Void ratio vs. Coefficient of permeability for sample 4 (static at wet of optimum) | 239 |
| 3.257. | Void ratio vs. Coefficient of permeability for sample 5 (dynamic at dry of optimum) | 240 |
| 3.258. | Void ratio vs. Coefficient of permeability for sample 5 (dynamic at optimum moisture content) | 240 |
| 3.259. | Void ratio vs. Coefficient of permeability for sample 5 (dynamic at wet of optimum) | 241 |
| 3.260. | Void ratio vs. Coefficient of permeability for sample 5 (static at dry of optimum) | 241 |
| 3.261. | Void ratio vs. Coefficient of permeability for sample 5 (static at optimum moisture content) | 242 |
| 3.262. | Void ratio vs. Coefficient of permeability for sample 5 (static at wet of optimum) | 242 |
| 4.1. | Void ratio vs consolidation pressure curve for S1(dry) | 79 |
| 4.2. | Void ratio vs consolidation pressure curve for S2(dry) | 80 |
| 4.3. | Void ratio vs consolidation pressure curve for S3(dry) | 80 |
| 4.4. | Void ratio vs consolidation pressure curve for S4(dry) | 81 |
| 4.5. | Void ratio vs consolidation pressure curve for S5(dry) | 81 |

| | | |
|-------|--|----|
| 4.6. | Void ratio vs consolidation pressure curve for S1(OMC) | 83 |
| 4.7. | Void ratio vs consolidation pressure curve for S2 (OMC) | 83 |
| 4.8. | Void ratio vs consolidation pressure curve for S3(OMC) | 84 |
| 4.9. | Void ratio vs consolidation pressure curve for S4(OMC) | 84 |
| 4.10. | Void ratio vs consolidation pressure curve for S5(OMC) | 85 |
| 4.11. | Void ratio vs consolidation pressure curve for S1(wet) | 87 |
| 4.12. | Void ratio vs consolidation pressure curve for S2(wet) | 87 |
| 4.13. | Void ratio vs consolidation pressure curve for S3(wet) | 87 |
| 4.14. | Void ratio vs consolidation pressure curve for S4(wet) | 88 |
| 4.15. | Void ratio vs consolidation pressure curve for S5(wet) | 88 |
| 4.16. | Void ratio vs consolidation pressure curve for S1 | 90 |
| 4.17. | Void ratio vs consolidation pressure curve for S2 | 90 |
| 4.18. | Void ratio vs consolidation pressure curve for S3 | 91 |
| 4.19. | Void ratio vs consolidation pressure curve for S4 | 91 |
| 4.20. | Void ratio vs consolidation pressure curve for S5 | 92 |
| 4.21. | Void ratio vs consolidation pressure curve for S1 | 95 |
| 4.22. | Void ratio vs consolidation pressure curve for S2 | 95 |
| 4.23. | Void ratio vs consolidation pressure curve for S3 | 96 |
| 4.24. | Void ratio vs consolidation pressure curve for S4 | 96 |
| 4.25. | Void ratio vs consolidation pressure curve for S5 | 97 |
| 5.1. | Void Ratio (e) vs. Coefficient of Permeability (k) for S1(dry) | 98 |

| | | |
|-------|---|-----|
| 5.2. | Void Ratio (e) vs. Coefficient of Permeability (k) for S2(dry) | 99 |
| 5.3. | Void Ratio (e) vs. Coefficient of Permeability (k) for S3(dry) | 99 |
| 5.4. | Void Ratio (e) vs. Coefficient of Permeability (k) for S4(dry) | 100 |
| 5.5. | Void Ratio (e) vs. Coefficient of Permeability (k) for S5(dry) | 100 |
| 5.6. | Coefficient of Permeability (dynamic) vs. Coefficient of Permeability (static)(Dry) | 102 |
| 5.7. | Void Ratio (e) vs. Coefficient of Permeability (k) for S1(OMC) | 103 |
| 5.8. | Void Ratio (e) vs. Coefficient of Permeability (k) for S2(OMC) | 103 |
| 5.9. | Void Ratio (e) vs. Coefficient of Permeability (k) for S3(OMC) | 104 |
| 5.10. | Void Ratio (e) vs. Coefficient of Permeability (k) for S4(OMC) | 104 |
| 5.11. | Void Ratio (e) vs. Coefficient of Permeability (k) for S5(OMC) | 105 |
| 5.12. | Coefficient of Permeability (dynamic) vs. Coefficient of Permeability (static)(OMC) | 106 |
| 5.13. | Void Ratio (e) vs. Coefficient of Permeability (k) for S1(wet) | 107 |
| 5.14. | Void Ratio (e) vs. Coefficient of Permeability (k) for S2(wet) | 107 |
| 5.15. | Void Ratio (e) vs. Coefficient of Permeability (k) for S3(wet) | 108 |
| 5.16. | Void Ratio (e) vs. Coefficient of Permeability (k) for S4(wet) | 108 |
| 5.17. | Void Ratio (e) vs. Coefficient of Permeability (k) for S5(wet) | 108 |
| 5.18. | Coefficient of Permeability (dynamic) vs. Coefficient of Permeability (static)(Wet) | 110 |
| 5.19. | Void Ratio (e) vs. Coefficient of Permeability (k) for S1 (dynamic) | 111 |
| 5.20. | Void Ratio (e) vs. Coefficient of Permeability (k) for S2 (dynamic) | 111 |
| 5.21. | Void Ratio (e) vs. Coefficient of Permeability (k) for S3 (dynamic) | 112 |

| | | |
|-------|--|-----|
| 5.22. | Void Ratio (e) vs. Coefficient of Permeability (k) for S4 (dynamic) | 112 |
| 5.23. | Void Ratio (e) vs. Coefficient of Permeability (k) for S5 (dynamic) | 113 |
| 5.24. | Void Ratio (e) vs. Coefficient of Permeability (k) for S1 (static) | 114 |
| 5.25. | Void Ratio (e) vs. Coefficient of Permeability (k) for S2 (static) | 114 |
| 5.26. | Void Ratio (e) vs. Coefficient of Permeability (k) for S3 (static) | 115 |
| 5.27. | Void Ratio (e) vs. Coefficient of Permeability (k) for S4 (static) | 115 |
| 5.28. | Void Ratio (e) vs. Coefficient of Permeability (k) for S5 (static) | 116 |
| 5.29. | Permeability versus molding water content relationship for S1(dynamic) | 118 |
| 5.30. | Permeability versus molding water content relationship for S2(dynamic) | 119 |
| 5.31. | Permeability versus molding water content relationship for S3(dynamic) | 120 |
| 5.32. | Permeability versus molding water content relationship for S4(dynamic) | 121 |
| 5.33. | Permeability versus molding water content relationship for S5(dynamic) | 122 |
| 5.34. | Permeability versus molding water content relationship for S1(static) | 125 |
| 5.35. | Permeability versus molding water content relationship for S2(static) | 126 |
| 5.36. | Permeability versus molding water content relationship for S3(static) | 127 |
| 5.37. | Permeability versus molding water content relationship for S4(static) | 128 |
| 5.38. | Permeability versus molding water content relationship for S5(static) | 129 |

CONTENTS

| Title | Page No. |
|---|-----------|
| Declaration | ii |
| Certificate | iii |
| Certificate from the head of the department | iv |
| Acknowledgement | v |
| Abstract | vi |
| List of tables | vii-x |
| List of figures | xi-xxviii |
| Chapter 1: Introduction | 1-3 |
| Chapter 2: Literature Review | |
| 2.1: Introduction | 4 |
| 2.2: Review of Literature | 4-22 |
| Chapter 3: Experimental Procedure and Results | |
| 3.1: Introduction | 23 |
| 3.2: Test program | 23 |
| 3.2.1: Collection of soil sample | 24 |
| 3.2.2: Preparation of the disturbed samples for testing | 24 |
| 3.2.3: Determination of the physical properties of the soils | 24 |
| 3.2.4: Determination of the compaction properties of the soils | 24 |
| 3.2.4.1: Dynamic compaction method | 25 |
| 3.2.4.2: Static compaction method | 25 |
| 3.2.4.2.1: Static Compaction Test Procedure | 26 |
| 3.2.5: Determination of the consolidation properties of soils by consolidation test | 27 |
| 3.2.5.1: Consolidation test on dynamically compacted soil | 27 |
| 3.2.5.2: Consolidation test on statically compacted soil | 30 |
| 3.3. Test results | 31 |
| 3.3.1: Test results of the physical properties | 31 |
| 3.3.2: Test results of the compaction properties of the soil | 33 |
| 3.3.3: Determination of equivalent static pressure | 47 |
| 3.3.4: Test results of consolidation properties of the soil | 50 |
| 3.3.4.1: Consolidation test results of dynamically compacted soil samples | 50 |
| 3.3.4.1.1: Consolidation Test results at dry of optimum moisture content (OMC-3%) | 51 |
| 3.3.4.1.2: Consolidation Test results at optimum moisture content (OMC) | 53 |
| 3.3.4.1.3: Consolidation Test results at wet of optimum moisture content (OMC+3%) | 55 |
| 3.3.4.2: Consolidation test results of statically compacted | 58 |

| | |
|--|-----|
| soil samples | |
| 3.3.4.2.1: Consolidation Test results at dry of optimum moisture content (OMC-3%) | 58 |
| 3.3.4.2.2: Consolidation Test results at optimum moisture content (OMC) | 61 |
| 3.3.4.2.3: Consolidation Test results at wet of optimum moisture content (OMC+3%) | 63 |
| 3.3.4.3: Determination of Coefficient of consolidation (C_v) | 66 |
| 3.3.4.4: Determination of coefficient of compressibility (a_v) and coefficient of volume compressibility (m_v) | |
| 3.3.4.5: Determination of coefficient of permeability (k) | 73 |
| Chapter 4: Analysis of Compressibility characteristics | |
| 4.1: Analysis for compressibility characteristics at dry of optimum, optimum moisture content and wet of optimum moisture content. | 79 |
| 4.1.1: At dry of optimum moisture content | 79 |
| 4.1.2: At optimum moisture content | 82 |
| 4.1.3: At wet of optimum moisture content | 86 |
| 4.2: Analysis for the combined consolidation plots (at dry, OMC and wet) | 90 |
| 4.2.1: Analysis for the combined consolidation plots (at dry, OMC and wet) for dynamic compaction | 90 |
| 4.2.2: Analysis for the combined consolidation plots (at dry, OMC and wet) for static compaction | 90 |
| Chapter 5: Analysis of Permeability characteristics | 98 |
| 5.1: Analysis of permeability characteristics for static and dynamic compaction across dry side, optimal moisture content (OMC), and wet side of optimum | 98 |
| 5.1.1: Analysis of permeability characteristics for dynamic and static compaction at dry side of optimum | 98 |
| 5.1.2: Analysis of permeability characteristics for dynamic and static compaction at optimum moisture content | 102 |
| 5.1.3: Analysis of permeability characteristics for dynamic and static compaction at wet of optimum | 106 |
| 5.2: Analysis of permeability characteristics for dynamic compaction across dry side, optimal moisture content (OMC), and wet side of optimum | 110 |
| 5.3: Analysis of permeability characteristics for static compaction across dry side, optimal moisture content (OMC), and wet side of optimum | 113 |

| | |
|---|-----|
| 5.4: Analysis for Permeability versus molding water content relationship for dynamic and static compaction | 117 |
| 5.4.1: For dynamic compaction | 117 |
| 5.4.2: For static compaction | 124 |
| Chapter 6: Conclusions and Scope for future study | 132 |
| 6.1: Introduction | 132 |
| 6.2: Conclusions from compressibility characteristics of statically and dynamically compacted soil samples | 132 |
| 6.3: Conclusions from permeability characteristics of statically and dynamically compacted soil samples | 133 |
| 6.4: Scope for future study | 134 |
| References | 135 |
| Appendix I | 137 |
| Appendix II | 144 |
| Appendix III | 154 |
| Appendix IV | 223 |
| Appendix V | 231 |

CHAPTER 1

INTRODUCTION

Soil compaction is the practice of applying mechanical compactive effort to densify a soil by reducing the void space between soil particles. Compaction occurs when particles are pressed together to reduce the space between them. Highly compacted soils contain very few spaces resulting in soil with higher unit weight. The maximum density is achieved at optimum moisture content.

Soil compaction is necessary to increase the bearing capacity and stiffness of in-situ (natural state) or chemically modified soils. Compaction increases the shear strength of soils by adding friction from the interlocking of particles. Future settlement of soils is reduced by increasing the stiffness and eliminating voids creating a densified soil. The removal of voids reduces the chance of the soil settling or shrinking or expanding and it decreases water seepage that would lead to deleterious shrinking and swelling soil properties. Shrinking or swelling properties compromise the pavement structure thereby leading to premature failure of the pavement structure.

Particle size and critical water values play a large role in soil compaction. Different soil types react differently to compaction efforts. Soil types are classified by their particle size and, in fine-grained soils, by their Atterberg limits. Particle size is determined in a laboratory by separating a representative sample on a series of sieves, or screens, ranging from 4.75 mm (4-mesh) to 0.075 mm (200-mesh). Distribution of soil particles are either well graded, poorly graded or gap graded. Well graded soils that contain a wide range of particles are preferred in construction applications because they can be easily compacted, eliminating voids, interlocking the particles and resisting moisture absorption allowing the soil to support heavier loads as a very dense soil. Poorly graded soils contain a narrow range of particle sizes and are less conducive for construction purposes as shear strength is not associated with the non-interlocking particles because of their similar sizes. Gap graded soils contain a break in the overall distribution of grain sizes.

The degree of compaction of a soil is measured in terms of dry unit weight, which is a measure of the weight of the soil solids packed into a unit volume of the soil. The dry unit weight provides valuable information about the physical properties of the soil and is used by

engineers and construction professionals to design structures and foundations that can withstand the loads and stresses imposed on them by the soil.

Soil compaction is achieved through static or dynamic force and manipulation of the soil. Static force makes use of the dead weight of machines to apply downward, continuous pressure to increase compaction through compression of the top of the soil. Dynamic force uses movement in the form of vibrations or falling weight in conjunction with the static load of the machine to increase the density of the soil. Manipulation through kneading and shearing, helps to compact soil at greater depths.

In 1933, R.R. Proctor demonstrated a clear correlation between the moisture content at which soil is placed and its dry unit weight. The Bureau of Indian Standards has since adopted Proctor's compaction test with some minor adjustments, as outlined in IS: 2720 part-7. This test is commonly used to determine the optimum moisture content (OMC) and maximum dry unit weight (MDUW) for a specific type of fill, such as backfills, embankments, or earthen dams, that require minimal subgrade compaction. The modified Proctor test, on the other hand, is typically utilized for fills that will support heavy loads, such as roadways or runways.

In practical applications, soil compaction is typically accomplished using different types of rollers. To achieve the desired dry densities, the number of passes required for each type of soil encountered must be determined. In the field, the degree of compaction achieved is assessed by means of relative compactness, with a recommended value of 95-100% for various civil engineering projects.

However dynamic compaction given by R. R. Proctor applies standard energy for all types of soils and requires considerable time and effort and its application has a few imperfections. One of these imperfections is that we determine the MDD and OMC in soil laboratory using standard Proctor compaction method to decide for the MDD and OMC of subgrade, in which static compaction method is used to achieve compaction. In order to overcome this shortcoming of application of standard Proctor compaction test results to static compaction of subgrade soil, a method has been introduced in the laboratory to determine the MDD and OMC values through static compaction of soil. The soil is statically compacted in the standard Proctor mould by using a loading frame. In this study an attempt has been made to derive an equivalent static pressure in which MDD value at OMC can be obtained as determined from the standard Proctor compaction test. The study also concentrates in drawing comparison

between the static and standard Proctor compaction method so as to ascertain the variation in MDD and OMC values determined by the static and standard Proctor compaction test. The study also concentrates to find the effect of static compaction with the height of the soil. The experimental procedure, the description of the apparatus devised and the analysis of the test results obtained are discussed further in the work.

When a soil is loaded because of construction of a structure, its volume will decrease due to a rearrangement of soil particles. The decrease in soil volume by squeezing out of pore water on account of gradual dissipation of excess hydrostatic pressure induced by an imposed total stress is defined as consolidation. The compressibility of clays may be caused by three factors: a) the expulsion of double layer water from between the grains, b) slipping of the particles to new positions of greater density, and c) bending of particles as elastic sheets.

The objective of this study is to investigate the consolidation and permeability properties of soil that has been compacted using both static and dynamic compaction methods at the dry of optimum, at optimum moisture content and at wet of optimum moisture content. Using water content as (OMC-3%), OMC and (OMC+3%) and by using the corresponding dry unit weight, samples are to be prepared by dynamic compaction using the Standard Proctor test, and by static compaction method using the Proctor mould and a static compaction apparatus.

CHAPTER 2

LITERATURE REVIEW

2.1. INTRODUCTION:

There is a dearth of research on the compaction properties of soil using both static and dynamic methods, with only a limited amount of studies available. This chapter provides a brief overview of the research conducted by different scholars that predicts the compaction properties and compares the results obtained by the two methods.

2.2. Review of Literature:

Laboratory compaction is an important test to obtain maximum dry density and optimum moisture content values. Kenneth and Steven (1968); Reddy and Jagadish (1993); Mesbah et al (1999) and Hafez et al. (2010) presented the static compaction method as the main laboratory technique.

Hogentogler (1937) is considered to be the first researcher who coined the concept of static pressure equivalent to Proctor's compacting pressure. According to his findings equivalent static pressure equals to 896 kN/m^2 need to be imposed on the soil to get the maximum dry density same as that of Proctor's compaction.

Berenhard and Krynine (1952) compared the static and dynamic compaction efficiencies.

Kenneth and Steven (1968) in their research conducted kneading and static compaction method in the laboratory. The static compaction technique was conducted by forcing the soil into the mould with 1.4 inch diameter of metal plunger. Then the results obtained from kneading compaction and static compaction methods were compared. Based on the comparison, of the MDD and OMC curves, it was found that the value of MDD obtained from static compaction method was higher as compared to that of the kneading method. The MDD value obtained from static compaction was 94 lb/ft^3 , while that obtained from kneading compaction was 89 lb/ft^3

Diamond S. (1970) in his study investigated the microstructures of impact-compacted kaolinite and illite clays through various techniques including pore size-distribution measurements, X-ray orientation determinations, and scanning electron microscopy. The results showed that clays compacted at or above the optimum moisture content had a more

massive structure without large interdomain voids, while clays compacted on the dry side of the optimum moisture content exhibited a domain structure separated by interdomain voids. The study also identified significant volumes of pores in the 200-800 Å dia. Range in the kaolinite samples, which were classified as “intergrown” in character. The orientation indices were calculated for the compacted kaolinite and showed only a small degree of preferential orientation normal to the axis of compaction, with little difference between samples compacted either wet or dry of optimum. The results were consistent with scanning electron microscope interpretations, which suggested that the domains did not orient themselves significantly under the influence of the compaction employed.

Ahmed et al. (1974) conducted a study on a specific type of clay called Grundite. The study investigated the relationship between pore size distribution, compaction characteristics, and undrained strength and deformation data, and how they are affected by the molding water content and type of laboratory compaction. Mercury porosimetry was used to measure the pore size distribution, but this required dry samples, which were obtained by freeze drying. The measurements were obtained for a range of diameters. Samples that were compacted at moisture contents less than the Proctor optimum moisture contents showed brittle compressive failures at low strains, while samples that were compacted on the wet of the optimum moisture contents continued to deform to high strains.

Reddy and Jagadish (1993) presented a new static compaction test for soils, to be used in the production of compacted soil blocks. The static compaction test described in their work can be used to obtain a continuous relationship between compaction energy and OMC. In such a test the energy input per unit volume could easily be varied and thus, OMC becomes a function of the energy input for a given maximum dry density. Reddy and Jagadish (1993) produced two concepts of static compaction in the laboratory which are constant peak stress variable stroke compaction and variable peak stress-constant stroke compaction.

In the constant peak stress variable stroke compaction method, the applied stress is varied gradually at a definite rate (or a set of different rates) until a specific peak stress is reached. The thickness of the compacted specimen depends on the moisture content. Such tests have been carried out by various other researchers. Compaction curves similar to the Proctor curves were generated in these tests, but the energy input to the soil varied with the moisture content. Such a compaction curve cannot be interpreted with reference to a specific energy input. In

the variable peak stress-constant stroke compaction method, a static force is gradually applied to a soil mass until a specific final thickness (volume) is achieved. The force at the end of compaction can vary, depending on the moisture content of the soil.

Reddy and Jagadish (1993) in their work deduced the relationship of compaction energy, dry density and OMC obtained by static compaction of a soil into a small cube at different moisture contents while the energy input to the cube was monitored. This relationship provided specific information on the OMC to be used to achieve a given dry density when the compaction energy available in the static compaction device/ process was known.

Reddy and Jagadish (1993) also compared the results of static compaction and Proctor compaction by superimposing the curves obtained from both the methods as shown in Figure 2.1. On comparison it was obtained that the static compaction curves showed only the ‘rising’ portion of the Proctor compaction curve the ‘drooping’ portion beyond the OMC normally noticed in the Proctor curve was not present. The curves also showed that for the same input energy and OMC value, the static compaction produces a much higher dry density.

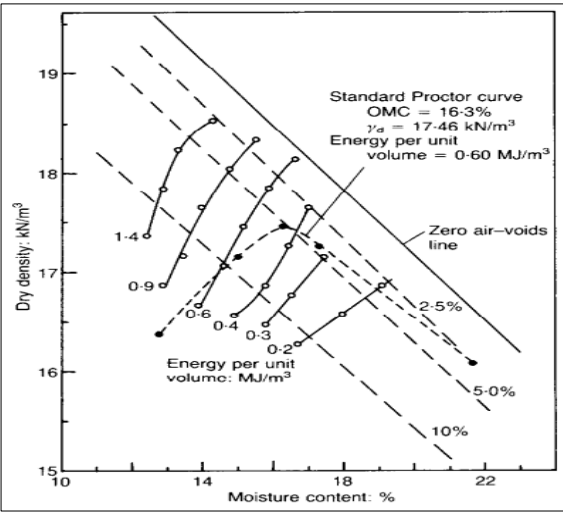


Figure 2.1: Comparison between static compaction method by Reddy and Jagadish (1993) and the standard Proctor compaction method.

Delage et al. (1996) described a study that was conducted to investigate the microstructure of a compacted silt. The researchers used a scanning electron microscope and mercury intrusion pore size distribution measurements to carry out the qualitative and quantitative analysis of the samples. The silt samples were statically compacted at three different water contents: one with less water than the optimum level determined by the standard Proctor test, one at the optimum

level, and one with more water than the optimum level. The results showed that the wet sample had a different structure than the other two, with a clayey fraction filling the voids and sticking to the silt-sized grains, while the other samples had a structure characterized by a skeleton made of silt grain aggregates linked together by clayey bridges. The researchers also describe the distribution of water and air within the microstructure of the compacted soil for each of the three compaction states.

Mesbah et al. (1999) described the quasi-static compaction technique in their technical paper. The technique involves pressing the soil into the mould in two way directions which are from the top and from the bottom. Based on quasi-static compaction design, the soil specimen was compacted homogenously. According to the technical paper of Mesbah et al. (1999), quasi static and dynamic compaction methods were compared to define which method present higher density.

As a conclusion, the higher density value was obtained by the quasi-static technique as compared to the standard Proctor technique although the same amount of energy was applied to both the methods.

Kenai S., Bahar R., Benazzoug M. (2006) summarized the results of an experimental study on the effect of different compaction methods on the performance of stabilized soil. The compaction methods investigated were either static compaction by applying a static pressure using a universal compression testing machine, dynamic compaction by a drop weight method, or static compaction coupled with vibration. All methods were applied on unstabilized soil or cement stabilized soil.

Hafez et al. (2010) introduced a new laboratory compaction method that is suitable to measure the degree of compaction for Malaysian cohesive soils. Most of the Malaysian road infrastructures are situated in cohesive soils where static road roller machine is commonly used in the field to achieve the required MDD. But in the laboratory the MDD is determined by the standard Proctor dynamic compaction. Thus, there is a gap between laboratory test and field method to measure the value of MDD. Therefore, a new static method of compaction has been developed to close the gap between compaction measured in the laboratory and in the field.

The static packing pressure test as designed by Hafez et.al applies a constant compression force to the soil by using a new static mould design with a certain amount of energy. The amount of energy is dependent on the characteristic and the conditions of each type of soils. Therefore, from static compaction test each soil has a certain amount of energy per unit volume compared to the standard Proctor compaction which applies a standard energy for all categories of soils.

The static packing pressure machine uses a load cell connected to a data logger to measure the force values and the compaction technique applies a gradually upward static force to the soil by using a hydraulic pump as shown in Figure 2.2. The static compaction was performed in one homogeneous layer and a new static mould was designed to ensure that the soil inside it has high degree of freedom to plunge out under excessive static compaction.

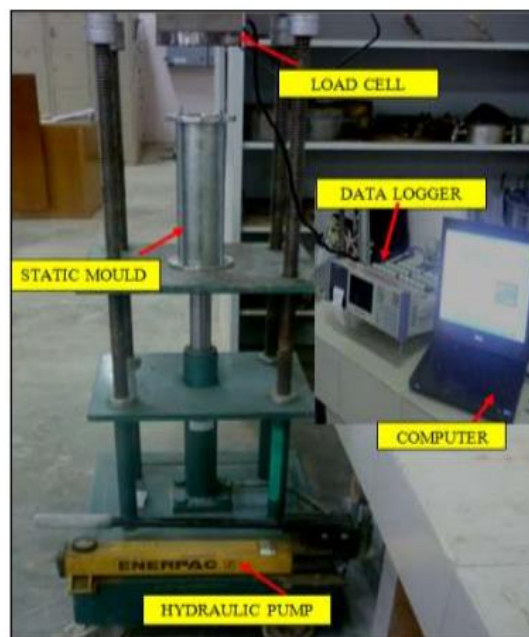


Figure 2.2: Static Packing Pressure Equipment by Hafez et al. 2010.

The technical paper also drew comparisons between the static packing pressure method and the standard Proctor method as shown in Figure 2.3 and obtained that the results from static compaction is higher in MDD value as compared to the standard Proctor compaction method. Therefore, the static compaction test can be used to measure the degree of compaction value in the laboratory to correlate with field data of static compaction technique.

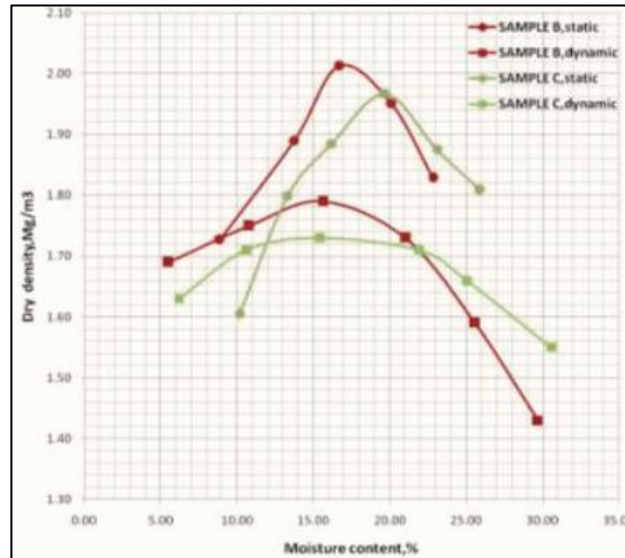


Figure 2.3: Comparison between static compaction method by Hafez et al. (2010) and the dynamic compaction method.

Dario et al. (2011), in their study investigated the effects of both static and dynamic laboratory compaction methods on the compaction curves and mechanical strength of two residual soils from the Zona da Mata Norte region in the state of Minas Gerais, Brazil. The study utilized two types of gneissic residual soils, one with a silty-sandy clay texture (soil 1) and the other with a clayey-silty sand texture (soil 2). The researchers compacted the specimens using the standard Proctor compaction effort and at three different moisture levels: the optimum water content (w_{ot}), $w_{ot} - 3\%$, and $w_{ot} + 2\%$. The study also included determination of the unconfined compressive strength of the compacted specimens, micromorphological analysis of thin sections of the compacted specimens using optical microscopy, and statistical analysis of the laboratory testing program data.

In an attempt to reproduce the compaction effort and water content commonly used in the field compaction of landfills and sub-grade soil layers, all specimens were compacted at the standard Proctor compaction effort adopting nine repetitions of the compaction curve at the following water contents: optimum (w_{ot}); optimum minus 3% ($w_{ot} - 3\%$); and optimum plus 2% ($w_{ot} + 2\%$). All specimens were compacted 24 hr after mixing in order to reach equilibrium water content in the soil mass. The compaction tests were carried out through dynamic and static compaction laboratory procedures to determine the dry unit weight (γ_d) at each selected water content.

The acceptance criteria adopted for specimen preparation was water content maximum deviation of $\pm 0.3\%$.

Table 2.1 – Compaction data of specimens from soils 1 and 2

| Soil Type | $w_{ot}-3\%$ (%) | γ_d (kN/m ³) | w_{ot} (%) | γ_{dmax} (kN/m ³) | $w_{ot}+2\%$ (%) | γ_d (kN/m ³) |
|-----------|------------------|---------------------------------|--------------|--------------------------------------|------------------|---------------------------------|
| 1 | 27.50 | 13.62 | 30.50 | 14.18 | 32.50 | 13.78 |
| 2 | 11.90 | 17.15 | 14.90 | 17.42 | 16.90 | 17.15 |

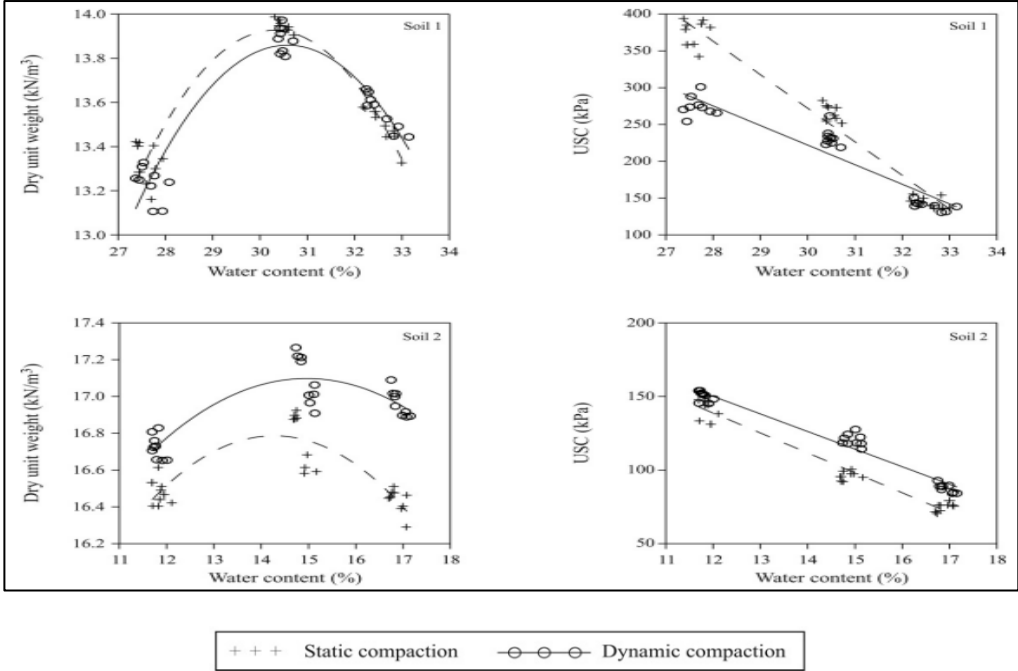


Figure 2.4: Compaction curves and unconfined compressive strength (UCS) of soils 1 and 2 (Dario et al. 2011)

From Fig. 2.4, it was clear that static compaction produced higher dry density and higher unconfined compressive strength for fine-grained soil 1 upto a particular water content (in the wet side of optimum) as shown in figure 2.4. After the specific water content, an opposite trend of dry density and mechanical strength is observed for the same soil. Hence it was evident that the static compaction mode produced soil specimens with higher and lower shear strength, respectively for soils 1 and 2, emphasizing the influence of soils formation processes in their mechanical strength.

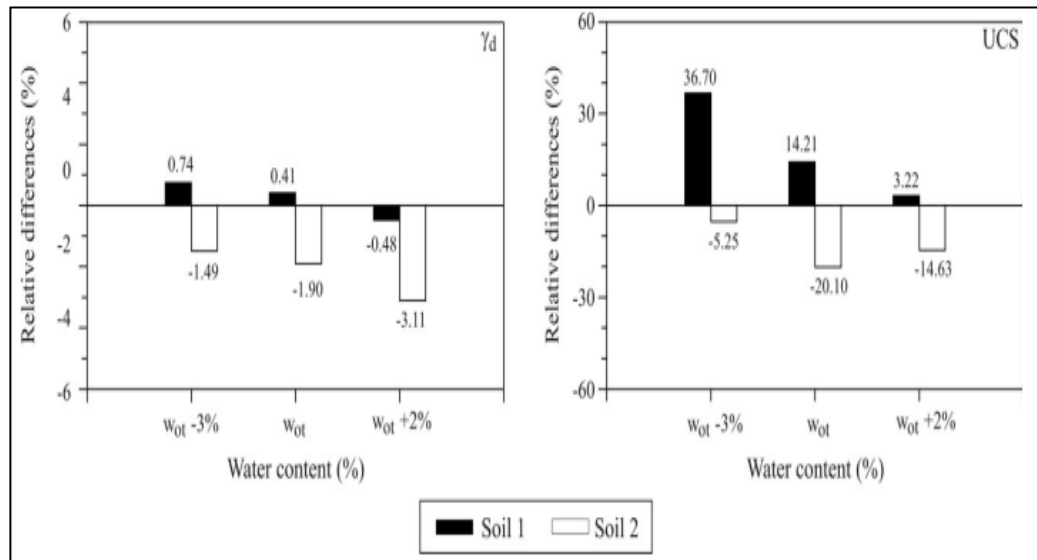


Figure 2.5: Relative differences between mean values of the parameters γ_d and RCNC of soils 1 and 2, adopting the dynamic compaction data as reference. (Dario et al. 2011)

Figure 2.5 shows relative differences between the mean values of the parameters γ_d and UCS of soils 1 and 2, adopting the dynamic compaction data as reference. For practical engineering applications, the relative differences between the γ_d mean values are not significant, not over 1% for soil 1 and 3% for soil 2; on the other hand, regarding the UCS mean values, the relative differences are higher, reaching approximately 37% for soil 1 and 20% for soil 2, which emphasizes the significant influence of the compaction procedure on soil mechanical strength.

From statistical analyses applied to γ_d and UCS data from soils 1 and 2 at the 5% significance level, it was concluded that regarding the parameter γ_d , there are significant statistical differences between the data from the static and the dynamic compaction procedures, except for specimens of soil 1 compacted at the water content $w_{ot} + 2\%$; on the other hand, considering the UCS parameter, the results of the statistical analysis confirm that the compaction procedure affects the soils mechanical strength, except for specimens of soil 1 compacted at the water content $w_{ot} + 2\%$.

Using the optical microscope, the micromorphological analysis was carried out on thin section of specimen which is compacted statically and dynamically at the water contents $w_{ot} -3\%$ and w_{ot} and respective porosity data is determined using the QUANTIPORO software.

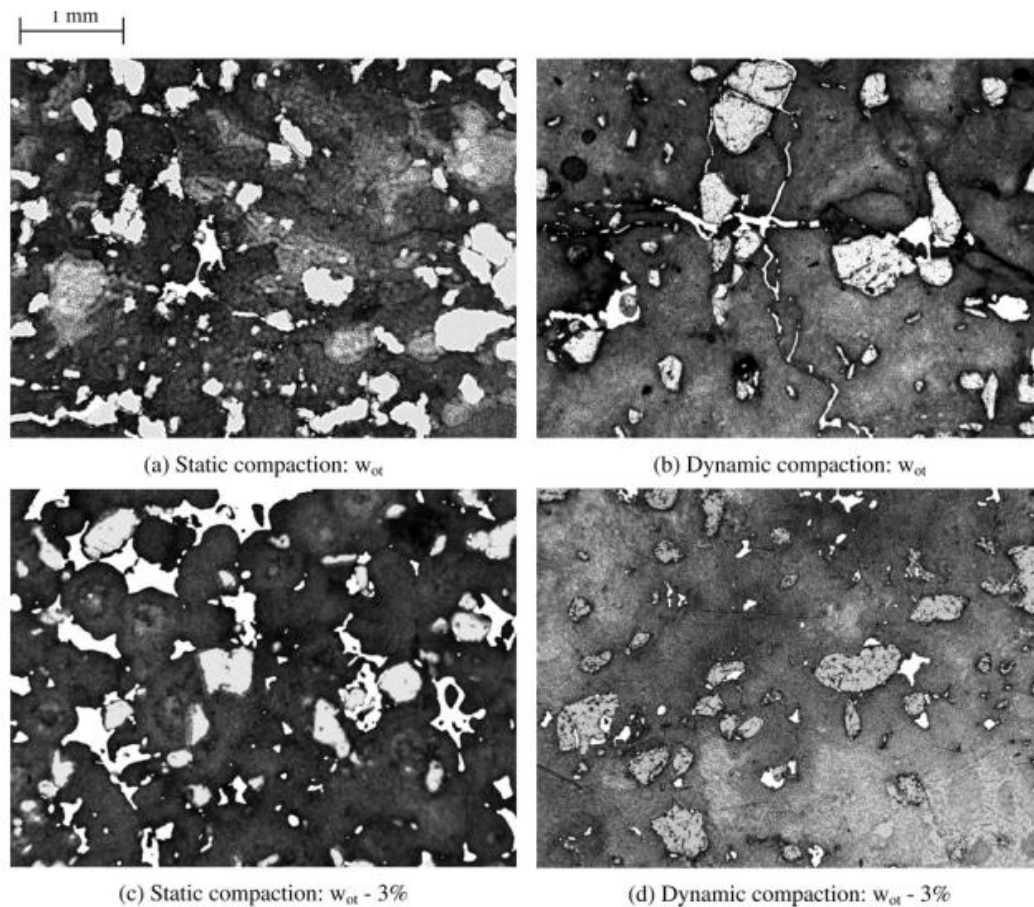


Figure 2.6 – Photomicrographs taken from thin section obtained from specimens of soils 1 and 2 statically and dynamically compacted at the water contents w_{ot} and $w_{ot} - 3\%$ (Dario et al. 2011)

Figures 2.6 present photomicrographs taken from thin section of specimens from soils 1 and 2 statically and dynamically compacted at the water contents $w_{ot} - 3\%$ and w_{ot} , and Fig. 2.7 introduces the respective porosity data determined using the QUANTIPORO software (Fernandes Filho & Viana, 2001). At OMC, figure 2.6(a) shows that the statically compacted specimens of soil 1 present features of original microaggregation, noticing original nodules, formation of isolated gaps and fissured and oriented porosity, and low porosity, around 3%. On the other hand, at this same water content, figure 2.6(b) shows that dynamically compacted specimens present a few original microaggregation features, with porosity almost all lost, around 2%. On the dry side of optimum, at water content $w_{ot} - 3\%$, as observed in figure 2.6(c) and figure 2.6(d) the static compaction applied to soil 1 produced structure with strong features of original microaggregation and gaps, and porosity around 11%. From another standpoint, the dynamic compaction produced partially bonded microstructured argillaceous

plasma, with the original microaggregation destroyed, and porosity reaching around 2%, which is much lower than the one imposed by the static compaction.

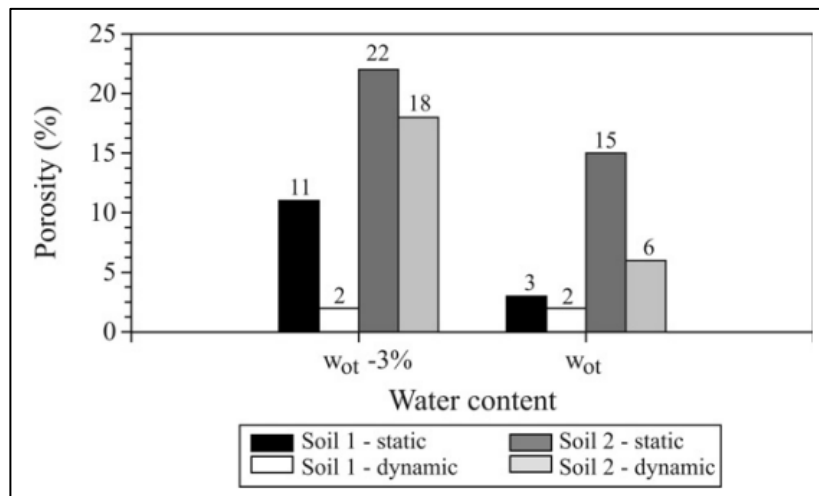


Figure 2.7 – Porosity data obtained from photomicrographs taken from thin sections of specimens of soils 1 and 2 (Dario et al. 2011)

From the above discussion it can be concluded that at OMC and dry of optimum, porosity is greater for statically compacted soil than dynamically compacted soil.

It should be emphasized that soil 1 exhibits silty-sandy clay texture, with significant clay fraction of 66%. Geotechnically, it is classified as mature residual soil, and pedologically, as red-yellow latosol, indicating occurrence of advanced pedogenetic formation processes. It also presents granular structure, with well individualized granules and highly porous aspect that can present potential collapse according to Azevedo (1999). Therefore, in soil specimen 1, there can be predominance of interparticle forces that were affected or destroyed by the dynamic compaction, producing structures with lower shear strength. This kind of behaviour¹³ is compatible with the one described by Bueno et al. (1992) when analyzing¹³ the effect of dynamic compaction in a red-yellow latosol in comparison with its mechanical response under undisturbed field condition.

After the conduction of the necessary tests, the researchers have concluded that the static procedure produced specimens with higher UCS for the clayey soil (soil 1), and lower UCS for the granular soil (soil 2), bringing up the importance of soils formation processes in their mechanical responses as compared to dynamic compaction. Considering the applied compaction methods, statistically significant differences were identified in the parameters γ_d

and UCS of both soils, except for specimens of soil 1 compacted 2% above the optimum. Therefore, the use of the static compaction procedure in laboratory to obtain compaction and mechanical strength parameters of soils for field applications requires careful study. Also incorporation of the micromorphological analysis to the present study allowed to identifying differences in the structures produced by the static and dynamic compaction procedures.

Sharma et al. (2016) had studied compaction characteristics of fine-grained soil by static compaction method in the laboratory and also derived the equivalent static pressure required to obtain the MDUW and OMC as obtained from the standard Proctor test. For this purpose the static compaction test was performed on a known weight of soil, at a known moisture content, which was placed into the mould upto a particular height and it was statically compacted in a standard Proctor mould of capacity 1000 cc. The experiments were carried out in 3 different layers of initial thicknesses 25mm, 55mm, and 100mm respectively, to ascertain whether there can be variation in dry density with initial layer thickness. A metal plate of diameter 98 mm and thickness 16 mm was placed on top of the soil sample in the mould. The entire assembly was placed under a cylindrical plunger of diameter 50 mm in the loading frame. Load was then statically applied to the soil through a proving ring having a proving ring constant of 0.99 kg/div. The plunger is a rigid plunger in contact with the plate, and uniform settlement of the plate was obtained. The height of penetration of the metal plate from the top surface was measured carefully corresponding to different applied static loads. The known load was applied until the penetration of the metal plate ceased or the measured height of the soil inside the mould became constant.

Upon analysing the superimposed curves corresponding to three different initial soil thicknesses, it was observed that the dry unit weight did not exhibit any significant variation when the soil was compacted in three different thicknesses. It was determined that the relationship between moisture content and dry unit weight for a particular soil under a given static pressure follows a parabolic pattern. This relationship remained parabolic at all other static pressures as well. The study further found that at lower static pressures, there was a significant variation in the dry unit weight, but this variation became negligible as static pressure increased, and after reaching a certain point, the dry unit weight became constant.

The superimposed static compaction curves corresponding to different static pressures were compared to the standard Proctor compaction curve, revealing that higher maximum dry unit

weight (MDUW) was obtained at higher static pressures than that obtained from the standard Proctor test. The equivalent static pressure required to achieve the MDUW at the optimum moisture content (OMC) as determined by the standard Proctor test was approximately 820 kN/m³, and this result was consistent across all eight different soil samples tested using three separate soil thicknesses.

The study also demonstrated that the static compaction test can be used to determine both the MDUW and OMC, with a static pressure of around 820 kN/m³ being the recommended value. Sharma and Talukdar (2014) previously presented an early version of this work in their technical paper.

Sharma and Deka (2016) attempted to obtain compaction characteristic using static compaction method, using the same mechanism as proposed by Sharma et al.(2016) to determine the equivalent static pressure corresponding to different dynamic compaction effort i.e. Standard Proctor test, Reduced Standard Proctor test, Modified Proctor test and Reduced Modified Proctor test. The maximum height to which soil could be filled in the compaction mould was 100mm. Similar consistent results were generated in the entire soil sample as that of Sharma and Talukdar (2014) regardless of variation in liquid limits of the soils from 30% to 79 % and the plastic limits from 16% to 23%.

The relationship between static pressure and dry unit weight, corresponding to different water contents had been plotted in the form of curves and it was found to be non-linear. For a particular static pressure and water content, the dry unit weight was obtained. The relationship between water content and dry unit weight for a particular soil at a particular static pressure is found to be parabolic in nature. Similarly, at all other static pressures, this relationship is found to be parabolic. One common characteristic in all the curves in all the soil samples was that, beyond a static pressure of around 1513kN/m², further increase in dry unit weight was not possible. To understand this analysis, plot of static pressure vs degree of saturation value at each water content for all the seven number of soil samples were made. These plots were found to be non-linear in nature. It was observed that degree of saturation could reach a maximum value of 93% to 98% depending on the soil sample at around the optimum water contents.

The static compaction curves of a particular soil sample corresponding to different static pressures were superimposed with the dynamic compaction curves of the Standard Proctor test, Modified Proctor test, Reduced Standard Proctor test and Reduced Modified Proctor test. It was observed that a static pressure in the range of 750 kN/m² to 875 kN/m² was required to obtain the maximum dry unit weight value at OMC for standard Proctor test and reduced standard Proctor test and a static pressure in the range of 1375 kN/m² to 1500 kN/m² was required to obtain the maximum dry unit weight value for reduced modified Proctor test curves in all the seven soil samples.

Mitchell et al. (1965) developed a simple and reliable device to test how easily water could pass through compressed clay. The device allowed accurate measurement and control of water saturation using back pressure. With this device, researchers were able to study the permeability of compressed clay in much greater detail than before.

To specifically examine the impact of structure on permeability, they had prepared samples of silty clay by compacting and kneading them at various moisture levels but to a consistent density of 108 pounds per cubic foot, as depicted in the lower section of figure 2.8. The permeability values at saturation levels of 90% and 95% was determined and compared

It was observed that for specimens compacted below the optimal moisture content, the permeability slightly increased as the water content increased. However, there was a significant decrease in permeability around the optimal moisture content. Notably, the samples prepared with a higher moisture content than the optimum exhibited permeability nearly three orders of magnitude lower than those prepared with a lower moisture content.

Previous studies by Seed and Chan extensively examined the structure and strength characteristics of the silty clay used in these tests. They provided evidence that this soil is highly sensitive to its structure, meaning that compaction methods involving significant shear strains, such as kneading compaction, result in a dispersed structure when the soil is compacted with a moisture content higher than the optimum. The significant influence of this dispersion on permeability is clearly demonstrated by the data presented in figure 2.8.

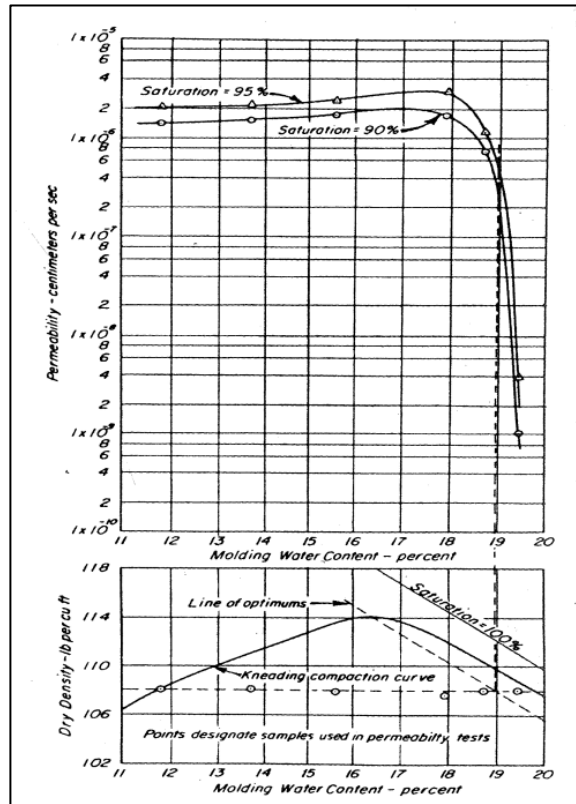


Figure 2.8: Permeability as a function of moulding water content for samples silty clay prepared to constant density by kneading compaction

Previous research by Lambe, Bjerrum, and Huder showed that adding more water to samples initially compacted below the optimal moisture content resulted in a steady decrease in permeability. However, in this study, it was observed that a slight increase in permeability when additional water was added to such samples.

The discrepancy may be due to the compaction process. As the molding water content increased for samples initially compacted below the optimal moisture content, the compaction effort needed to achieve a density of 108 pounds per cubic foot decreased. This reduced compaction effort caused less dispersion of the soil structure, leading to a slight increase in permeability instead of the expected decrease with higher water content.

The explanation does not fully explain the observed behavior, as seen in figure 2.9, where permeability varies with different water contents under the same compactive effort. Figure 2.9 shows that permeability initially reaches a minimum at 5.2% water content, then increases to a maximum at 12.5%, and finally decreases sharply at around 13% due to soil structure dispersion.

Tests on a different soil, a silty clay from the AASHO road test site, Ottawa III, revealed a smaller range of water contents below the optimum (figure 2.10) compared to figure 2.9. The behaviour of specimens prepared below the optimum may be influenced by the soil type, compactive effort, increased dispersion with higher water content, and possible non-uniform saturation. Additionally, significant hydraulic gradients (ranging from 50 to 120) may cause fine particle migration, creating seepage forces within the clay.

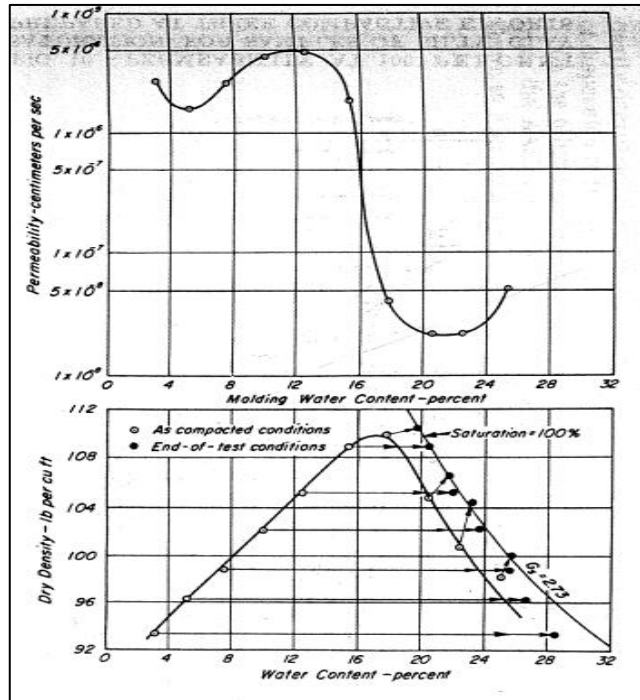


Figure 2.9: Permeability vs molding water content relationship for silty clay kneading compaction

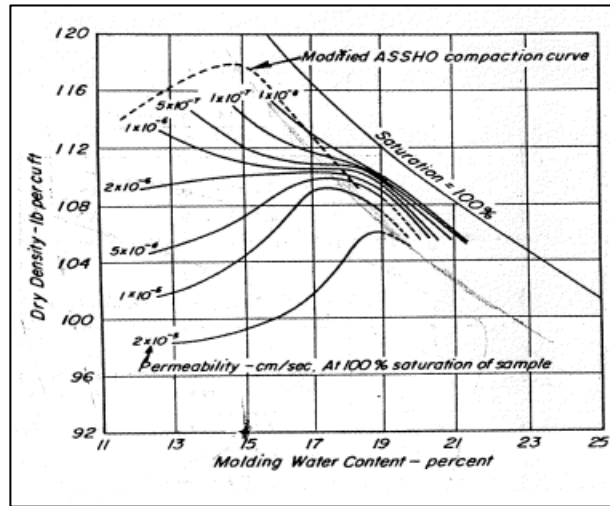


Figure 2.11: Contours of equal permeability for samples of silty clay prepared by kneading compaction

The compaction method significantly affected the permeability of the silty clay used in the study, especially when wet of optimum moisture content. Fig 2.12 showed varying shear strain and dispersion levels with different compaction procedures in the order- static, vibratory, and kneading.

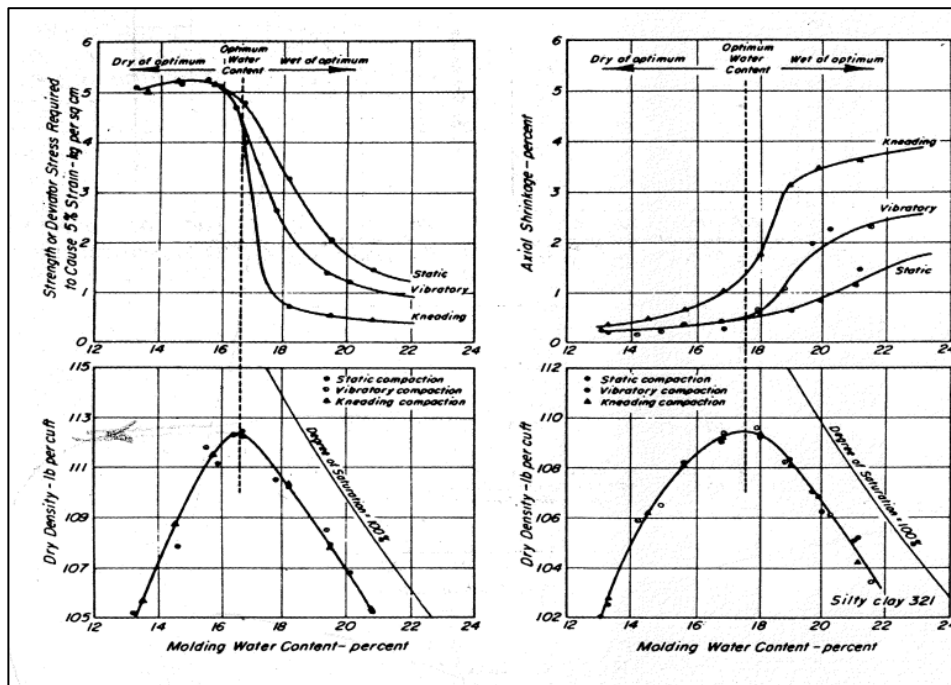


Figure 2.12: Influence of method of compaction of strength and shrinkage of silty clay

Furthermore, they anticipated lower permeabilities in kneading-compacted samples compared to statically compacted ones, particularly when molding water content exceeded optimal

levels. To validate this, silty clay samples were prepared using both static and kneading methods, ensuring uniformity through 2.8-inch diameter and 1-inch height molds. Additional tests were conducted on samples kneading-compacted in 3.5-inch-high molds. Results in Fig 2.13 confirmed the prediction: statically compacted samples were notably more permeable than kneading-compacted ones, especially for moisture contents surpassing the optimum. However, the differences were less pronounced than initially expected.

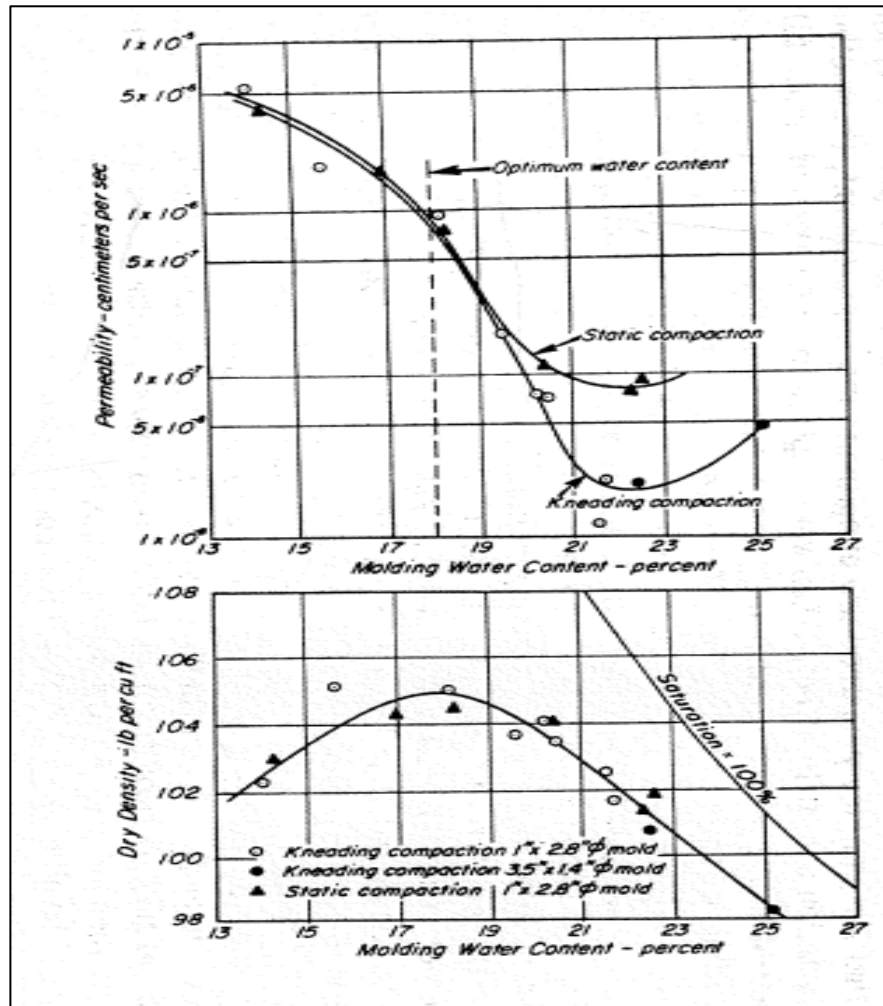


Figure 2.13: Influence of method of compaction on the permeability

Notably, the research explored the permeability behavior of various structural clays, attributing the significant drop in permeability beyond optimal water content in statically compacted samples to Olsen's cluster concept of soil structure. The clusters, formed even during controlled mixing before compaction, resisted deformation, with this resistance expected to decline as water content increased. Olsen highlighted that permeability in a cluster structure relied on flow through intercluster pores more than within the clusters themselves.

As water content increased, clusters weakened, potentially becoming smaller due to pre-compaction mixing, distorting more with higher water content and reducing intercluster pore size. Despite this, the structure retained its flocculent nature after static compaction beyond the optimal water content, but the heightened water content distorted clusters, significantly reducing average pore size.

Based on the literature review, it has been discovered that a comparison can be drawn between the static compaction method and the standard Proctor compaction method. According to Dario et al. (2011), a comparison of the compaction characteristics for both methods can be made at the optimum moisture content, dry of optimum, and wet of optimum, among other factors. The purpose of our study is to investigate the consolidation and compressibility properties of soil that has been statically and dynamically compacted at the same dry unit weight and at both the dry of optimum, optimum moisture content and wet of optimum moisture contents. This research is an attempt to address the same issue.

CHAPTER 3

EXPERIMENTAL PROCEDURE AND RESULTS

3.1 INTRODUCTION:

This chapter reports about the different tests performed in the laboratory and the results of these tests have been presented in the form of tables and graphs.

3.2 Test Program:

The main objectives of the test program are:

1. To determine the maximum dry density and optimum moisture content of different types of soil in the laboratory by static compaction and standard Proctor compaction methods, to make a comparison of the compaction properties by both the methods
2. To determine various consolidation soil properties like void ratio vs consolidation pressure, coefficient of compressibility (a_v), coefficient of volume compressibility (m_v), coefficient of compression or compression or compression index (C_c) and coefficient of consolidation (C_v) for five different soil samples where the consolidation samples are prepared from the static compaction and standard Proctor compaction method maintaining the same moisture content at dry of optimum, optimum moisture content and wet of optimum and at same maximum dry unit weight respectively for a particular type of soil and same procedure is followed for the different types of soil samples with the help of consolidation test.

Thus, after careful planning the entire test program is divided into five phases as follows:

1. Collection of the soil samples.
2. Preparation of the disturbed samples for testing.
3. Determination of the physical properties of the soils.
4. Determination of the compaction properties of soils by static and standard Proctor compaction test.
5. Determination of the consolidation properties of soils by consolidation test.

3.2.1. Collection of the soil samples:

Soil samples were gathered from five distinct locations in and around Guwahati. A region measuring approximately 4ft. x 4ft. was chosen at each site, and the upper 1ft. to 2ft. layer of soil was excavated using hoes and spades. This layer may have contained organic materials such as grass, leaves, and vegetable roots. After removing this layer, the ground surface was levelled, and approximately 100 kg of soil was collected from each site.

3.2.2 Preparation of the disturbed samples for testing:

Soil samples obtained from the field need to be prepared by standard method before testing so that reproducible results can be obtained. The usual procedure consists of drying of the soil sample followed by pulverization and removal of stones before testing. Subsequently, the soil samples were air dried at room temperature. This process was adhered to for both dynamic and static compaction of the soil.

3.2.3 Determination of the physical properties of the soils:

1. Determination of liquid limit was performed by cone penetration method according to IS 2720 (Part 5) 1985.
2. Determination of plastic limit was carried out in the laboratory according to IS 2720 (Part 5) 1985.
3. Determination of specific gravity was performed according to IS 2720 (Part 3) 1980.
4. Determination of gradation of the soil samples by wet sieve analysis was performed according to IS 2720 (Part 4) 1985.

3.2.4. Determination of the compaction properties of soils:

In laboratory, compaction properties of soil are mainly determined by dynamic compaction method and static compaction method. Both the methods have been discussed below:

3.2.4.1. Dynamic compaction method:

The soil sample, which was air-dried, was sieved using a 4.75mm IS Sieve. A 2.5 kg soil sample was taken and its initial moisture content was determined immediately using the Infra-red-torsion balance meter method before adding water. Once the existing moisture content was determined, the necessary amount of water was added to achieve the desired water content for the specific soil sample. The soil sample was then placed in an airtight container, inside a polythene bag, for at least 24 hours for maturation. The same process was repeated for the other four samples with different water contents of the same soil. After the maturation process, the standard Proctor's compaction test was conducted in the laboratory to determine the optimum moisture content corresponding to the maximum dry unit weight in accordance with IS: 2720 (Part 7) 1980.

3.2.4.2. Static compaction method:

In order to determine the compaction properties via static compaction, a laboratory method was developed which is similar to the method used by Sharma et al. (2016) in their research as discussed in Chapter 2. Sharma et al. found that the maximum dry unit weight achieved via static compaction was almost the same for three different layers in a standard Proctor mould. Thus, in this present study, the static compaction test was performed on a single soil layer with a height of 106 mm for all soil samples of varying types and water contents. The remaining thickness of the Proctor mould was filled with two metal plates, one with a diameter of 98 mm and a thickness of 5 mm, and the other with a thickness of 16 mm. The 5 mm plate was placed over the soil sample in the Proctor mould, and the 16 mm plate was placed over it so that the upper surface of the 16 mm plate coincided with the upper edge of the Proctor mould. The experimental setup for the static compaction test is illustrated in Figure 3.1.



Figure 3.1 Static Compaction Test Set up

In this method, the soil sample preparation process is exactly same as that of standard Proctor test. Only difference is that 1.0 kg of air-dried sample was taken instead of 2.5 kg as used in standard Proctor test.

3.3.4.2.1. Static Compaction Test Procedure:

A soil sample weighing approximately 1.0 kg, which had been kept in an airtight container for 24 hours for maturation, was taken. A small amount of the sample was kept in an oven for determining its water content in accordance with IS: 2720 (part 2)-1973. The remaining soil sample was placed in the Proctor mould until it reached a height of 106 mm from the bottom. Subsequently, 5 mm and 16 mm metal plates were placed over the sample. The entire assembly was placed under a cylindrical plunger with a diameter of 50 mm in a loading frame, and the gear lever of the machine was set at a penetration rate of 1.25 mm per minute.

Before switching on of the machine it should be checked that the upper surface of the plate matches the top edge of the Proctor mould. Then the experiment was started and the height of penetration of the metal plate from the top surface of the mould was measured corresponding to different load levels. The different loads applied to the soil sample are obtained from dial gauge readings attached to the proving ring with a constant of 0.05 kN/div.

For different applied loads, the amount by which the soil was compacted can be calculated by measuring the height of the soil inside the mould which got reduced as the load went increasing. The load was applied till the penetration ceased or the measured height of the soil inside the mould became constant with further increase in load. After measuring the heights corresponding to a number of load levels the compacted soil inside the mould was completely removed. Again, the mould was filled with soil of different moisture content and the entire aforementioned process was repeated.

The height of the soil specimen can be calculated by subtracting the measured height and thickness of the two metal plates from the total height of the Proctor mould (i.e., 127 mm). The static pressure was calculated by dividing the different applied load values by the area to which it was applied. With the measured height of the soil inside the mould for different load values, the corresponding bulk density of the soil was determined. Knowing the moisture content and bulk density of a soil, the dry unit weight of the soil for a particular static pressure was determined. By this procedure, corresponding to a number of static pressures the dry unit weight of the soil was determined. In this manner all the soil sample were tested.

3.2.5. Determination of the consolidation properties of soils by consolidation test:

Consolidation test was performed to determine the consolidation properties of statically and dynamically compacted soil at the same dry unit weight and same moisture content at dry of optimum, OMC and wet of optimum respectively. The consolidation test process was carried out according to the guidelines outlined in IS 2720 (Part 15)-1986. Both the processes have been discussed below:

3.2.5.1 Consolidation test on dynamically compacted soil:

The experimentation encompassed three moisture conditions: the dry side of optimum, the optimum moisture content (OMC), and the wet side of optimum. To prepare the soil samples for this procedure, the air-dried soil was mixed with water content that was 3% lower than the OMC for the dry side of optimum. For the OMC condition, the air-dried sample was mixed with water content corresponding to the OMC. Lastly, for the wet side of optimum, the air-dried soil was mixed with water content 3% higher than the OMC, a value obtained from section 3.2.4.1 (dynamic compaction method) for the specific soil type. The following day, a standard Proctor test was conducted on the soil sample following the IS: 2720 (Part 7) 1980

standard. Figure 3.2 showcases a soil sample dynamically compacted at the OMC for a particular soil type.



Figure 3.2: Dynamically Compacted Soil at Dry of Optimum

In this compacted soil specimen consolidation ring was inserted by hammering smoothly or by pressing statically in the UCS machine keeping in mind that the soil surfaces inside the consolidation ring is not touched and affected by the loading action. A picture of the insertion of consolidation ring into the compacted soil mass is shown below:



Figure 3.3: Insertion of consolidation ring in compacted soil mass

The soil sample recovered with the consolidation ring is shown in the figure below:



Figure 3.4: Recovered soil sample from the Proctor mould

If we find some cavities while extruding the soil sample from the compacted soil mass that means the thickness of the consolidation sample is less than that of 20 mm then we have to discard the soil sample and we repeat the process again. After that trimming and smoothening was done of the surfaces of soil samples inside the consolidation ring with the help of very thin knife. The consolidation sample thus prepared is shown in the figure below



Figure 3.5: Upper surface of consolidation sample



Figure 3.6: Lower surface of consolidation sample

Now the consolidation sample is placed inside the consolidation cell which is then placed in the loading frame and the test was started according to IS: 2720 (Part 15) – 1986. The same process is followed for the other soil samples. Complete consolidation set up is shown below:



Figure 3.7: Consolidation cell under the loading frame



Figure 3.8: The whole consolidation setup

3.2.5.2. Consolidation test on statically compacted soil:

The procedure was conducted across three moisture conditions: dry of optimum, optimum moisture content (OMC), and wet of optimum. In this method, the air-dried soil sample was combined with water content that was 3% below the optimum moisture content for the dry side of optimum. For the OMC condition, the air-dried sample was mixed with water content corresponding to the OMC. Similarly, for the wet side of optimum, the air-dried soil was blended with water content 3% higher than the OMC, a value derived from section 3.2.4.1 (dynamic compaction method) specific to the soil type. Following this, the soil sample was allowed to settle for a day and compacted statically to a level where its maximum dry unit weight matched the value acquired in section 3.2.4.1. The subsequent stages of the test followed the identical procedures outlined in section 3.2.5.1.

3.3. Test results:

The experimental results obtained from the various tests performed are shown below in the form of tables and graphs.

3.3.1. Test results of the physical properties:

Table 3.1 gives the test results of the physical properties for the five soil samples.

Table 3.1. Physical properties of soil

| Sample No. | Site Location | Depth from G.L. (m) | Colour | Odour | Specific Gravity (G _s) | Liquid Limit W _L (%) | Plastic Limit W _P (%) | Plasticity Index PI (%) | Soil Type |
|------------|---------------|---------------------|-------------|-------|------------------------------------|---------------------------------|----------------------------------|-------------------------|-----------|
| 1 | Panikhaity | 0.5 | Grey | NIL | 2.67 | 37.56 | 22.96 | 14.60 | CI |
| 2 | Beharbari | 1 | Light Brown | NIL | 2.71 | 58.44 | 23.17 | 35.27 | CH |
| 3 | Maligaon | 1.5 | Red | NIL | 2.68 | 68.7 | 31.03 | 37.67 | CH |
| 4 | Dipor Bil | 0.3 | Pale yellow | NIL | 2.65 | 39.3 | 22.82 | 16.48 | CI |
| 5 | Boko | 0.6 | Light Grey | NIL | 2.72 | 36.42 | 20.01 | 16.41 | CI |

Table 3.2 gives the results of the particle size distribution of all the soil samples.

Table 3.2. Particle Size distribution results of the soil samples.

| Sample No. | % of sand | % of fines (silt+clay) |
|------------|-----------|------------------------|
| 1 | 2.99 | 97.01 |
| 2 | 28.15 | 71.85 |
| 3 | 9.83 | 90.17 |
| 4 | 8.26 | 91.74 |
| 5 | 27.87 | 72.13 |

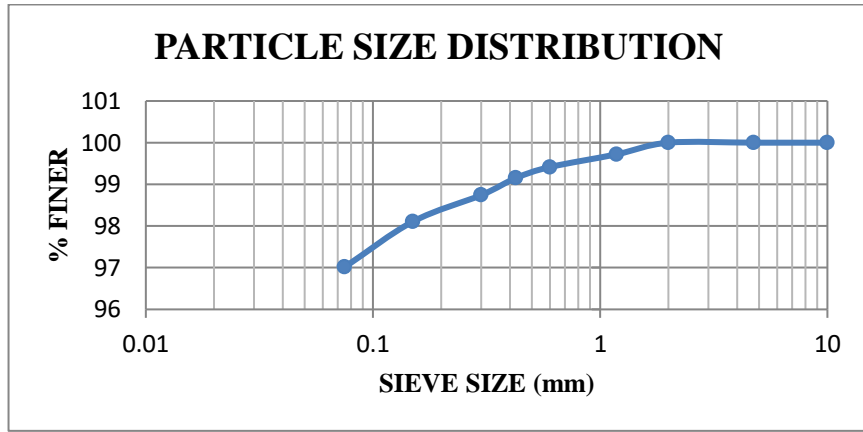


Figure 3.9 Gradation curve for sample 1

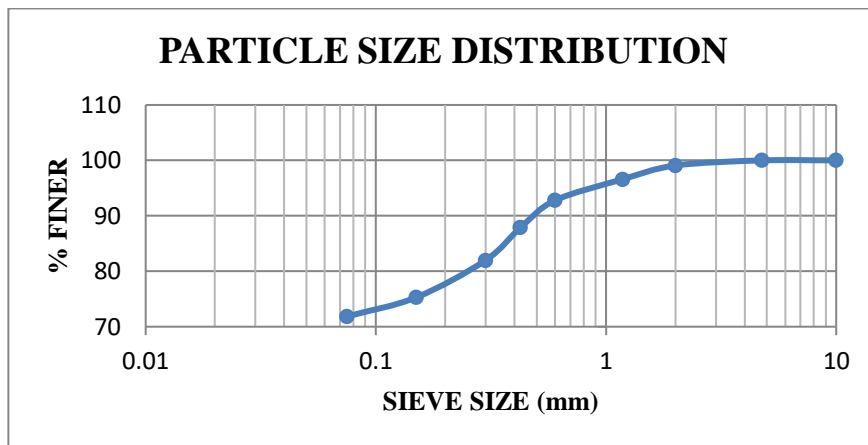


Figure 3.10: Gradation curve for sample 2

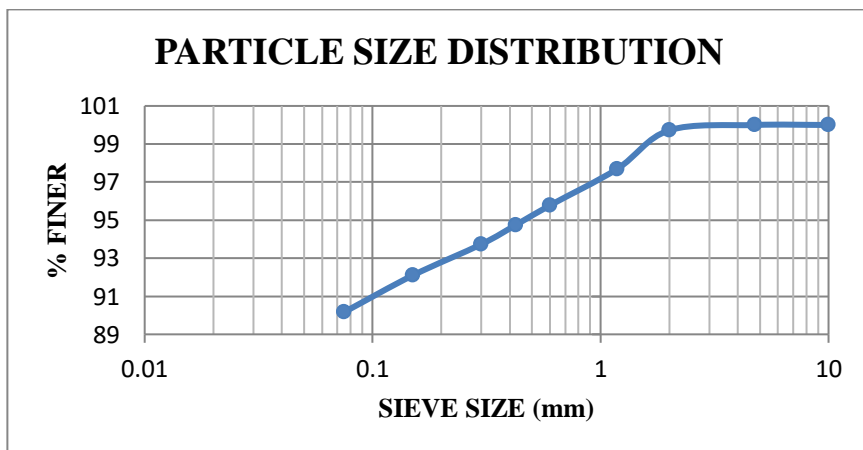


Figure 3.11 Gradation curve for sample 3

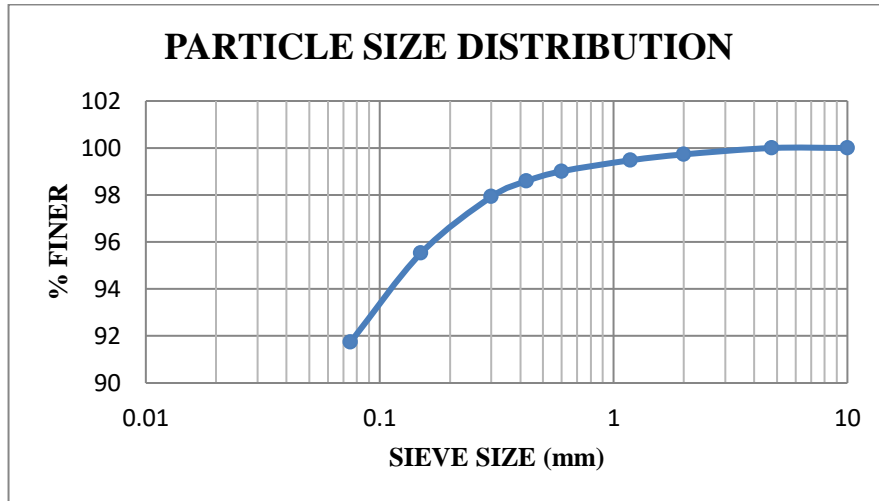


Figure 3.12 Gradation curve for sample 4

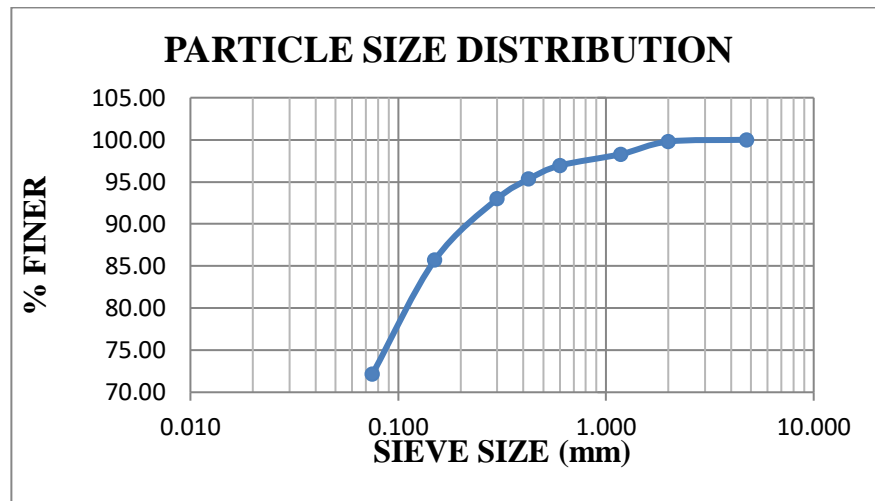


Figure 3.13 Gradation curve for sample 5

3.3.2. Test results of the compaction properties of the soil:

The soil samples were tested using the standard Proctor compaction test, and the results of the five different soil samples are presented in Table 3.2.

Table 3.3. Optimum moisture content and maximum dry unit weight by Standard Proctor compaction test

| Sample No. | Site Location | Maximum Dry Unit Weight (MDUW) (kN/m ³) | Optimum Moisture Content (OMC) (%) |
|------------|---------------|---|------------------------------------|
| 1 | Panikhaity | 16.500 | 18 |
| 2 | Beharbari | 14.900 | 23 |
| 3 | Maligaon | 14.790 | 24 |
| 4 | Dipor Bil | 16.766 | 18 |
| 5 | Boko | 16.850 | 17 |

The compaction curves are shown from Figure 3.13 to Figure 3.17.

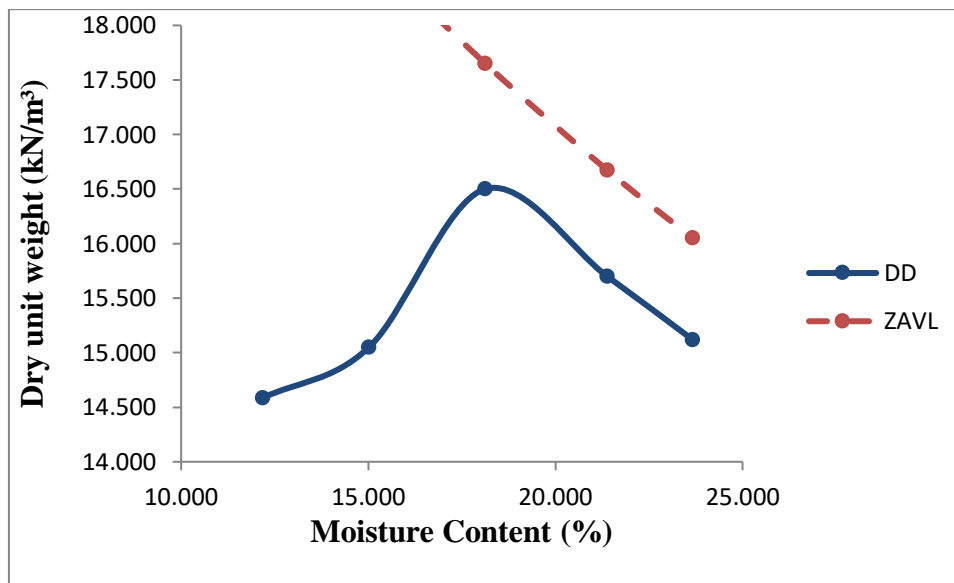


Figure 3.14: Standard Proctor Curve for sample 1

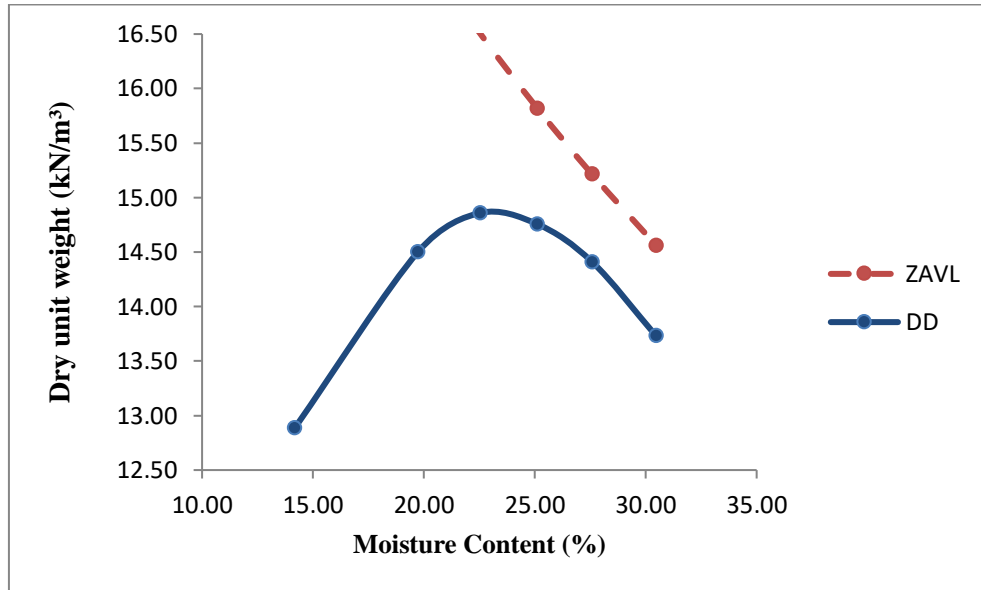


Figure 3.15: Standard Proctor curve for sample 2

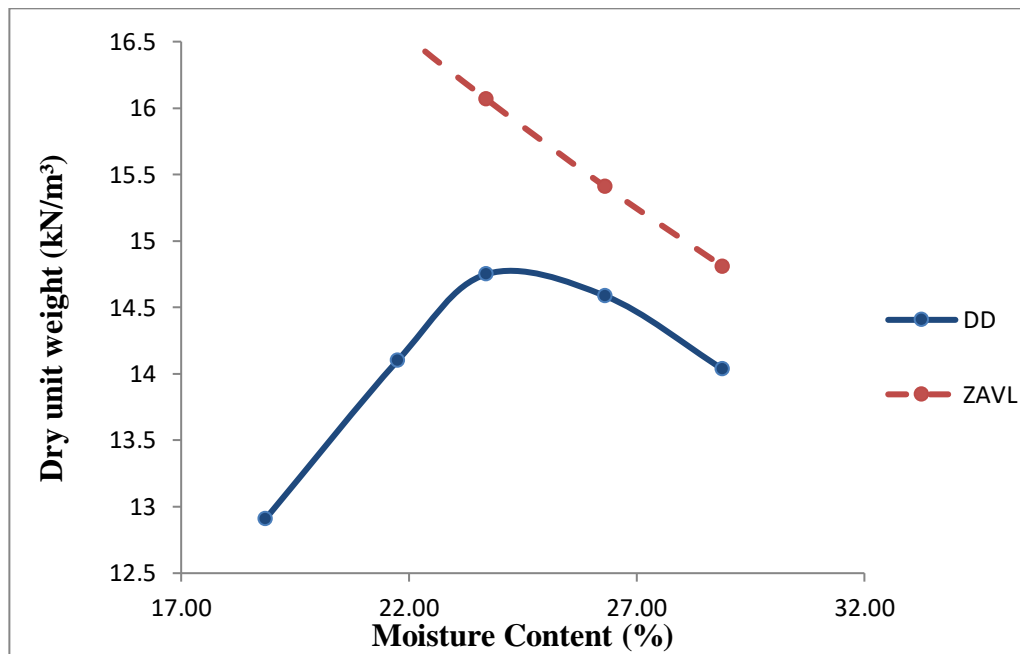


Figure 3.16: Standard Proctor Curve for sample 3

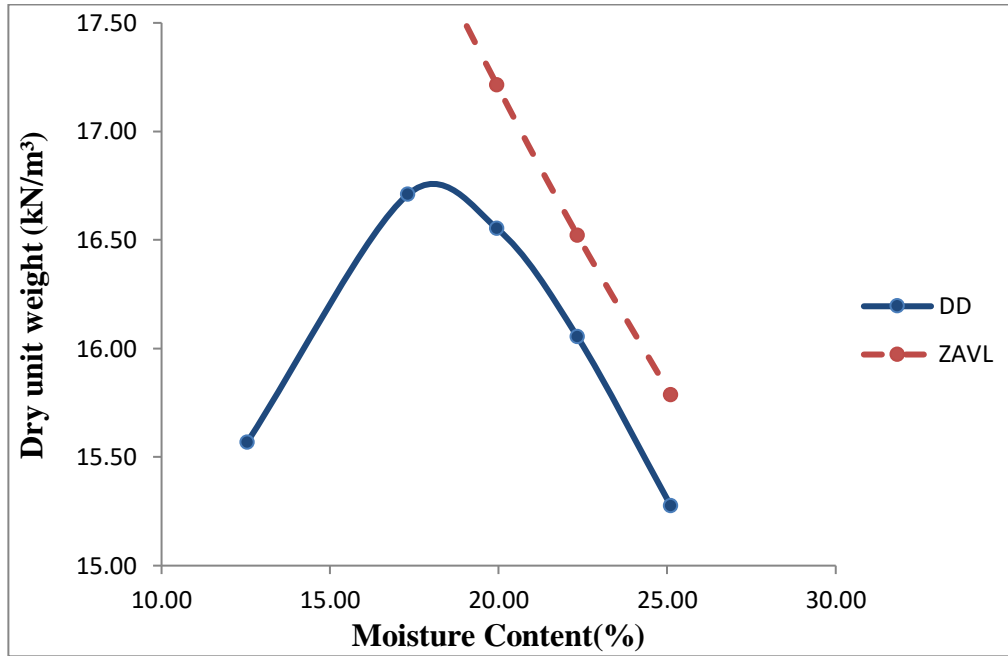


Figure 3.17: Standard Proctor curve for sample 4

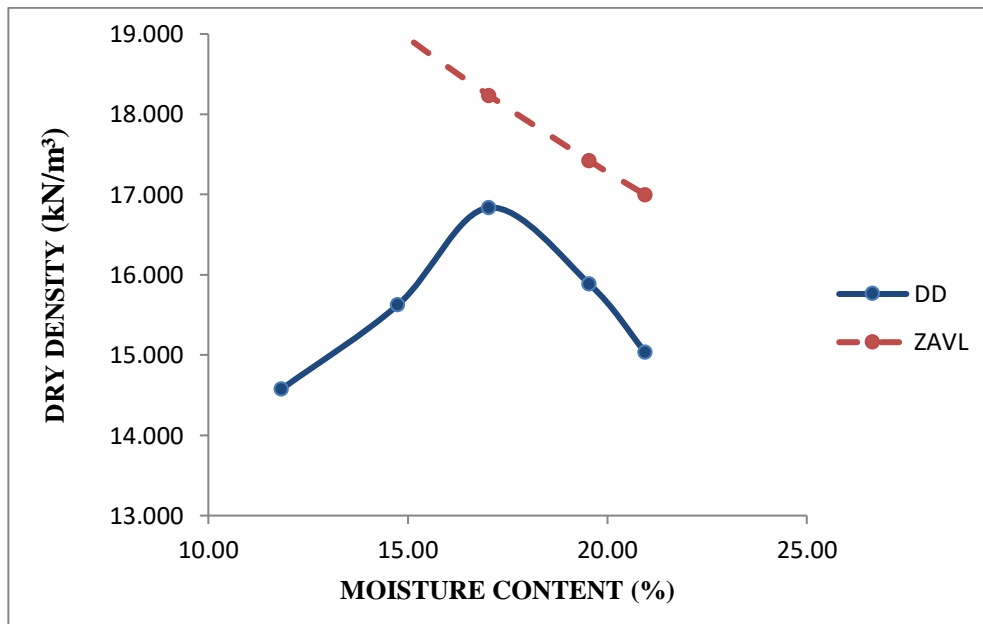


Figure 3.18: Standard Proctor curve for sample 5

The Proctor mould was utilized to conduct the Static compaction test until the height measured from the top surface of the Proctor mould became constant in spite of an increase in static pressure at a specific water content of a particular soil type. Experimental findings from the Static compaction test on soil samples gathered from five distinct sites are presented in graphs. The graphs display the correlation between dry unit weight and static pressure for all the soil samples tested with varying moisture contents. These graphs are shown in figures 3.19 to 3.28, while additional curves for the remaining soil samples are shown in Appendix I.

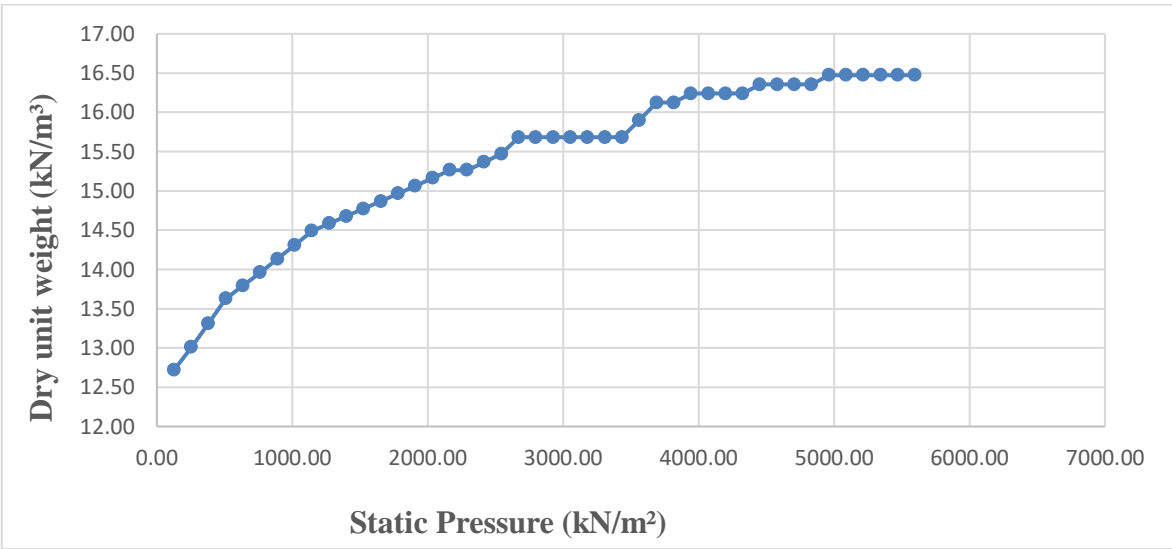


Figure 3.19: Dry unit weight vs Static Pressure curve of sample 1 at 9.03% water content

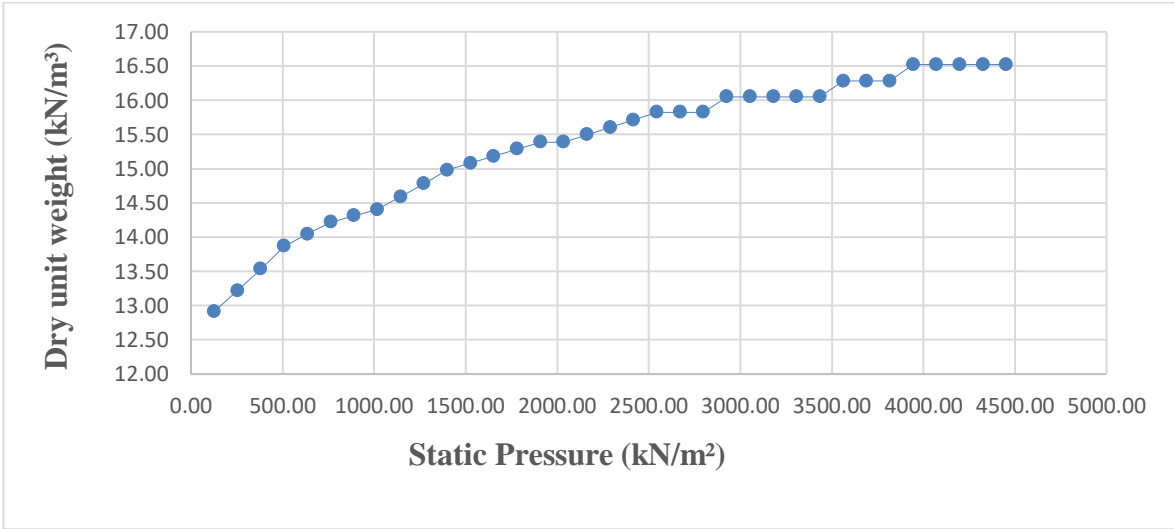


Figure 3.20: Dry unit weight vs Static Pressure curve for sample 1 at 11.10% water content

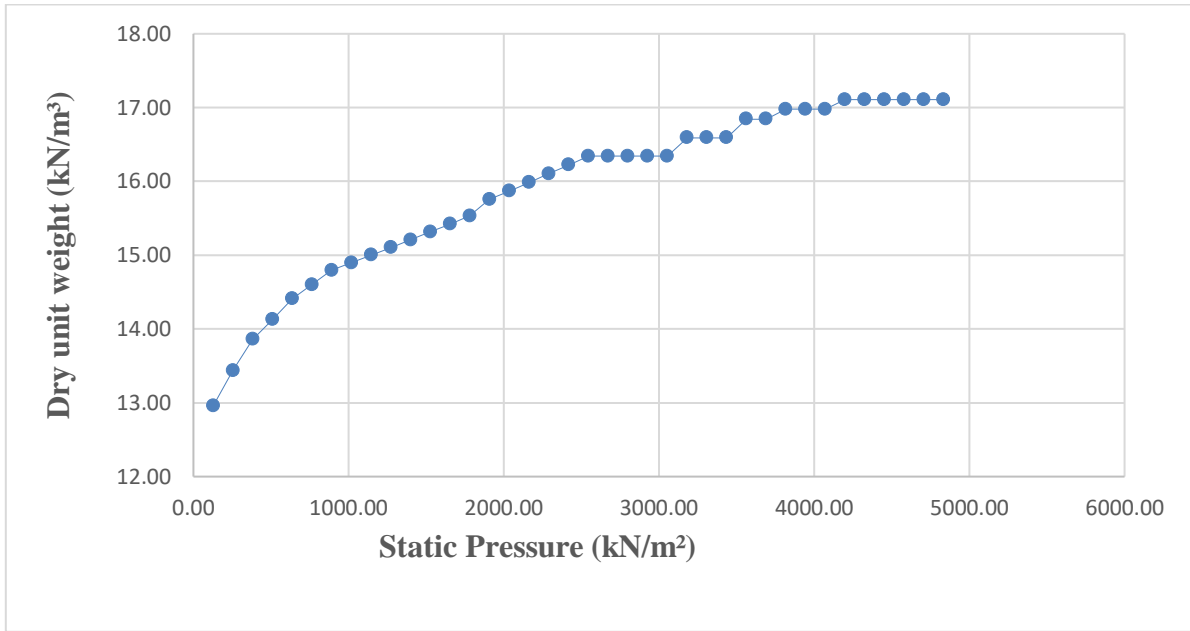


Figure 3.21: Dry unit weight vs Static Pressure curve for sample 1 at 14% water content

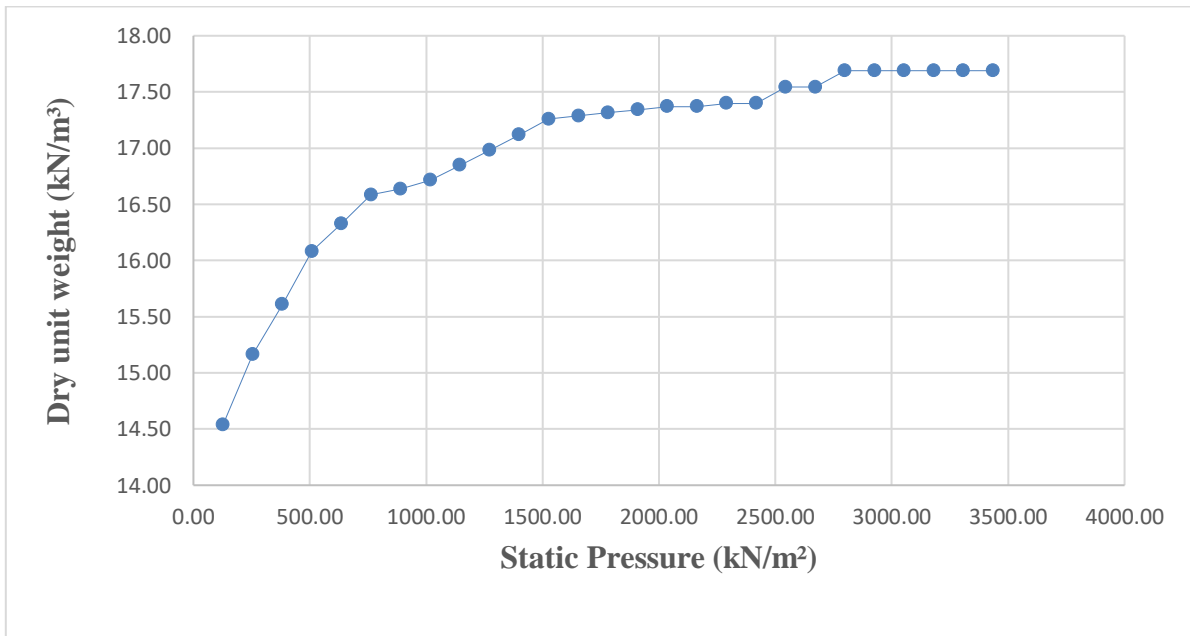


Figure 3.22: Dry unit weight vs Static Pressure curve for sample 1 at 17.60% water content

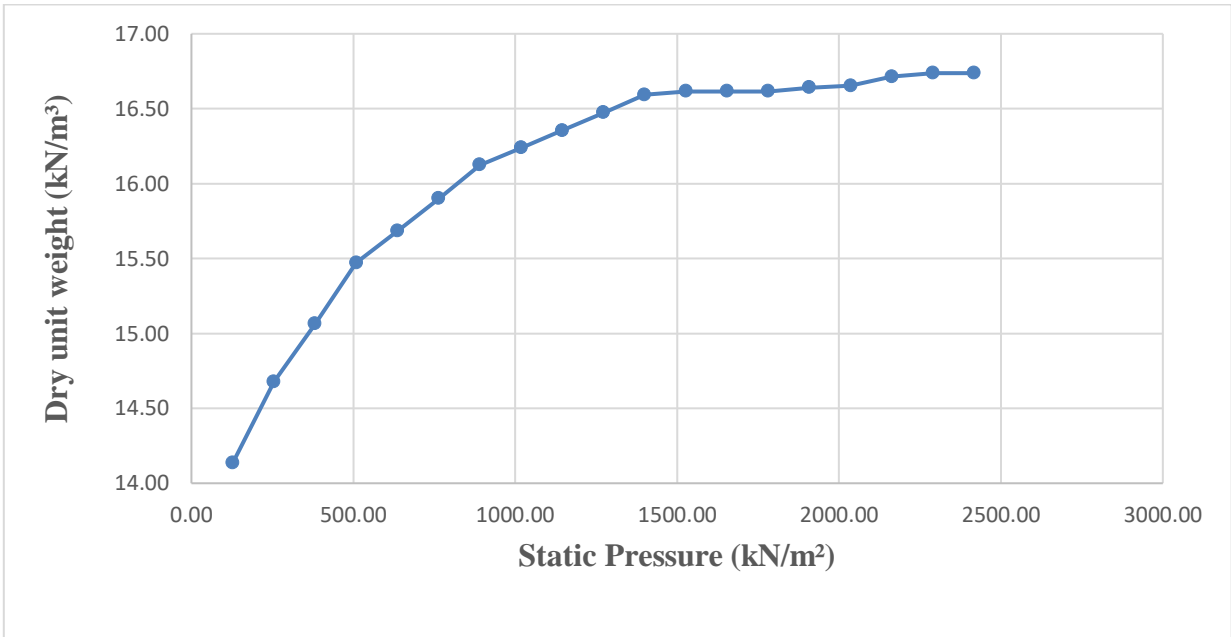


Figure 3.23: Dry unit weight vs Static Pressure curve for sample 1 at 20.61% water content

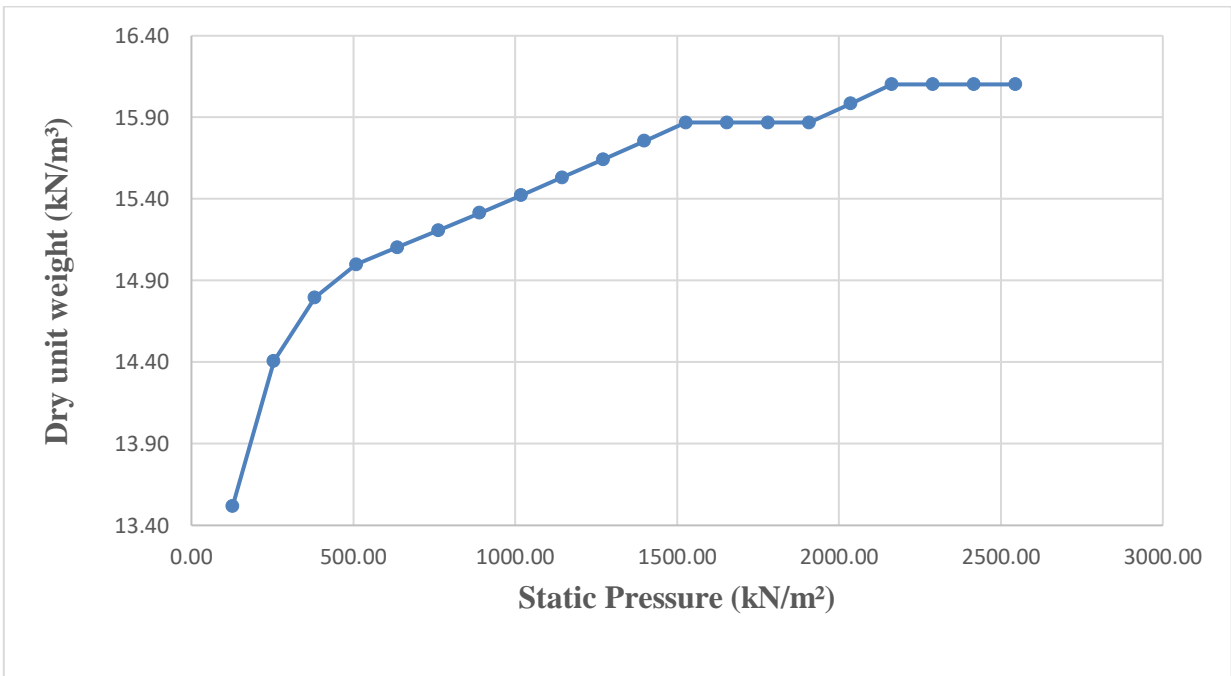


Figure 3.24: Dry unit weight vs Static Pressure curve for sample 1 at 22.49% water content

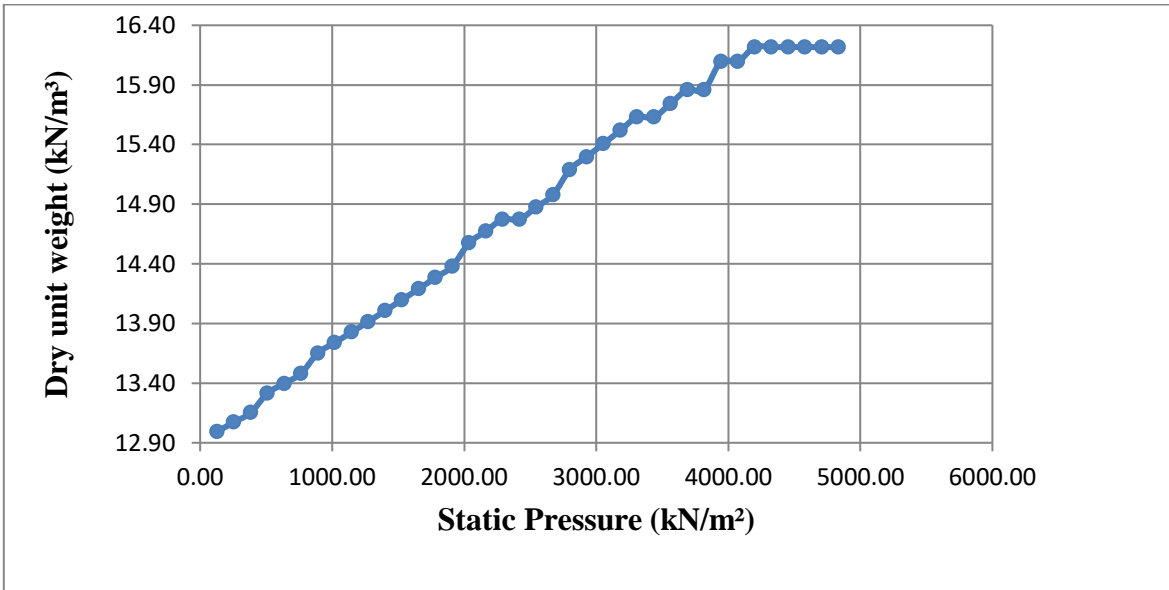


Figure 3.25: Dry unit weight vs Static Pressure curve for sample 2 at 15.74% water content

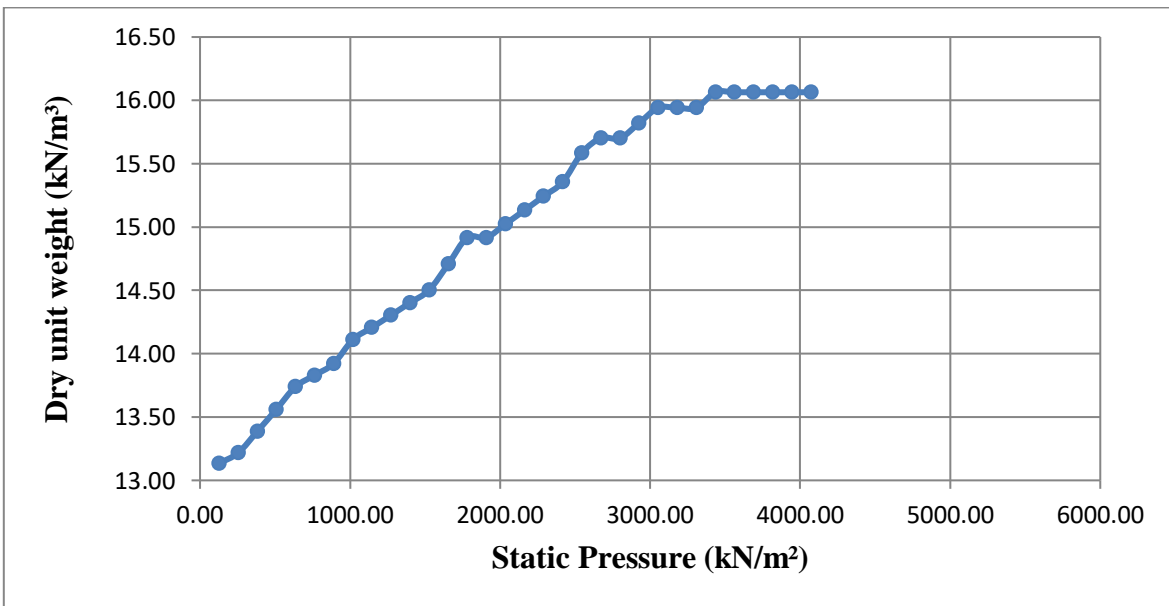


Figure 3.26: Dry unit weight vs Static Pressure curve for sample 2 at 19.54% water content

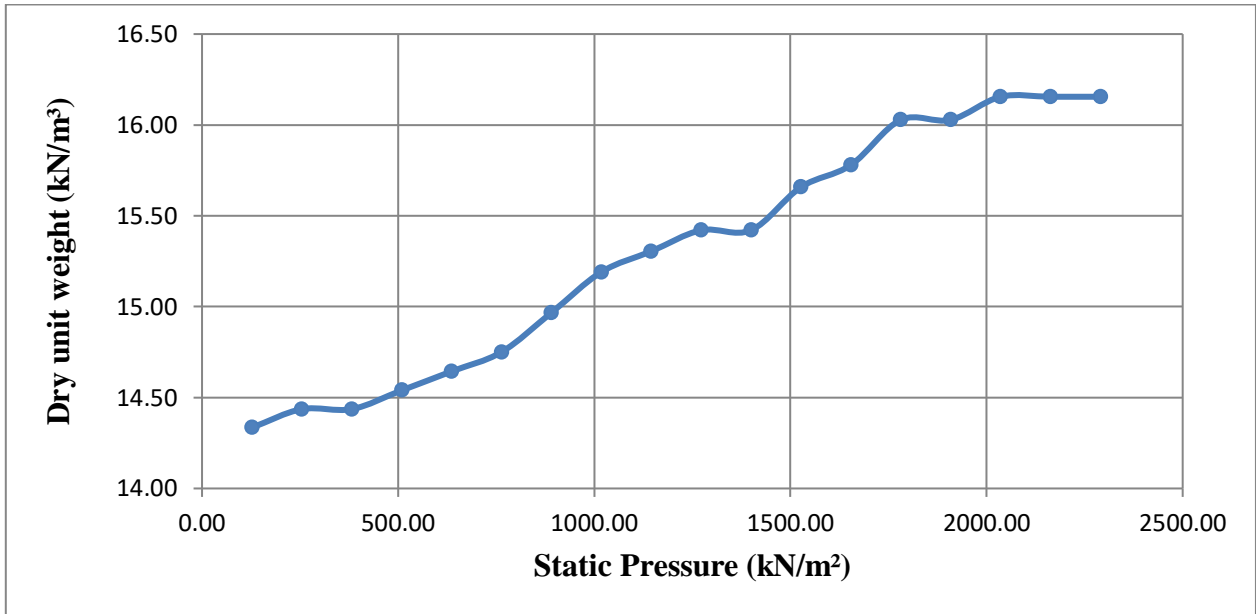


Figure 3.27: Dry unit weight vs Static Pressure curve for sample 2 at 22.64% water content

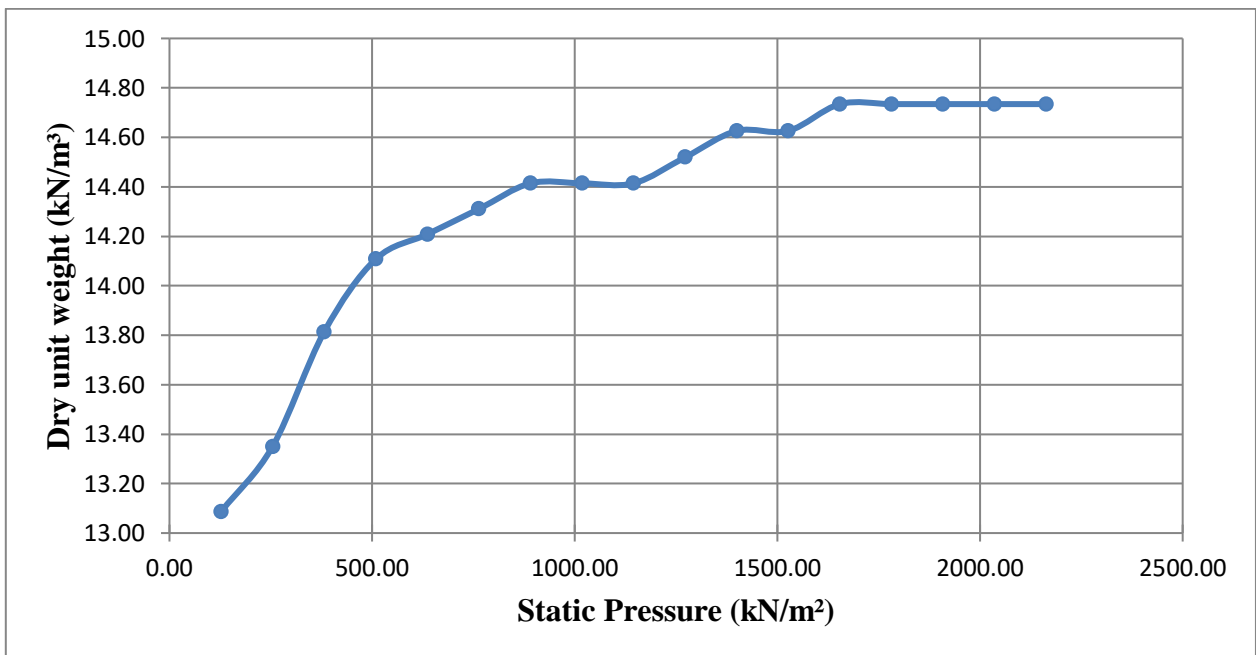


Figure 3.28: Dry unit weight vs Static Pressure curve for sample 2 at 25.50% water content

When the results of the static compaction test are plotted as curves between dry unit weight and static pressure, it was evident that all five soil samples display a similar non-linear pattern. It was noticed that there was a significant fluctuation in dry unit weight at lower static pressure, which becomes insignificant as the static pressure increases. Eventually, the dry unit weight reaches a constant value after a specific static pressure. As a result, it can be inferred

that in a static compaction test, there is a non-linear rise in dry unit weight as static pressure increases for all soil samples, irrespective of their moisture contents.

The static compaction test results have provided the relationship between dry unit weight and static pressure for various moisture contents of a soil sample. To determine the relationship between moisture content and dry unit weight for all soil samples at different static pressures, curves have been constructed. These curves are obtained by superimposing the moisture content vs. dry unit weight curves for both static and dynamic compaction tests for each soil sample. Figures 3.43 to 3.47 illustrate these curves. It can be observed that both static and dynamic compaction curves exhibit a parabolic nature.

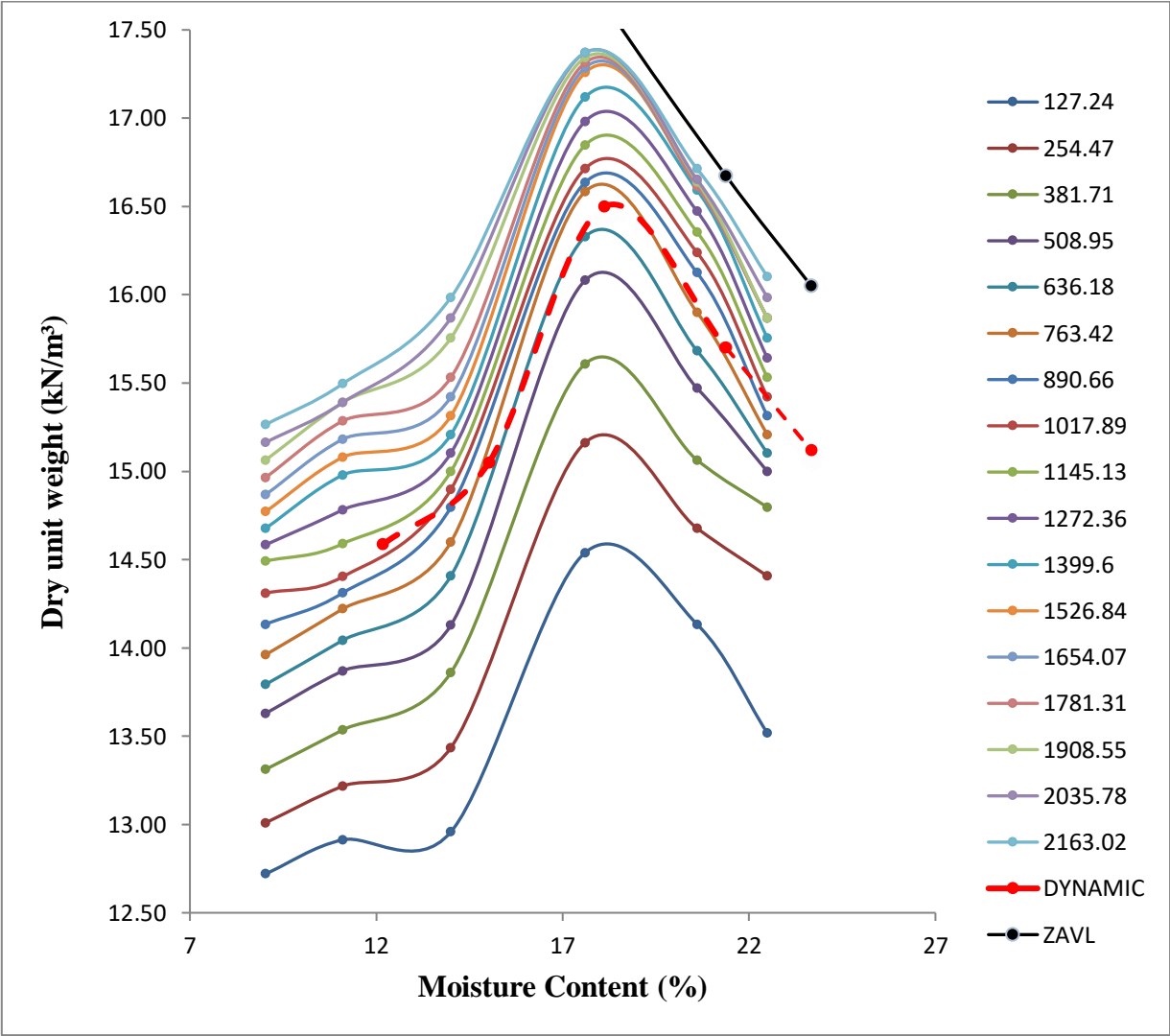


Figure 3.43: Static and dynamic compaction curve for sample 1

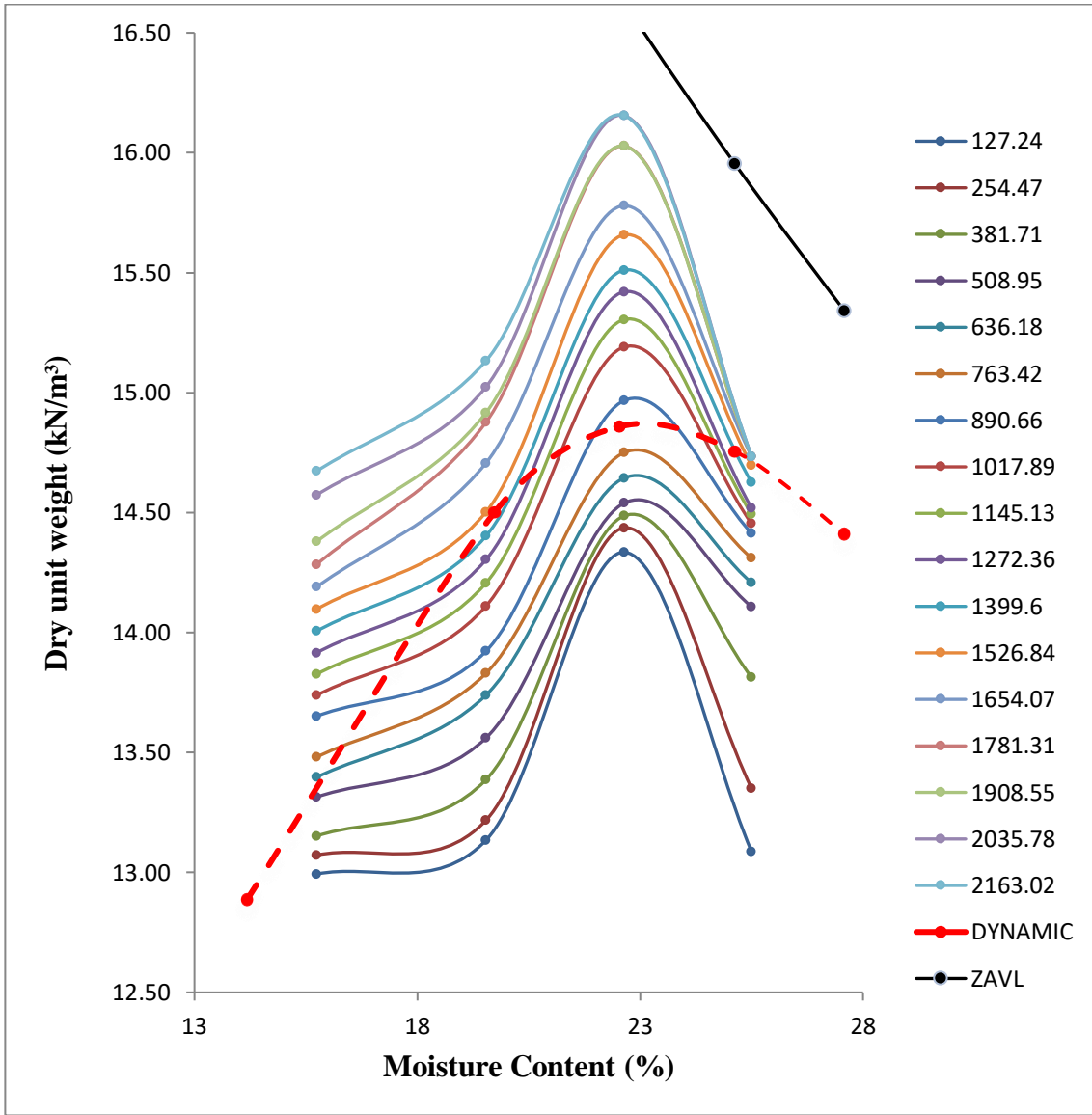


Figure 3.44: Static and dynamic compaction curve for sample 2

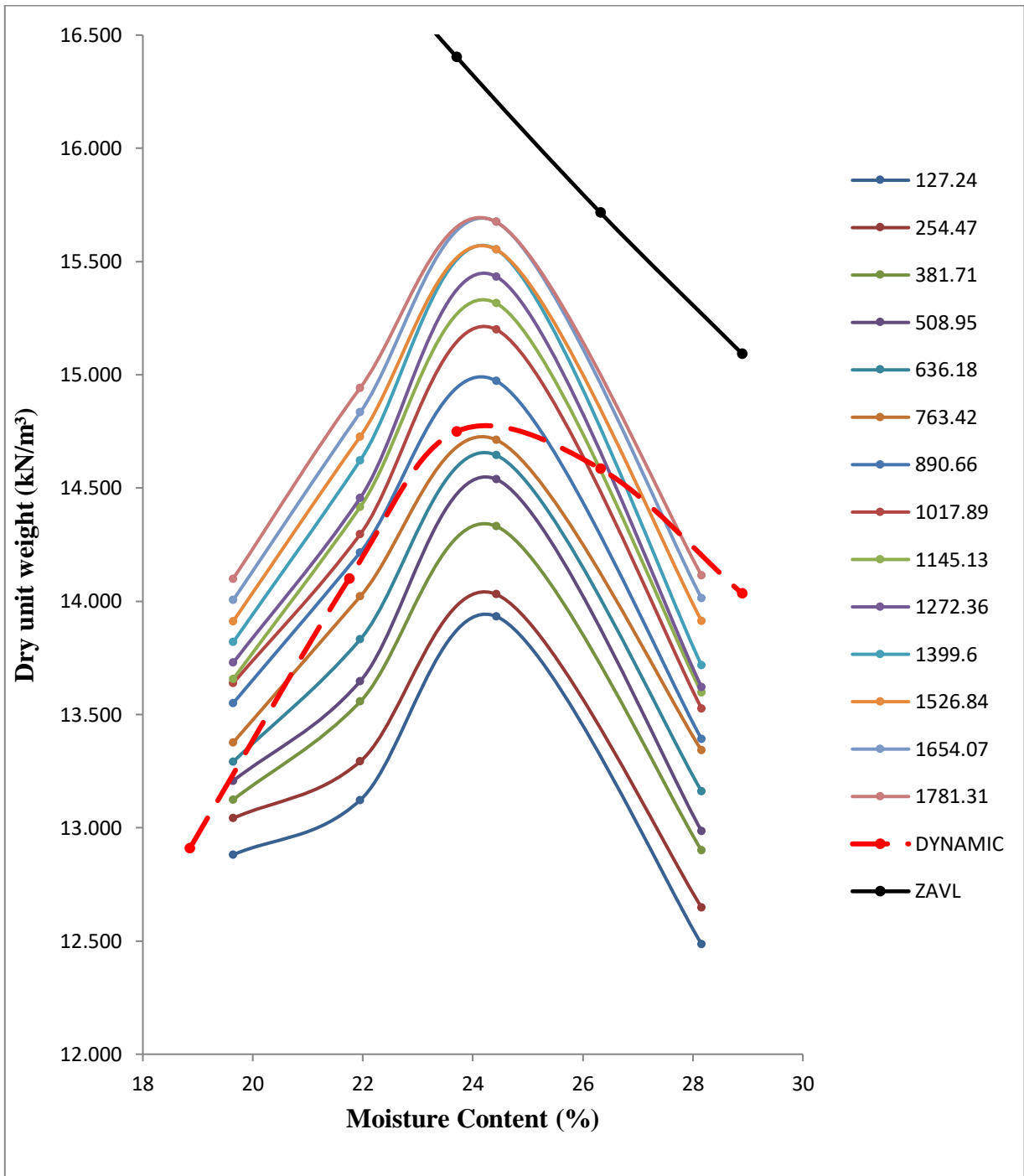


Figure 3.45: Static and dynamic compaction curve for sample 3

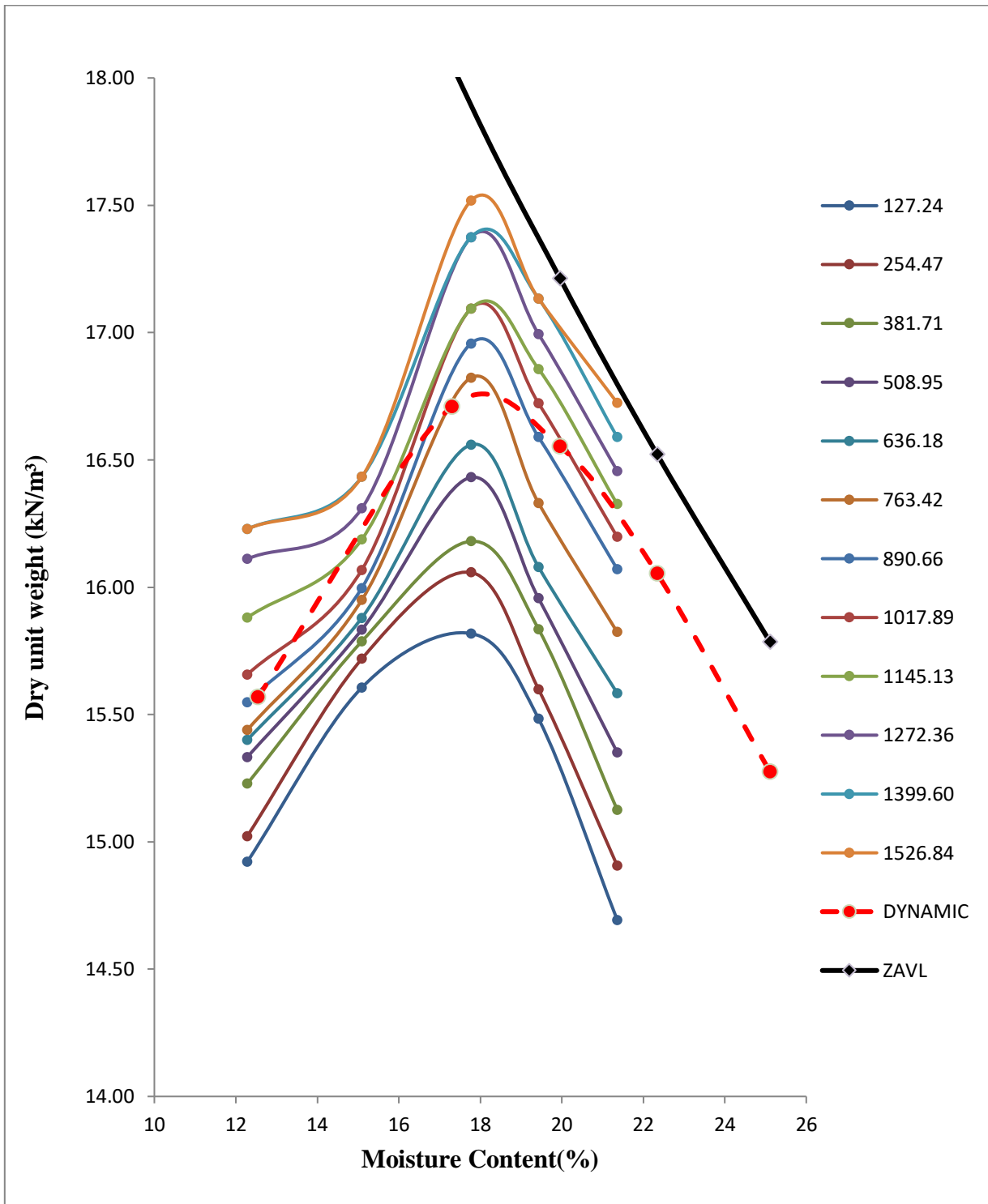


Figure 3.46: Static and dynamic compaction curve for sample 4

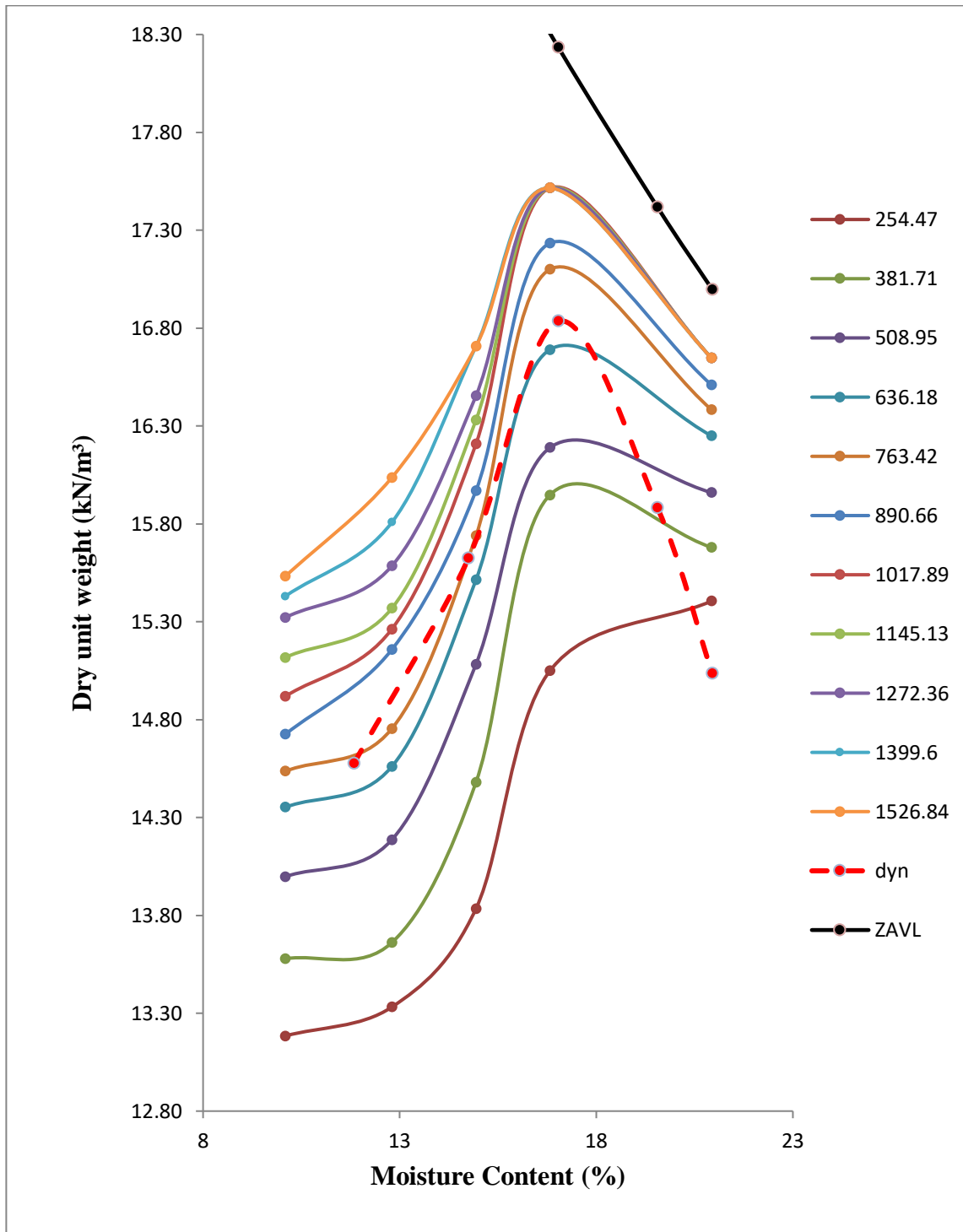


Figure 3.47: Static and dynamic compaction curve for sample 5

The curves revealed that as the static pressure increases, the maximum dry unit weight also increases, but the optimum moisture content remains unchanged. A variation in dry unit weight is observed at lower static pressures, but as the static pressure increases, the variation

in dry unit weight becomes negligible. The difference in optimum moisture content between the static compaction curve and dynamic compaction curve for a specific soil sample is negligible. For all types of soil samples examined in this study, a higher dry unit weight can be achieved at the same optimum moisture content with a higher value of static energy than with dynamic energy.

3.3.3. Determination of equivalent static pressure:

To determine the equivalent static pressure for the maximum dry unit weight at the optimum moisture content (OMC) obtained from the Standard Proctor test, a graph is plotted between the static pressure and dry unit weight. In this process, two static pressures are selected, which correspond to the maximum dry unit weights obtained from the static compaction method at OMC that lie just above and below the maximum dry unit weight achieved from the Standard Proctor test at the OMC. The values of the maximum dry unit weights corresponding to the two selected static pressures are then plotted in the form of curves. This process is repeated for all five of the soil samples to determine their respective equivalent static pressures.

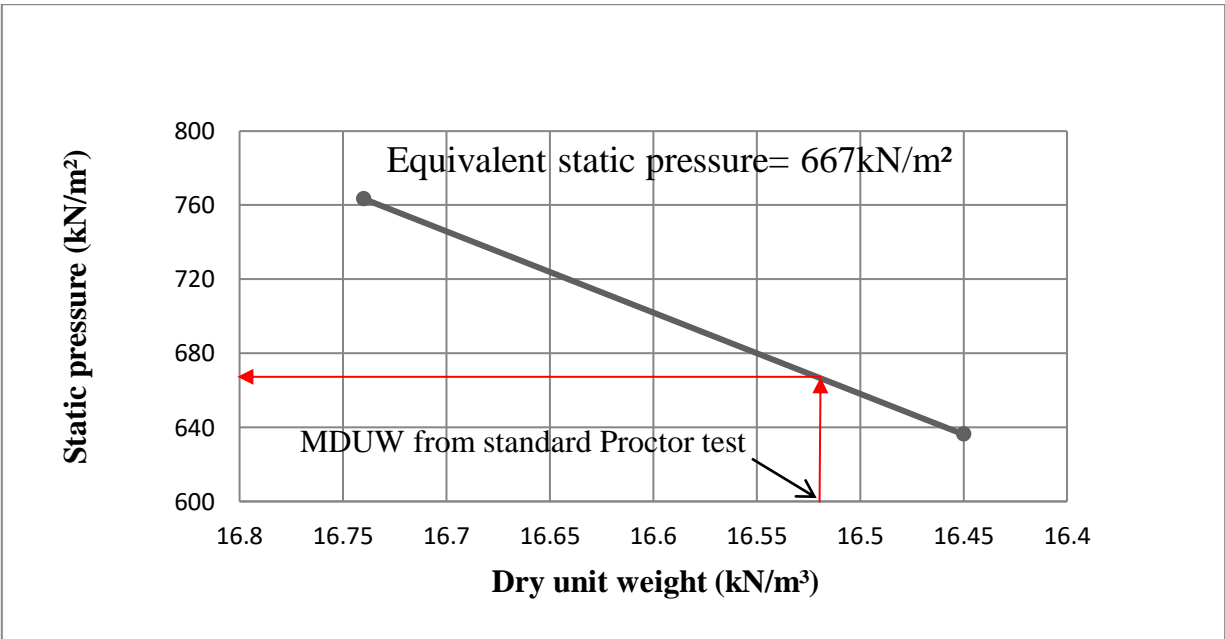


Figure 3.48: Determination of equivalent static pressure of sample 1

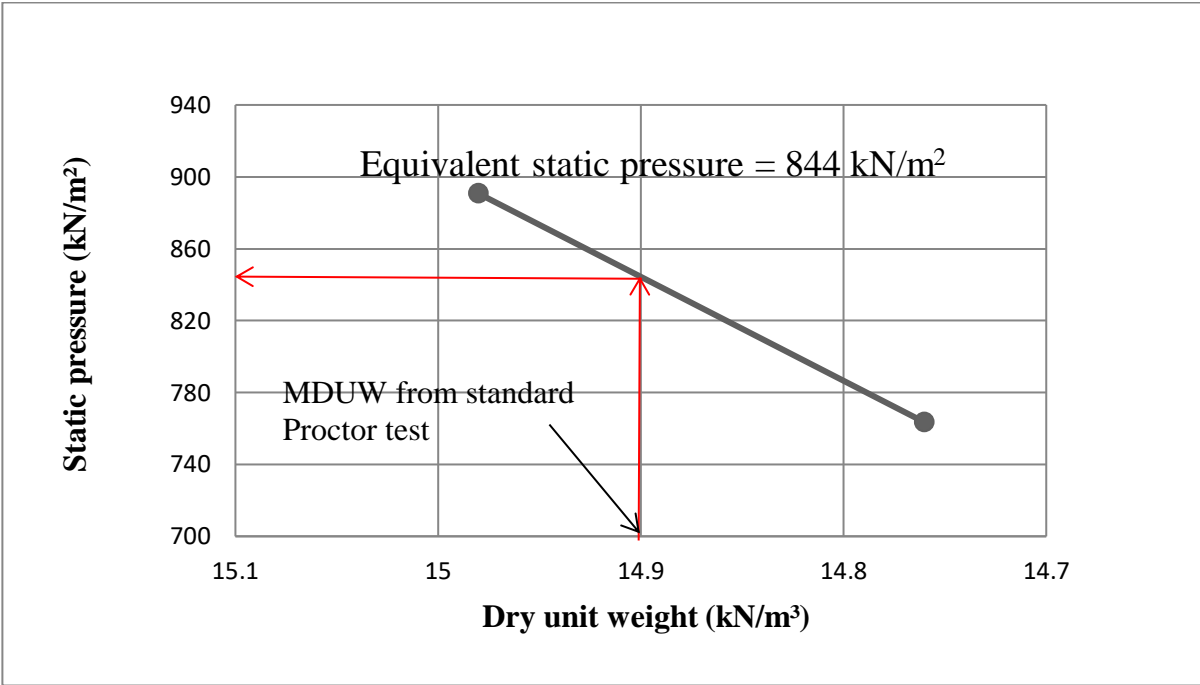


Figure 3.49: Determination of equivalent static pressure of sample 2

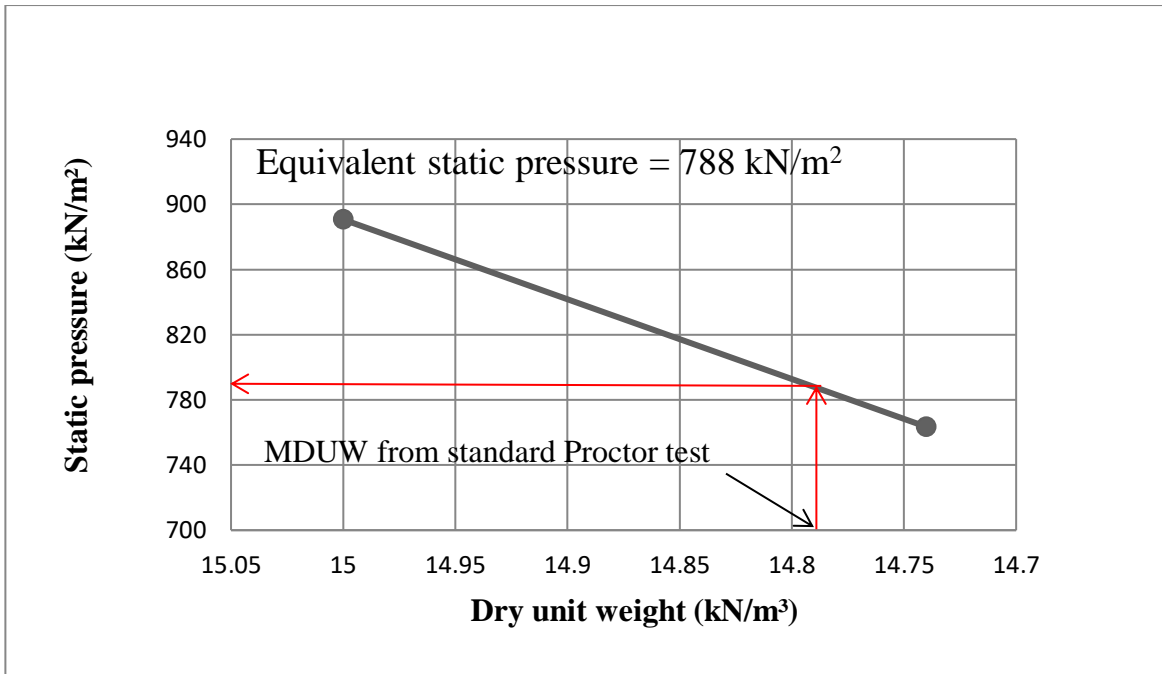


Figure 3.50: Determination of equivalent static pressure of sample 3

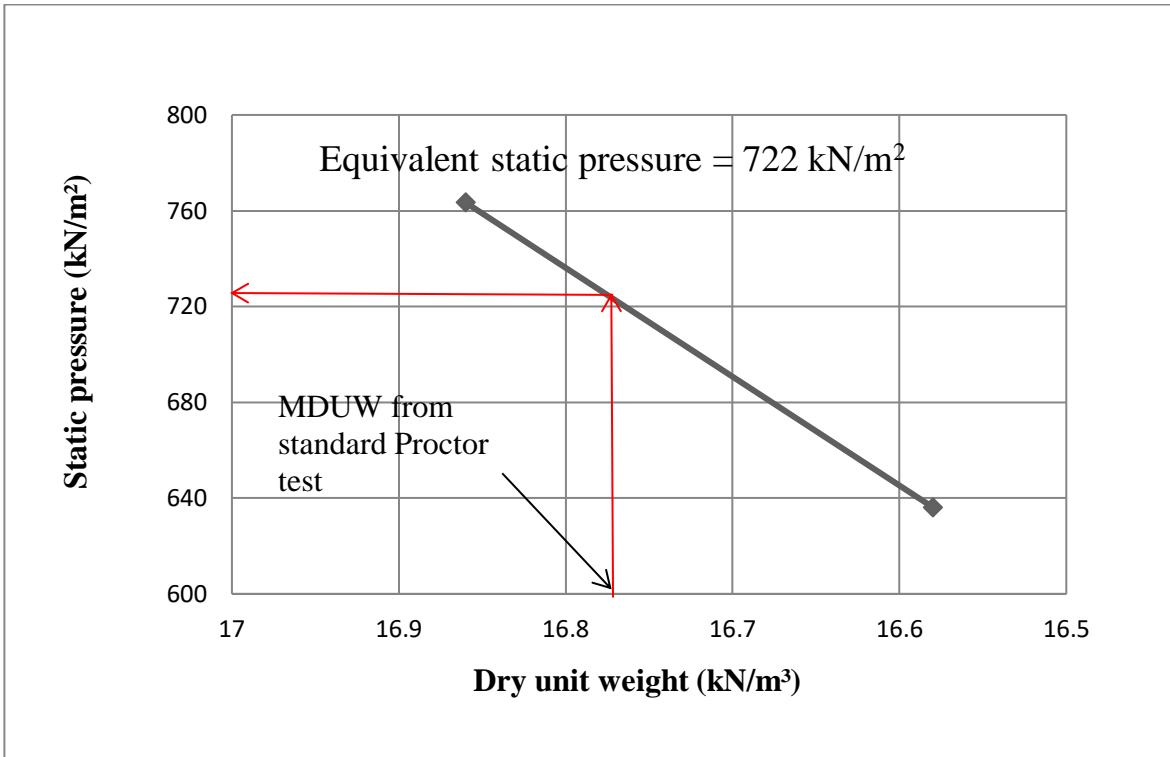


Figure 3.51: Determination of equivalent static pressure of sample 4

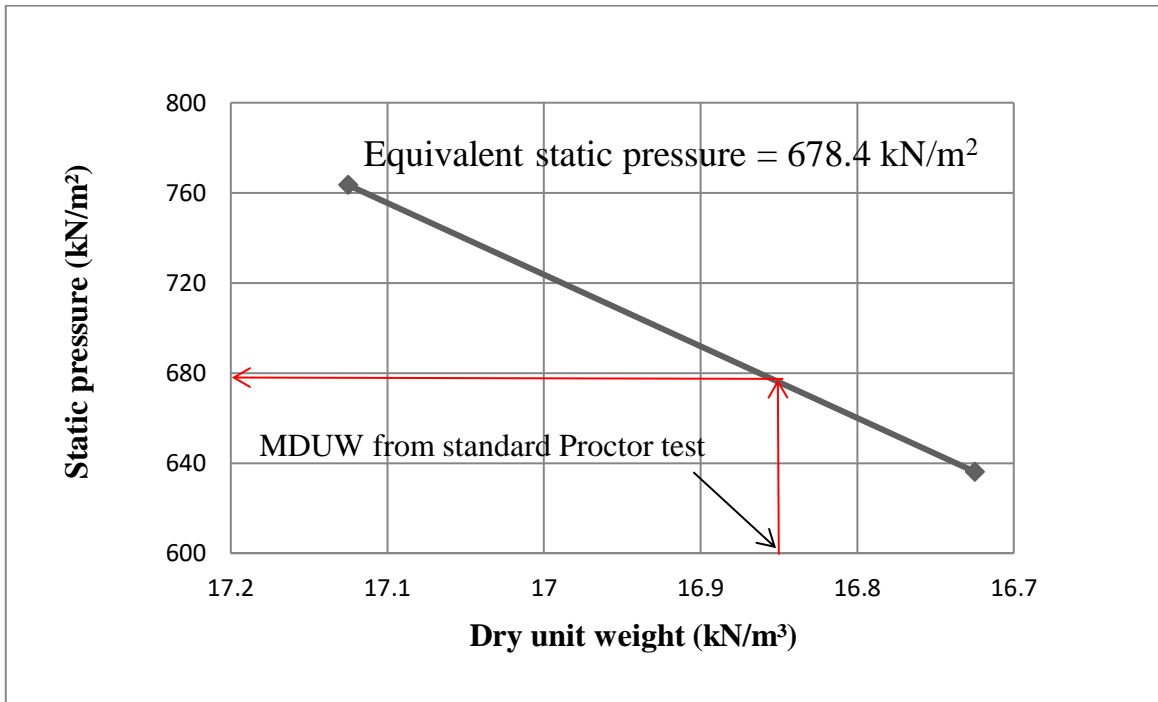


Figure 3.52: Determination of equivalent static pressure of sample 5

The equivalent static pressures for all the five samples have been listed down in Table 3.3.

Table 3.4. Equivalent static pressures of all the five soil samples

| Sample No. | Equivalent Static Pressure (kN/m²) |
|-------------------|--|
| 1 | 667 |
| 2 | 844 |
| 3 | 788 |
| 4 | 722 |
| 5 | 678.4 |

In our study, we found that the average equivalent static pressure for the five different soil samples was 740 kN/m², which was almost close to the value obtained by Sharma et al. (2016). Our primary goal was to replicate real field situations as closely as possible while minimizing specimen compaction time and effort. We recognized that the standard Proctor compaction test results may not be directly applicable to the static compaction of subgrade soil because the compaction method used to achieve compaction may vary.

To overcome this limitation, a laboratory static compaction method was introduced that would bridge the gap between field and laboratory situations. Our study aimed to replicate the compaction characteristics through the static compaction test in the laboratory and determine the equivalent static pressure required to obtain the maximum dry unit weight and optimum moisture content as determined from the standard Proctor test.

3.3.4. Test results of consolidation properties of the soil:

Consolidation test was performed for five different soil samples to determine the consolidation properties of statically and dynamically compacted soil at dry of optimum (OMC-3%), optimum moisture content (OMC) and at wet of optimum (OMC+3%).

3.3.4.1. Consolidation test results of dynamically compacted soil samples:

Below are the graphs illustrating the relationship between the void ratio and consolidation pressure (log scale), as determined through the consolidation test performed on soil samples that underwent dynamic compaction. The calculated values for the specimen height and void ratio, corresponding to each applied pressure, are tabulated in Appendix II, specifically in Table 3.5 to 3.34.

3.3.4.1.1. Consolidation Test results at dry of optimum moisture content (OMC-3%)

The consolidation curves obtained for all the samples compacted dynamically at dry of optimum moisture content are presented below from Fig 3.53 to Fig 3.57.

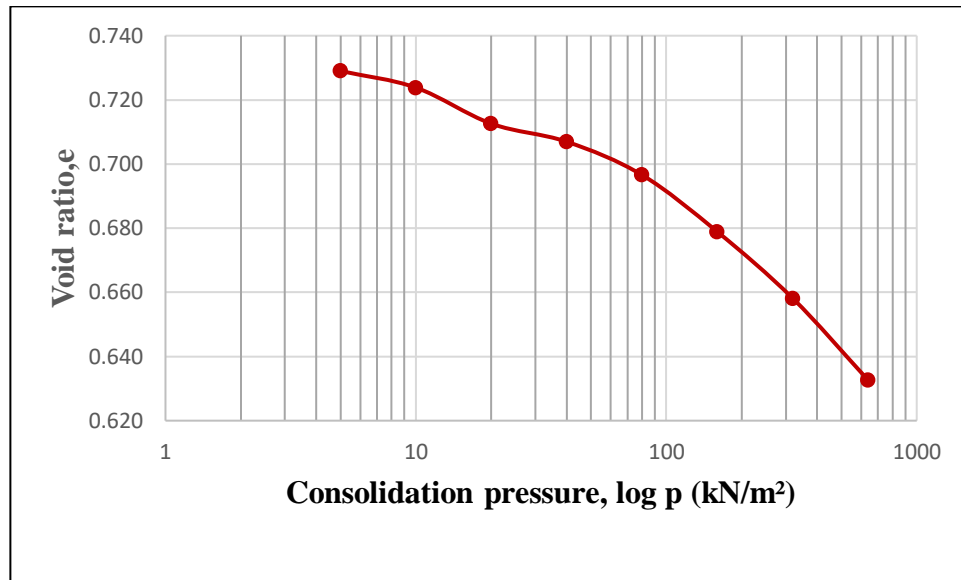


Figure 3.53: Consolidation pressure-void ratio curve of sample 1(dynamic at dry of optimum)

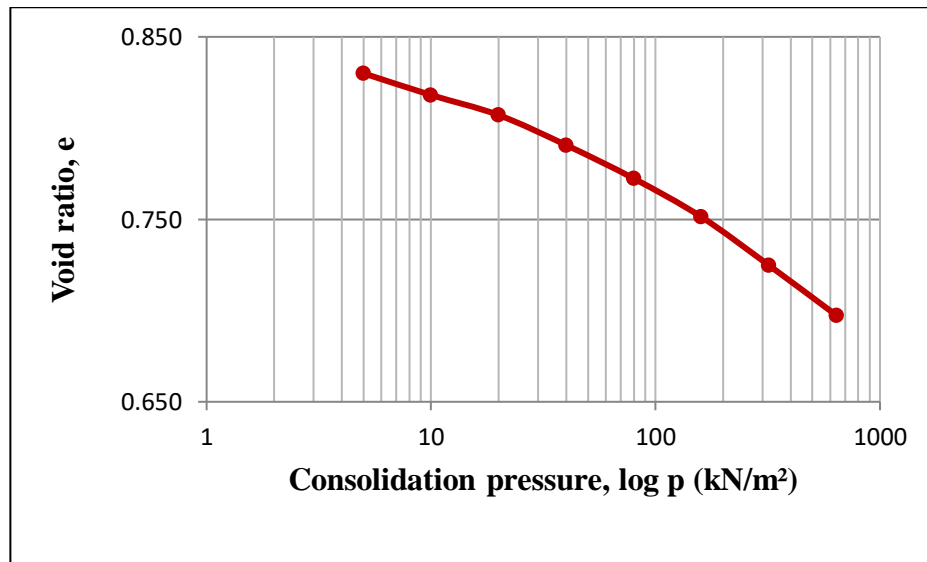


Figure 3.54: Consolidation pressure-void ratio curve of sample 2(dynamic at dry of optimum)

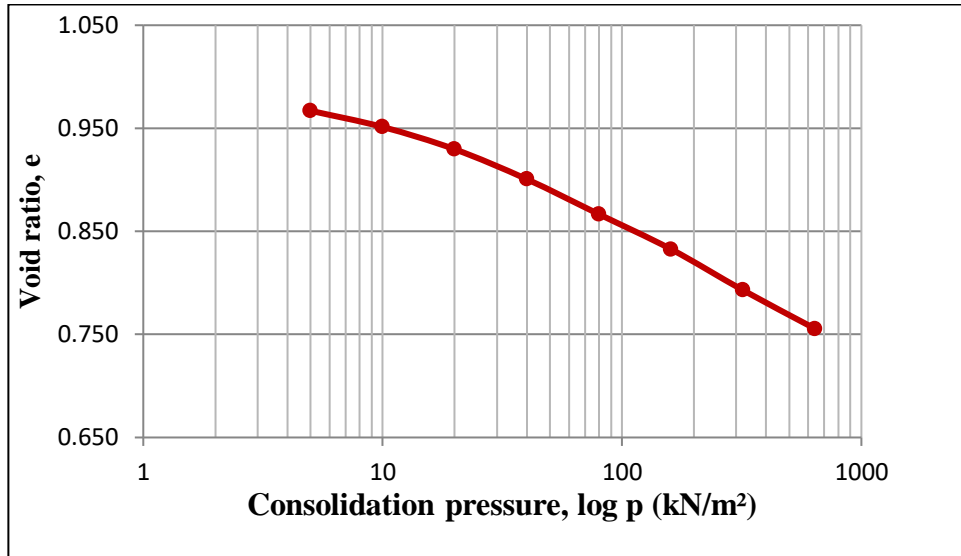


Figure 3.55: Consolidation pressure-void ratio curve of sample 3(dynamic at dry of optimum)

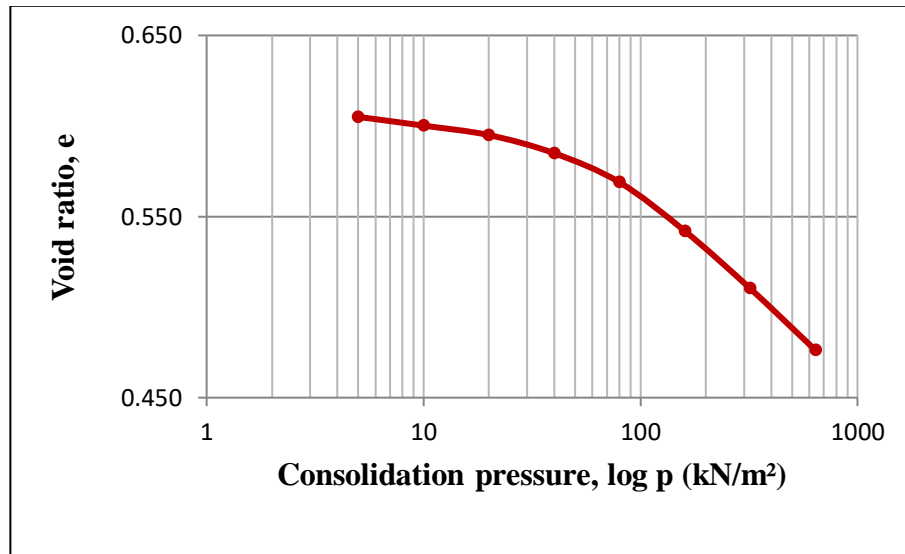


Figure 3.56: Consolidation pressure-void ratio curve of sample 4(dynamic at dry of optimum)

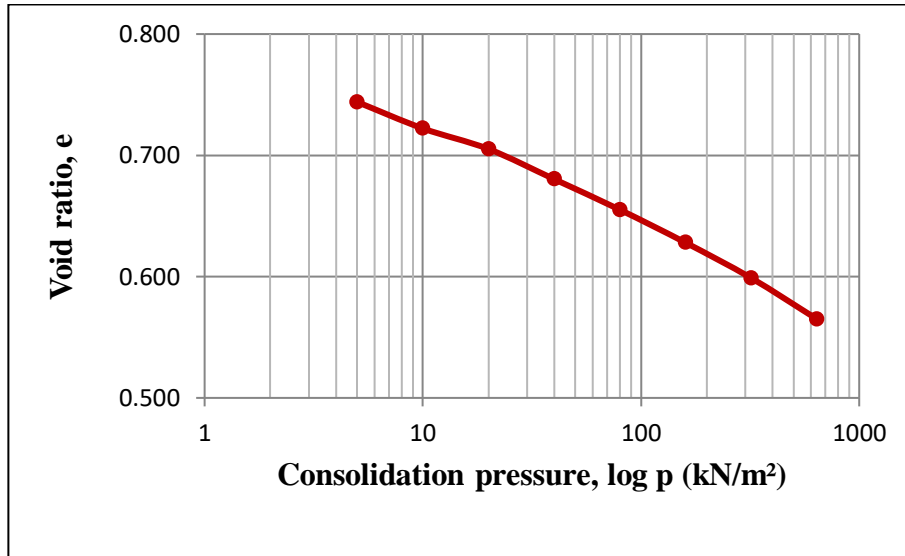


Figure 3.57: Consolidation pressure-void ratio curve of sample 5(dynamic at dry of optimum)

3.3.4.1.2. Consolidation Test results at optimum moisture content (OMC)

The consolidation curves derived from the dynamic compaction of all samples at the optimum level are displayed sequentially in the figures ranging from Figure 3.58 to Figure 3.62 below.

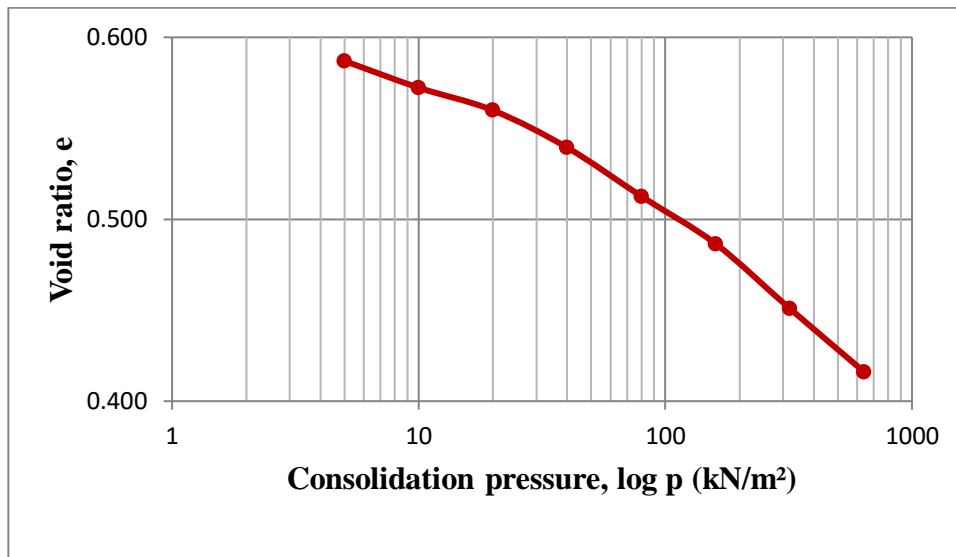


Figure 3.58: Consolidation pressure-void ratio curve of sample 1(dynamic at OMC)

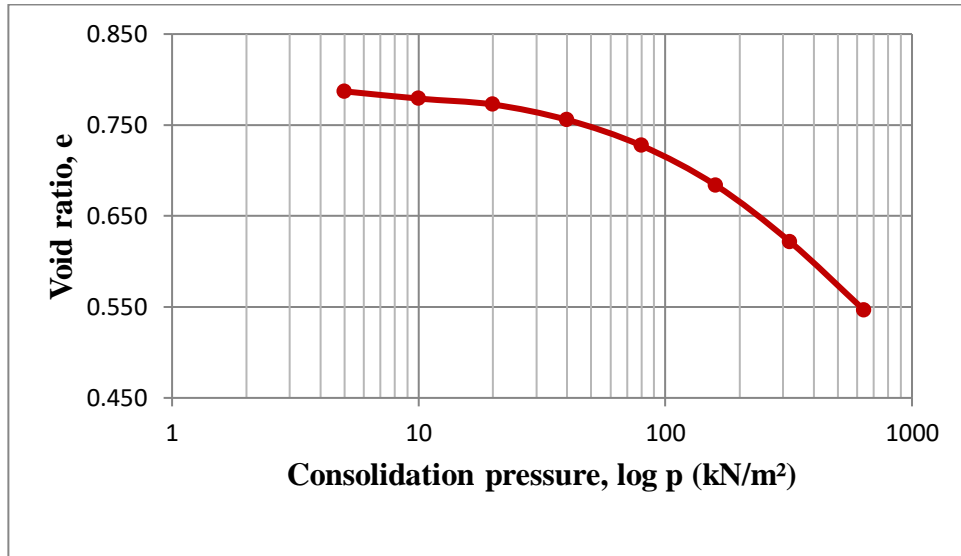


Figure 3.59: Consolidation pressure-void ratio curve of sample 2(dynamic at OMC)

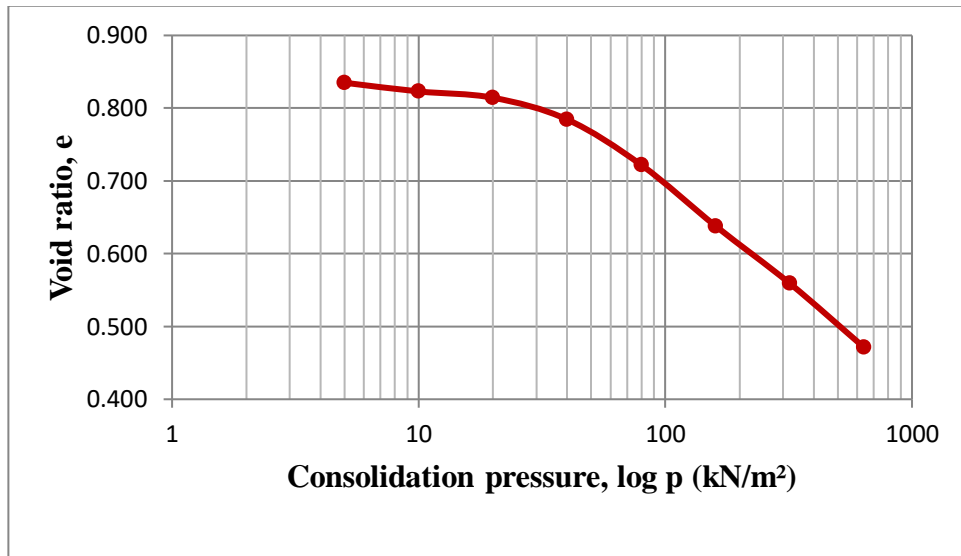


Figure 3.60: Consolidation pressure-void ratio curve of sample 3(dynamic at OMC)

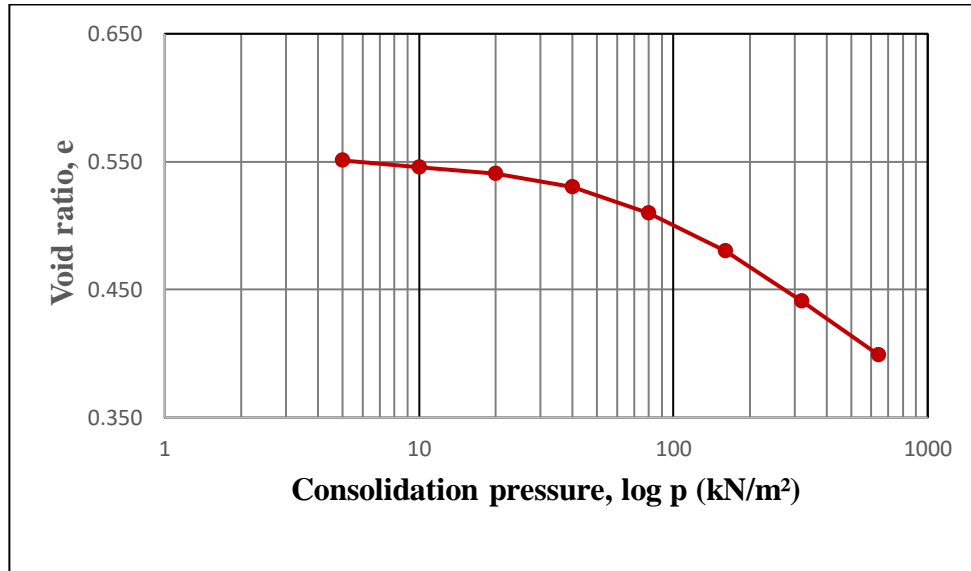


Figure 3.61: Consolidation pressure-void ratio curve of sample 4(dynamic at OMC)

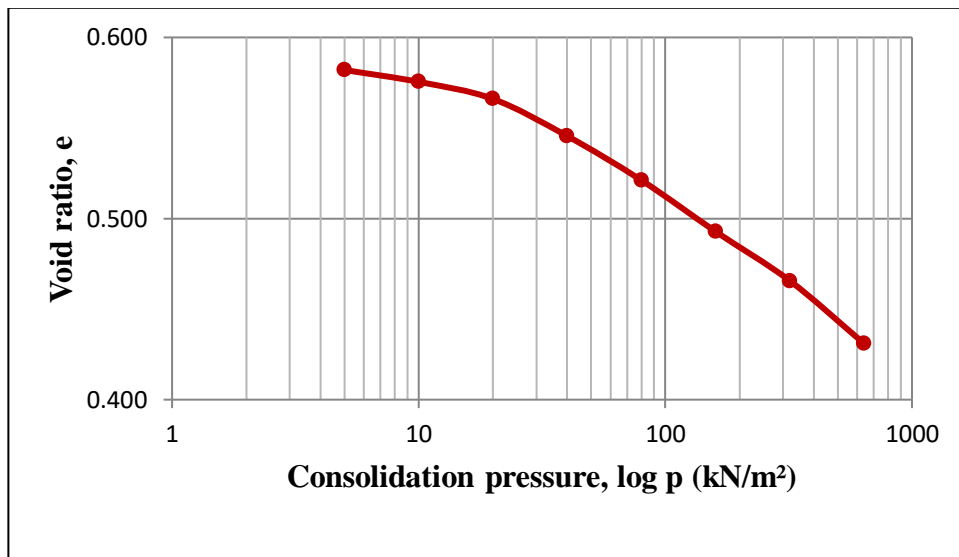


Figure 3.62: Consolidation pressure-void ratio curve of sample 5(dynamic at OMC)

3.3.4.1.3. Consolidation Test results at wet of optimum moisture content (OMC+3%)

Presented below, spanning from Figure 3.63 to Figure 3.67, are the consolidation curves resulting from the dynamic compaction of all samples at their respective wet of optimum moisture content.

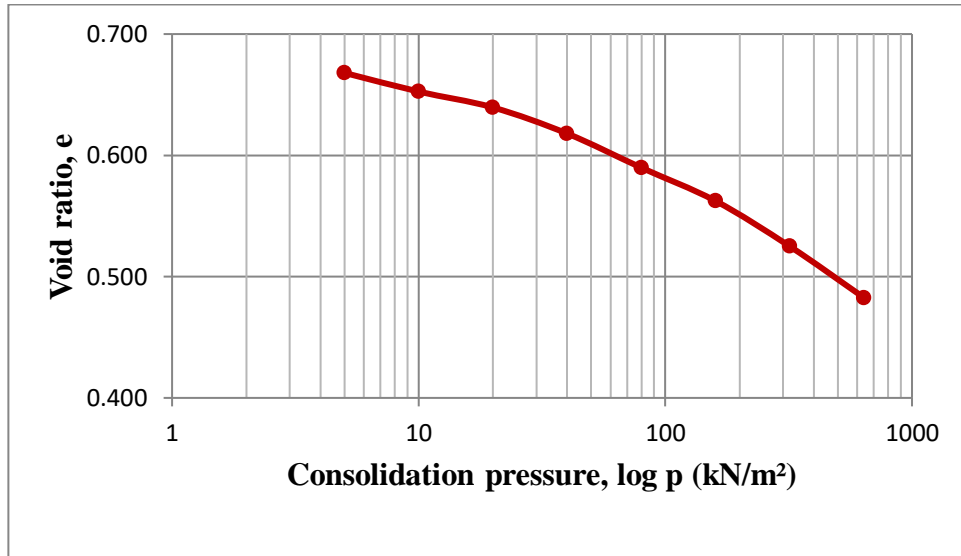


Figure 3.63: Consolidation pressure-void ratio curve of sample 1(dynamic at wet of optimum)

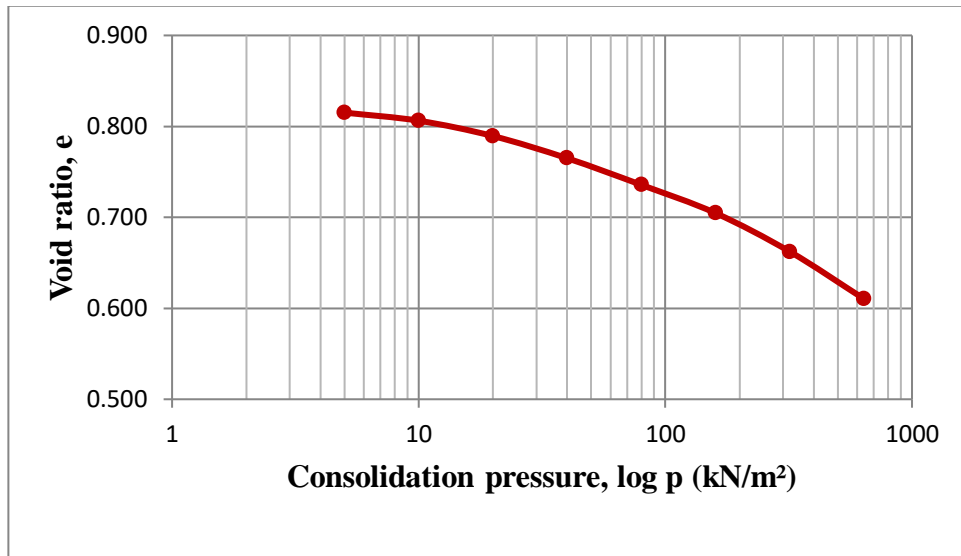


Figure 3.64: Consolidation pressure-void ratio curve of sample 2(dynamic at wet of optimum)

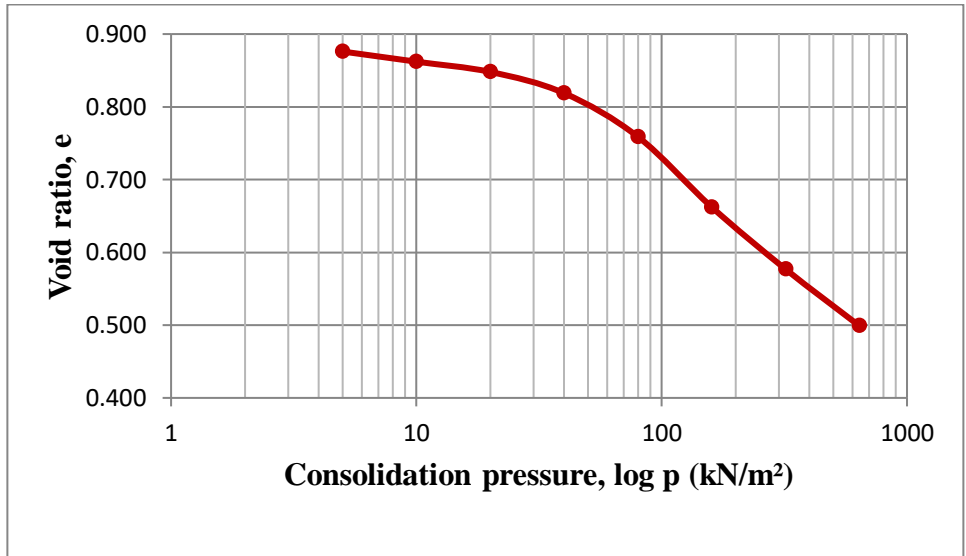


Figure 3.65: Consolidation pressure-void ratio curve of sample 3 (dynamic at wet of optimum)

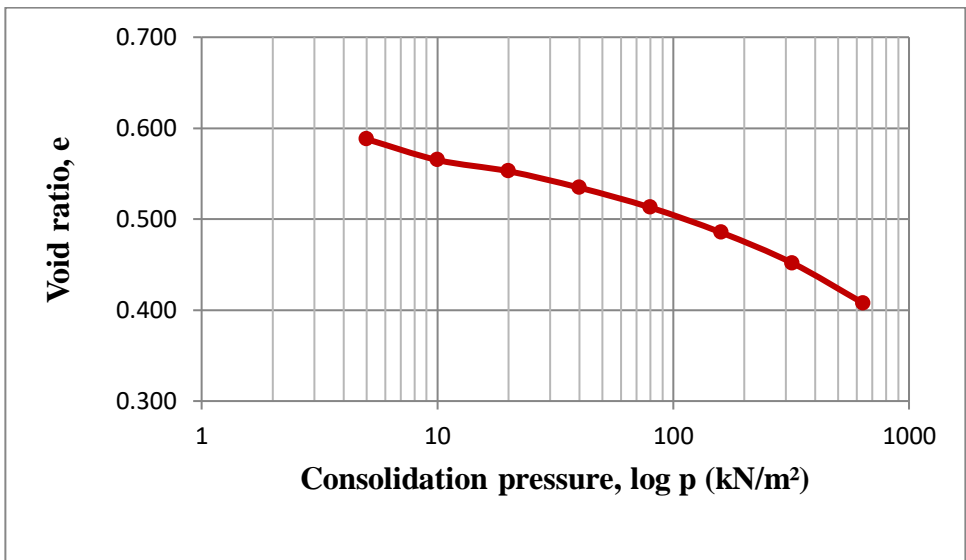


Figure 3.66: Consolidation pressure-void ratio curve of sample 4 (dynamic at wet of optimum)

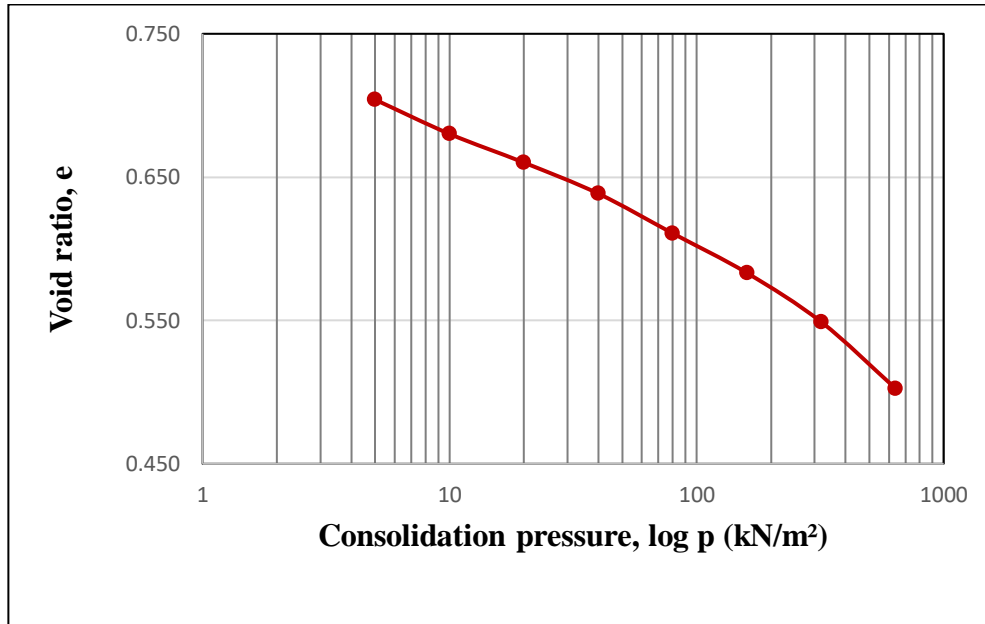


Figure 3.67: Consolidation pressure-void ratio curve of sample 5 (dynamic at wet of optimum)

3.3.4.2. Consolidation test results of statically compacted soil samples:

Below are the graphs illustrating the relationship between the void ratio and consolidation pressure (log scale), as determined through the consolidation test performed on soil samples that underwent static compaction.

3.3.4.2.1. Consolidation Test results at dry of optimum moisture content (OMC-3%)

The consolidation curves obtained for all the samples compacted statically at dry of optimum moisture content are presented below from Fig 3.68 to Fig 3.72.

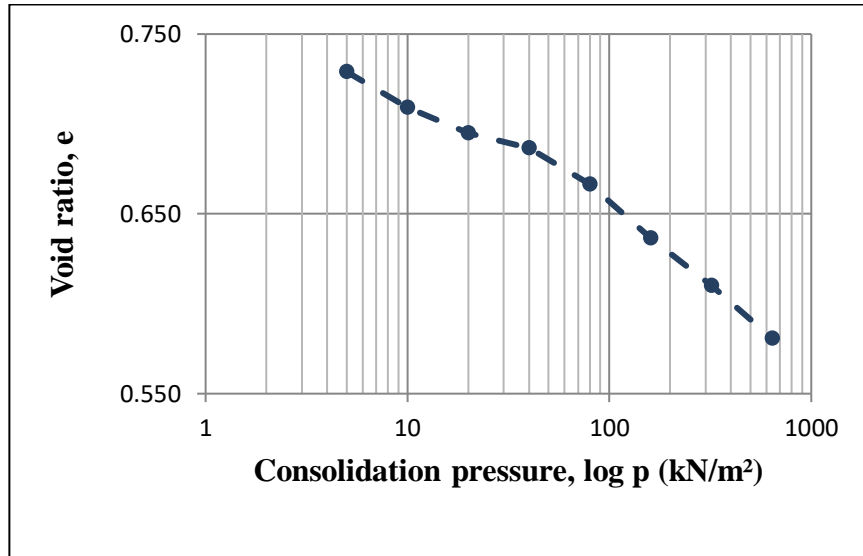


Figure 3.68: Consolidation pressure-void ratio curve of sample 1 (static at dry of optimum)

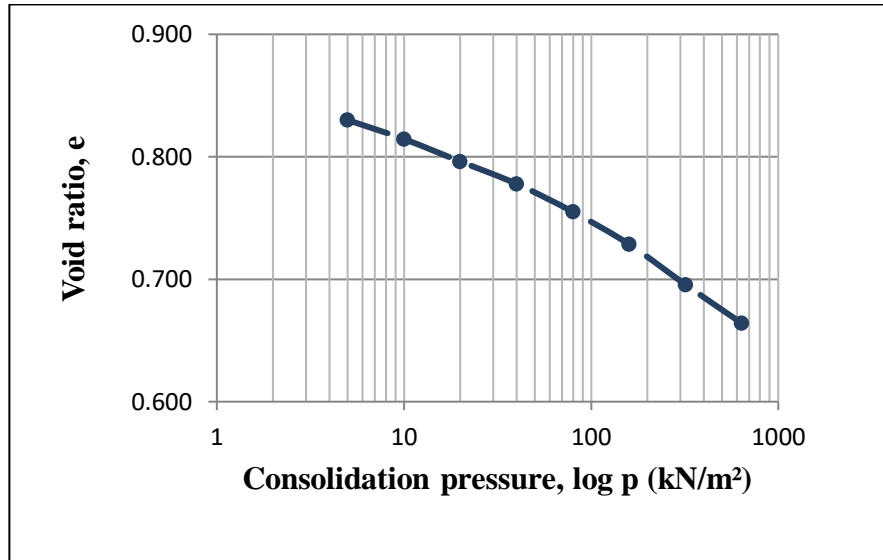


Figure 3.69: Consolidation pressure-void ratio curve of sample 2 (static at dry of optimum)

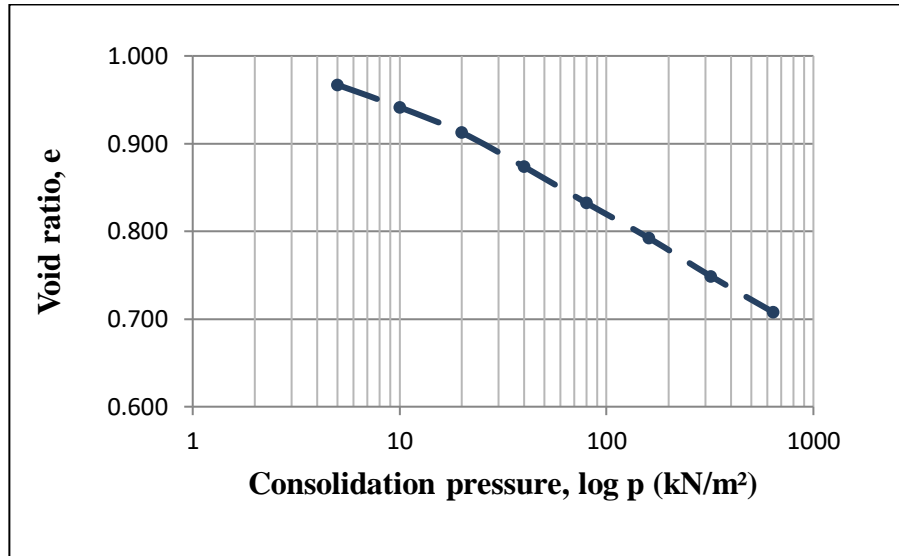


Figure 3.70: Consolidation pressure-void ratio curve of sample 3(static at dry of optimum)

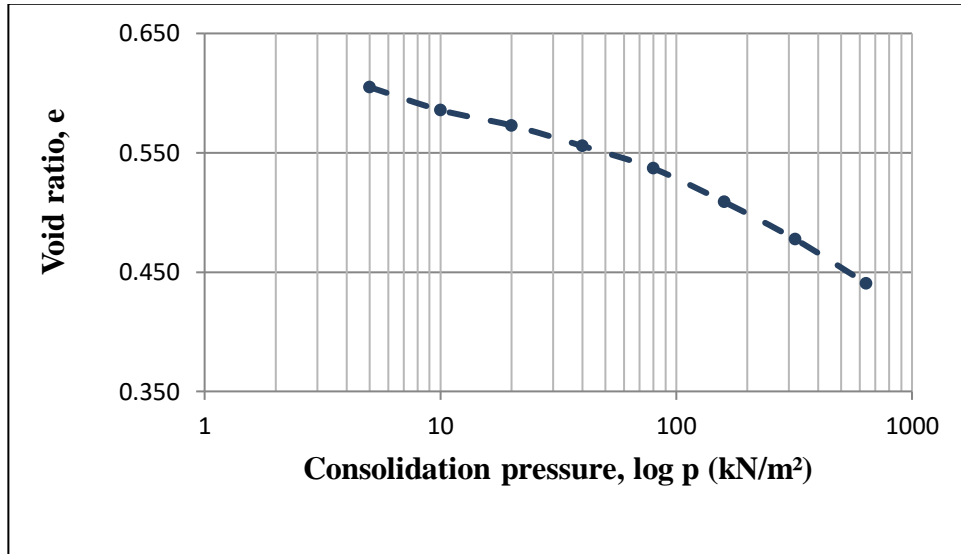


Figure 3.71: Consolidation pressure-void ratio curve of sample 4(static at dry of optimum)

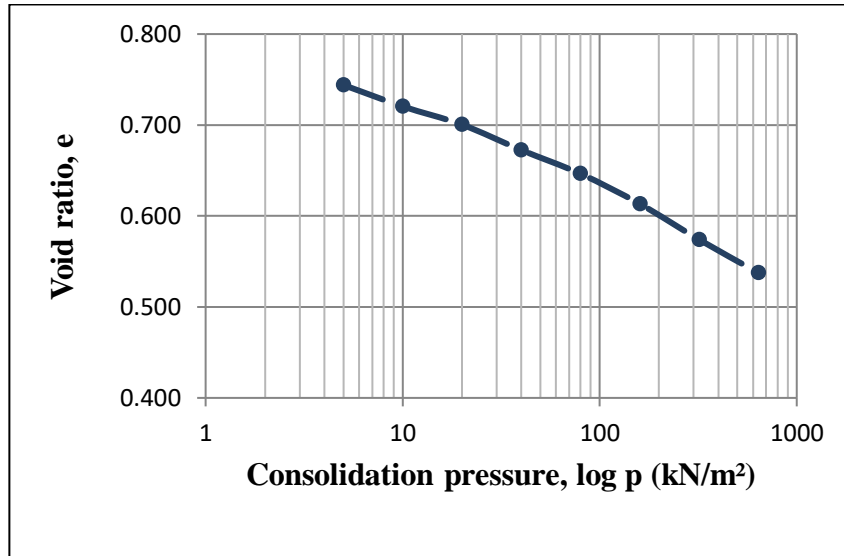


Figure 3.72: Consolidation pressure-void ratio curve of sample 5 (static at dry of optimum)

3.3.4.2.2. Consolidation Test results at optimum moisture content (OMC)

The consolidation curves obtained for all the samples compacted statically at optimum moisture content are presented below from Fig 3.73 to Fig 3.77.

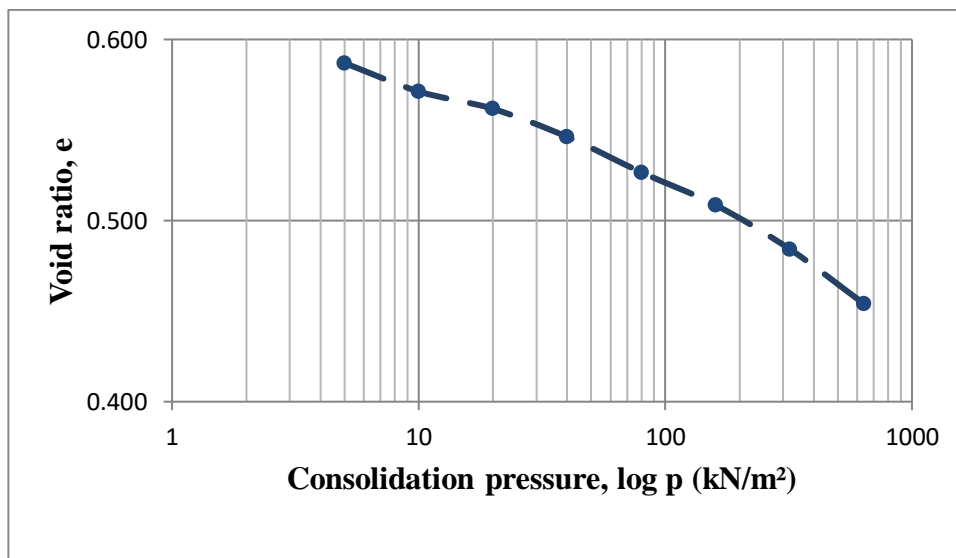


Figure 3.73: Consolidation pressure-void ratio curve of sample 1 (static at OMC)

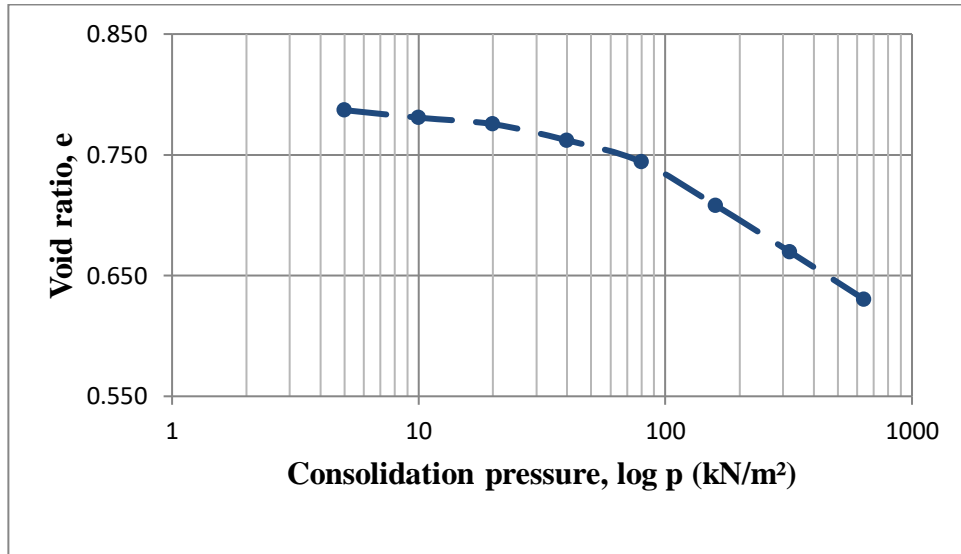


Figure 3.74: Consolidation pressure-void ratio curve of sample 2(static at OMC)

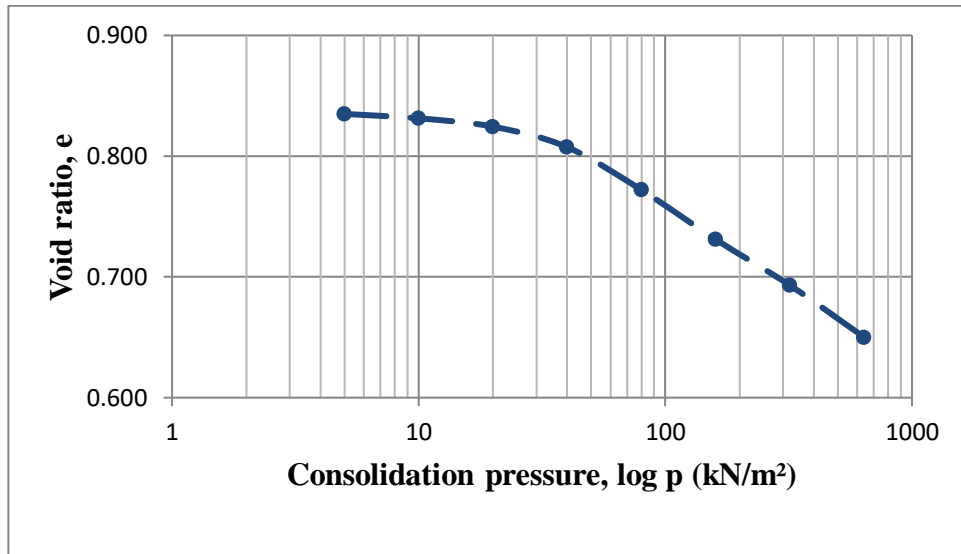


Figure 3.75: Consolidation pressure-void ratio curve of sample 3(static at OMC)

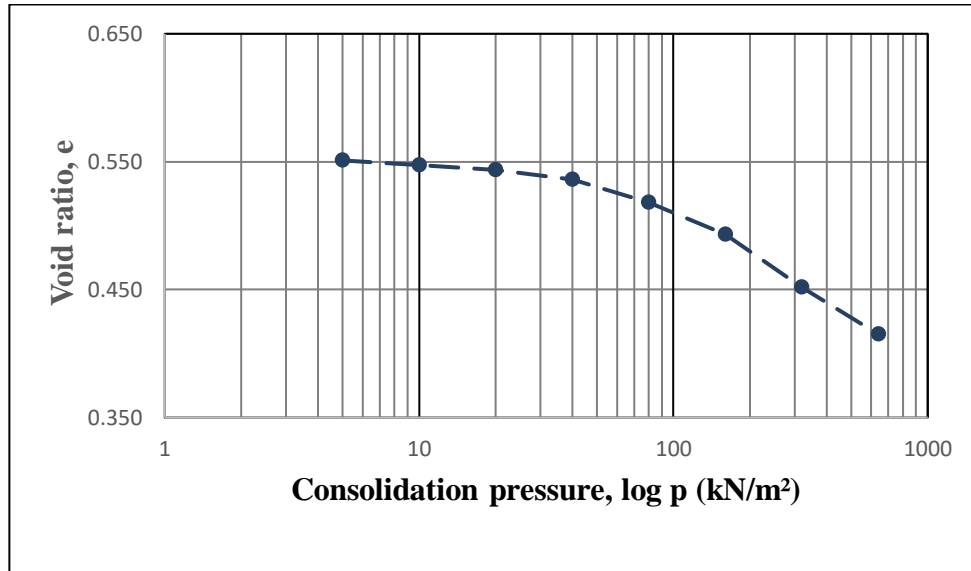


Figure 3.76: Consolidation pressure-void ratio curve of sample 4 (static at OMC)

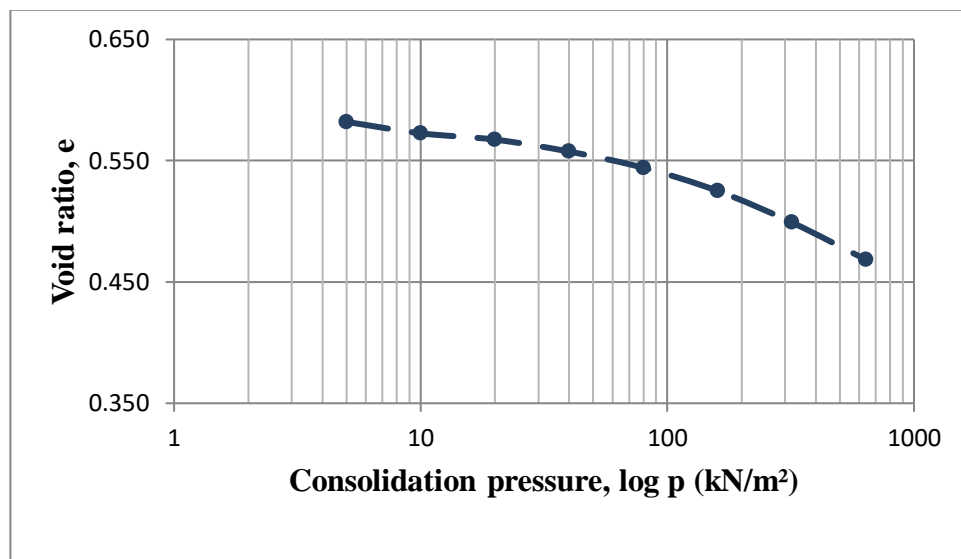


Figure 3.77: Consolidation pressure-void ratio curve of sample 5 (static at OMC)

3.3.4.2.3. Consolidation Test results at wet of optimum moisture content (OMC+3%)

The consolidation curves obtained for all the samples compacted statically at wet of optimum moisture content are presented below from Fig 3.78 to Fig 3.82.

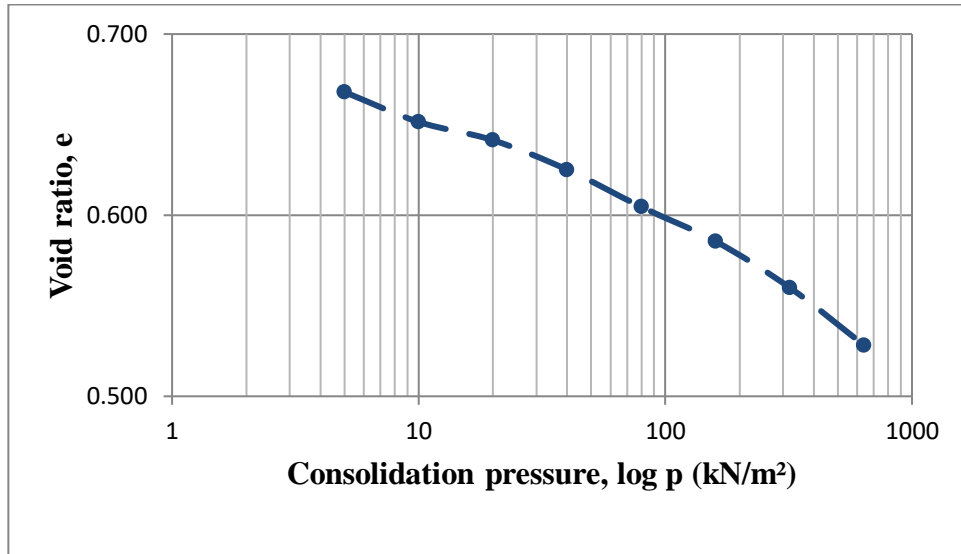


Figure 3.78: Consolidation pressure-void ratio curve of sample 1(static at wet of optimum)

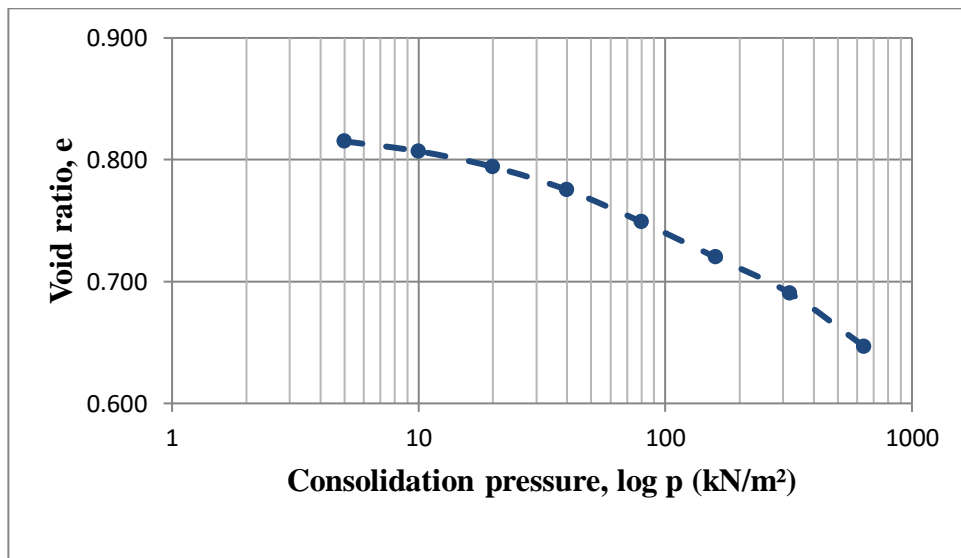


Figure 3.79: Consolidation pressure-void ratio curve of sample 2(static at wet of optimum)

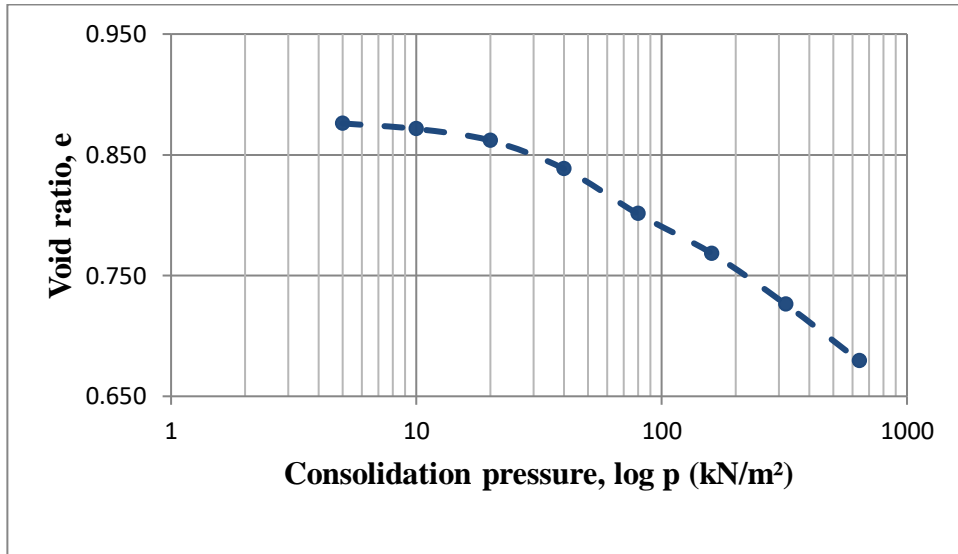


Figure 3.80: Consolidation pressure-void ratio curve of sample 3(static at wet of optimum)

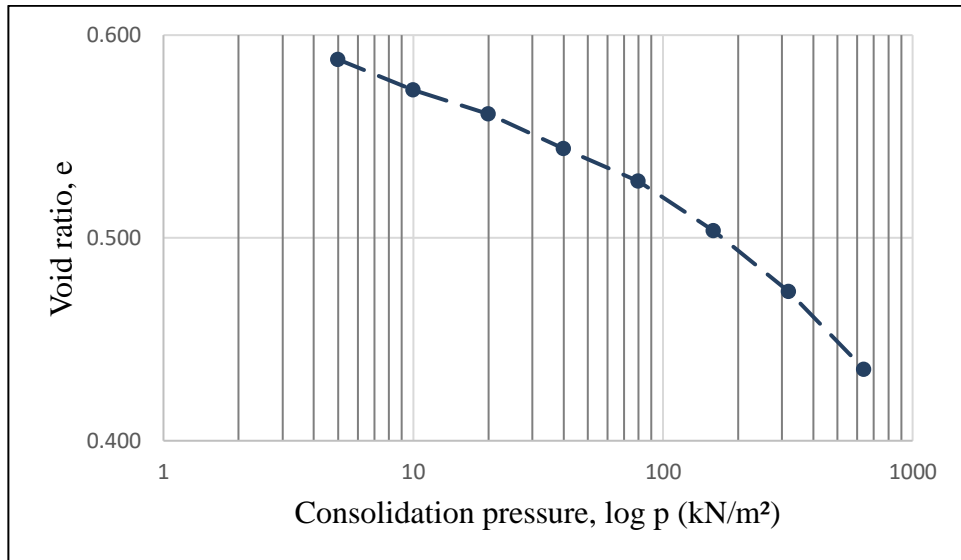


Figure 3.81: Consolidation pressure-void ratio curve of sample 4(static at wet of optimum)

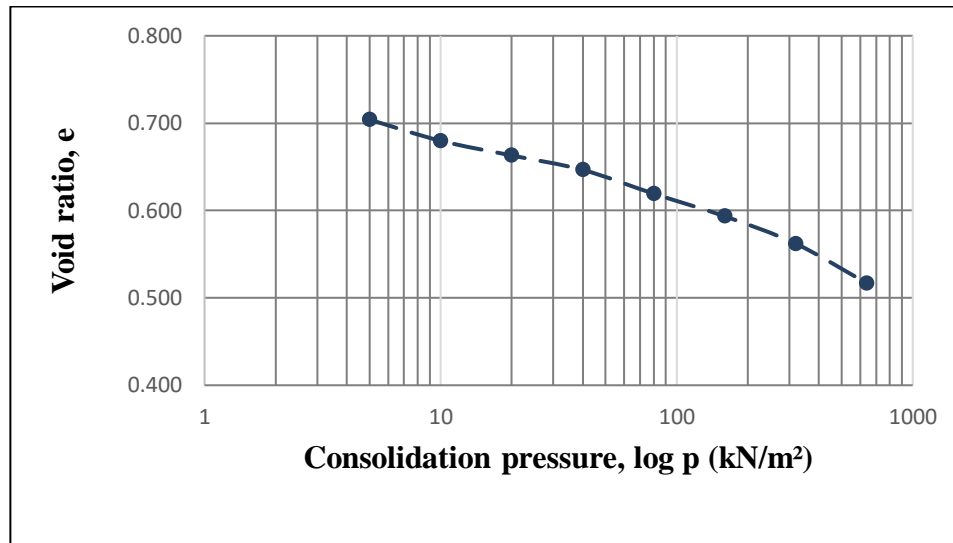


Figure 3.82: Consolidation pressure-void ratio curve of sample 5 (static at wet of optimum)

The consistent trend observed in the consolidation pressure versus void ratio curves of all samples, subjected to static and dynamic compaction at different moisture levels (dry, wet, and optimum) and corresponding dry unit weights, is clearly indicative. This consistent behaviour can be ascribed to the pre-consolidation pressure of the soil, given that all soil samples exhibit an over-consolidated state. In the initial stages of the consolidation test, the pressure is lower than the pre-consolidation pressure specific to that soil, resulting in a curvilinear shape of the curve until reaching the pre-consolidation pressure. Subsequently, the curves adopt a linear trajectory. These curves provide valuable insights into various consolidation properties of soils, which will be elaborated in the subsequent chapter.

3.3.4.3. Determination of Coefficient of consolidation (C_v):

The coefficient of consolidation was calculated using the Square root of time fitting method for all specimens subjected to both static and dynamic compaction at dry of optimum, optimum moisture content and at wet of optimum. These are presented below from Fig. 3.83 to Fig. 3.94.

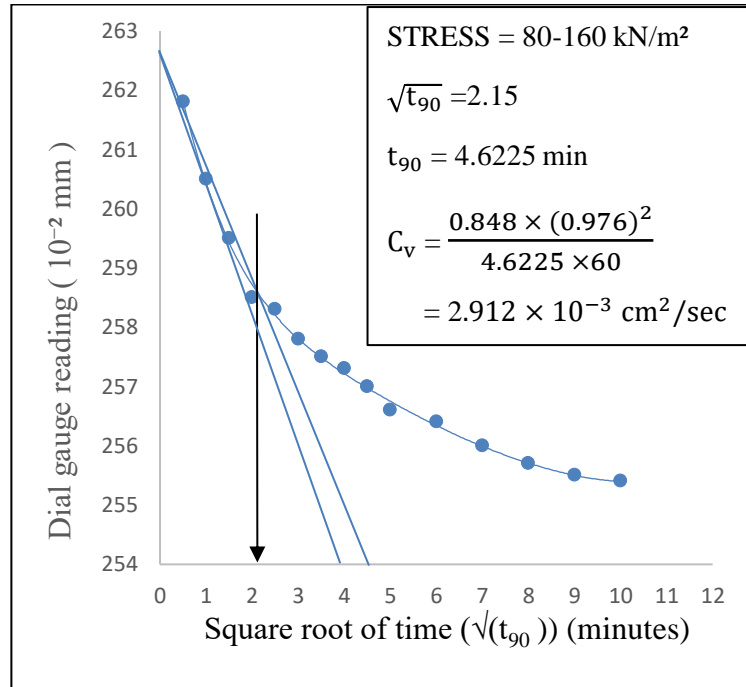


Figure 3.83: Time-consolidation curve of sample 1 (dynamic at dry of optimum) at 80-160kPa

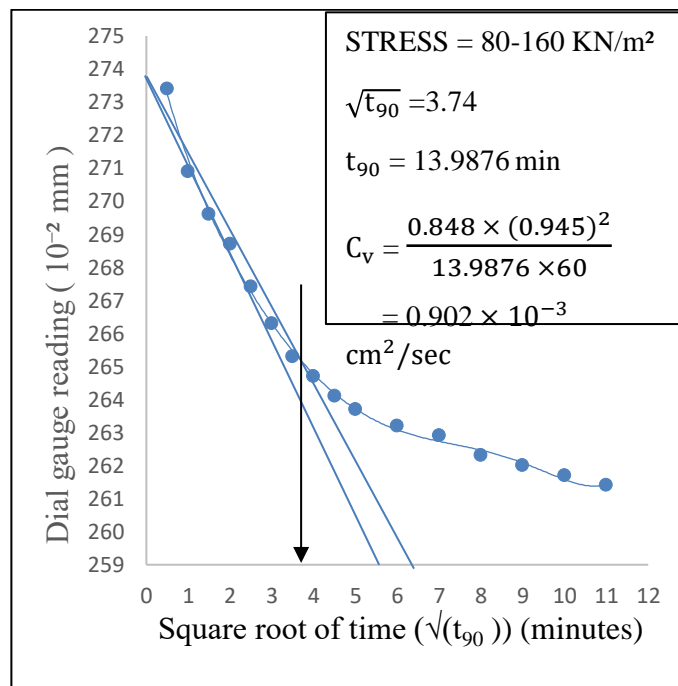


Figure 3.84: Time-consolidation curve of sample 1 (dynamic at OMC) at 80-160kPa

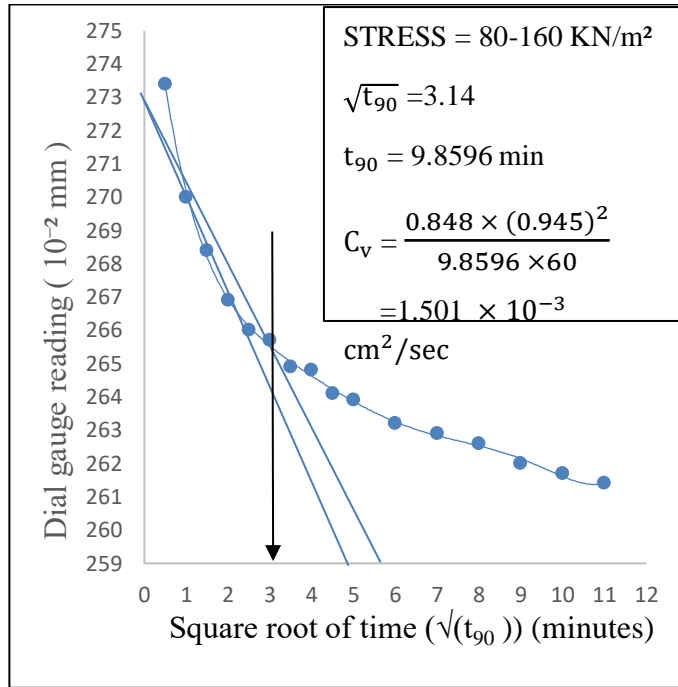


Figure 3.85: Time-consolidation curve of sample 1 (dynamic at wet of optimum) at 80-160kPa

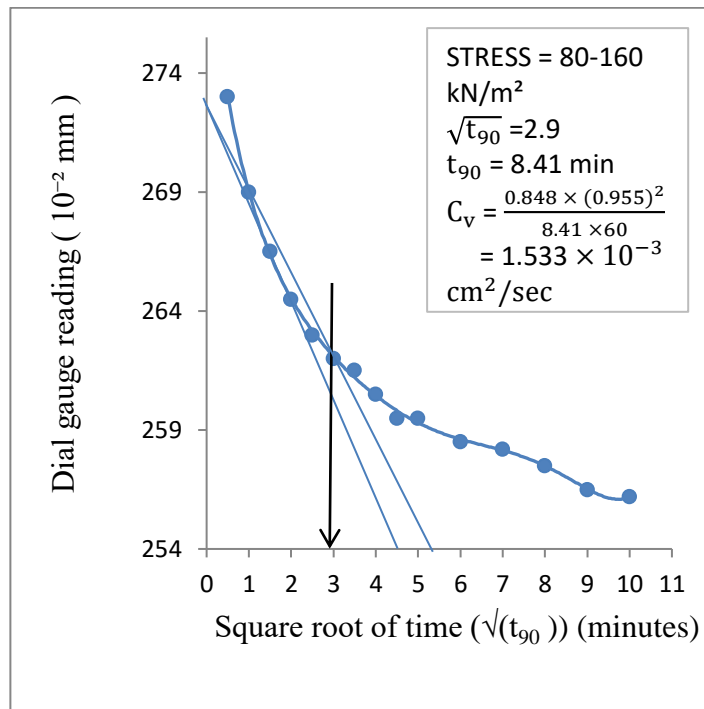


Figure 3.86: Time-consolidation curve of sample 1 (static at dry of optimum) at 80-160kPa

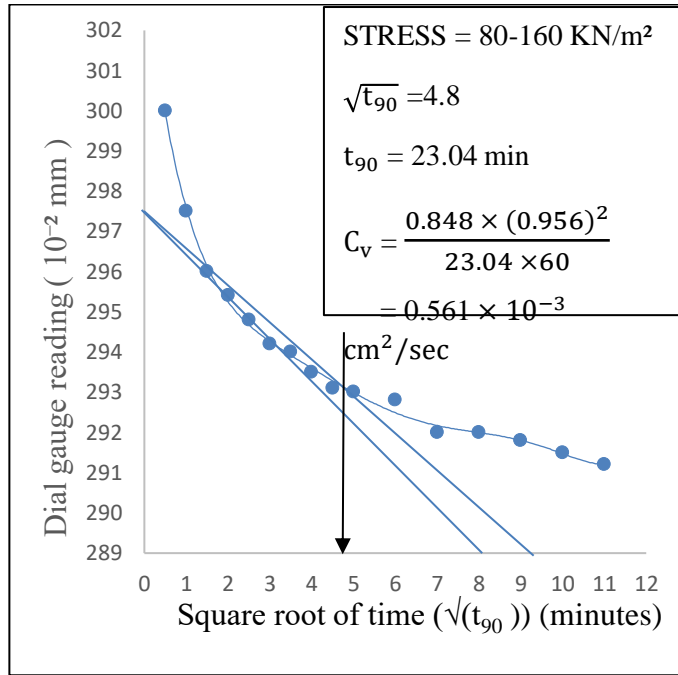


Figure 3.87: Time-consolidation curve of sample 1 (static at OMC) at 80-160kPa

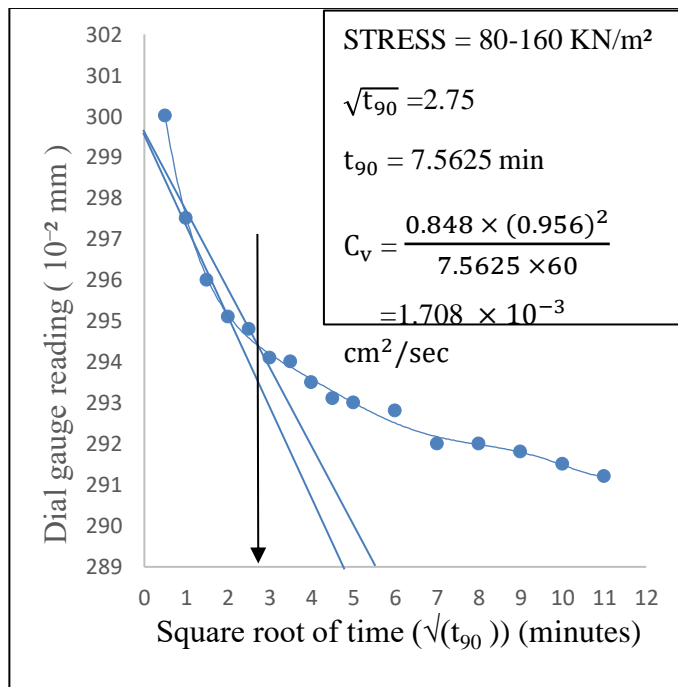


Figure 3.88: Time-consolidation curve of sample 1 (static at wet of optimum) at 80-160kPa

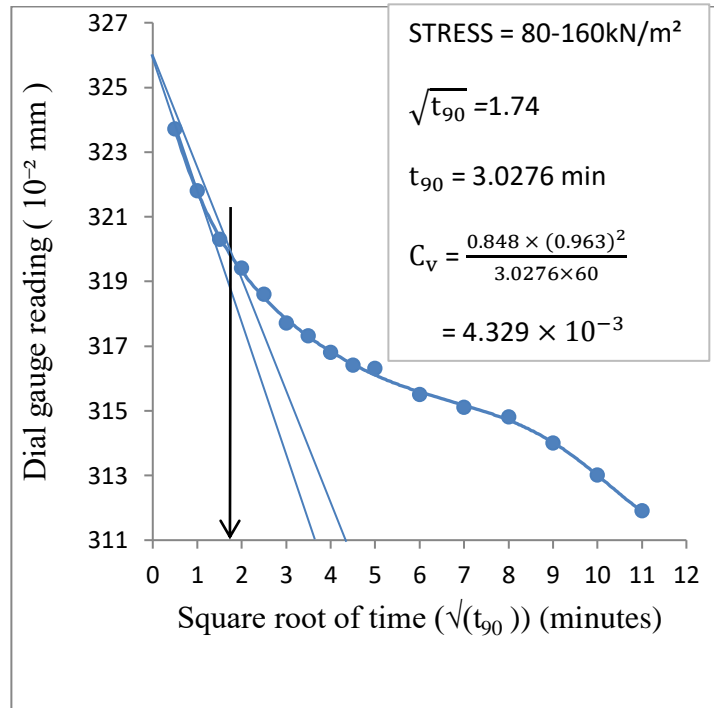


Figure 3.89: Time-consolidation curve of sample 2 (dynamic at dry of optimum) at 80-160kPa

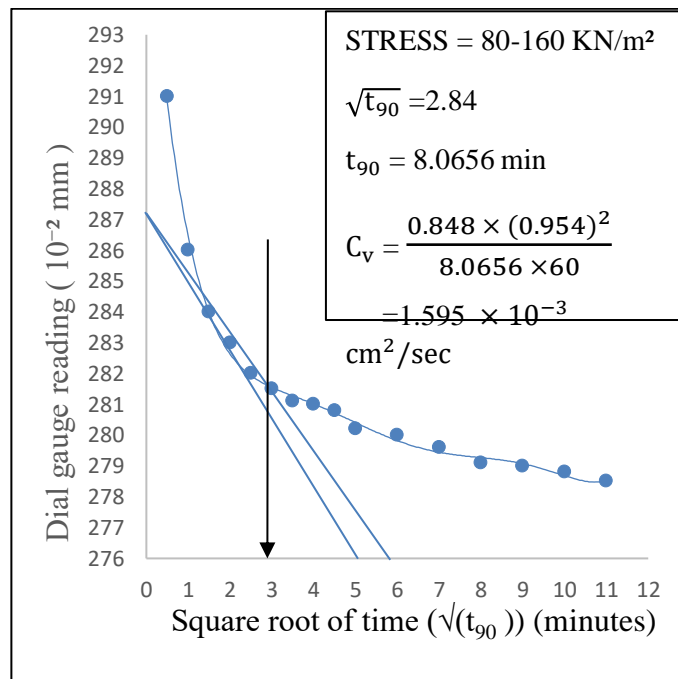


Figure 3.90: Time-consolidation curve of sample 2 (dynamic at optimum moisture content) at 80-160kPa

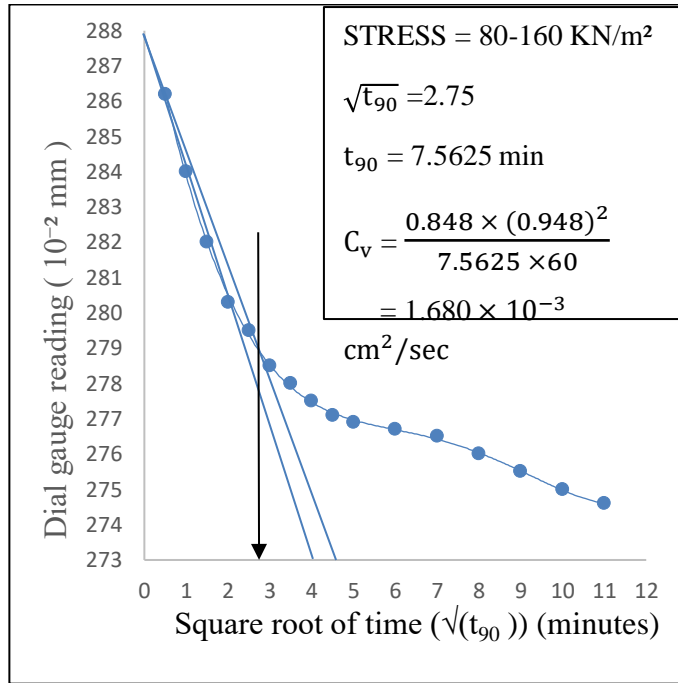


Figure 3.91: Time-consolidation curve of sample 2 (dynamic at wet of optimum) at 80-160kPa

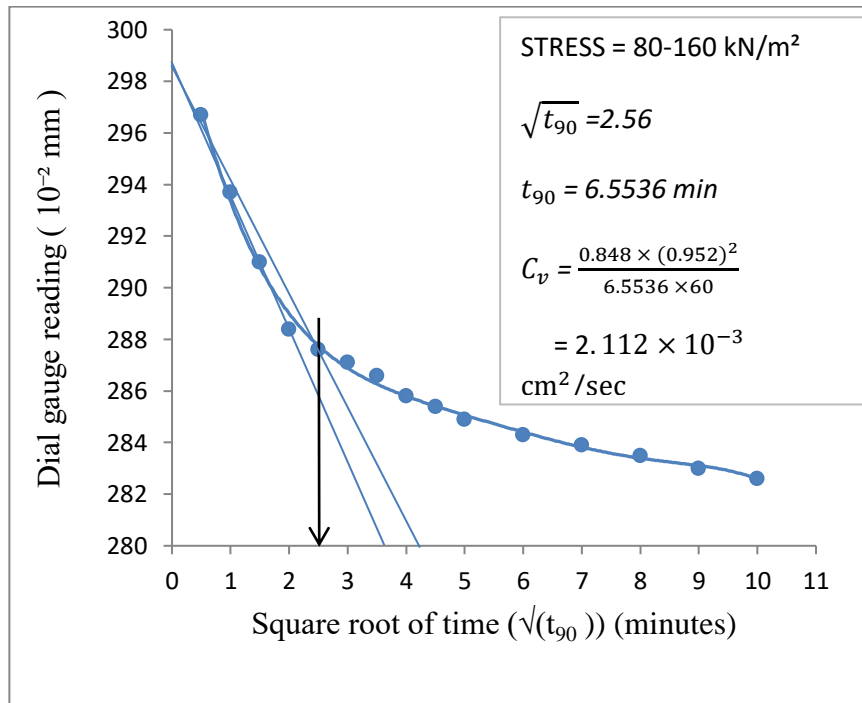


Figure 3.92: Time-consolidation curve of sample 2 (static at dry of optimum) at 80-160kPa

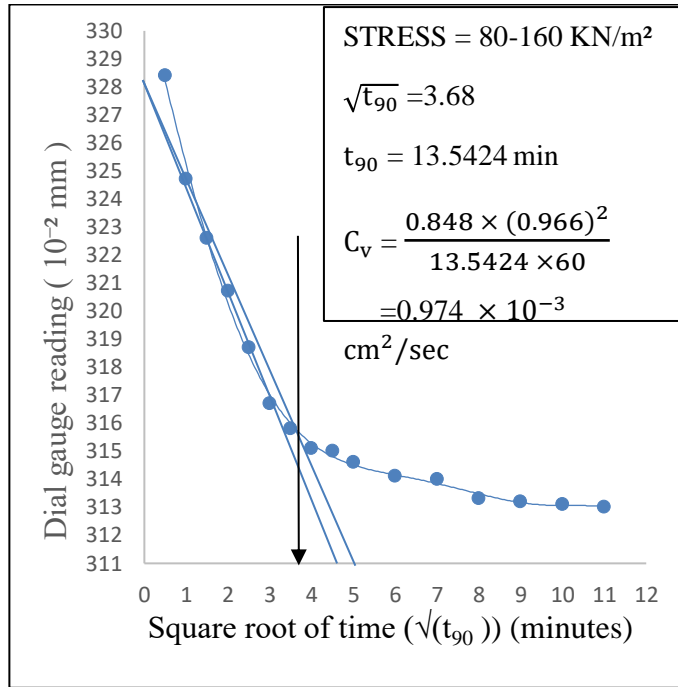


Figure 3.93: Time-consolidation curve of sample 2 (static at optimum moisture content) at 80-160kPa

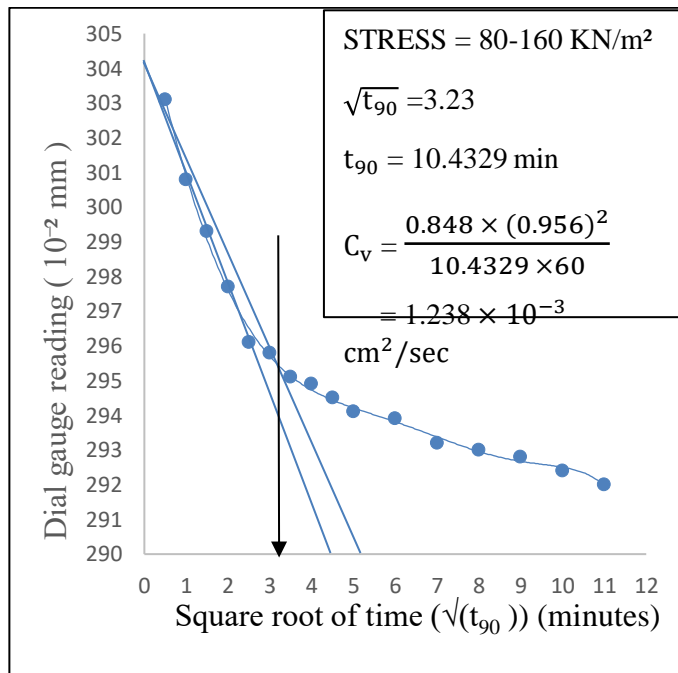


Figure 3.94: Time-consolidation curve of sample 2 (static at wet of optimum) at 80-160kPa

The remaining graphs are shown in Appendix III from Figure 3.95 to Figure 3.232 of all the remaining samples.

3.3.4.4. Determination of coefficient of compressibility (a_v) and coefficient of volume compressibility (m_v)

These two parameters can be calculated from the graphs shown in section 3.3.4.3.

3.3.4.5. Determination of coefficient of permeability (k):

Once we have the values for m_v and C_v , we can use the following equation to determine the value of k :

$$k = C_v m_v \gamma_w$$

The values are shown in table below:

Table 3.35. Consolidation and permeability properties of sample 1(dynamic at dry of optimum)

| Applied Pressure | Void ratio | Coefficient of compressibility, a_v (m^2/kN) | Coefficient of volume compressibility, m_v (m^2/kN) | Coefficient of consolidation, C_v (cm^2/sec) | Coefficient of permeability, k (cm/sec) |
|------------------|------------|--|---|--|---|
| kN/m^2 | e | | | | |
| 5 | 0.729 | | | | |
| 10 | 0.724 | 1.037×10^{-3} | 0.600×10^{-3} | | |
| 20 | 0.713 | 1.124×10^{-3} | 0.652×10^{-3} | | |
| 40 | 0.707 | 0.281×10^{-3} | 0.164×10^{-3} | 5.140×10^{-3} | 8.272×10^{-8} |
| 80 | 0.697 | 0.259×10^{-3} | 0.152×10^{-3} | 4.224×10^{-3} | 6.296×10^{-8} |
| 160 | 0.679 | 0.222×10^{-3} | 0.131×10^{-3} | 2.912×10^{-3} | 3.730×10^{-8} |
| 320 | 0.658 | 0.130×10^{-3} | 0.077×10^{-3} | 2.04×10^{-3} | 1.546×10^{-8} |
| 640 | 0.633 | 0.080×10^{-3} | 0.048×10^{-3} | 1.533×10^{-3} | 0.723×10^{-8} |

Table 3.36. Consolidation and permeability properties of sample 1(dynamic at OMC)

| Applied Pressure | Void ratio | Coefficient of compressibility, a_v (m^2/kN) | Coefficient of volume compressibility, m_v (m^2/kN) | Coefficient of consolidation, C_v (cm^2/sec) | Coefficient of permeability, k (cm/sec) |
|------------------|------------|--|---|--|---|
| kN/m^2 | e | | | | |
| 5 | 0.587 | | | | |
| 10 | 0.572 | 2.936×10^{-3} | 1.850×10^{-3} | | |
| 20 | 0.560 | 1.246×10^{-3} | 0.792×10^{-3} | | |
| 40 | 0.539 | 1.024×10^{-3} | 0.656×10^{-3} | 0.882×10^{-3} | 5.678×10^{-8} |
| 80 | 0.513 | 0.672×10^{-3} | 0.436×10^{-3} | 0.752×10^{-3} | 3.213×10^{-8} |
| 160 | 0.486 | 0.326×10^{-3} | 0.216×10^{-3} | 0.903×10^{-3} | 1.911×10^{-8} |
| 320 | 0.451 | 0.223×10^{-3} | 0.150×10^{-3} | 0.822×10^{-3} | 1.208×10^{-8} |
| 640 | 0.416 | 0.109×10^{-3} | 0.075×10^{-3} | 1.021×10^{-3} | 0.750×10^{-8} |

Table 3.37. Consolidation and permeability properties of sample 1(dynamic at wet of optimum)

| Applied Pressure | Void ratio | Coefficient of compressibility, a_v (m^2/kN) | Coefficient of volume compressibility, m_v (m^2/kN) | Coefficient of consolidation, C_v (cm^2/sec) | Coefficient of permeability, k (cm/sec) |
|------------------|------------|--|---|--|---|
| kN/m^2 | e | | | | |
| 5 | 0.668 | | | | |
| 10 | 0.653 | 3.086×10^{-3} | 1.850×10^{-3} | | |
| 20 | 0.639 | 1.309×10^{-3} | 0.792×10^{-3} | | |
| 40 | 0.618 | 1.076×10^{-3} | 0.656×10^{-3} | 1.016×10^{-3} | 6.541×10^{-8} |
| 80 | 0.590 | 0.705×10^{-3} | 0.436×10^{-3} | 1.033×10^{-3} | 4.414×10^{-8} |
| 160 | 0.562 | 0.343×10^{-3} | 0.216×10^{-3} | 1.277×10^{-3} | 2.703×10^{-8} |
| 320 | 0.525 | 0.234×10^{-3} | 0.150×10^{-3} | 1.124×10^{-3} | 1.652×10^{-8} |
| 640 | 0.483 | 0.132×10^{-3} | 0.087×10^{-3} | 0.957×10^{-3} | 0.815×10^{-8} |

Table 3.38. Consolidation and permeability properties of sample 1(static at dry of optimum)

| Applied Pressure | Void ratio | Coefficient of compressibility, a_v (m^2/kN) | Coefficient of volume compressibility, m_v (m^2/kN) | Coefficient of consolidation, C_v (cm^2/sec) | Coefficient of permeability, k (cm/sec) |
|------------------|------------|--|---|--|---|
| kN/m^2 | e | | | | |
| 5 | 0.729 | | | | |
| 10 | 0.709 | 3.977×10^{-3} | 2.300×10^{-3} | | |
| 20 | 0.695 | 1.426×10^{-3} | 0.835×10^{-3} | | |
| 40 | 0.687 | 0.411×10^{-3} | 0.242×10^{-3} | 4.172×10^{-3} | 9.916×10^{-8} |
| 80 | 0.666 | 0.508×10^{-3} | 0.301×10^{-3} | 1.581×10^{-3} | 4.670×10^{-8} |
| 160 | 0.637 | 0.373×10^{-3} | 0.224×10^{-3} | 1.533×10^{-3} | 3.365×10^{-8} |
| 320 | 0.610 | 0.165×10^{-3} | 0.101×10^{-3} | 1.589×10^{-3} | 1.570×10^{-8} |
| 640 | 0.581 | 0.092×10^{-3} | 0.057×10^{-3} | 1.781×10^{-3} | 0.997×10^{-8} |

Table 3.39. Consolidation and permeability properties of sample 1(static at OMC)

| Applied Pressure | Void ratio | Coefficient of compressibility, a_v (m^2/kN) | Coefficient of volume compressibility, m_v (m^2/kN) | Coefficient of consolidation, C_v (cm^2/sec) | Coefficient of permeability, k (cm/sec) |
|------------------|------------|--|---|--|---|
| kN/m^2 | e | | | | |
| 5 | 0.587 | | | | |
| 10 | 0.571 | 3.142×10^{-3} | 1.980×10^{-3} | | |
| 20 | 0.562 | 0.960×10^{-3} | 0.611×10^{-3} | | |
| 40 | 0.546 | 0.774×10^{-3} | 0.495×10^{-3} | 0.640×10^{-3} | 3.110×10^{-8} |
| 80 | 0.527 | 0.490×10^{-3} | 0.317×10^{-3} | 0.626×10^{-3} | 1.946×10^{-8} |
| 160 | 0.509 | 0.226×10^{-3} | 0.148×10^{-3} | 0.561×10^{-3} | 0.815×10^{-8} |
| 320 | 0.484 | 0.152×10^{-3} | 0.101×10^{-3} | 0.503×10^{-3} | 0.498×10^{-8} |
| 640 | 0.454 | 0.094×10^{-3} | 0.064×10^{-3} | 0.485×10^{-3} | 0.303×10^{-8} |

Table 3.40. Consolidation and permeability properties of sample 1 (static at wet of optimum)

| Applied Pressure | Void ratio | Coefficient of compressibility, a_v (m ² /kN) | Coefficient of volume compressibility, m_v (m ² /kN) | Coefficient of consolidation, C_v (cm ² /sec) | Coefficient of permeability, k (cm/sec) |
|-------------------|------------|--|---|--|---|
| kN/m ² | e | | | | |
| 5 | 0.668 | | | | |
| 10 | 0.651 | 3.303×10^{-3} | 1.980×10^{-3} | | |
| 20 | 0.641 | 1.009×10^{-3} | 0.611×10^{-3} | | |
| 40 | 0.625 | 0.813×10^{-3} | 0.495×10^{-3} | 1.505×10^{-3} | 7.314×10^{-8} |
| 80 | 0.605 | 0.515×10^{-3} | 0.317×10^{-3} | 1.471×10^{-3} | 4.573×10^{-8} |
| 160 | 0.586 | 0.238×10^{-3} | 0.148×10^{-3} | 1.708×10^{-3} | 2.482×10^{-8} |
| 320 | 0.560 | 0.160×10^{-3} | 0.101×10^{-3} | 1.662×10^{-3} | 1.646×10^{-8} |
| 640 | 0.528 | 0.099×10^{-3} | 0.064×10^{-3} | 1.793×10^{-3} | 1.120×10^{-8} |

The rest of the tables of consolidation and permeability properties of rest of the samples are shown in Appendix IV.

It is evident from the above results that, as the consolidation pressure increases, the coefficient of compressibility and volume compressibility decrease for all soil samples. This is because as the pressure increases, the soil becomes denser and less permeable, so it takes longer for the pore water pressure to dissipate and soil to consolidate.

The correlation between the coefficient of permeability and void ratio is illustrated below for sample 1 with the help of some graphs:

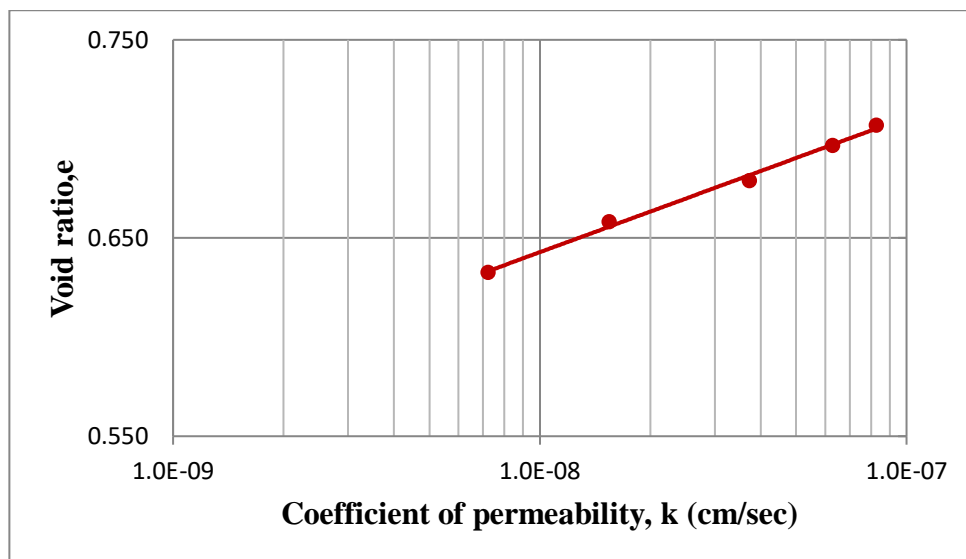


Figure 3.233 Void ratio vs. Coefficient of permeability for sample 1 (dynamic at dry of optimum)

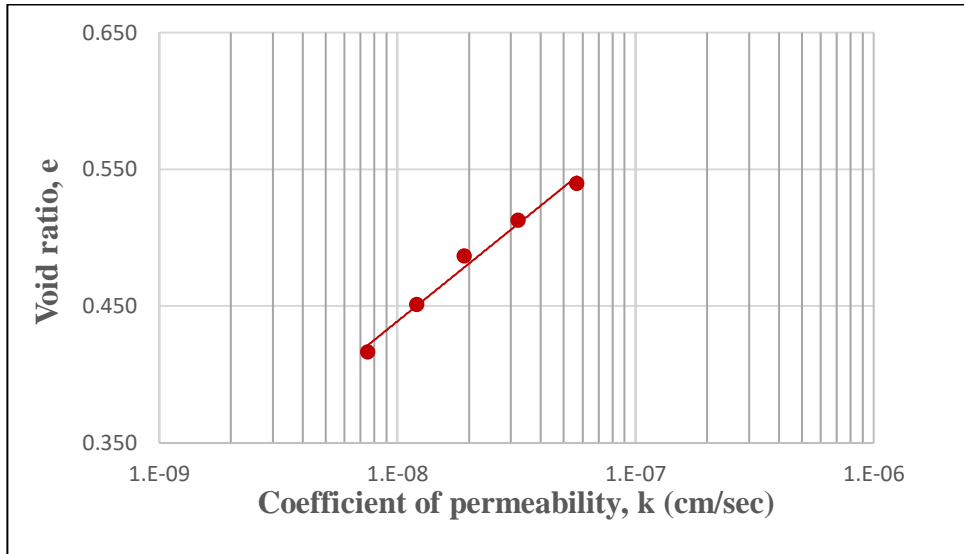


Figure 3.234: Void ratio vs. Coefficient of permeability for sample 1 (dynamic at optimum moisture content)

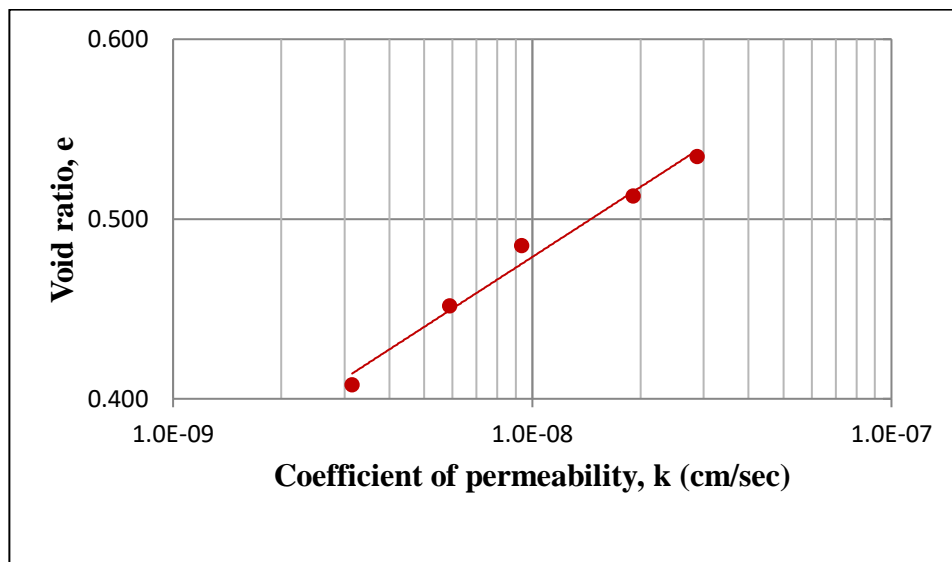


Figure 3.235: Void ratio vs. Coefficient of permeability for sample 1 (dynamic at wet of optimum)

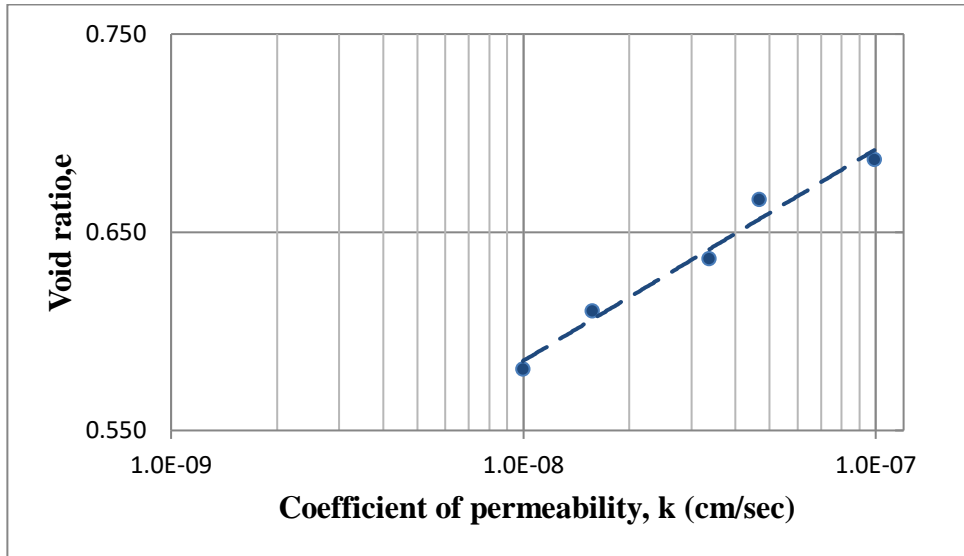


Figure 3.236: Void ratio vs. Coefficient of permeability for sample 1 (static at dry of optimum)

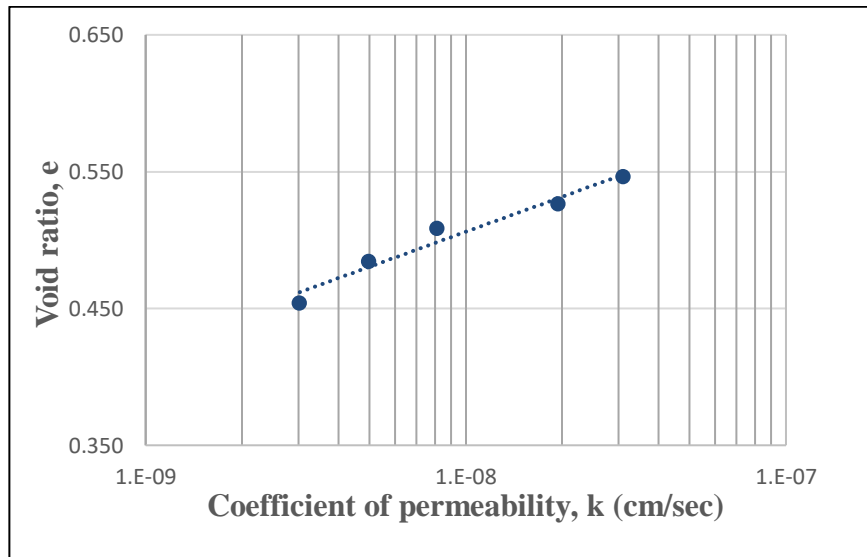


Figure 3.237: Void ratio vs. Coefficient of permeability for sample 1 (static at optimum moisture)

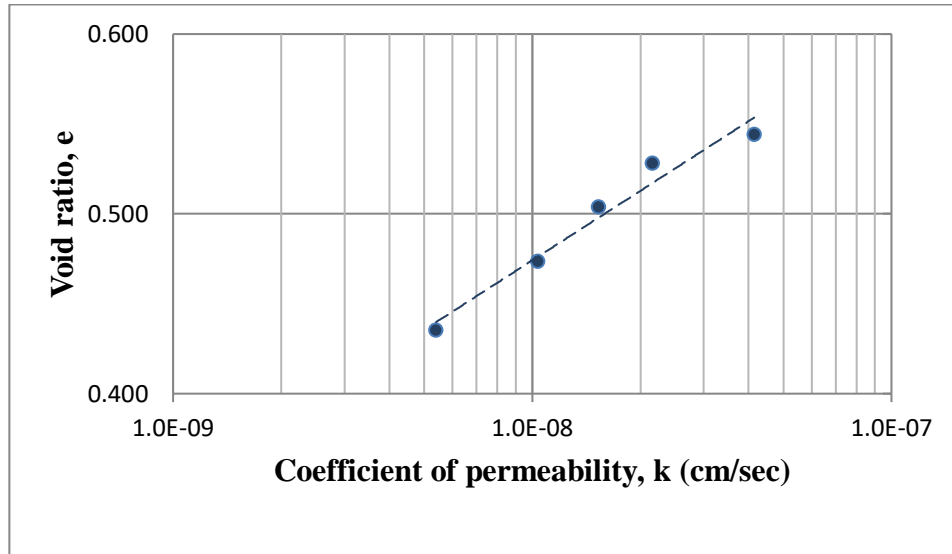


Figure 3.238: Void ratio vs. Coefficient of permeability for sample 1 (static at wet of optimum)

The graphs illustrate a consistent trend wherein the coefficient of permeability declines as the void ratio decreases. This signifies that in all soil samples, an increase in consolidation pressure leads to a decrease in permeability. As consolidation pressure intensifies, soil particles move closer, causing a compression in the size and structure of the voids between them. Permeability pertains to the flow rate resulting from seepage through these voids; thus, a reduction in the dimensions of the seepage pathway corresponds to a proportional drop in permeability.

The remaining graphs are shown in figure 3.239 to figure 3.262 in Appendix V.

CHAPTER 4

ANALYSIS OF COMPRESSIBILITY CHARACTERISTICS

4.1. Analysis for compressibility characteristics at dry of optimum, optimum moisture content and wet of optimum moisture content.

In the subsequent section, analysis is done about the compressibility findings derived from the consolidation process of soils subjected to both static and dynamic compaction. The analysis focuses on conditions at the dry of optimum, optimal moisture content (OMC), and wet of optimum.

4.1.1. At dry of optimum moisture content:

The compressibility traits resulting from both static and dynamic compaction at the dry side of the optimum have been superimposed onto a single graph for each sample. These graphical representations are displayed from Fig. 4.1 to Fig. 4.5 below.

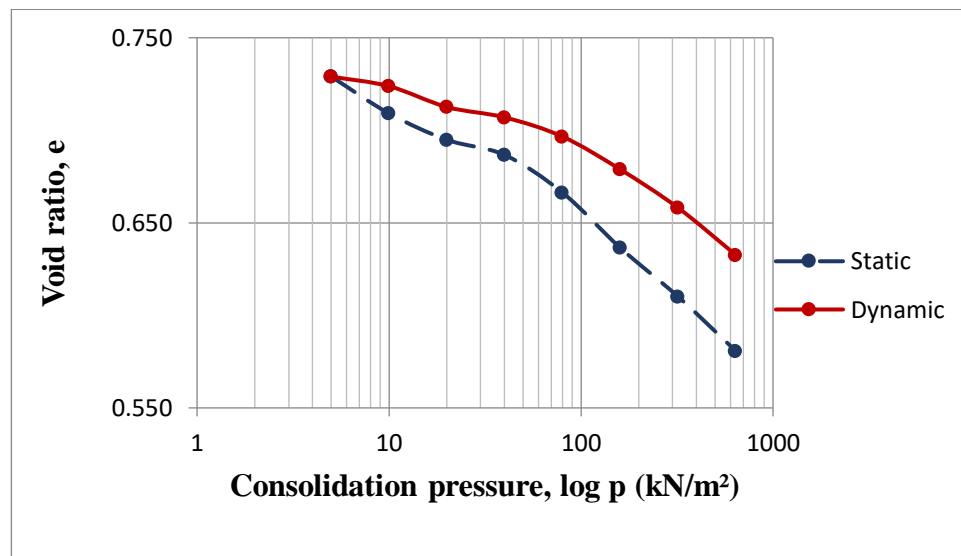


Figure 4.1: Void ratio vs consolidation pressure curve for S1(dry)

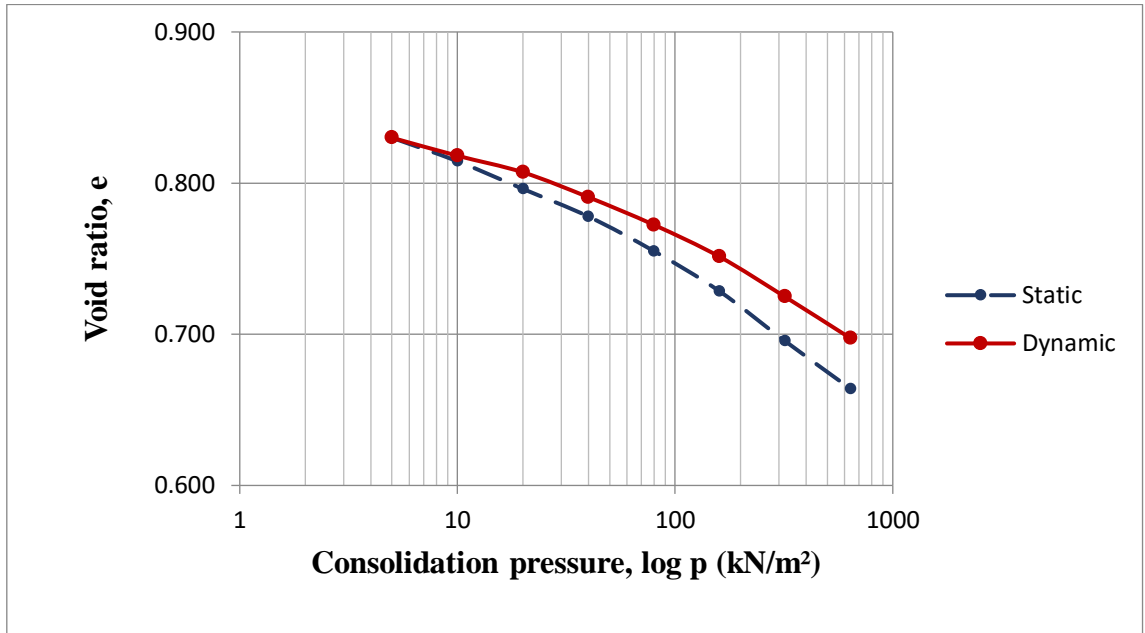


Figure 4.2: Void ratio vs consolidation pressure curve for S2(dry)

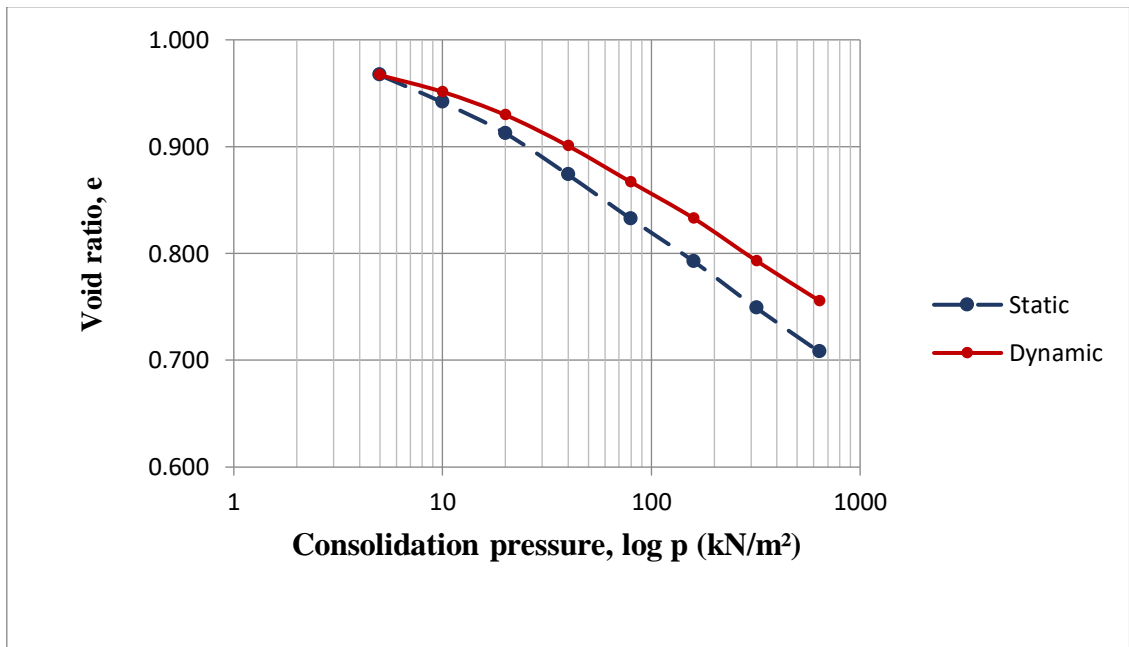


Figure 4.3: Void ratio vs consolidation pressure curve for S3(dry)

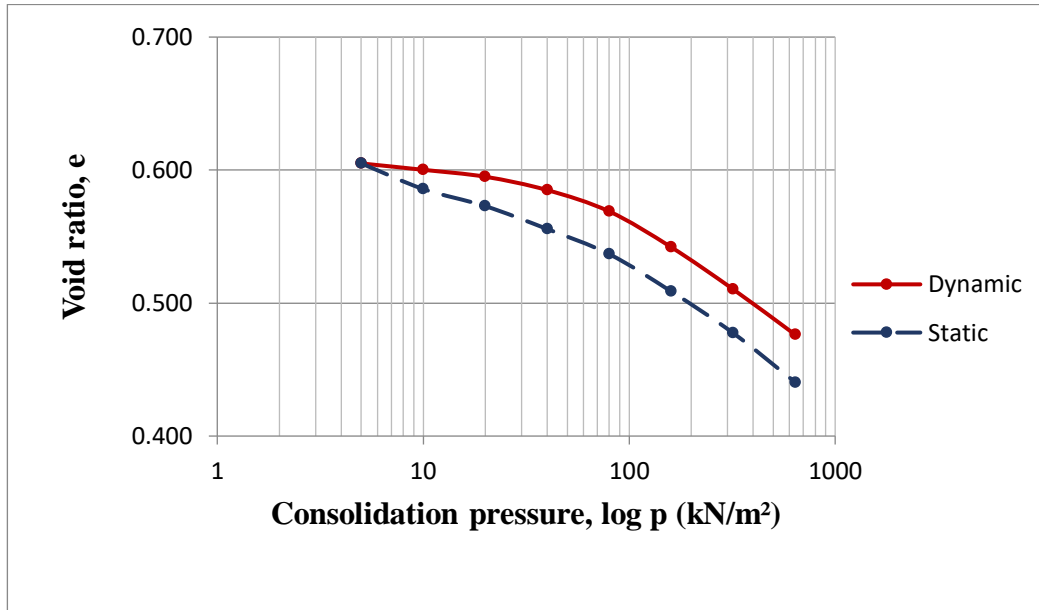


Figure 4.4: Void ratio vs consolidation pressure curve for S4(dry)

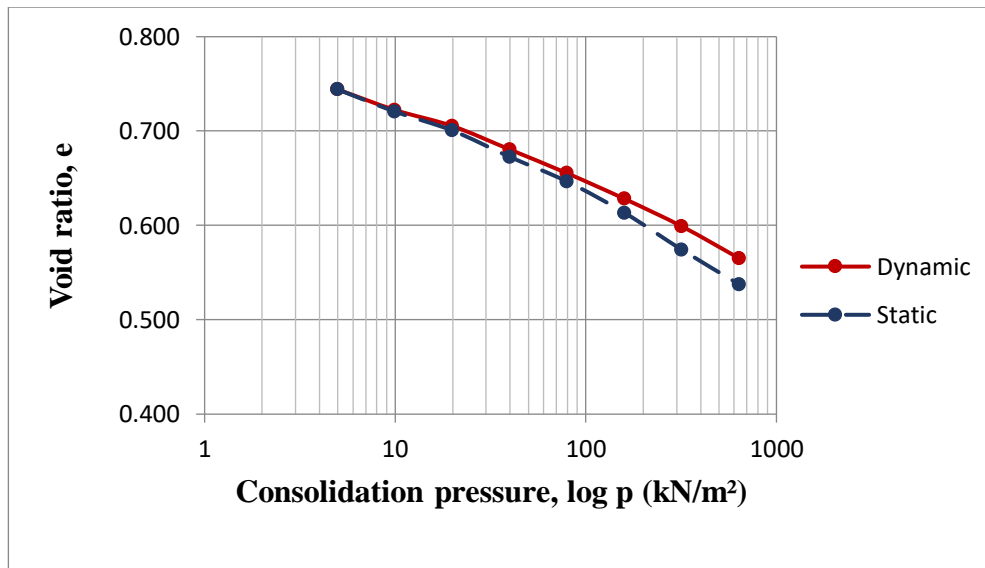


Figure 4.5: Void ratio vs consolidation pressure curve for S5(dry)

When consolidation was executed on the dry side of the optimum moisture content, for both statically and dynamically compacted soil, a consistent trend emerged in the plots of void ratio (e) against consolidation pressure (p) on a semi-logarithmic scale. Across all samples, the curve representing dynamically compacted soil consistently positioned itself above the curve associated with statically compacted soil.

The compression index (C_c) was assessed for all samples at stress levels of 320 kPa and 640 kPa. The corresponding values of Compression Index (C_c) are presented in the table below in Table 4.1.

Table 4.1: Compression Index (C_c) values for static and dynamic compaction at dry of optimum

| SAMPLE NO. | Compression Index (C_c) | |
|------------|-----------------------------|---------|
| | STATIC | DYNAMIC |
| S1 | 0.10 | 0.08 |
| S2 | 0.10 | 0.09 |
| S3 | 0.14 | 0.12 |
| S4 | 0.12 | 0.11 |
| S5 | 0.12 | 0.11 |

The table reveals that the compression index (C_c) value for statically compacted soil is slightly greater than that for dynamically compacted soil. This suggests that statically compacted soil exhibits higher compressibility compared to dynamically compacted soil.

As described by Delage et al. (1996), when situated on the dry side of the optimum, the soil's structure maintains a flocculated arrangement. This arrangement contributes to the samples augmented internal cohesion, primarily due to elevated suction levels. This increased cohesion serves to hinder complete disintegration or reconfiguration during the compaction process, leading to the emergence of aggregates and substantial inter-aggregate pores. On the other hand, as highlighted by Dario et al. (2011), it's conceivable that the prevalence of interparticle forces could be disrupted by dynamic compaction, giving rise to structures characterized by diminished shear strength.

However, in the above case it is seen that static compaction is overcoming the internal cohesion between the interparticles of soil than the dynamic compaction. This could be because the static pressure used in static compaction was better at disrupting the forces between particles, which dynamic compaction didn't achieve as effectively. This potentially explains by the fact that statically compacted soil is more compressible than dynamically compacted soil.

4.1.2. At optimum moisture content:

The compressibility characteristics arising from both static and dynamic compaction at the optimum moisture content have been combined onto a single graph for each sample. These visual representations are depicted in Figures 4.6 through 4.10 presented below.

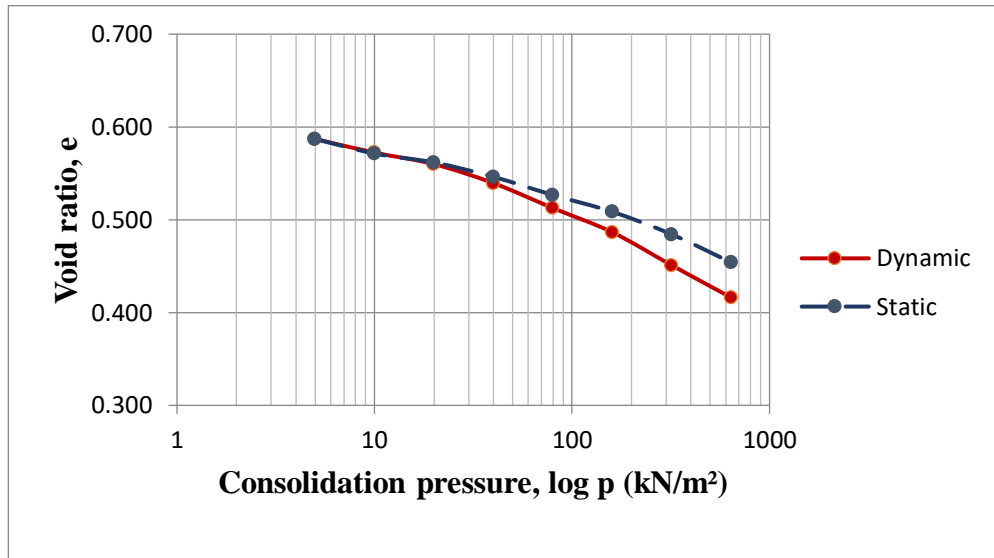


Figure 4.6: Void ratio vs consolidation pressure curve for S1(OMC)

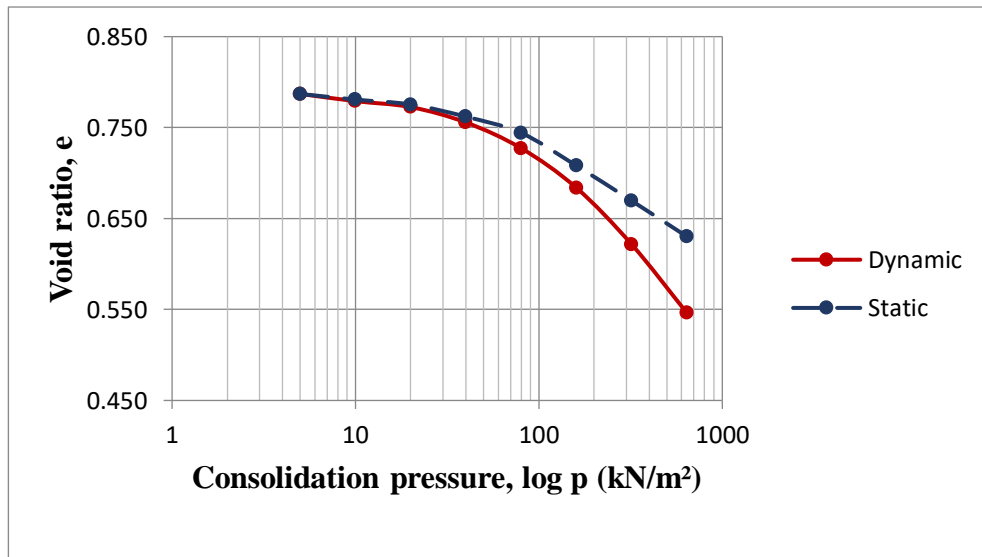


Figure 4.7: Void ratio vs consolidation pressure curve for S2 (OMC)

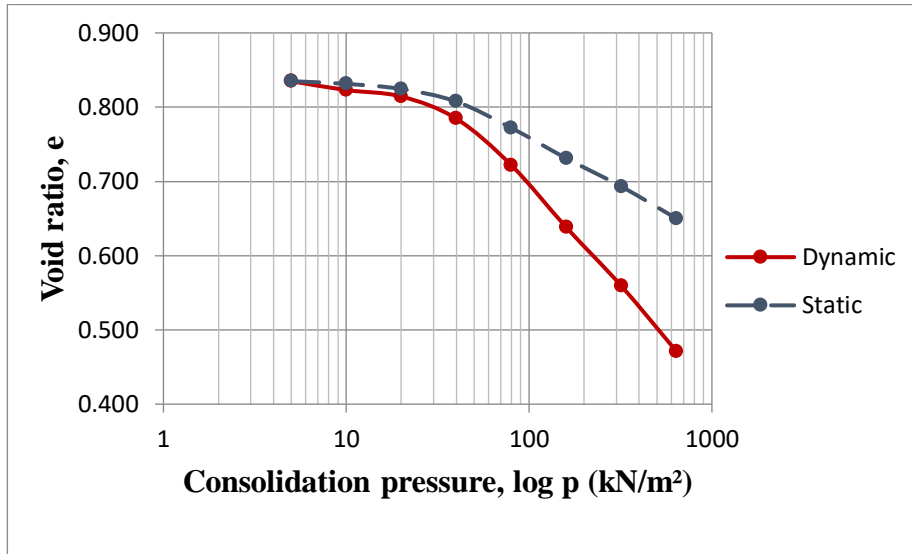


Figure 4.8: Void ratio vs consolidation pressure curve for S3(OMC)

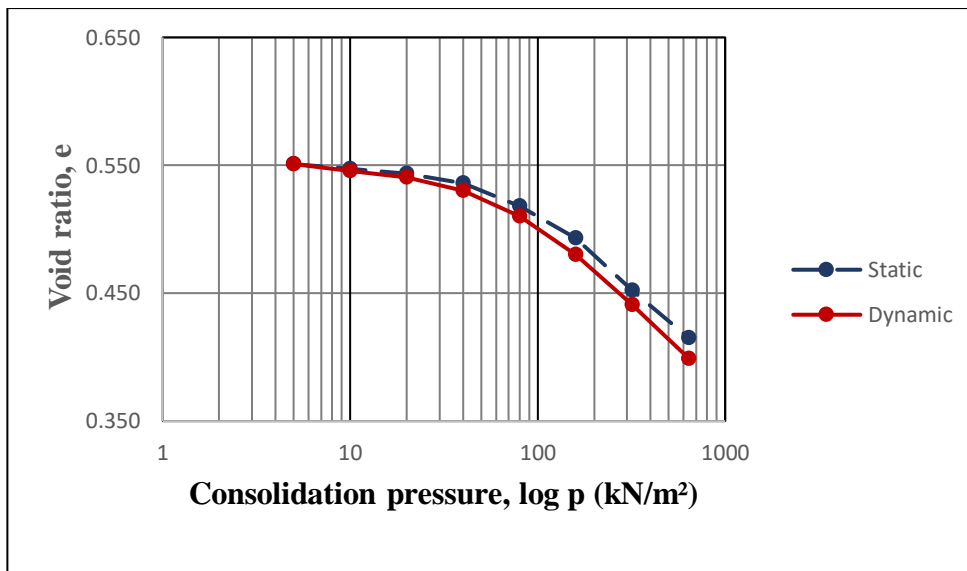


Figure 4.9: Void ratio vs consolidation pressure curve for S4(OMC)

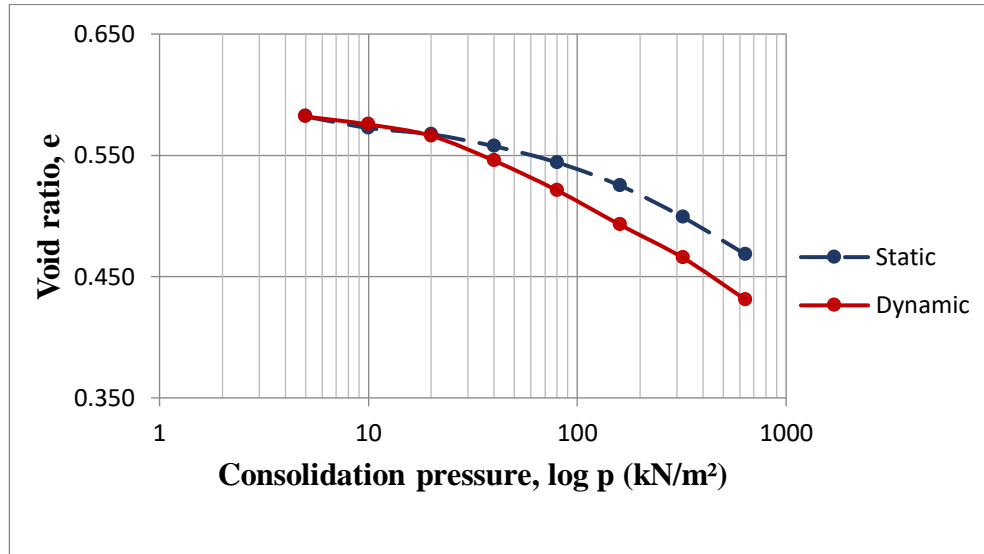


Figure 4.10: Void ratio vs consolidation pressure curve for S5(OMC)

When consolidation took place at the optimum moisture content for both statically and dynamically compacted soil, a uniform pattern became evident in the semi-logarithmic plots of void ratio (e) against consolidation pressure (p). Across all samples, the curve representing statically compacted soil consistently remained positioned above the curve corresponding to dynamically compacted soil.

The compression index (C_c) was evaluated for all samples under stress conditions of 320 kPa and 640 kPa. The corresponding C_c values are presented in the table below in Table 2.

Table 4.2: Compression Index (C_c) values for static and dynamic compaction at OMC

| SAMPLE NO. | Compression Index (C_c) | |
|------------|-----------------------------|---------|
| | STATIC | DYNAMIC |
| S1 | 0.10 | 0.12 |
| S2 | 0.13 | 0.25 |
| S3 | 0.14 | 0.29 |
| S4 | 0.12 | 0.14 |
| S5 | 0.11 | 0.12 |

The table illustrates that the compression index (C_c) value for dynamically compacted soil slightly surpasses that of statically compacted soil. This indicates that the dynamically compacted soil displays greater compressibility in comparison to the statically compacted counterpart.

Based on the research conducted by Dario et al. (2011), it has been noted that for clayey soil specimens compacted statically at optimal moisture content (OMC), distinct characteristics of original microaggregation are evident. These features include the presence of original nodules, formation of isolated gaps, and the development of fissured and oriented porosity (approximately 3%). Conversely, under the same moisture content conditions, specimens that were dynamically compacted exhibit fewer signs of original microaggregation, with nearly all porosity lost (around 2%).

According to Dario et al. (2011), the dominance of interparticle forces that were disrupted by dynamic compaction resulted in structures displaying reduced shear strength. A similar pattern was observed by Bueno et al. (1992) when investigating the impact of dynamic compaction on a red-yellow latosol and comparing its mechanical response to its undisturbed field condition.

Mitchell et al (1965) conducted a study and examined how the permeability of silty clay is affected by the compaction method. They observed that the clay's structure experiences significant changes due to shear strains caused by compaction performed. Furthermore, various compaction methods lead to varying levels of shear strain. Seed and Chan also investigated the impact of compaction methods on characteristics like swelling, shrinkage, and stress-strain behavior in compacted clays. The sequence of compaction procedures that results in increasing shear strain and thus greater dispersion is as follows: static, vibratory, and kneading.

Based on the preceding explanation, it can be concluded that dynamic compaction generates higher shear strain in the soil when compared to static compaction. This leads to the observation that soil compacted dynamically exhibits greater compressibility compared to soil compacted statically.

4.1.3. At wet of optimum moisture content:

The compressibility characteristics resulting from both static and dynamic compaction at the wet side of optimum moisture content have been integrated into a single graph for each sample. These graphical depictions are shown in Figures 4.11 through 4.15 provided below.

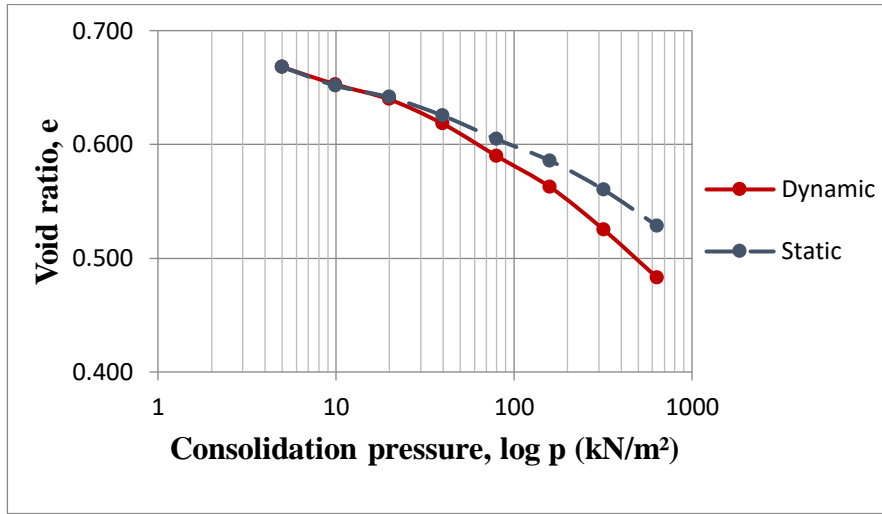


Figure 4.11: Void ratio vs consolidation pressure curve for S1(wet)

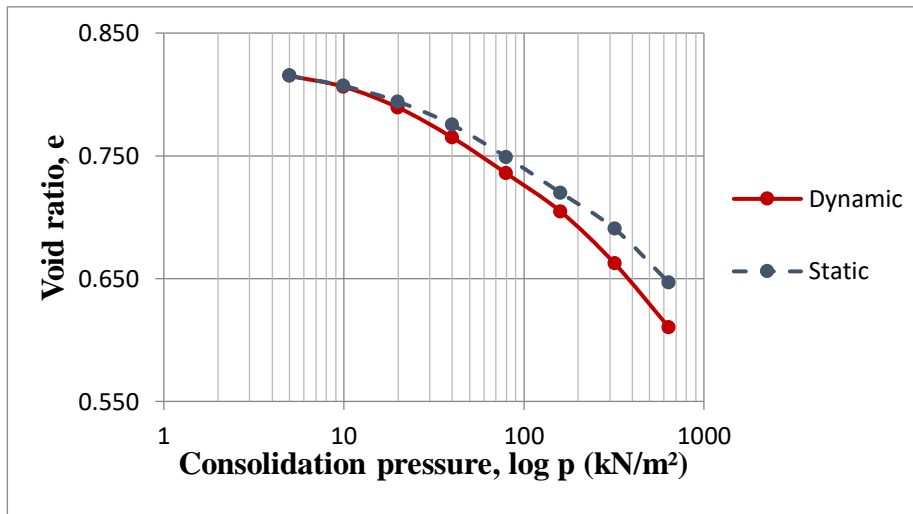


Figure 4.12: Void ratio vs consolidation pressure curve for S2(wet)

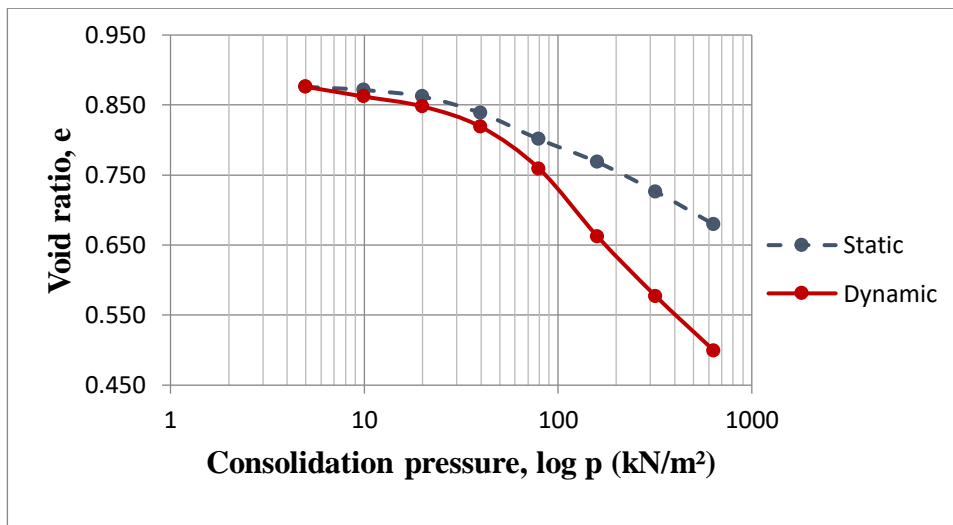


Figure 4.13: Void ratio vs consolidation pressure curve for S3(wet)

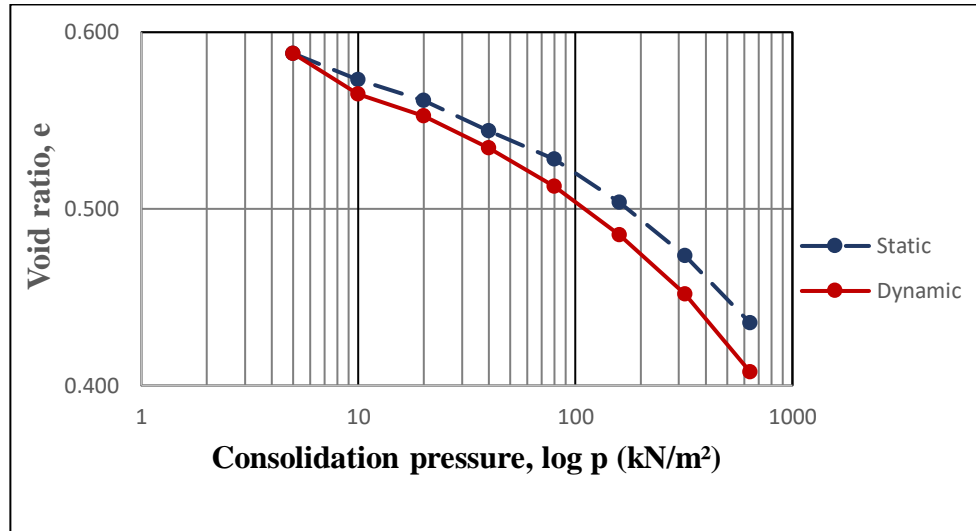


Figure 4.14: Void ratio vs consolidation pressure curve for S4(wet)

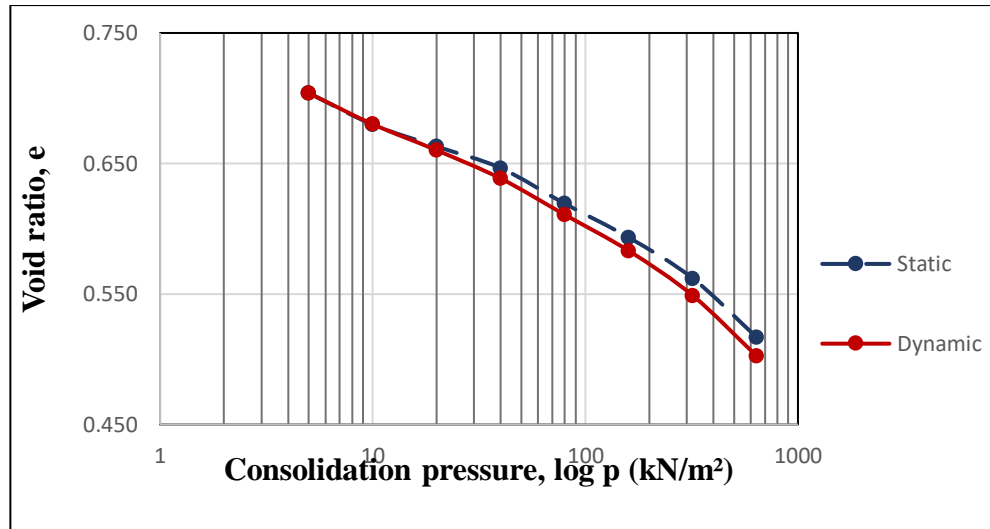


Figure 4.15: Void ratio vs consolidation pressure curve for S5(wet)

A uniform pattern became evident in the combined plots of void ratio (e) against consolidation pressure (p) using a semi-logarithmic scale when consolidation occurred at the wet side of the optimal moisture content for both statically and dynamically compacted soil. Across all samples, the curve representing statically compacted soil consistently maintained a position above the curve corresponding to dynamically compacted soil.

The compression index (C_c) was determined for all samples at stress levels of 320 kPa and 640 kPa. The corresponding C_c values are tabulated below in Table 3.

Table 4.3: Compression Index (C_c) values for static and dynamic compaction at wet of optimum

| SAMPLE NO. | Compression Index (C_c) | |
|------------|-----------------------------|---------|
| | STATIC | DYNAMIC |
| S1 | 0.11 | 0.14 |
| S2 | 0.14 | 0.17 |
| S3 | 0.16 | 0.26 |
| S4 | 0.13 | 0.15 |
| S5 | 0.15 | 0.16 |

The presented table indicates a slightly higher compression index (C_c) value for dynamically compacted soil in comparison to statically compacted soil. This indicates that the dynamically compacted soil showcases greater compressibility when contrasted with the statically compacted soil.

As moisture content surpasses the optimum level, a degree of swelling occurs alongside plastic deformation, contributing to an increased lubrication among soil particles. Mitchell et al. (1965) conducted a study to assess the influence of compaction methods on the permeability of silty clay. Their findings revealed significant alterations in the clay's structure due to shear strains induced by compaction performed beyond the line of optimum moisture content. Moreover, different compaction techniques yielded varying degrees of shear strain. Seed and Chan also examined the consequences of compaction methods on attributes such as swelling, shrinkage, and stress-strain behavior in compacted clays. The sequence of compaction procedures that results in increasing shear strain and thus greater dispersion is as follows: static, vibratory, and kneading.

Hence from the explanation provided earlier, it can be inferred that the dynamic compaction method induces a higher shear strain compared to static compaction. Consequently, soils compacted dynamically exhibit greater compressibility compared to those compacted statically.

4.2. Analysis for the combined consolidation plots (at dry, OMC and wet)

In this segment, the analysis on the compressibility traits acquired from the dry side of the optimum range, the Optimum Moisture Content (OMC), and the wet side of the optimum range is done and this analysis is carried out individually for both dynamic compaction and static compaction.

4.2.1. Analysis for the combined consolidation plots (at dry, OMC and wet) for dynamic compaction

The consolidation curves from dry of optimum, OMC and wet of optimum for dynamic compaction are superimposed in a graph for each sample and illustrated below from Fig. 4.16 to Fig. 4.20.

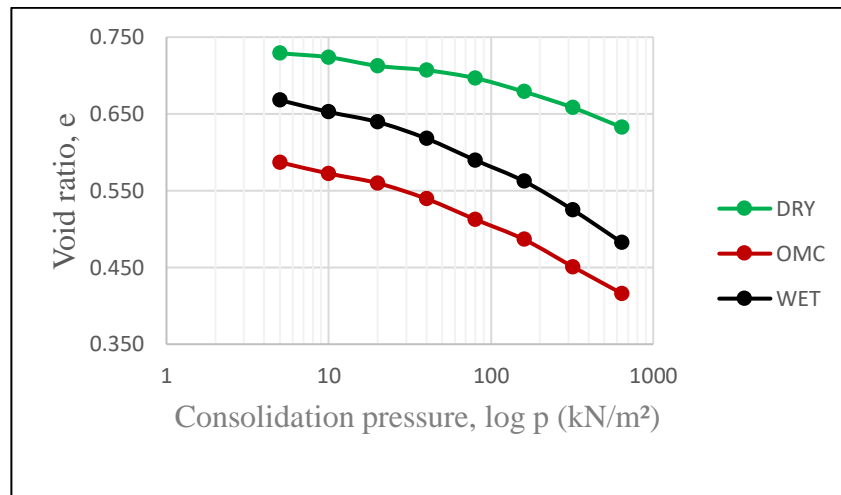


Figure 4.16. Void ratio vs consolidation pressure curve for S1

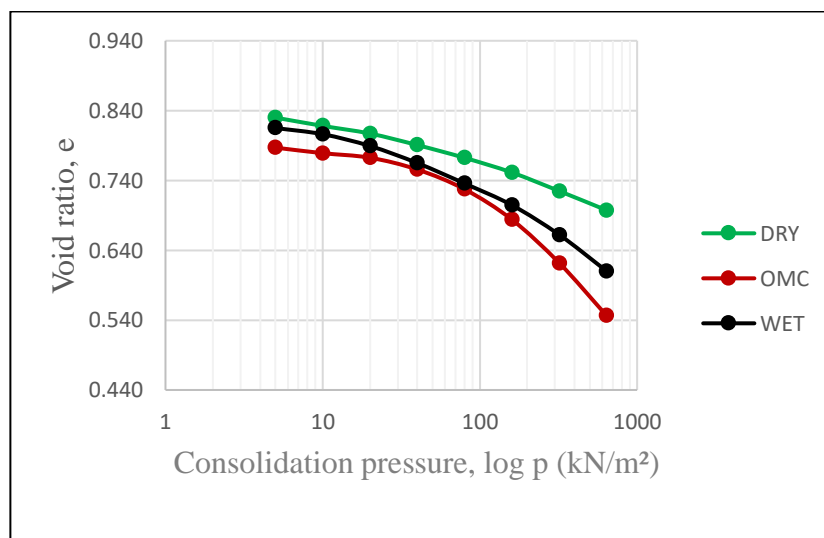


Figure 4.17: Void ratio vs consolidation pressure curve for S2

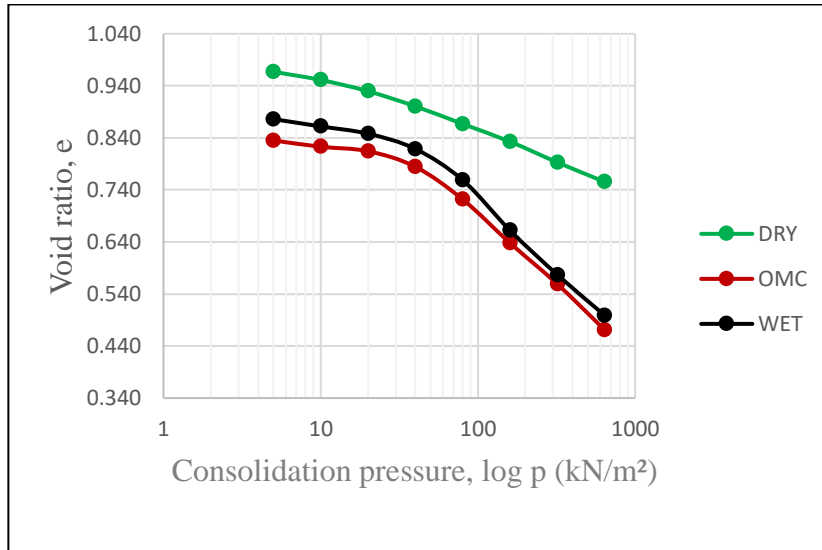


Figure 4.18: Void ratio vs consolidation pressure curve for S3

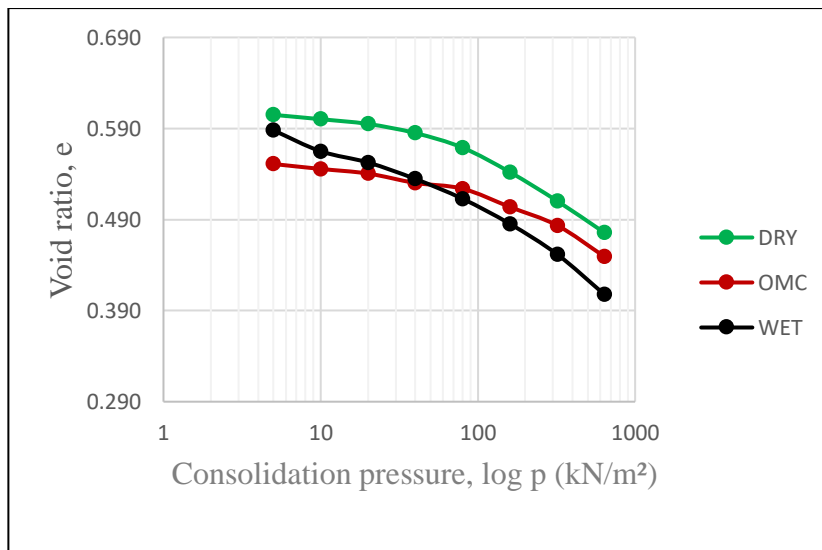


Figure 4.19: Void ratio vs consolidation pressure curve for S4

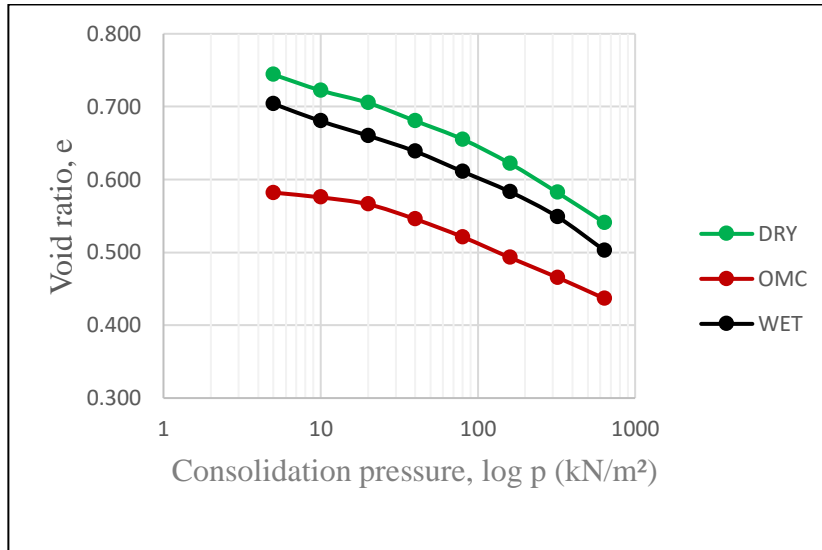


Figure 4.20: Void ratio vs consolidation pressure curve for S5

By examining the superimposed plots of void ratio (e) against consolidation pressure (p) acquired for dynamic compaction at the dry of optimum, optimal moisture content (OMC), and wet of optimum, a consistent trend emerges. In most instances, the consolidation curve corresponding to the dry of optimum condition is positioned at the uppermost point, followed by the curve for the wet side, and then the OMC curve.

This suggests that the void ratio on the dry side of the optimum is greater compared to those on the wet side and at OMC. Additionally, the void ratio on the wet side is marginally higher than the void ratio at OMC in nearly all samples subjected to both static and dynamic compaction.

In Diamond's (1970) investigation, the microstructure of compacted kaolinite and illite was scrutinized using scanning electron microscopy and mercury intrusion porosimetry. The outcomes revealed that on the dry side of the specimens, there were clusters of platelets measuring around $5 \mu\text{m}$, alongside substantial pores averaging $0.5 \mu\text{m}$ in diameter located between these aggregates. Conversely, the structure on the wet side exhibited a higher density and lacked significant pores. Diamond inferred that the formation of platelet clusters on the dry side was influenced by capillary effects, and the existence of larger pores mitigated shrinkage on this side.

Ahmed et al. (1974) harnessed advancements in dehydration techniques and embraced the freeze-drying approach, which involves rapid freezing using liquid nitrogen followed by vacuum-induced sublimation. This method was employed to remove water without inducing

shrinkage due to air-water capillary forces. The researchers scrutinized the microstructure of compacted illite within a porosimeter, and they compared particle size distribution (PSD) curves of specimens compacted through distinct methods: dynamic compaction in a Proctor mold, static compaction, and kneading. The findings revealed minimal disparity among these three laboratory preparation techniques, with the presence of comparable minute pores measuring less than 0.1 μm . This observation pointed toward analogous porosity characteristics. Consequently, the porosity attributes remain consistent for soil samples compacted either statically or dynamically, provided they share identical maximum dry unit weight and optimum moisture content.

Delage et. al (1996) performed a static compaction experiment on air-dried soil specimens, compacting them in three layers using a 38mm cylindrical mold. They discovered that subjecting the sample to the same maximum stress (845 kPa) while compacting it at the optimum moisture content (OMC) yielded a consistent dry unit weight across all three soil layers within acceptable margins. They enhanced the freeze-drying method utilized by Ahmed et al. (1974) by accelerating the freezing process to minimize changes in volume.

Mercury intrusion analysis of pore size distribution revealed that the sample at OMC exhibited the smallest overall pore volume, which correlated with its highest dry unit weight. Nevertheless, the remaining two samples displayed differing total pore volumes despite sharing the same dry unit weight. Through scanning electron microscopy, it was observed that the sample at the optimum water content displayed individual grains without clearly defined aggregates or pores between aggregates. This suggested the absence of larger pores in the dry sample, which were instead substituted by a less organized distribution of pore sizes ranging from 0.6 to 20 μm .

Comparing the dry, wet, and OMC curves, it becomes evident that an intermediary phase exists between the substantial pores of the dry sample and the saturated sample. At the OMC, these large pores are no longer present.

At the dry side of the optimum, soil samples exhibit heightened internal cohesion due to increased suction. This increased suction prevents complete breakdown or remolding during compaction, resulting in the presence of aggregates and significant inter-aggregate pores. When at the optimal moisture content (OMC), the aggregates within the samples become

more malleable and susceptible to breaking, leading to the creation of a compact and solid matrix microstructure.

Conversely, on the wet side of the spectrum, a distinct scenario emerges. As a result of hydration and an equivalent clay content, the volume occupied by clay particles increases, and silt grains become enveloped by a clay paste. This permits compaction to occur primarily through the plastic deformation of the clay paste, as opposed to the breakdown and remolding of granular aggregates. Water, previously under suction in its powder state, transitions to neutral or positive pressures and could potentially store some elastic energy, subsequently released when compaction stress is relieved.

As suggested by Delage et. al (1996), in the dry sample, the aggregates retain pore water, while inter-aggregate pores contain air. In the OMC sample, air occupies the larger, poorly sorted porosity with radii exceeding 1-2 μm . In the wet sample, the clay matrix seems to be saturated with water, and air is only found in a restricted number of pores larger than 1-2 μm in radius.

This provides a distinct understanding that the highest void ratio is observed on the dry side of the optimum, followed by the wet side, and then at the optimal moisture content (OMC).

4.2.2. Analysis for the combined consolidation plots (at dry, OMC and wet) for static compaction

The consolidation curves related to static compaction, encompassing the dry side of the optimum range, the Optimum Moisture Content (OMC), and the wet side of the optimum range, are superimposed on a graph for each sample. This graphical depiction extends from Fig. 4.21 to Fig. 4.25.

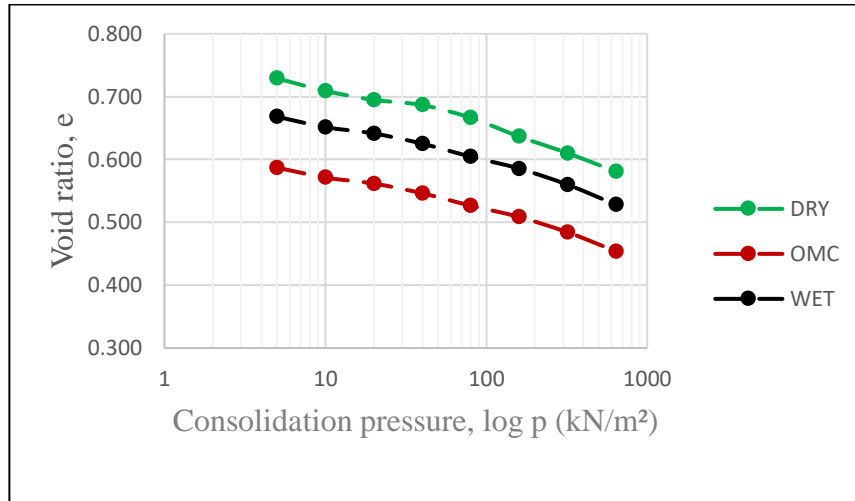


Figure 4.11. Void ratio vs consolidation pressure curve for S1

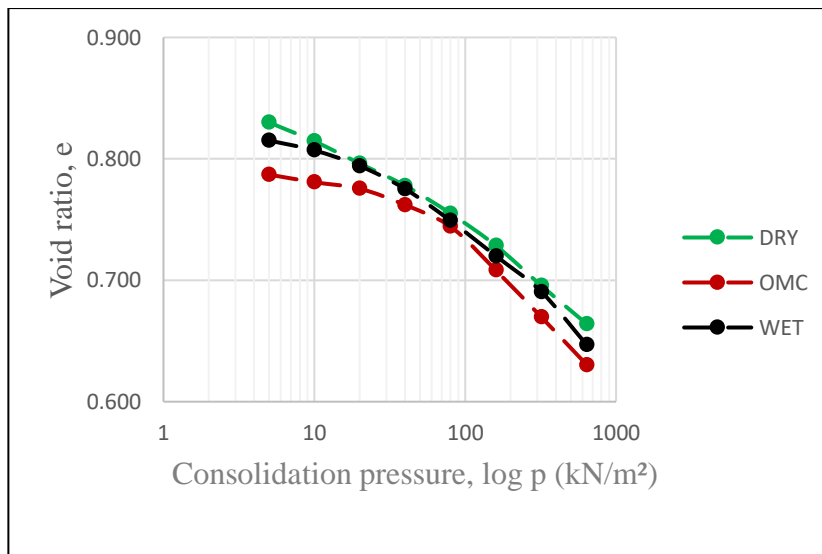


Figure 4.22: Void ratio vs consolidation pressure curve for S2

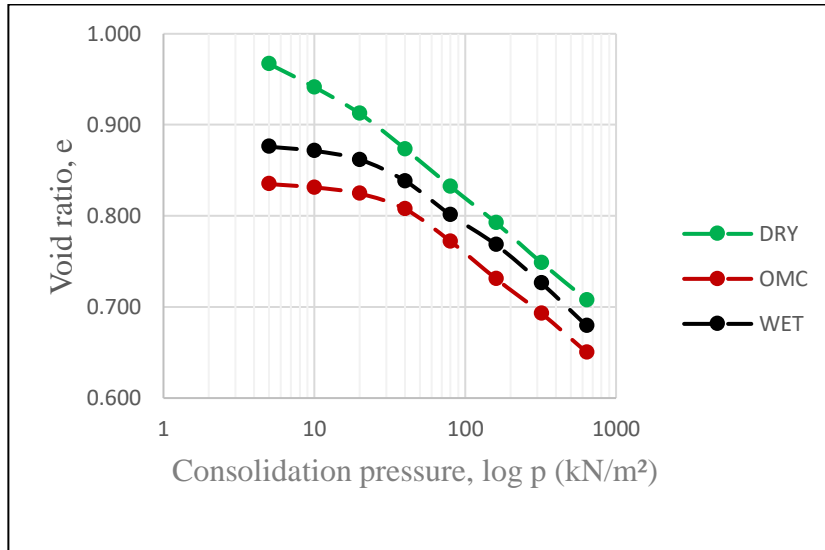


Figure 4.23: Void ratio vs consolidation pressure curve for S3

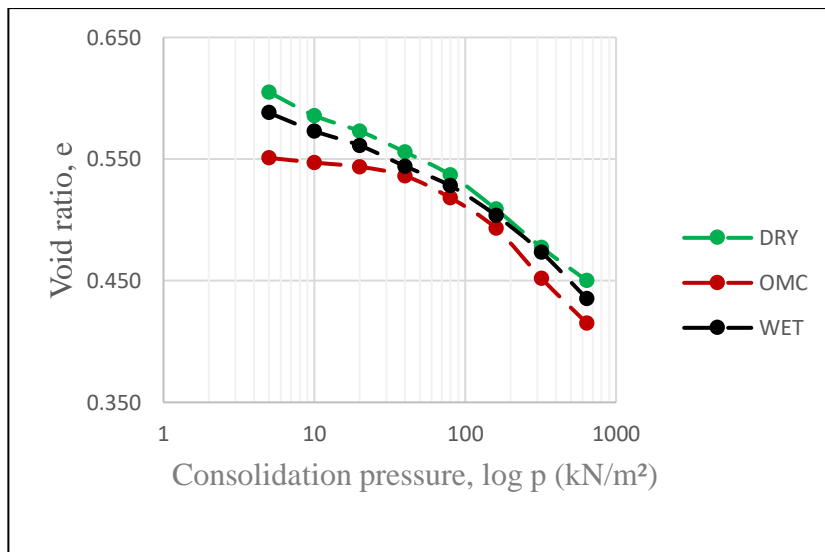


Figure 4.24: Void ratio vs consolidation pressure curve for S4

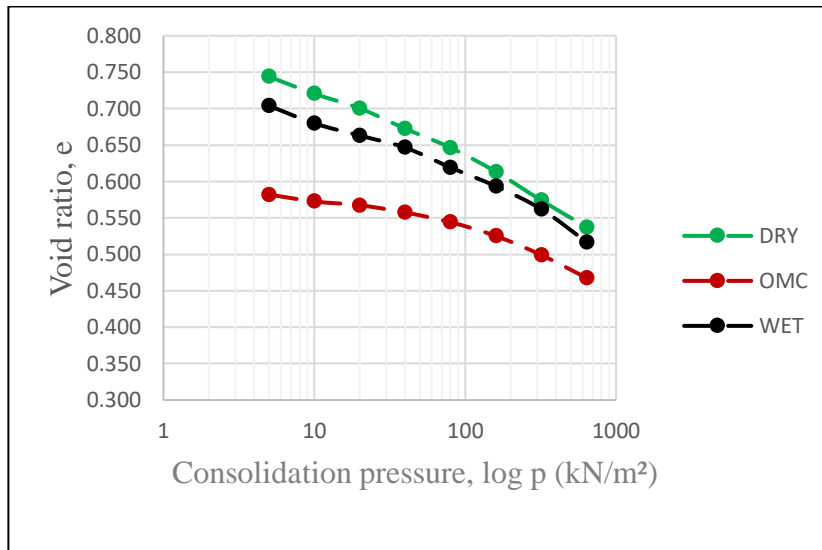


Figure 4.25: Void ratio vs consolidation pressure curve for S5

Upon analyzing the superimposed plots of void ratio (e) against consolidation pressure (p) obtained through static compaction at different moisture levels—the dry side of optimum, optimal moisture content (OMC), and wet side of optimum—a consistent trend becomes apparent. In all cases, the consolidation curve corresponding to the dry side of optimum condition is situated at the highest point, followed by the curve representing the wet side, and then the OMC curve.

This trend suggests that the void ratio on the dry side of the optimum displays a larger value compared to those observed on the wet side and at the OMC. Furthermore, the void ratio on the wet side shows a minor increase relative to the void ratio at the OMC across the majority of samples subjected to static compaction.

The insights provided within section 4.2.1 of the chapter contribute to comprehending the underlying factors behind the observed trends in compressibility. This section explores the mechanisms governing the connection between soil moisture content and compressibility. By referring to the explanations outlined in this specific segment of the chapter, a clearer understanding emerges regarding the reasons driving the patterns in soil compressibility observed. This integration of knowledge from section 4.2.1 assists in illuminating the interplay of factors that influence the highlighted compressibility trends within the observations.

This provides a distinct understanding that the highest void ratio is observed on the dry side of the optimum, followed by the wet side, and then at the optimal moisture content (OMC).

CHAPTER 5

ANALYSIS FOR PERMEABILITY CHARACTERISTICS

5.1. Analysis of permeability characteristics for static and dynamic compaction across dry side, optimal moisture content (OMC), and wet side of optimum

The examination of permeability characteristics for both static and dynamic compaction across the dry side, optimal moisture content (OMC), and wet side of the optimum is elaborated upon below.

5.1.1. Analysis of permeability characteristics for dynamic and static compaction at dry side of optimum

The graphs from Figure 5.1 to Figure 5.5 depict the superimposed void ratio (e) vs coefficient of permeability (k) plot for both dynamic and static compaction on the dry side of the optimum range.

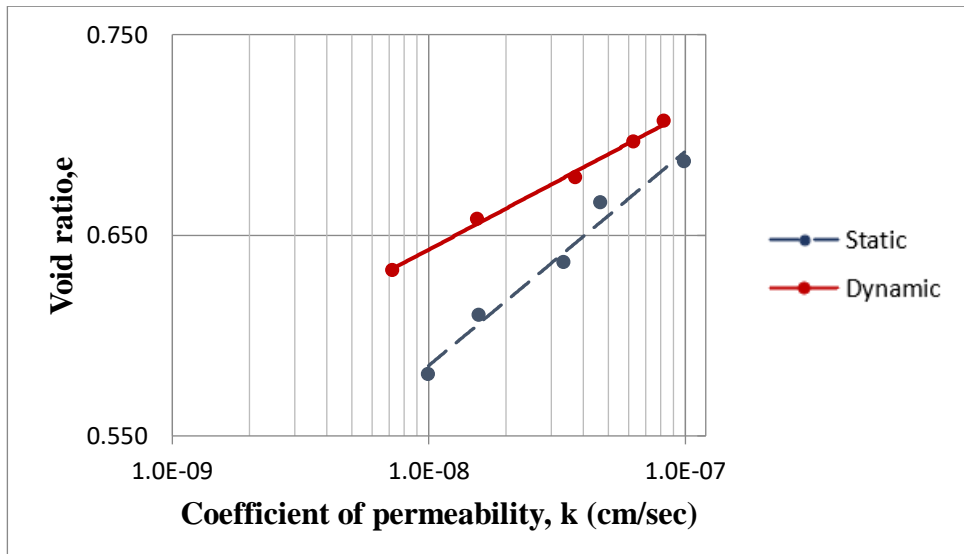


Figure 5.2. Void Ratio (e) vs. Coefficient of Permeability (k) for S1(dry)

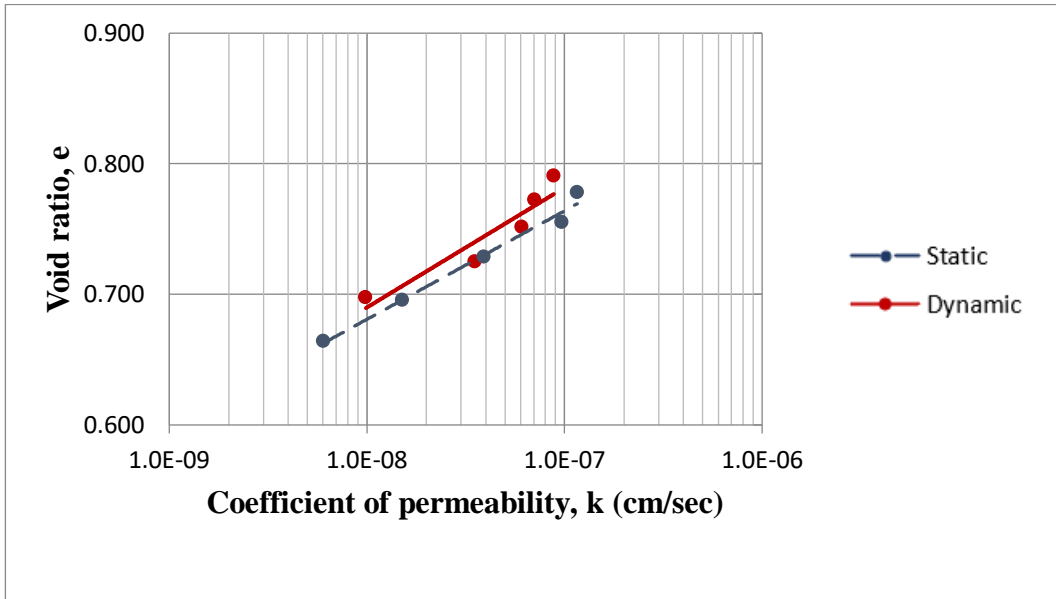


Figure 5.2: Void Ratio (e) vs. Coefficient of Permeability (k) for S2(dry)

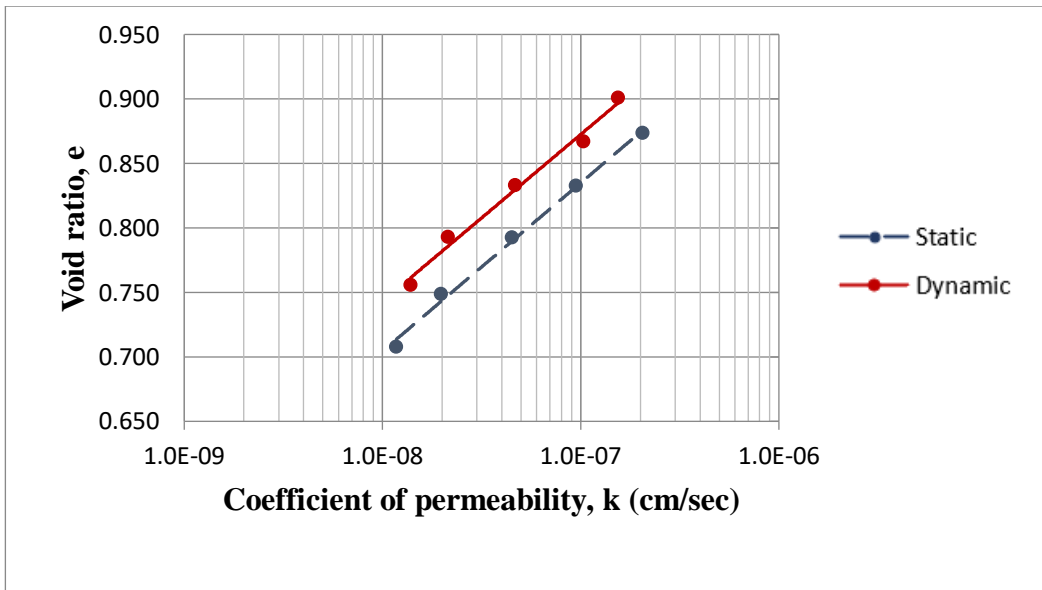


Figure 5.3: Void Ratio (e) vs. Coefficient of Permeability (k) for S3(dry)

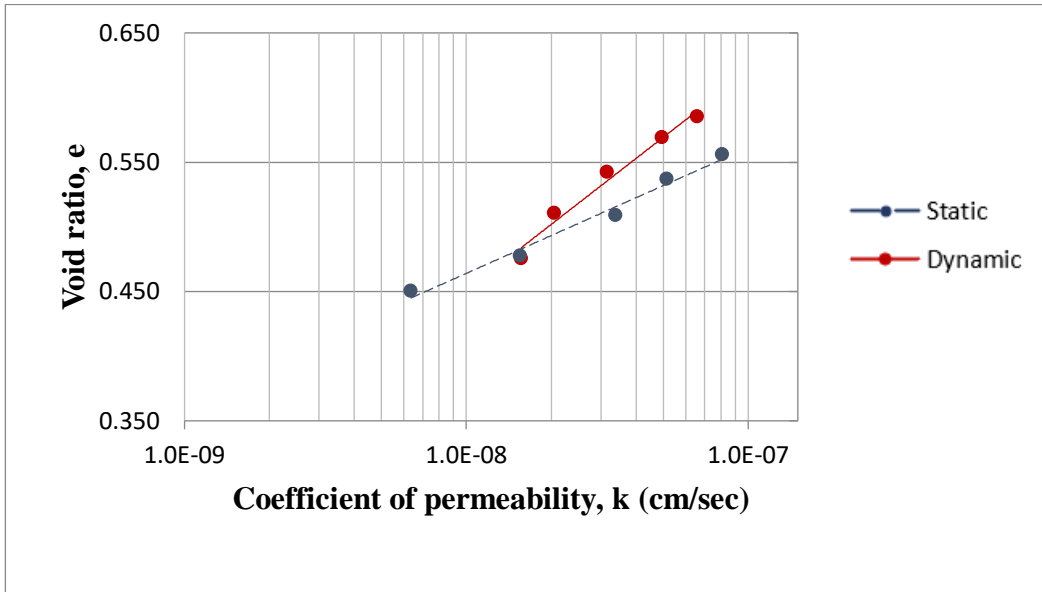


Figure 5.4: Void Ratio (e) vs. Coefficient of Permeability (k) for S4(dry)

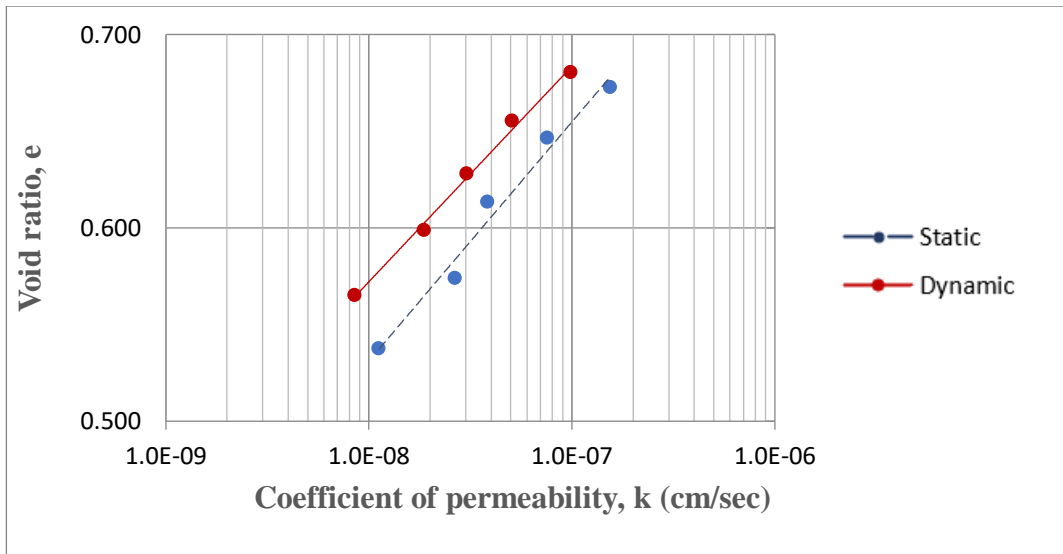


Figure 5.5: Void Ratio (e) vs. Coefficient of Permeability (k) for S5(dry)

The trends observed above suggest that permeabilities observed are within the same range between the coefficients of permeability for soil that has been subjected to static compaction and soil that has undergone dynamic compaction. In other words, the permeability coefficients of these two compaction methods exhibit a degree of resemblance. This finding implies that, despite the distinct compaction techniques employed, the rate at which water or other fluids can flow through the soil remains relatively consistent.

As demonstrated in a study by Dario et al. (2011) on silty clay soil, where porosity was measured using the mercury intrusion technique, distinct findings emerged. On the dry side of

the optimum moisture content, the soil compacted statically displayed a structure characterized by noticeable original micro-aggregation and gaps, leading to a porosity of approximately 11%. In contrast, the soil compacted dynamically exhibited a micro-structured argillaceous plasma with partial bonding, causing the breakdown of the original micro-aggregation. As a result, the porosity was considerably lower, around 2%, which marked a substantial reduction compared to the static compaction scenario. This suggests that dynamic compaction might have influenced or weakened the interparticle forces, resulting in structures with diminished shear strength.

Therefore, based on the explanation given by Dario et al. (2011), it can be deduced that the permeability of soil compacted statically is slightly higher than that of soil compacted dynamically. However, the slight variation in porosity, whether it's 11% or 2%, does not seem to have a significant impact on permeability. As a result, the permeabilities of statically compacted soil and dynamically compacted soil appear to be quite similar in their order.

To explore further into the investigation, a graph was constructed, featuring the coefficient of permeability of statically compacted soil on the x-axis and the coefficient of permeability of dynamically compacted soil on the y-axis. The graph representation incorporated data from all the samples, effectively visualized within a unified plot, as depicted in Figure 5.6.

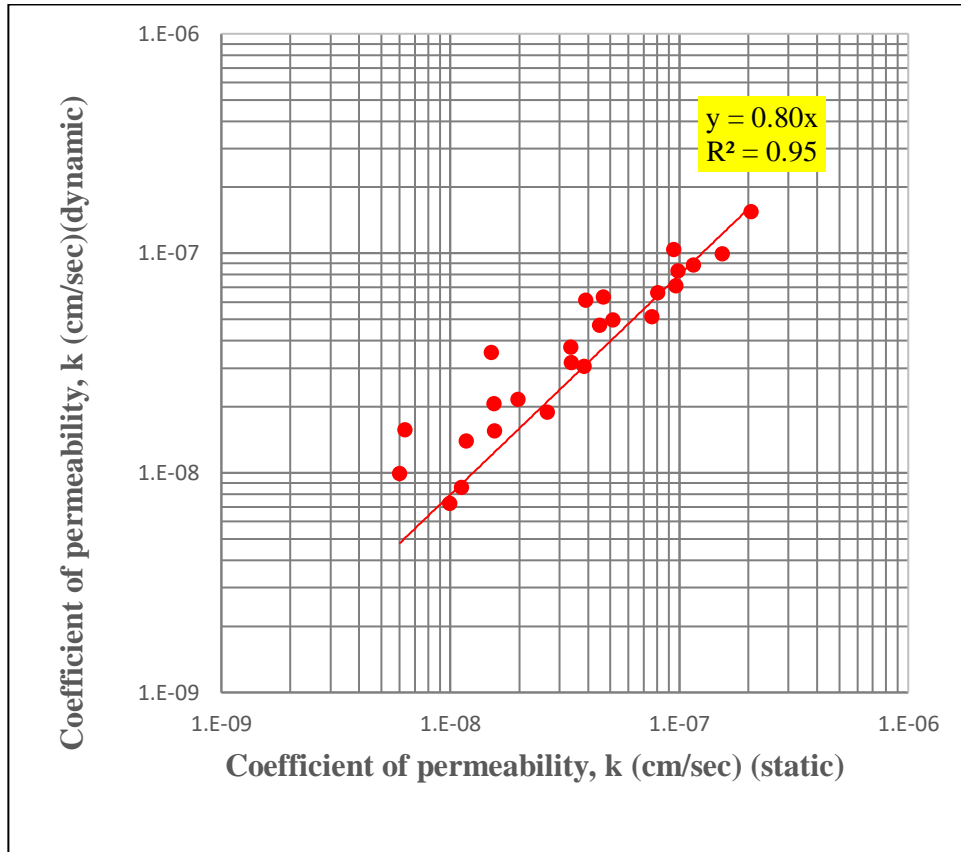


Figure 5.6: Coefficient of Permeability (dynamic) vs. Coefficient of Permeability (static)(Dry)

With a coefficient of determination (R^2) of 0.95, it becomes evident that a strong positive correlation exists between the dynamic coefficient of permeability and the static coefficient of permeability.

A coefficient of determination of 0.95 means that 95% of the variation in the permeability coefficient of statically compacted soil can be explained by the variation in the permeability coefficient of dynamically compacted soil.

5.1.2. Analysis of permeability characteristics for dynamic and static compaction at optimum moisture content

The figures ranging from Figure 5.7 to Figure 5.11 illustrate the superimposed plot of void ratio (e) against coefficient of permeability (k) for both dynamic and static compaction at the optimum moisture content.

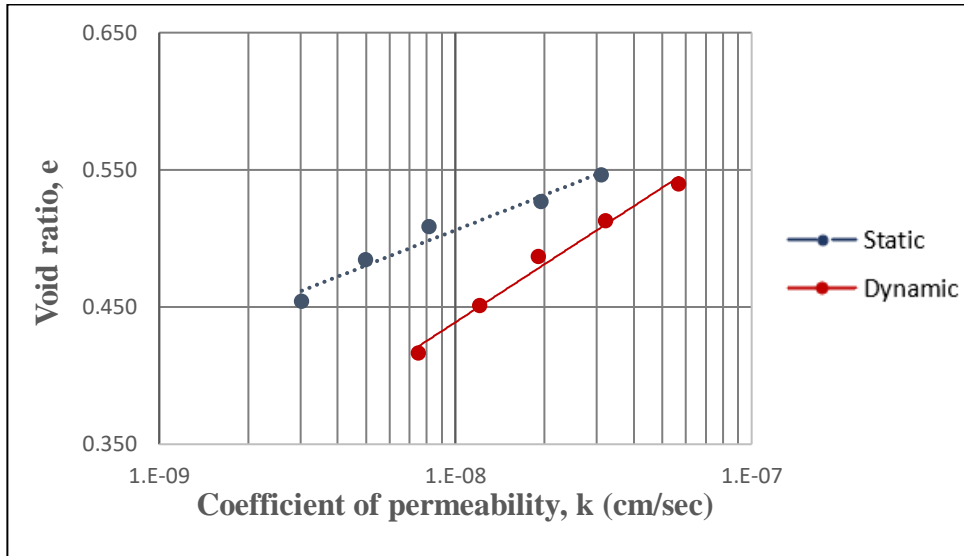


Figure 5.7. Void Ratio (e) vs. Coefficient of Permeability (k) for S1(OMC)

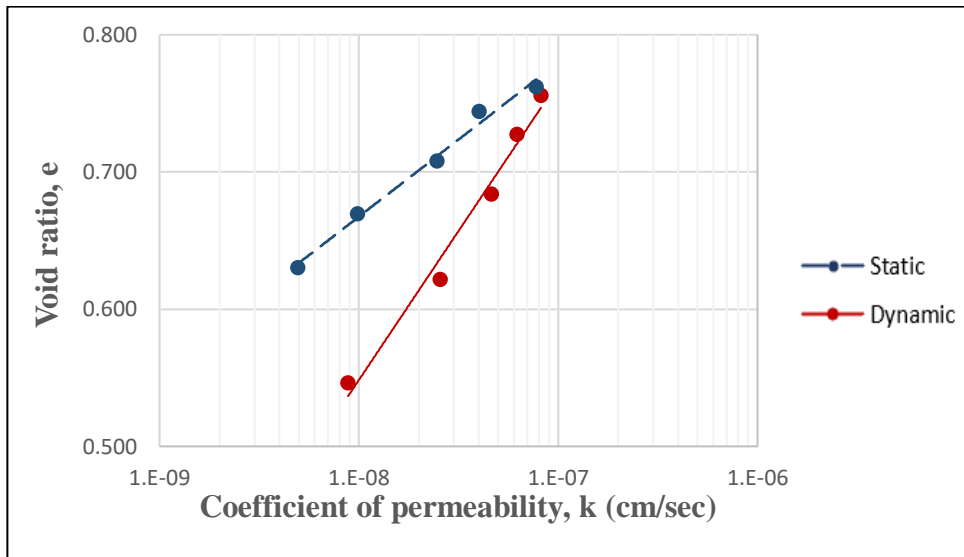


Figure 5.8: Void Ratio (e) vs. Coefficient of Permeability (k) for S2(OMC)

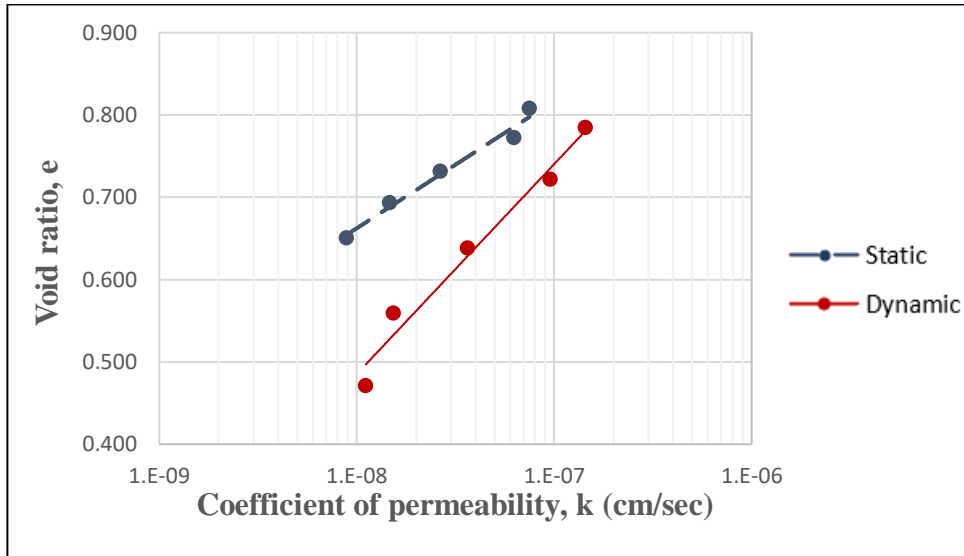


Figure 5.9: Void Ratio (e) vs. Coefficient of Permeability (k) for S3(OMC)

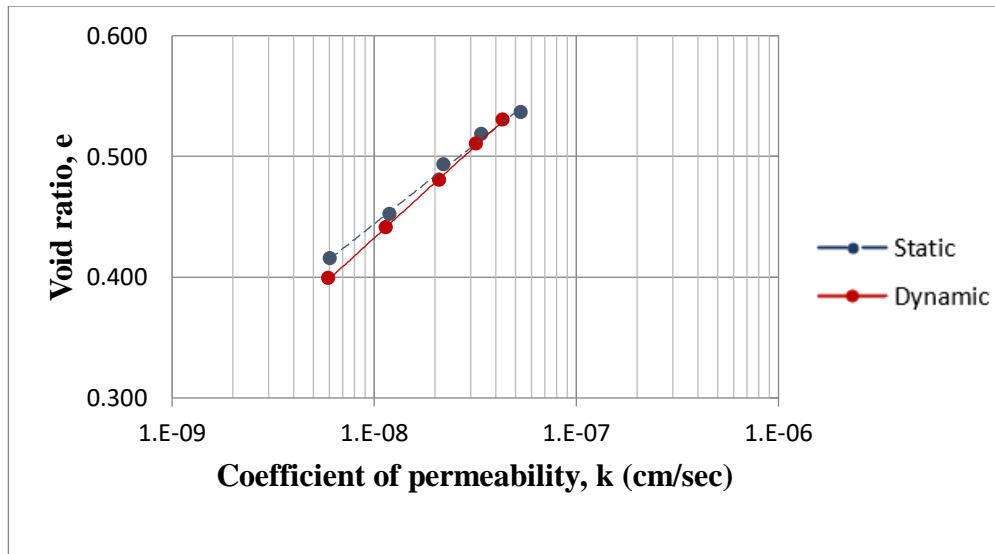


Figure 5.10: Void Ratio (e) vs. Coefficient of Permeability (k) for S4(OMC)

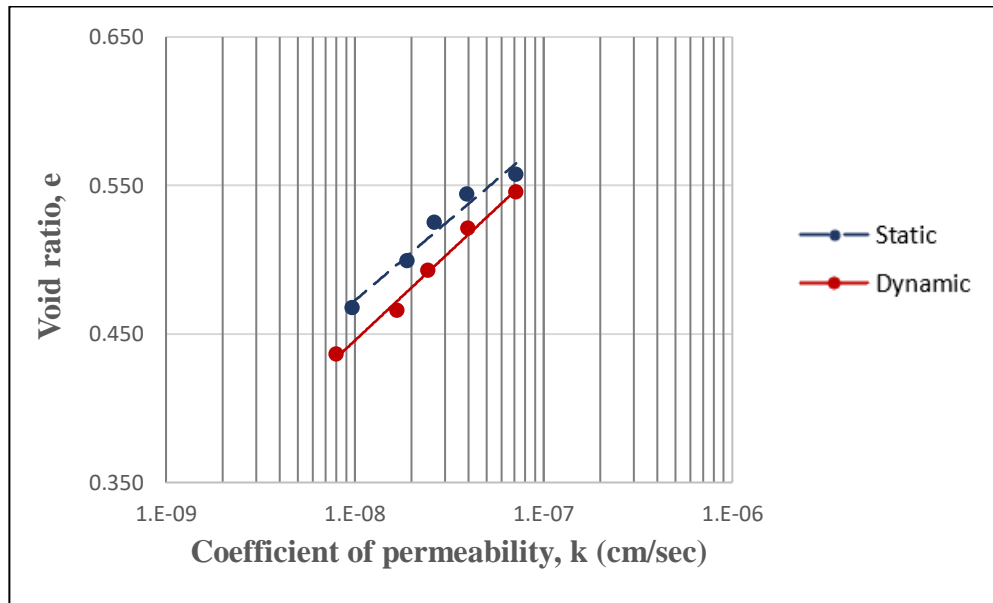


Figure 5.11: Void Ratio (e) vs. Coefficient of Permeability (k) for S5(OMC)

Based on the observed patterns, it seems that there are only small variations in the permeability characteristics when comparing soil that was compacted statically with soil that was compacted dynamically.

According to the research conducted by Dario et al. (2011) on gneissic residual soil pedologically classified as red yellow latosol to study the porosity using mercury intrusion technique, observations reveal that at the optimum moisture content (OMC), the clayey soil specimens compacted statically exhibit characteristics of the original micro-aggregation, retaining initial nodules. This is accompanied by the emergence of isolated gaps, fissures, and oriented porosity (approximately 3%). In contrast, under the same moisture content, the specimens subjected to dynamic compaction display a few features of the original micro-aggregation, but nearly all porosity is lost (around 2%). This observation could potentially reveal the underlying cause for the slight differences observed in permeability characteristics between static compaction and dynamic compaction. As a result, it can be inferred that the permeabilities in both scenarios tend to be relatively similar.

A graph was next plotted to represent the coefficient of permeability of soil that underwent static compaction on the x-axis, while the coefficient of permeability of soil subjected to dynamic compaction was plotted on the y-axis which is shown in Figure 5.12. This provides a detailed illustration of the relationship between the two permeability coefficients across the sample set.

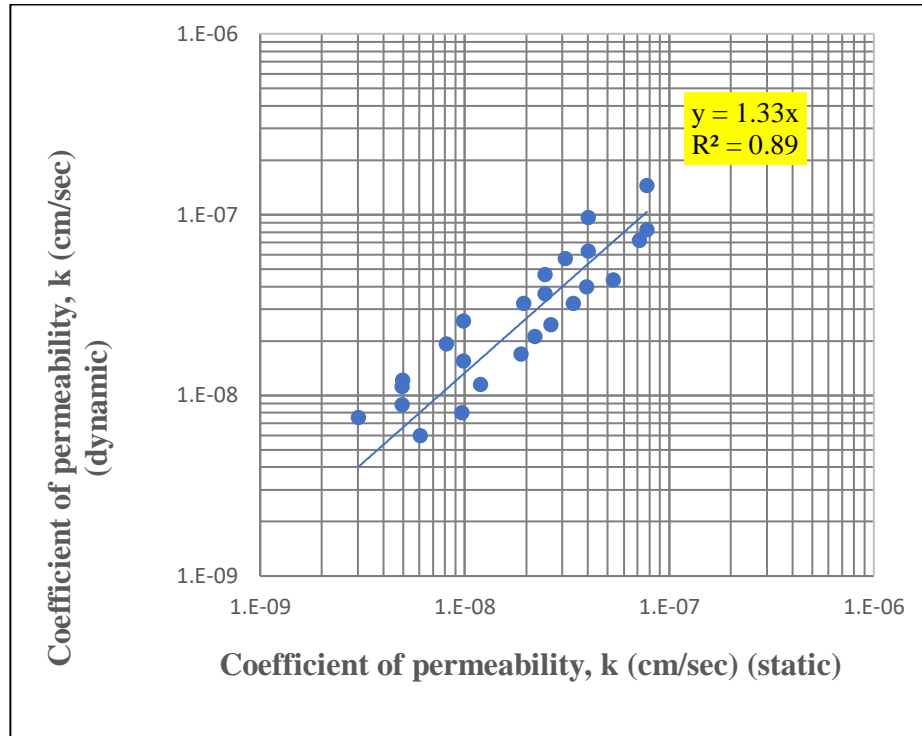


Figure 5.12: Coefficient of Permeability (dynamic) vs. Coefficient of Permeability (static)(OMC)

With the calculated determination coefficient (R^2) of 0.89, a distinct positive correlation between the dynamic coefficient of permeability and the static coefficient of permeability becomes evident. To be more precise, this value of 0.89 signifies that around 89% of the total variability in the permeability coefficient of the statically compacted soil samples can be explained by considering the corresponding changes in the permeability coefficient resulting from dynamic compaction.

5.1.3. Analysis of permeability characteristics for dynamic and static compaction at wet of optimum

From Figure 5.13 to Figure 5.17, the superimposed plot of void ratio (e) against coefficient of permeability (k) for both dynamic and static compaction at the wet of optimum is illustrated.

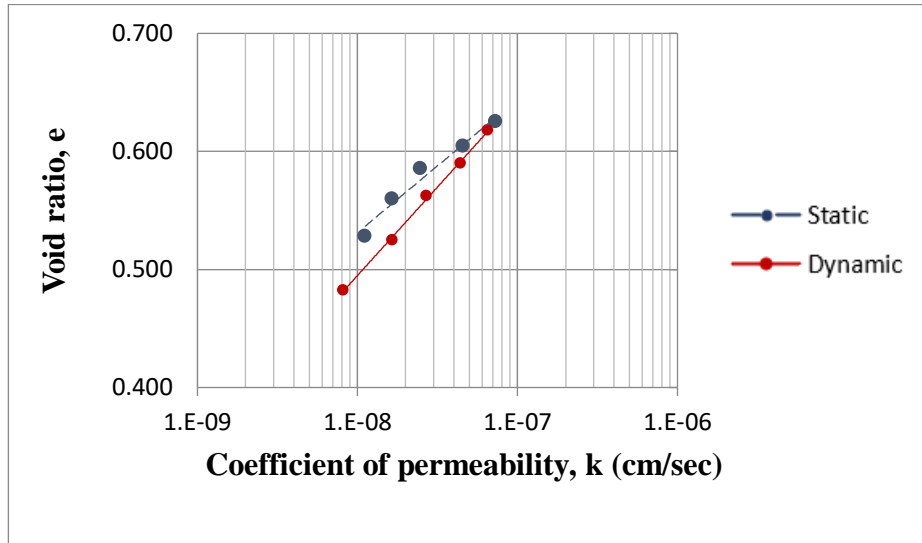


Figure 5.13. Void Ratio (e) vs. Coefficient of Permeability (k) for S1(wet)

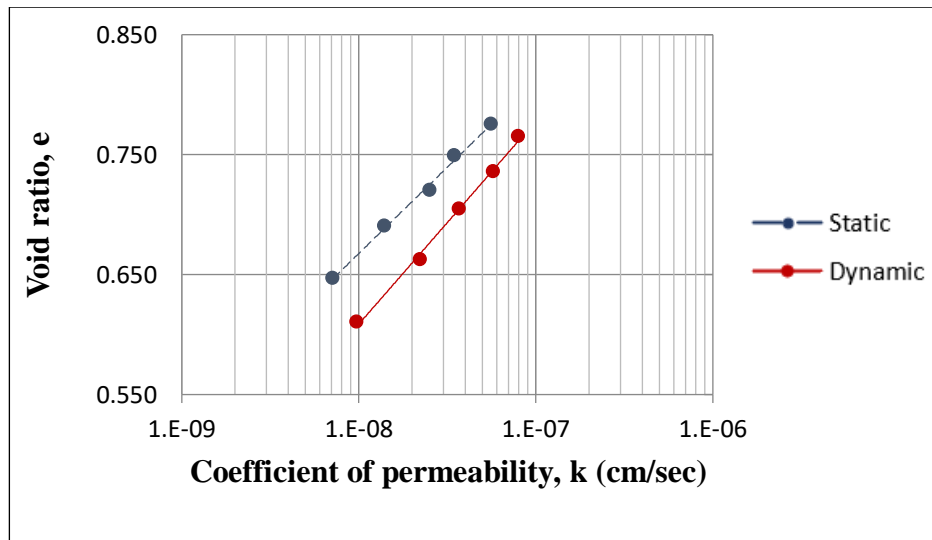


Figure 5.14: Void Ratio (e) vs. Coefficient of Permeability (k) for S2(wet)

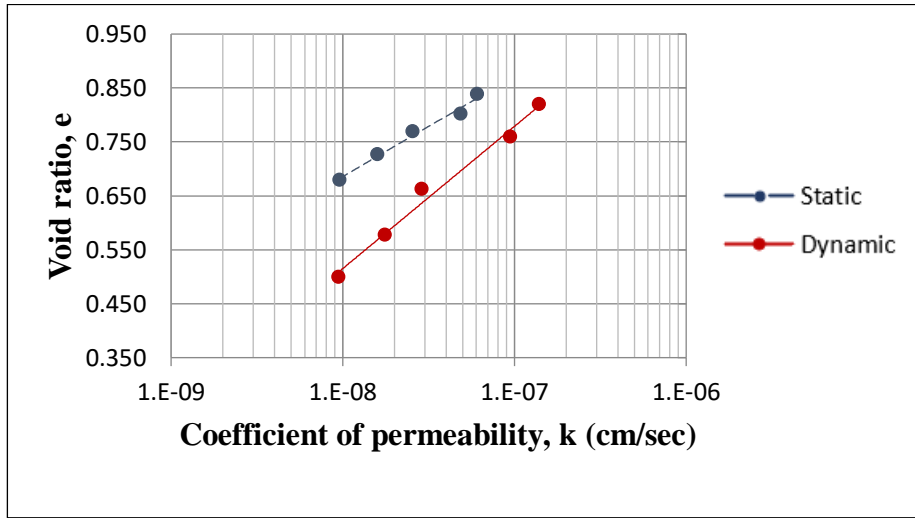


Figure 5.15: Void Ratio (e) vs. Coefficient of Permeability (k) for S3(wet)

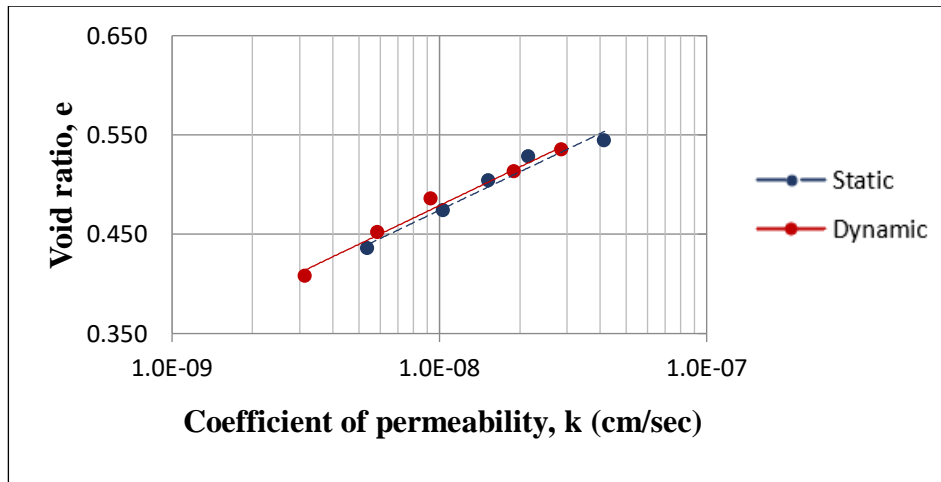


Figure 5.16: Void Ratio (e) vs. Coefficient of Permeability (k) for S4(wet)

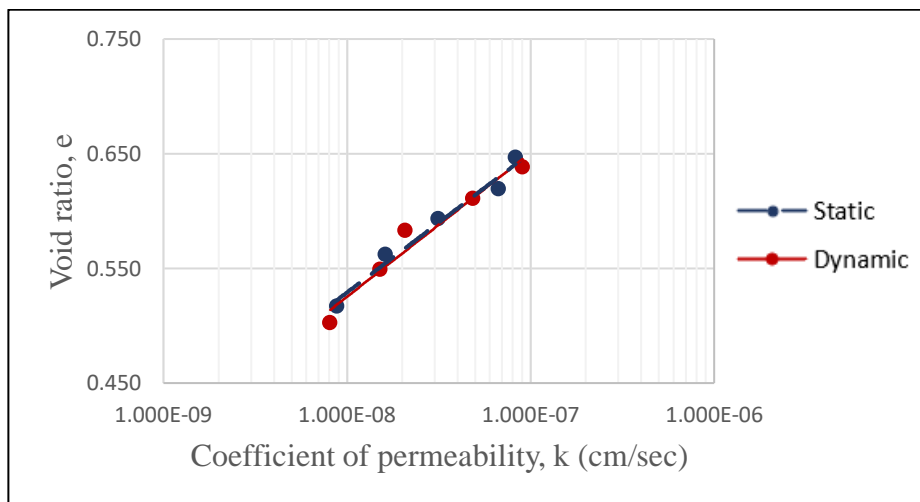


Figure 5.17: Void Ratio (e) vs. Coefficient of Permeability (k) for S5(wet)

From the patterns indicated above, there are only small differences noticeable in the permeability characteristics. derived from both static and dynamic compaction. Mitchell et al. (1965) investigated compaction methods' impact on silty clay permeability, expecting varied shear strain levels beyond the optimal point with different techniques. Similarly, Seed and Chan studied compaction methods' effects on clay behaviors like swelling, shrinking, and stress-strain traits. Their findings suggested increasing shear strain and dispersion in the sequence: static, vibratory, and kneading compaction methods.

Furthermore, they anticipated lower permeabilities in kneading-compacted samples compared to statically compacted ones, particularly when molding water content exceeded optimal levels. To validate this, silty clay samples were prepared using both static and kneading methods, ensuring uniformity through 2.8-inch diameter and 1-inch height molds. Additional tests were conducted on samples kneading-compacted in 3.5-inch-high molds. Results confirmed the prediction: statically compacted samples were notably more permeable than kneading-compacted ones, especially for moisture contents surpassing the optimum. However, the differences were less pronounced than initially expected.

Consequently, it can be deduced that while the permeability of statically compacted soil slightly exceeds that of dynamically compacted soil, the previously mentioned differences are notably subdued. Therefore, it is reasonable to conclude that the permeabilities in both static and dynamic compaction methods align in a similar order.

All samples were incorporated into this graphical representation, consolidated within a single plot, as depicted in Figure 5.18. This plot offers a comprehensive illustration of the relationship between the two permeability coefficients across the complete sample set.

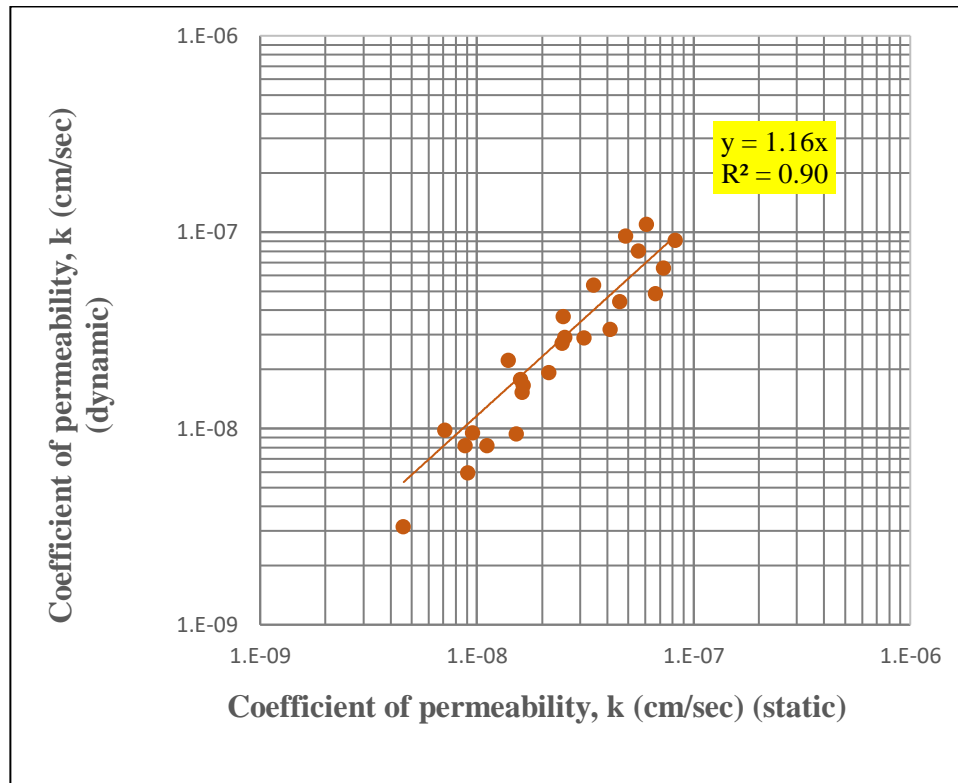


Figure 5.18: Coefficient of Permeability (dynamic) vs. Coefficient of Permeability (static)(Wet)

The calculated determination coefficient (R^2) of 0.90 indicates a strong positive connection between the dynamic and static permeability coefficients. This value signifies that around 90% of the variability observed in the permeability coefficient of statically compacted soil samples can be explained by the variations in the permeability coefficient resulting from dynamic compaction. In essence, the higher the correlation coefficient, the more closely changes in dynamic compaction align with changes in static compaction regarding the soil's permeability attributes.

5.2. Analysis of permeability characteristics for dynamic compaction across dry side, optimal moisture content (OMC), and wet side of optimum

Graphs were constructed for Void Ratio (e) against Coefficient of Permeability (k) using a semi-logarithmic scale for dynamic compaction separately. These graphs encompassed permeability values for the dry state, optimal moisture content (OMC), and wet conditions, all within a single graphical representation.

These are represented below from Fig. 5.19 to Fig. 5.23.

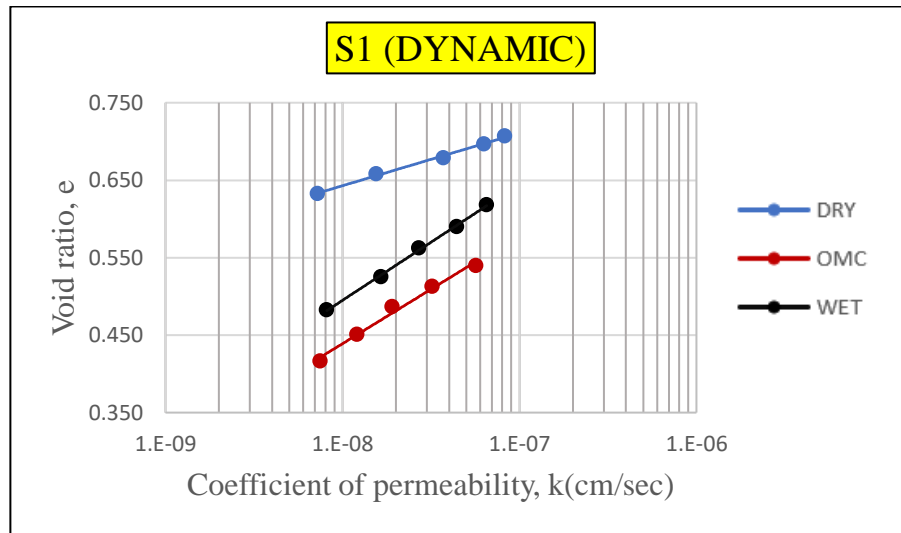


Figure 5.19: Void Ratio (e) vs. Coefficient of Permeability (k) for S1 (dynamic)

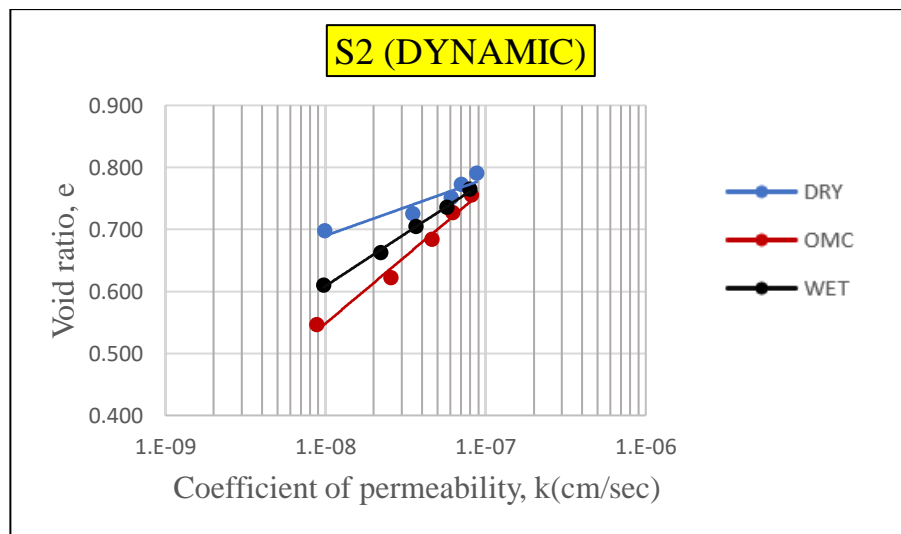


Figure 5.20: Void Ratio (e) vs. Coefficient of Permeability (k) for S2 (dynamic)

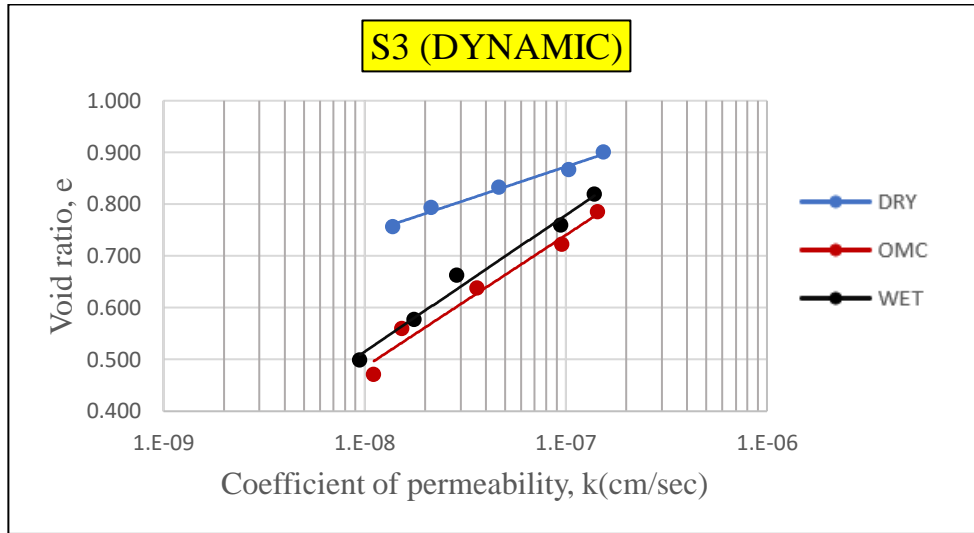


Figure 5.21. Void Ratio (e) vs. Coefficient of Permeability (k) for S3 (dynamic)

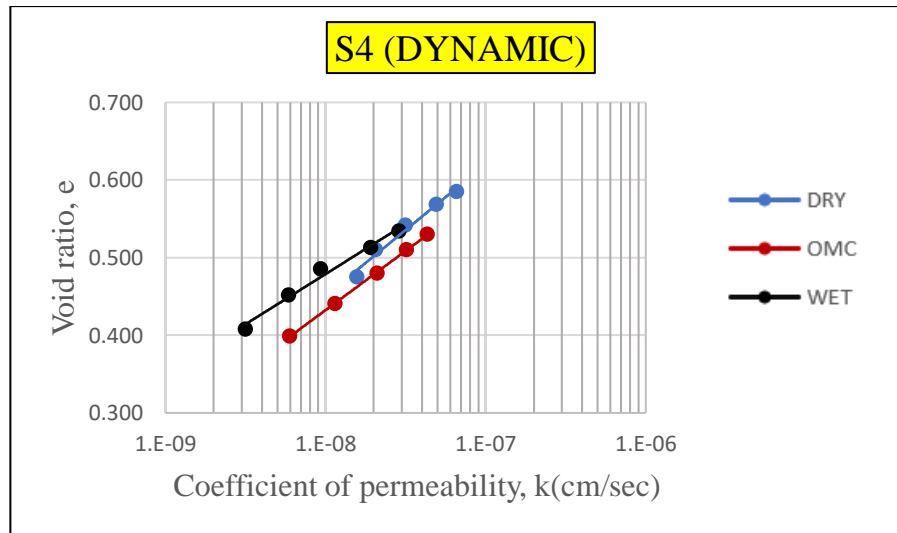


Figure 5.22: Void Ratio (e) vs. Coefficient of Permeability (k) for S4 (dynamic)

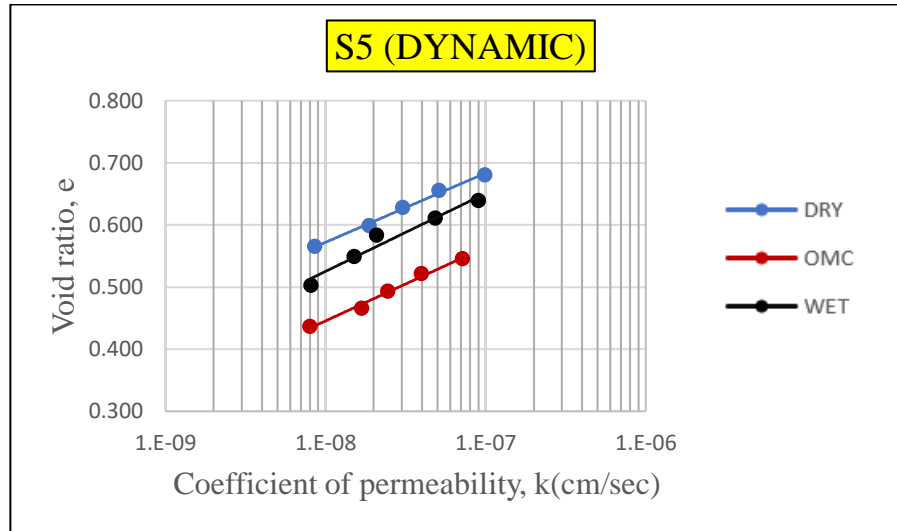


Figure 5.23: Void Ratio (e) vs. Coefficient of Permeability (k) for S5 (dynamic)

In certain samples, the graphs display distinct variations in void ratio, with the lines representing dry, wet, and OMC conditions neatly stacked in that order. Yet, in other samples, the void ratio differences are less apparent. Nevertheless, the permeability values corresponding to the dry, optimum moisture content (OMC), and wet side demonstrate slight variations, yet they maintain a remarkable alignment on the semi-logarithmic charts.

5.3. Analysis of permeability characteristics for static compaction across dry side, optimal moisture content (OMC), and wet side of optimum

Utilizing a semi-logarithmic scale, distinct graphs were generated for Void Ratio (e) in relation to Coefficient of Permeability (k) specifically for static compaction. These graphs comprehensively covered permeability values across the dry, optimal moisture content (OMC), and wet conditions, all encapsulated within a singular graphical portrayal. These visualizations are illustrated in Figures 5.24 through 5.28 below.

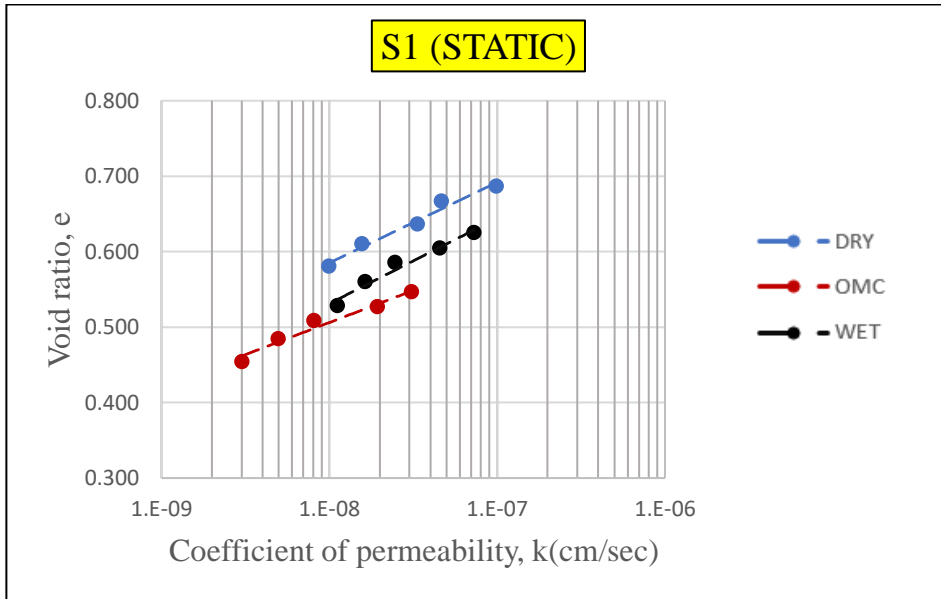


Figure 5.24: Void Ratio (e) vs. Coefficient of Permeability (k) for S1 (static)

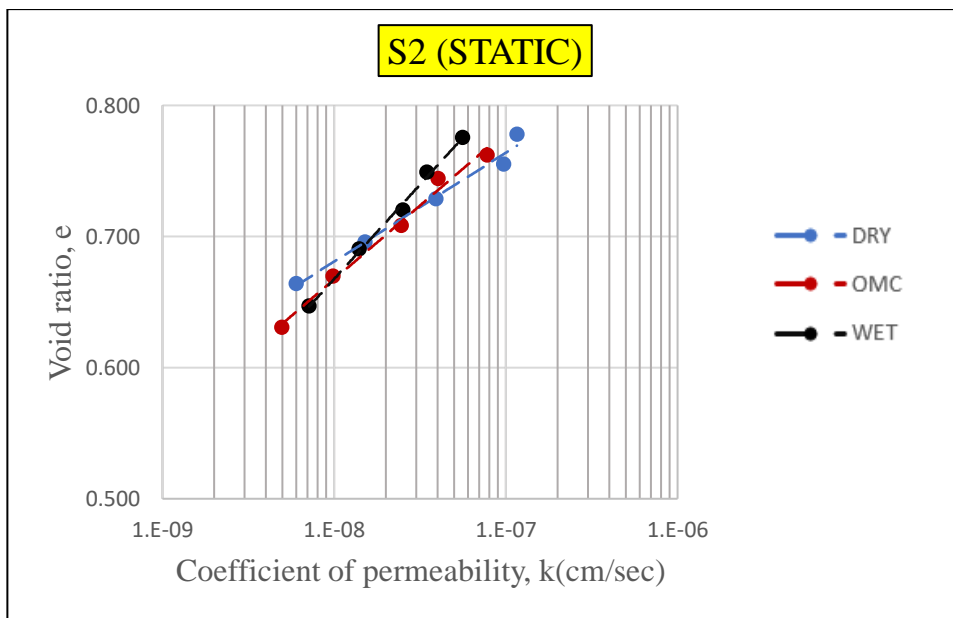


Figure 5.25: Void Ratio (e) vs. Coefficient of Permeability (k) for S2 (static)

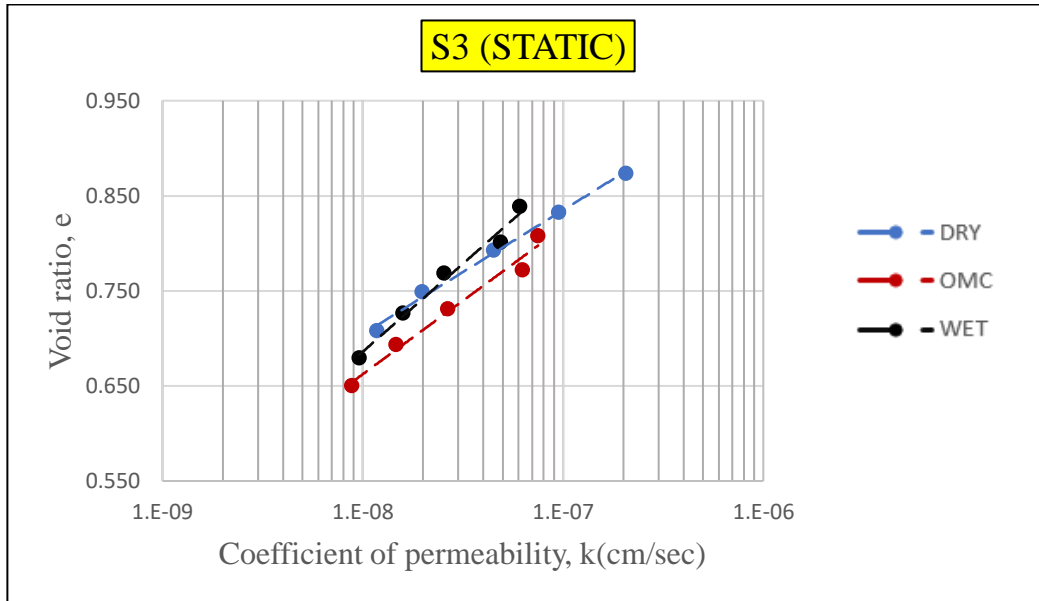


Figure 5.26. Void Ratio (e) vs. Coefficient of Permeability (k) for S3 (static)

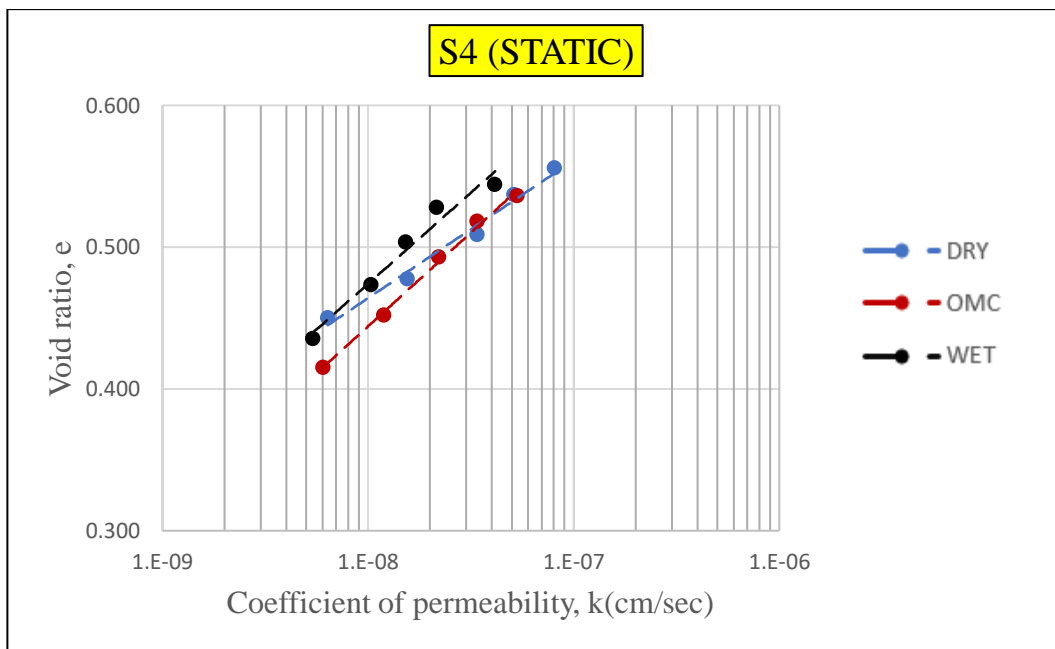


Figure 5.27: Void Ratio (e) vs. Coefficient of Permeability (k) for S4 (static)

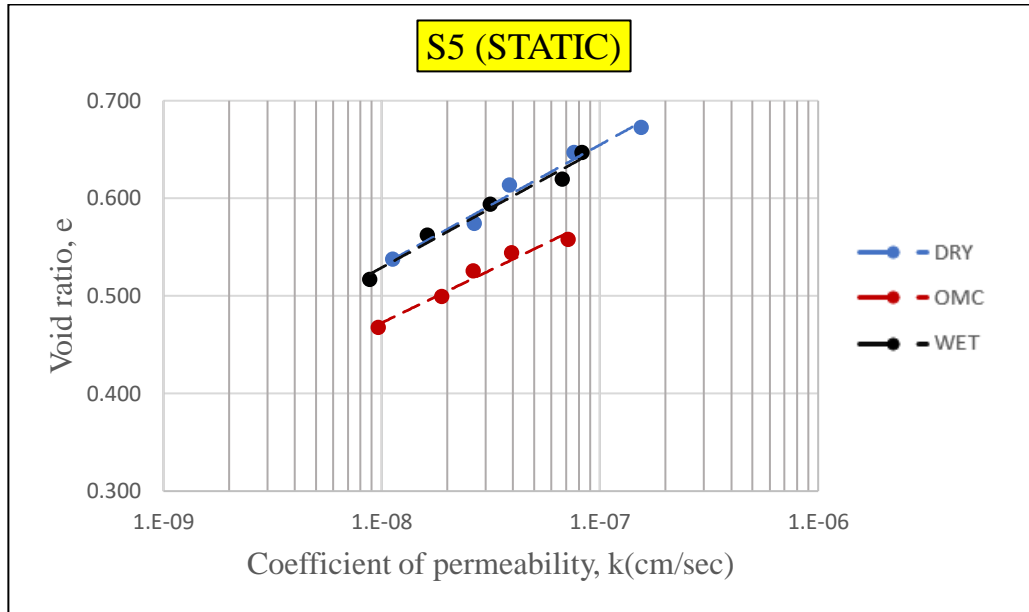


Figure 5.28: Void Ratio (e) vs. Coefficient of Permeability (k) for S5 (static)

In some instances, the graphs exhibit noticeable fluctuations in void ratio, where the lines representing dry, wet, and OMC states are clearly arranged in that sequence. However, in other samples, the distinctions in void ratio are less conspicuous. Nonetheless, the permeability values for the dry, OMC, and wet extents of the range show marginal variations and closely coincide on the semi-logarithmic graphs.

Based on the trends presented in figures 5.6, 5.12, and 5.18, and also the graphs in both section 5.2 and section 5.3 of this chapter, it becomes evident that the permeability values of statically and dynamically compacted soil, situated on the dry side of the optimum moisture content (OMC), at the OMC, and on the wet side of the optimum, respectively, exhibit a closely similar pattern with minimal to negligible distinctions. This observation aligns with the findings documented in the research conducted by Delage et al. (1996).

Delage et al. (1996) conducted a comprehensive analysis of the microstructure of compacted silt at three distinct points along the Proctor curve—dry, optimal moisture content (OMC), and wet. This investigation utilized the methodology outlined by Diamond (1970), where scanning electron microscopy and mercury intrusion porosimetry was utilized to examine the microstructure of compacted kaolinite and illite, and encompassed both qualitative and quantitative aspects. Qualitative insights were derived through scanning electron microscope (SEM) examinations, while quantitative examination relied on mercury intrusion pore size distribution (PSD) measurements to elucidate the porous medium's structure. The pore size

distribution observed in the compacted silt aligns with findings from various studies on distinct pure clays such as illite and kaolinite. The authors suggest that this similarity lends broader credibility to their conclusions regarding compacted fine-grained soils.

Ahmed et al. (1974) facilitated a comparative study by analysing PSD curves from samples prepared using different compaction methods: dynamic compaction in a Proctor mould, static compaction, and kneading compaction. Surprisingly, minimal disparity was observed among these three laboratory preparation techniques. Pores smaller than $0.1\ \mu\text{m}$ displayed a similar pattern, while the dry sample exhibited a population of pores averaging $28\ \mu\text{m}$ in size. In the Proctor optimum sample, pores were primarily situated between 1 and $10\ \mu\text{m}$, while the wet sample contained most pores between 0.1 and $1\ \mu\text{m}$. Consequently, when considering identical dry unit weight (DUW) and moisture content (MC), the porosity profile remains consistent for both statically and dynamically compacted soil samples.

This uniformity potentially contributes to the closely comparable coefficients of permeability values exhibited by the dynamically and statically compacted soils.

5.4. Analysis for Permeability versus molding water content relationship for dynamic and static compaction

To provide a more comprehensive understanding, graphs were constructed comparing the Coefficient of Permeability (k) against the molding water content for both dynamic and static compaction across the dry side, optimal moisture content (OMC), and wet side of the optimum.

5.4.1. For dynamic compaction

The graphical representations presented in figures ranging from Figure 5.29 to Figure 5.33 depict the connection between permeability and molding water content for samples that underwent dynamic compaction. These figures visually illustrate how the permeability changes at various moisture content levels throughout the dynamic compaction procedure.

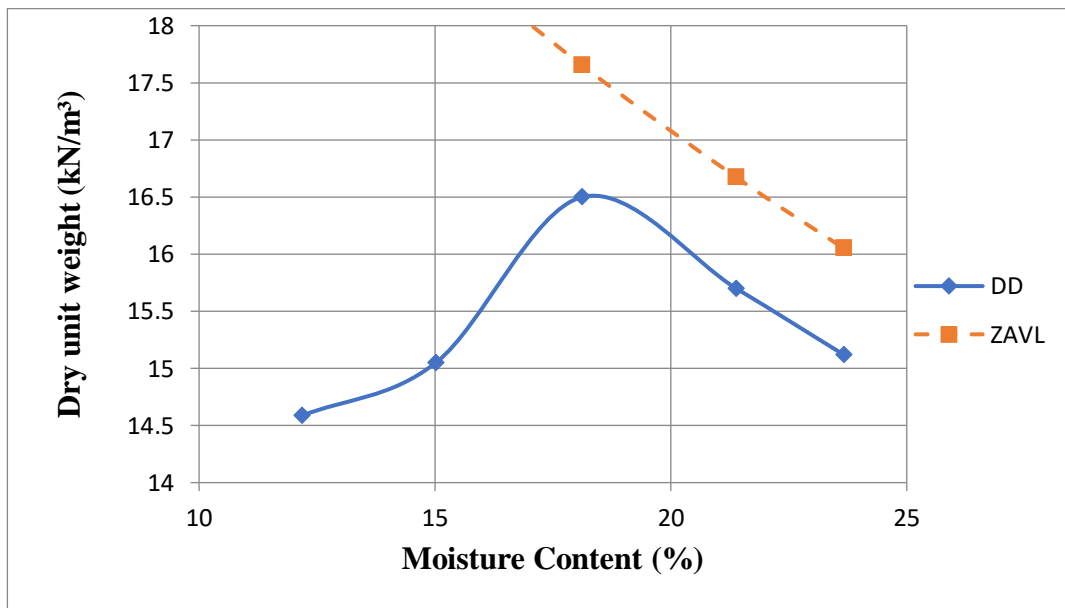
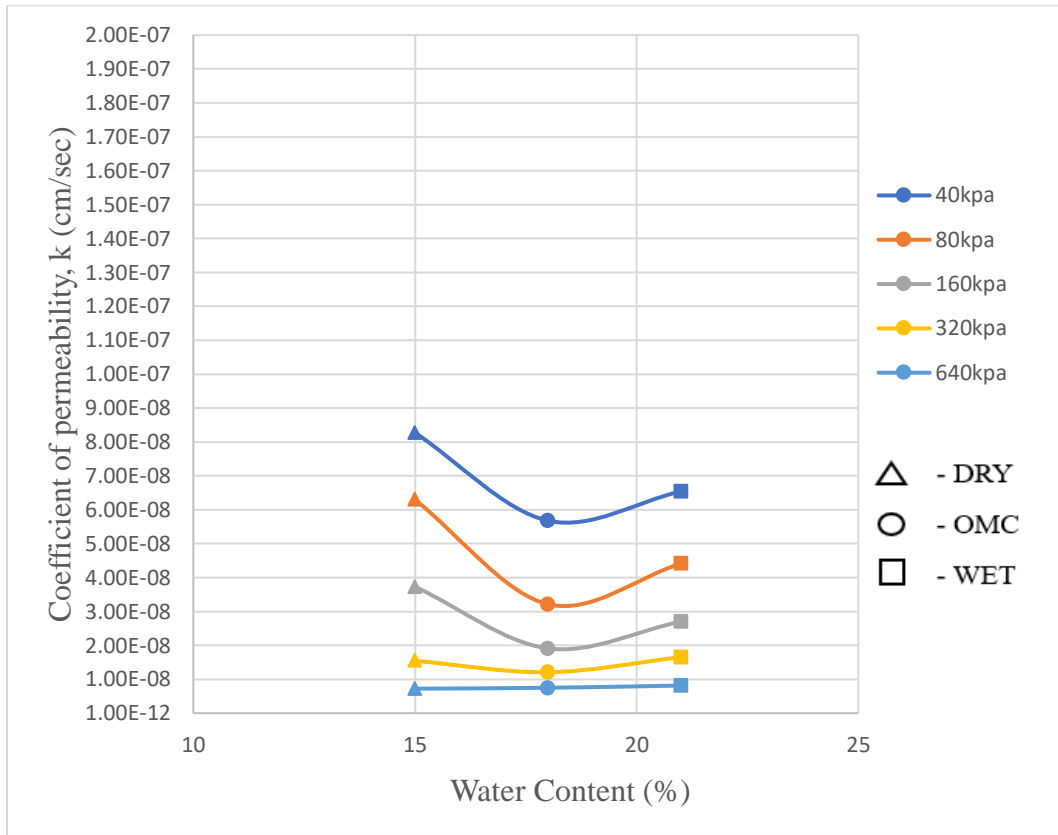


Figure 5.29: Permeability versus molding water content relationship for S1(dynamic)

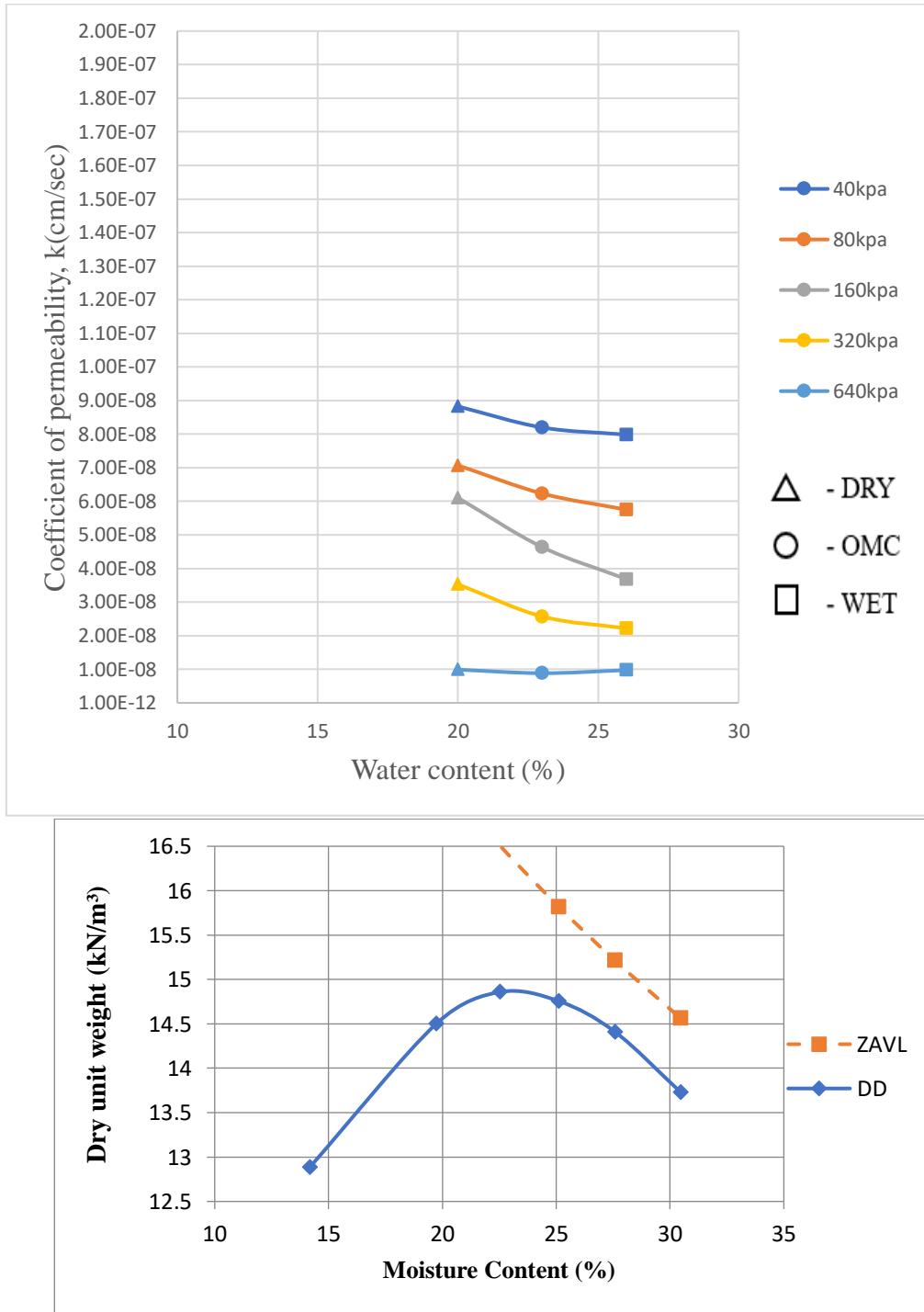


Figure 5.30: Permeability versus molding water content relationship for S2(dynamic)

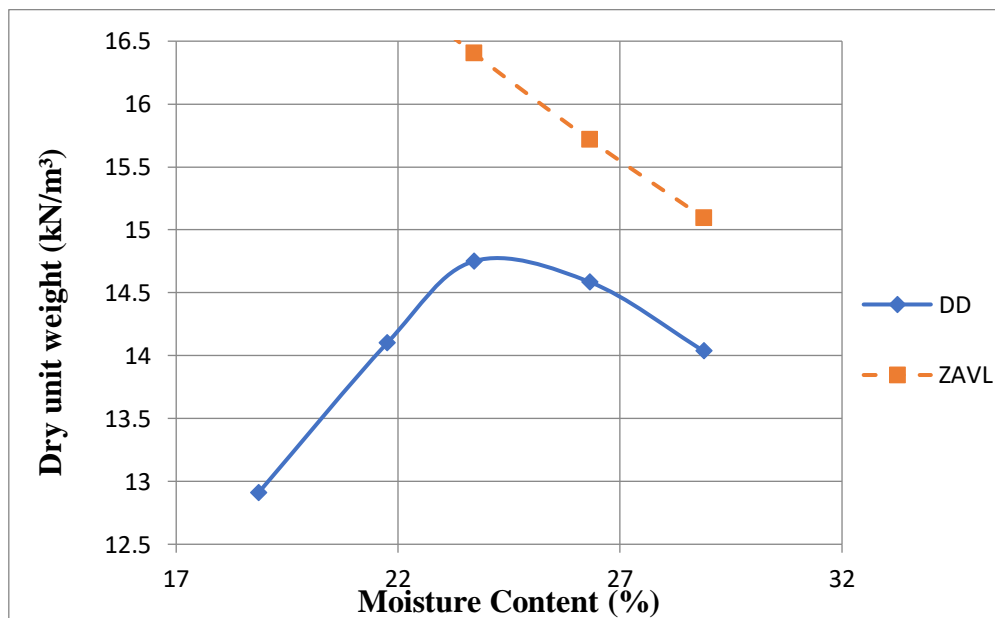
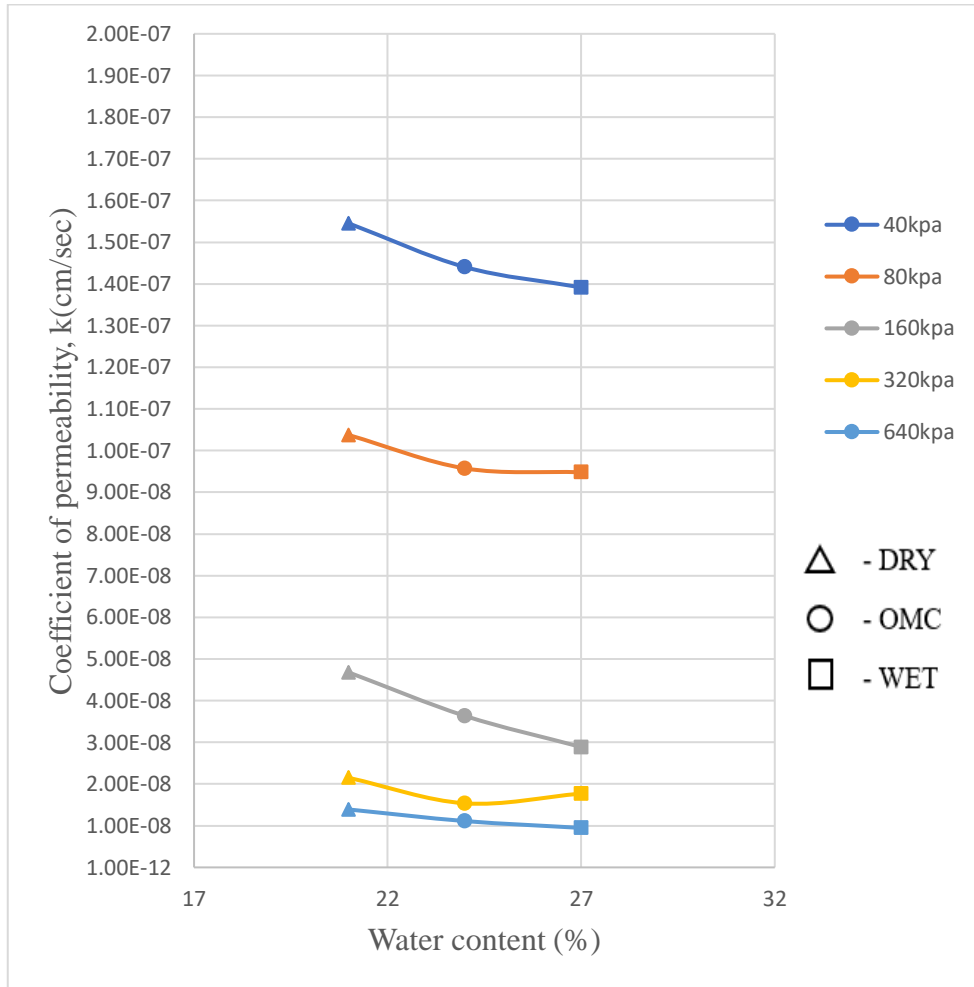


Figure 5.31: Permeability versus molding water content relationship for S3(dynamic)

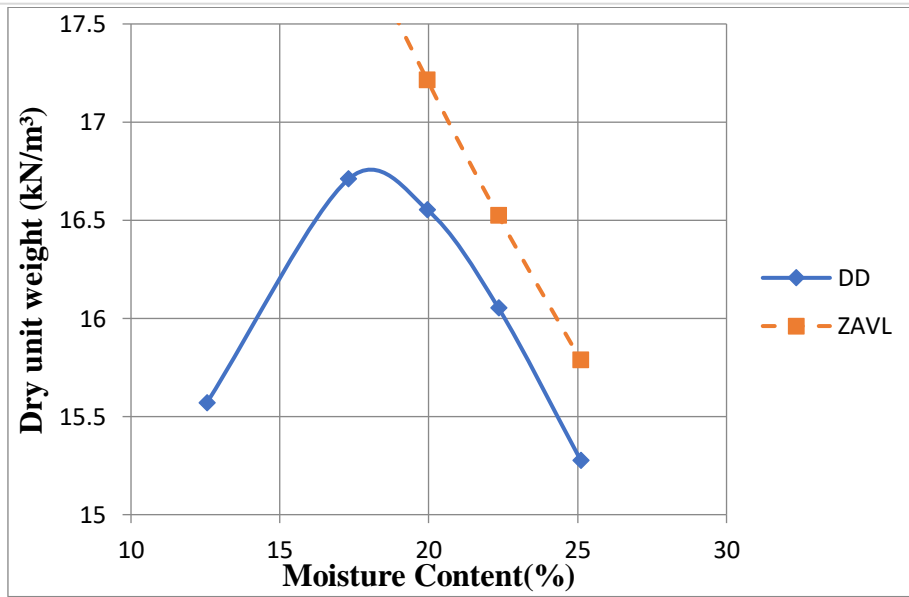
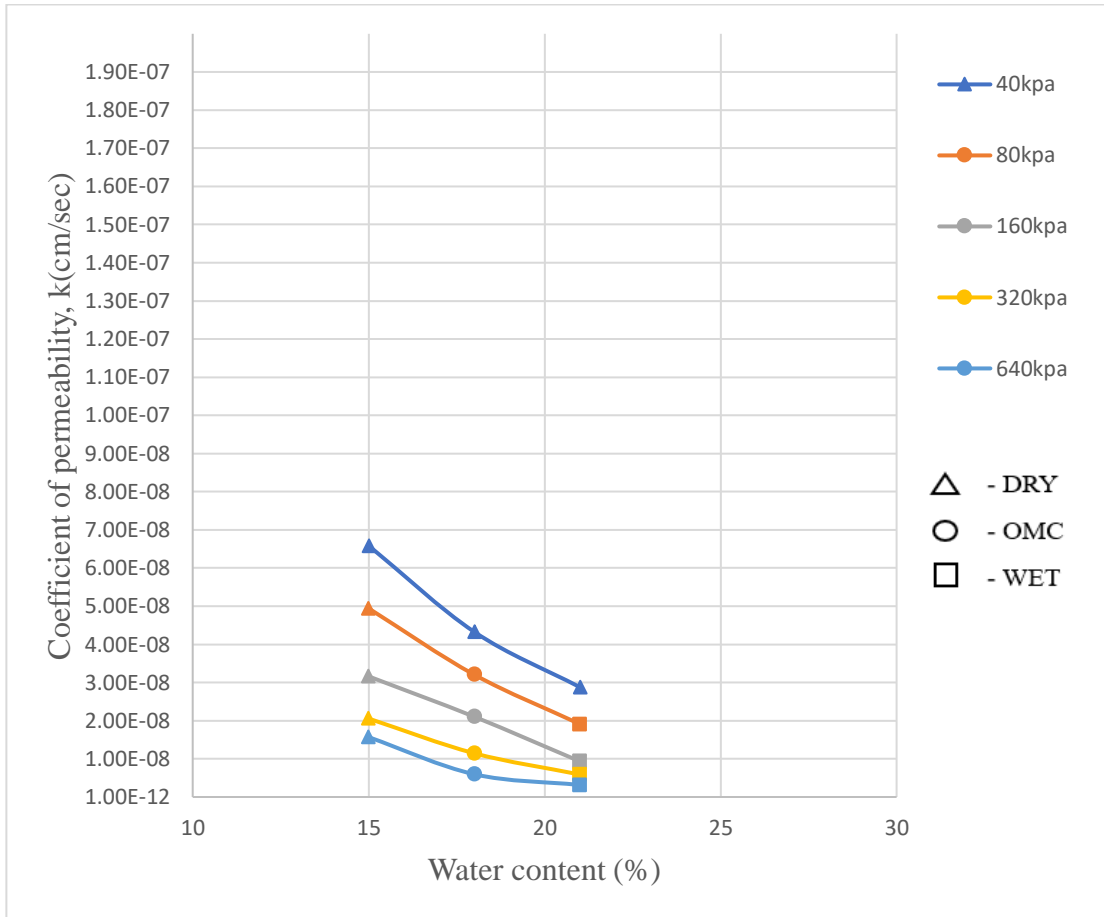


Figure 5.32: Permeability versus molding water content relationship for S4(dynamic)

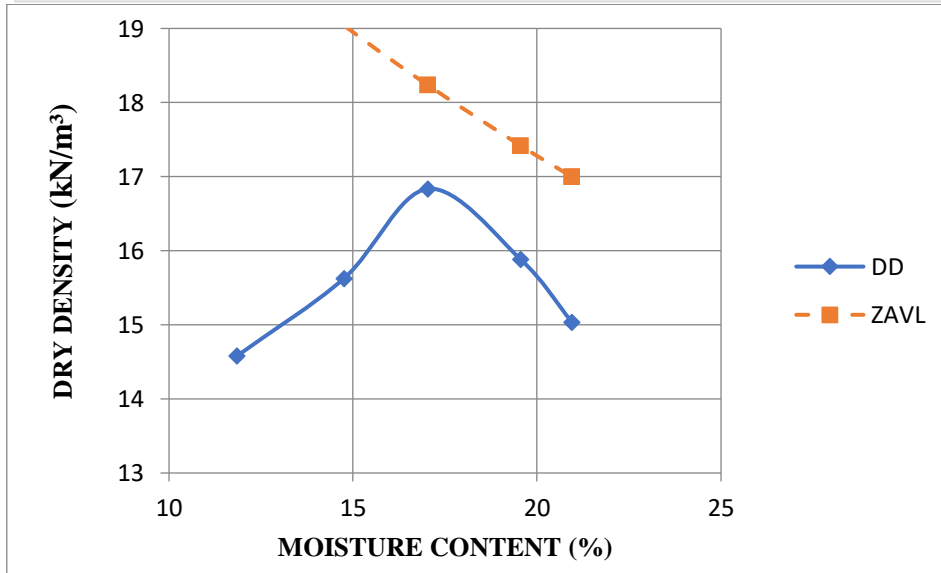
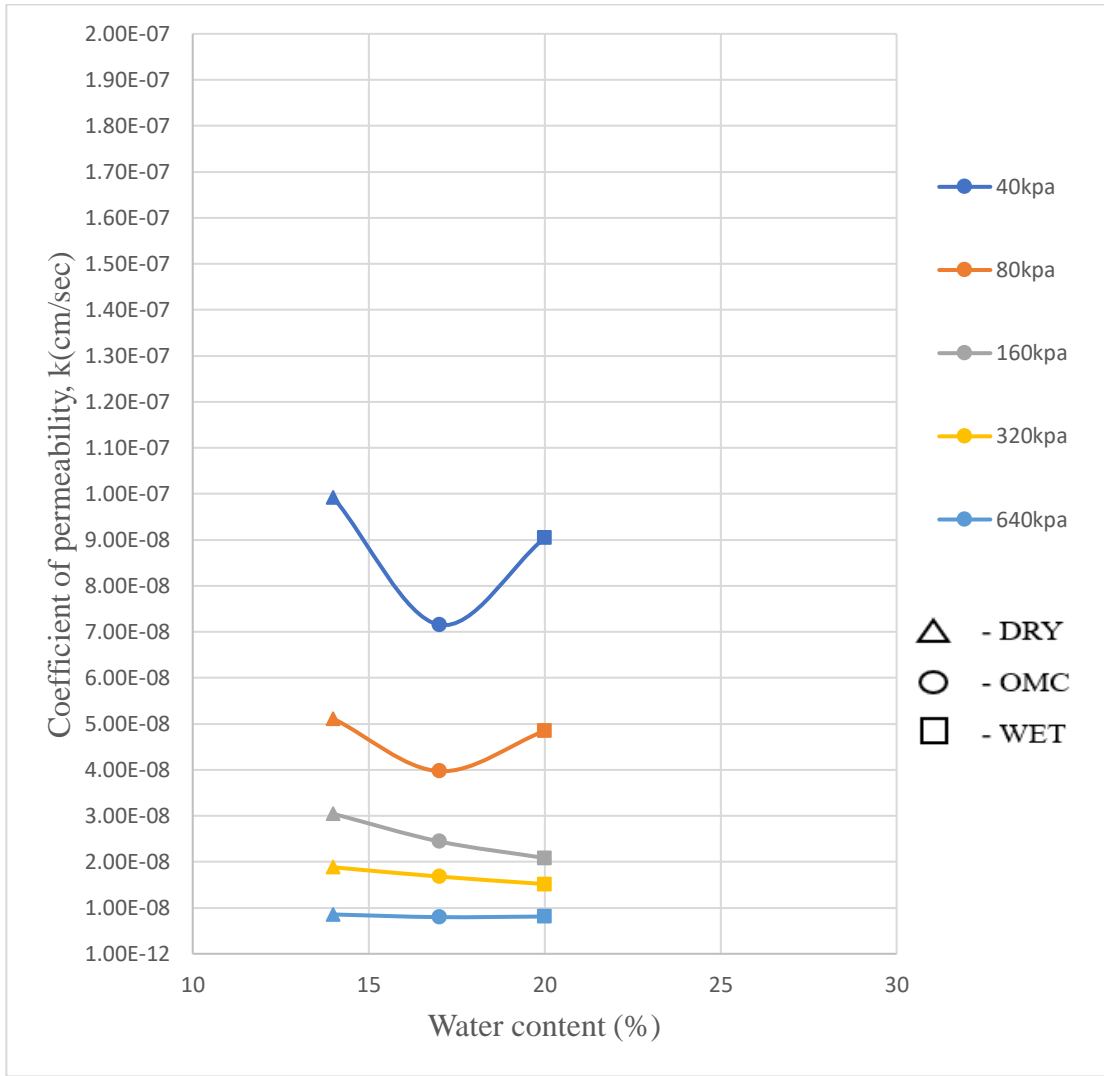


Figure 5.33: Permeability versus molding water content relationship for S5(dynamic)

A noticeable pattern became evident within specific samples that underwent dynamic compaction across various moisture levels. This encompassed conditions both before and after the optimum moisture content: the dry side of optimum, the optimum moisture content (OMC), and the wet side of optimum. These values revealed a consistent trend, progressing in a sequence. They exhibited higher values on the dry side of the optimum moisture content, followed by a reduction at the OMC, and culminating in their lowest levels when the soil was positioned on the wet side of the optimum spectrum. Notably, in certain samples, the permeability values on the wet side were marginally higher than those at the OMC, dry side of optimum values remaining the highest.

This observed pattern can be explained by referring to the research conducted by Mitchell et al. in their work titled "Permeability of Compacted Clay" in 1965.

Mitchell et al. (1965) in their study found that for specimens compacted below the optimal moisture content, the permeability showed a slight increase as the water content increased. However, there was a significant reduction in permeability around the optimal moisture content. Notably, samples prepared with a moisture content exceeding the optimum displayed permeability values nearly three orders of magnitude lower than those prepared with lower moisture content.

Earlier investigations by Seed and Chan extensively examined the structure and strength characteristics of the silty clay utilized in these tests. They presented evidence that this particular soil type is highly sensitive to changes in its structure. This sensitivity becomes evident when employing compaction methods that involve considerable shear strains, such as kneading compaction. Specifically, when the soil is compacted with a moisture content exceeding the optimum level, it results in a dispersed structure.

Nevertheless, in some of the samples, it was noted that the permeability values at the wet side of the optimum moisture content (OMC) are marginally greater than the permeability values observed at the OMC.

This occurrence could potentially be attributed to the phenomenon that, as the moisture content exceeds the optimal moisture level (OMC), there may be a likelihood of soil swelling taking place within its structure. This expansion in the soil's arrangement might effectively enhance the ease of water passage through its pores.

This observation aligns with the findings presented in the research conducted by Delage et al. (1996), titled "Microstructure of a compacted silt." In their study, they explicitly discuss that the heightened moisture content prompts a process known as hydration in the soil's clay particles. During hydration, water molecules are absorbed by these clay particles, leading to their expansion and an increase in volume. This phenomenon can contribute to the overall enlargement of the soil's structure, potentially enabling smoother water flow through its pore spaces.

However, under increased consolidation pressures, it was noticed that the curves displayed a notably shallower slope, implying that the permeability values for the dry of optimum, optimal moisture content (OMC), and wet of optimum conditions were relatively similar. Higher consolidation pressure leads to increased compaction and particle packing within the soil matrix. This tighter arrangement of particles reduces the void spaces through which water would normally flow. As a result, the differences in permeability between the dry, OMC, and wet conditions become less pronounced, as the compacted soil becomes more uniformly dense. As consolidation pressure increases, the pore spaces within the soil become narrower and more interconnected. This reduction in pore size and connectivity restricts the movement of water, making it harder for the permeability values to vary significantly between different moisture content levels.

5.4.2. For static compaction

The following figures, spanning from Figure 5.34 to Figure 5.38, visually represent the relationship between permeability and molding water content for samples subjected to static compaction. These figures provide a graphical overview of how permeability varies with different levels of moisture content during the static compaction process.

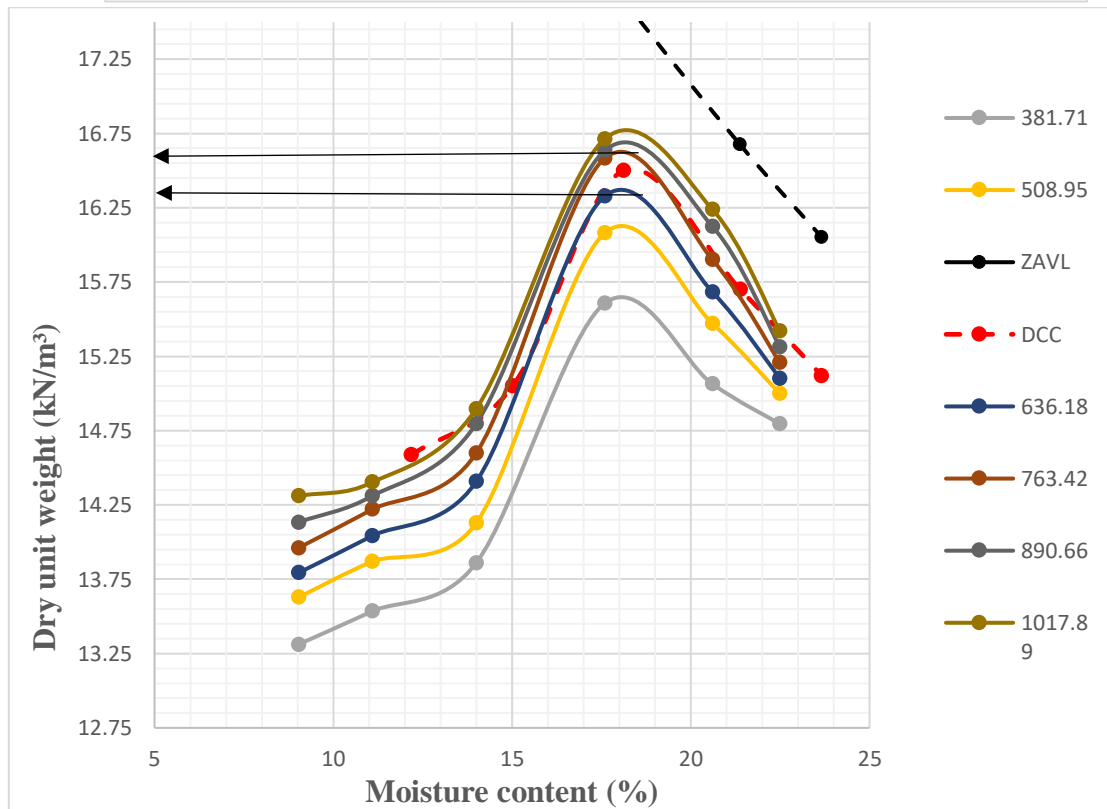
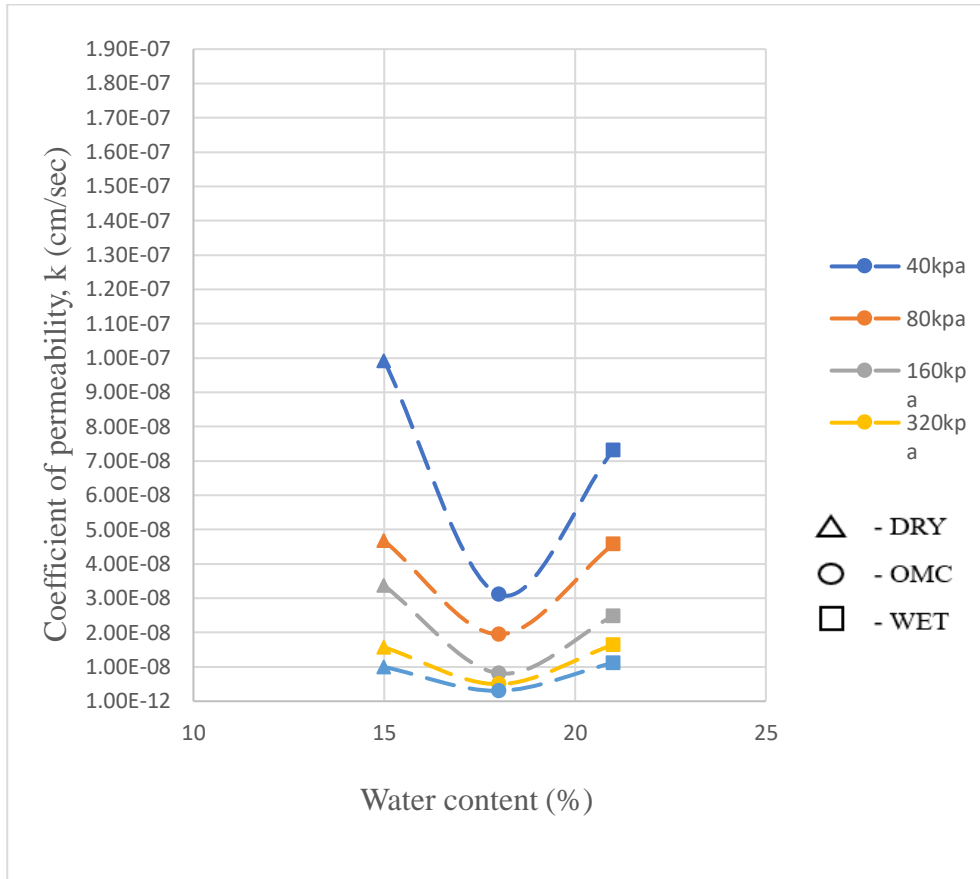


Figure 5.34: Permeability versus molding water content relationship for S1(static)

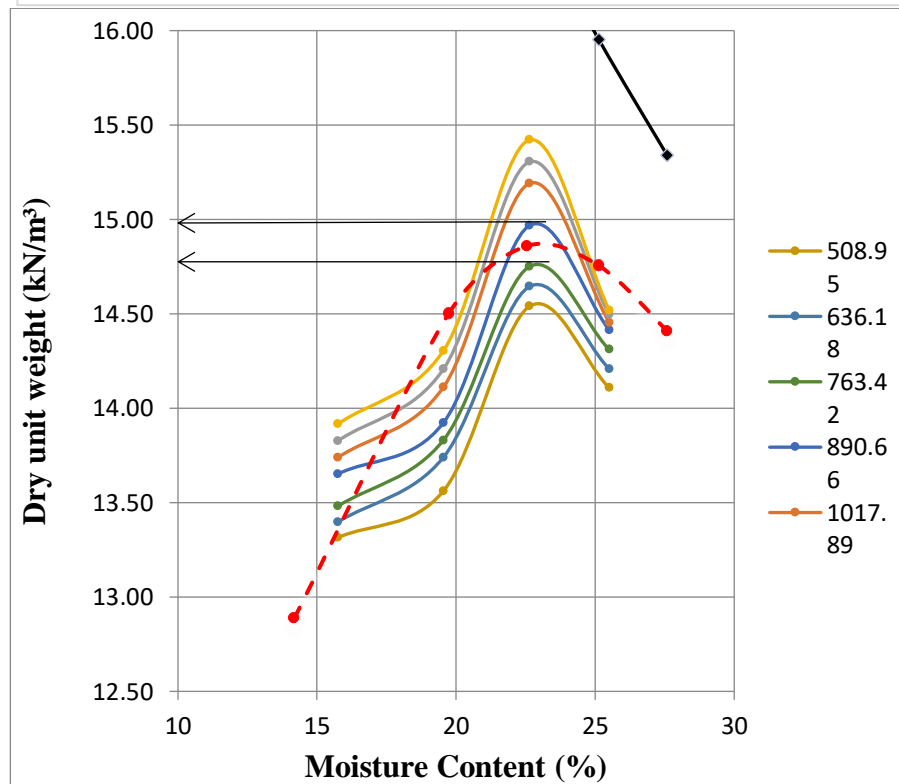
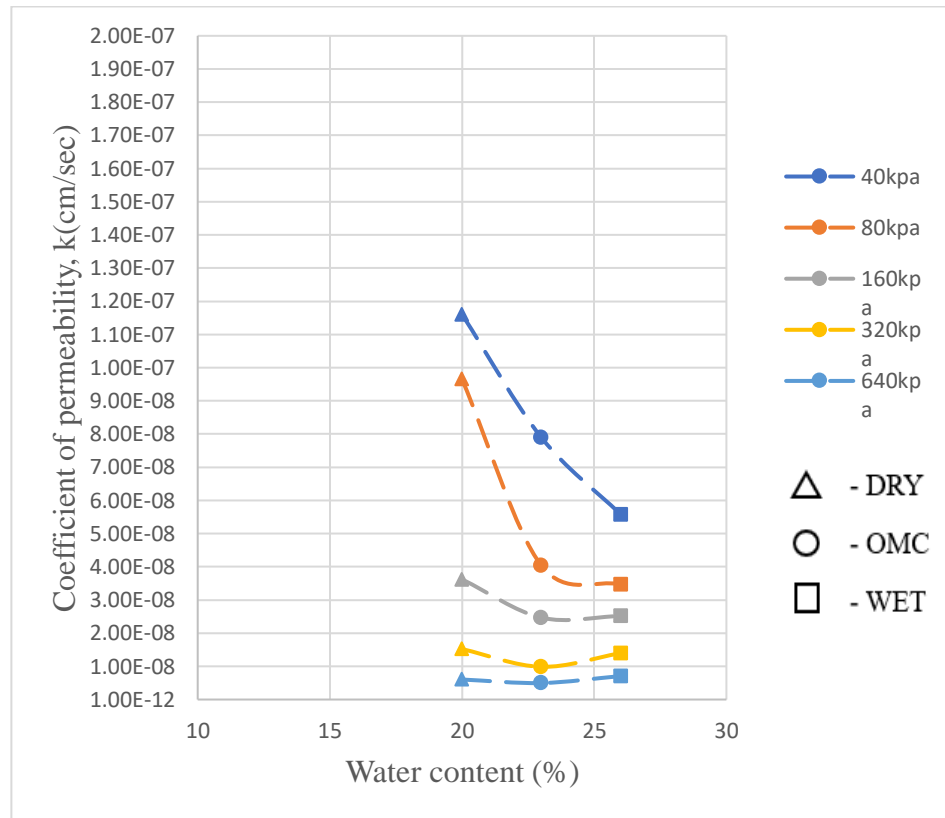


Figure 5.35: Permeability versus molding water content relationship for S2(static)

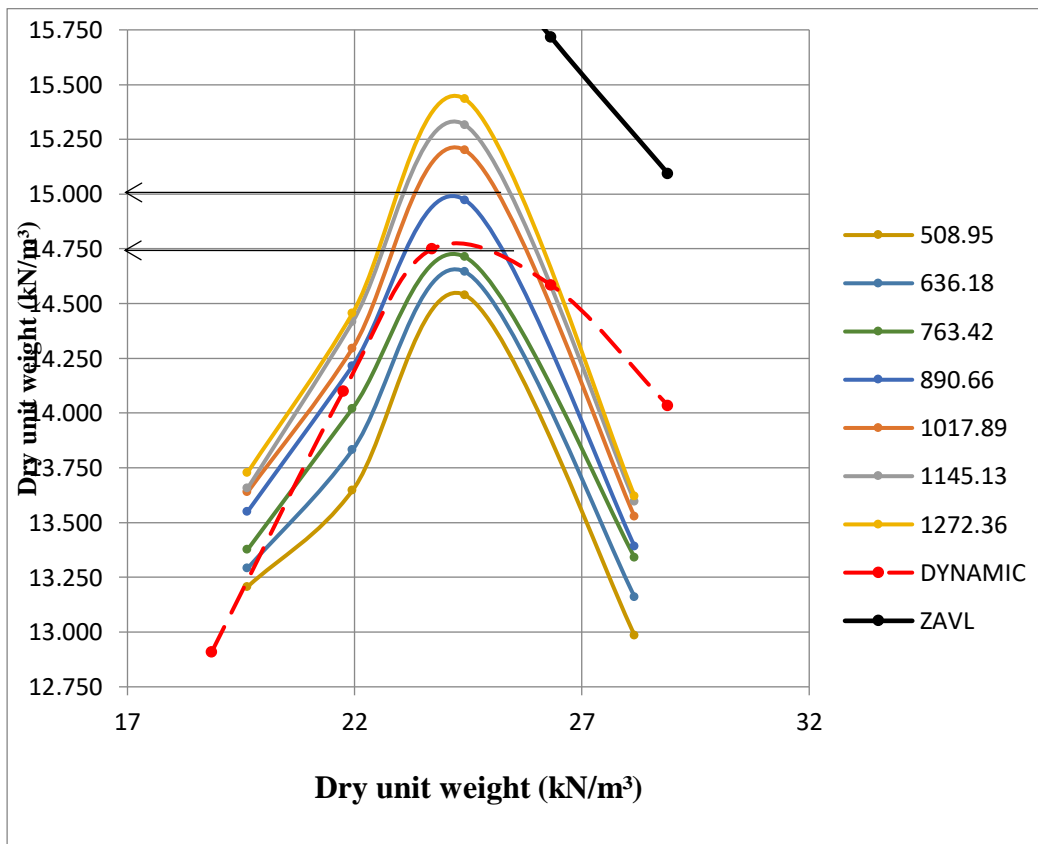
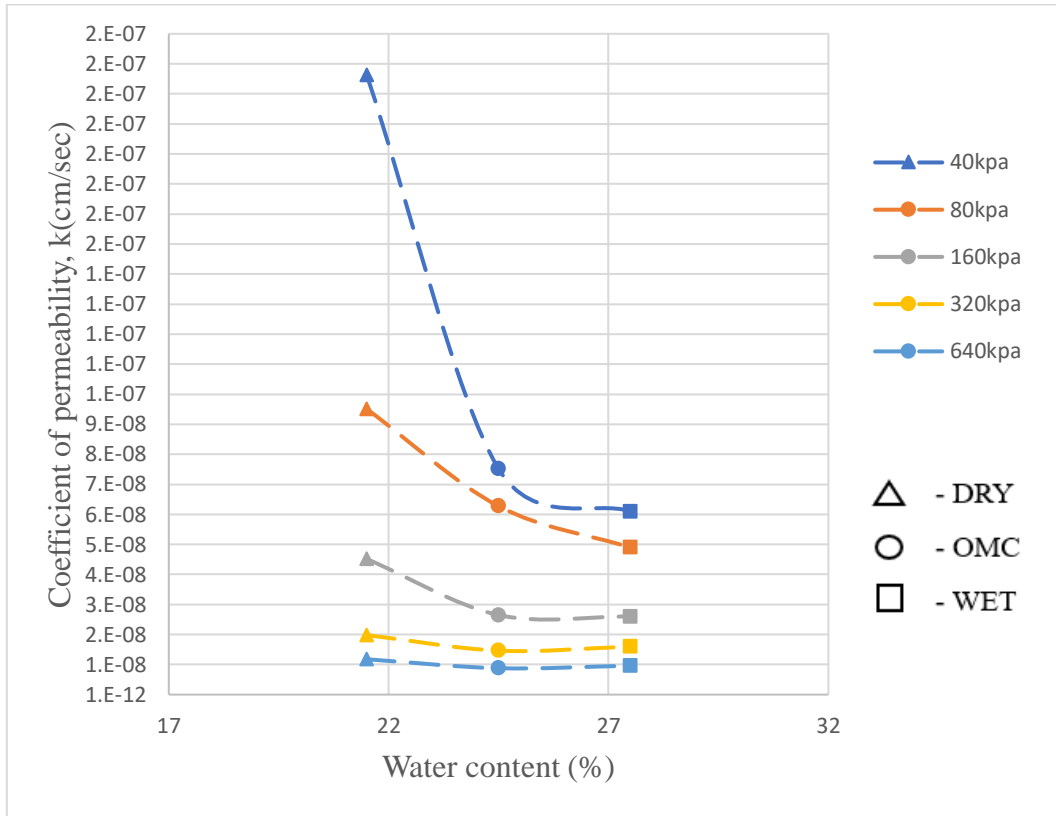


Figure 5.36: Permeability versus molding water content relationship for S3(static)

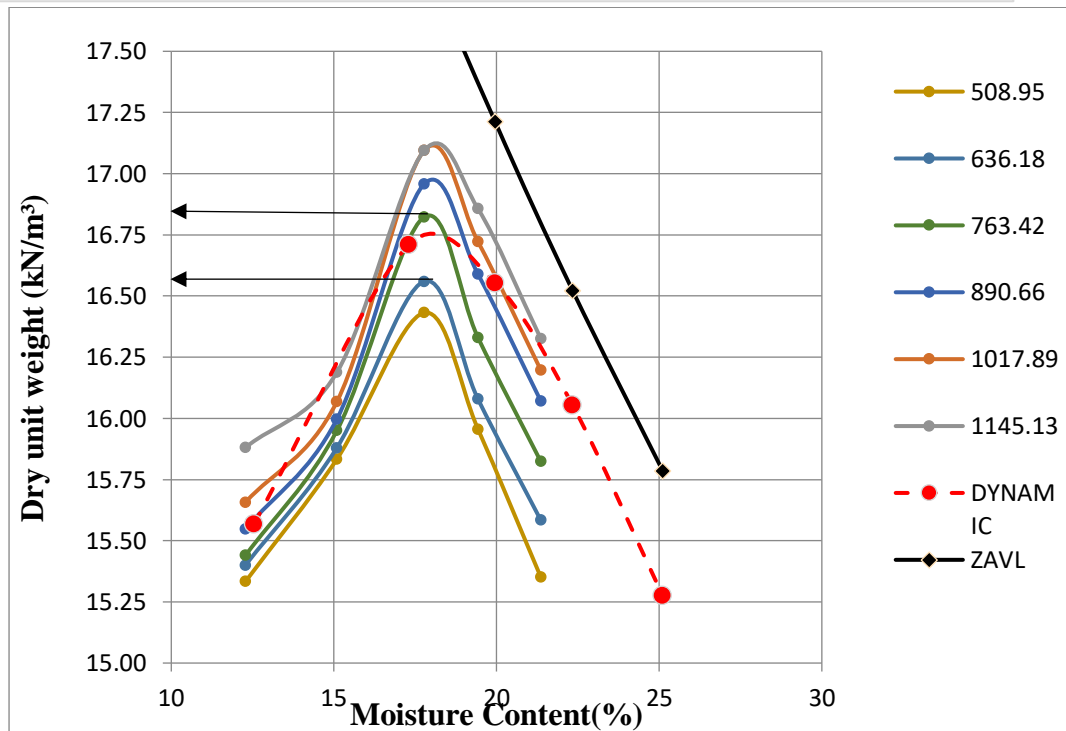
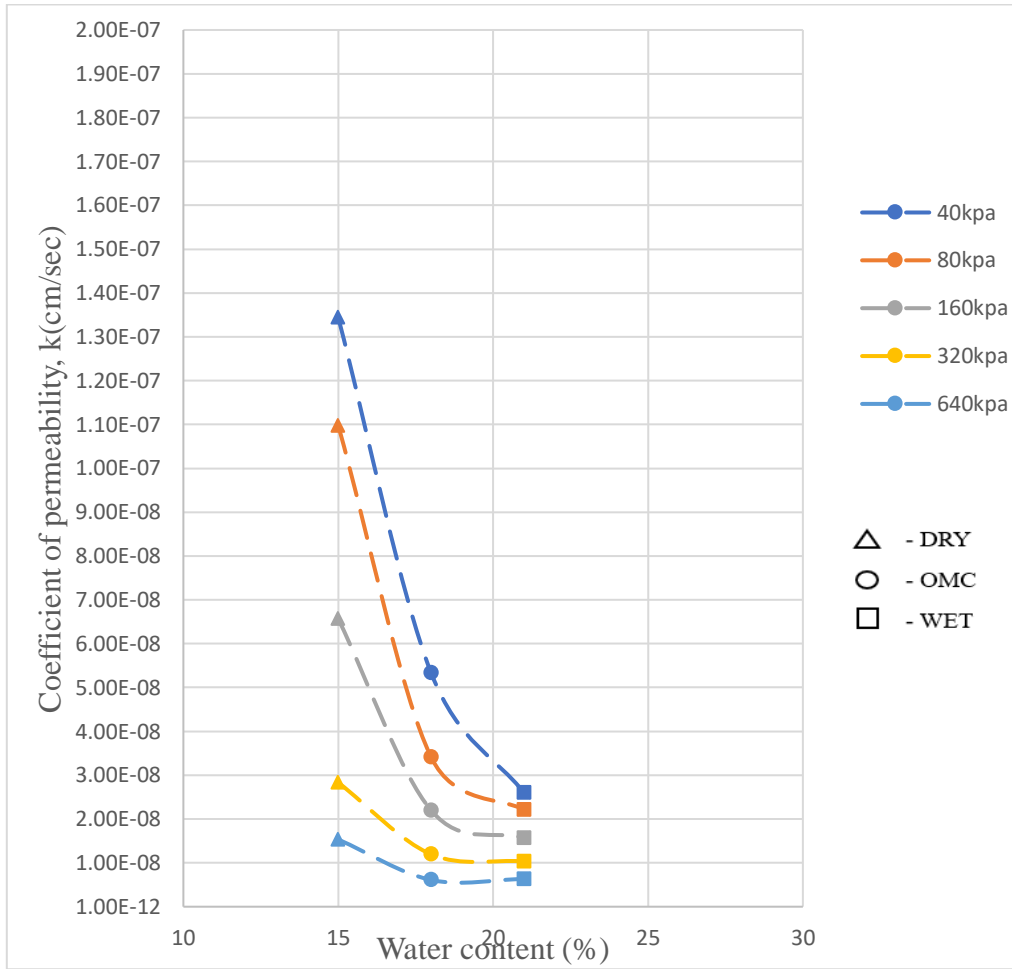


Figure 5.37: Permeability versus molding water content relationship for S4(static)

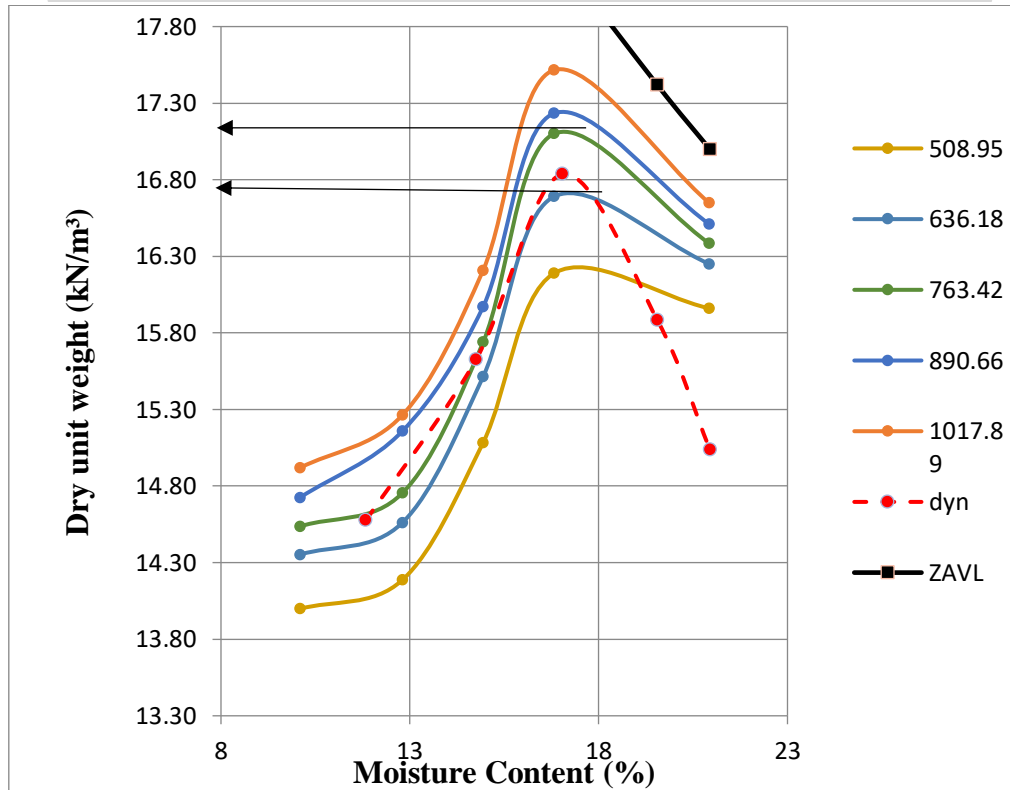
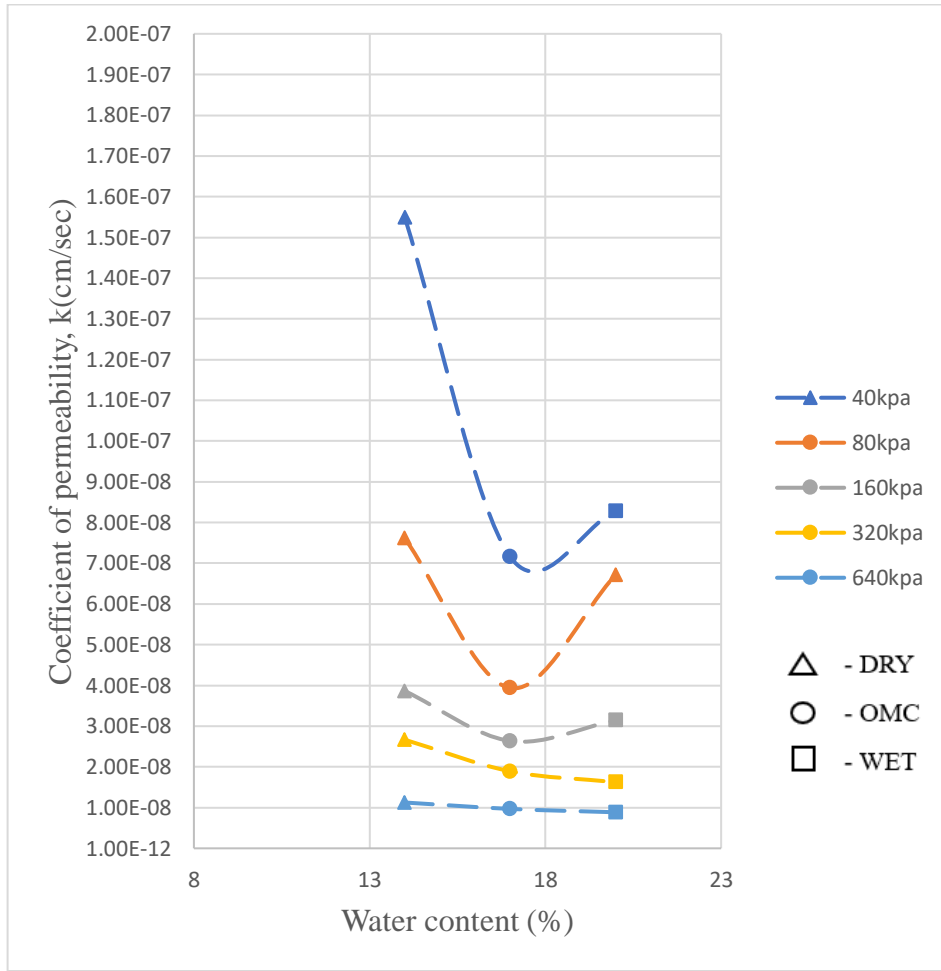


Figure 5.38: Permeability versus molding water content relationship for S5(static)

A distinct pattern emerged within specific samples subjected to both static compaction across various moisture levels. This encompassed conditions both before and after the optimum moisture content: the dry side of optimum, the optimum moisture content (OMC), and the wet side of optimum. These values revealed a consistent trend, progressing in a sequence. They exhibited higher values on the dry side of the optimum moisture content, followed by a reduction at the OMC, and culminating in their lowest levels when the soil was positioned on the wet side of the optimum spectrum. Significantly, in specific samples, the permeability values on the wet side demonstrated a slight elevation compared to those at the OMC, while the values on the dry side of optimum maintained their supremacy.

The explanation provided in section 5.4.1 of this chapter can be applied here to elaborate on the observed results in this context. This explanation explores the finer details of the relationship between moisture content and permeability, offering insights that help clarify the trends that have been witnessed. By employing the concepts presented in that specific section, the reasons behind the observed patterns in the data can be illuminated. This process further enriches the understanding of how the dynamic interplay between moisture levels and permeability plays a role in the variations present within the observed results.

Mitchell et al. (1965) examined how the compaction method affects the permeability of silty clay. It was anticipated that the structure would be greatly influenced by shear strains linked to compaction beyond the optimal line, and that different compaction methods would induce varying degrees of shear strain. Seed and Chan also looked into the effects of compaction methods on the swelling, shrinking, and stress-strain characteristics of compacted clays. Their test data revealed that the degree of shear strain and dispersion increases in the following sequence for different compaction methods: static, vibratory, and kneading.

Mitchell et al. (1965) had predicted that that samples compacted via kneading would display lower permeabilities than those compacted using static methods, particularly when molding water content exceeded the optimal level. To validate these predictions, silty clay samples were prepared using both static and kneading compaction techniques. The molds were 2.8 inches in diameter and 1 inch in height, ensuring uniformity. Furthermore, two tests were conducted on samples compacted through kneading in 3.5-inch-high molds. The results confirmed the earlier predictions, revealing that samples compacted statically were significantly more permeable than those compacted through kneading, specifically for samples

with moisture contents beyond the optimum. However, the differences were not as pronounced as initially expected.

To explain the permeability behavior of various structural clays, especially the notable decrease in permeability at optimum moisture and beyond the optimum water content for samples compacted statically, the concept of soil structure clusters by Olsen was considered.

Even under careful mixing before compaction, clay particles formed random aggregates or clusters. These clusters resisted deformation, but their resistance was expected to lessen with higher water content. Olsen illustrated that permeability in a cluster structure is primarily determined by flow through intercluster pores, rather than within the clusters themselves. With increasing molding water content, the clusters weakened, potentially becoming smaller due to mixing before compaction. This weakening, combined with higher water content, resulted in cluster distortion, causing reduced void spaces between clusters. Consequently, intercluster pore size decreased. Despite this, the structure maintained its flocculent nature beyond the optimal water content following static compaction, as evidenced by seed and Chan's analysis of swelling, shrinking, and strength properties. However, the heightened water content was sufficient to significantly distort the clusters and reduce average pore size.

Based on this observation, one can infer that the differences in permeabilities between the optimum moisture content (OMC) and the wet side of OMC are generally slight, particularly in the context of statically compacted soil.

CHAPTER 6

CONCLUSIONS AND SCOPE FOR FURTHER STUDY

6.1 INTRODUCTION:

Within this chapter, the conclusions extracted from the investigation of the compressibility and permeability traits pertaining to both statically and dynamically compacted soil at dry of optimum, optimum moisture content and wet of optimum are encapsulated. Furthermore, this chapter offers insights into potential avenues for future research in the field.

6.2 Conclusions from compressibility characteristics of statically and dynamically compacted soil samples:

- i. For the dry side of optimum moisture content, it was observed that the statically compacted curve exhibited a slightly greater compressibility compared to the dynamic curve across all samples
- ii. In contrast, both at the optimum moisture content (OMC) and on the wet side of optimum, the dynamically compacted curve displayed a slightly higher compressibility compared to the statically compacted curve for all samples.
- iii. Upon superimposing the consolidation curves of dynamically compacted soil samples from the dry side of optimum, OMC, and wet side of optimum onto a single graph, a distinct pattern emerged. The consolidation curve corresponding to the dry side was positioned atop, followed by the wet side curve, and finally, the OMC curve. This arrangement indicated that the void ratio was greatest at the dry side of optimum, followed by the wet side, and then the OMC.
- iv. Likewise, when the consolidation curves of statically compacted soil samples at the dry side of optimum, OMC, and wet side of optimum were overlaid on a single graph for all samples, a similar pattern emerged. The consolidation curve related to the dry side was positioned at the highest point, followed by the wet side curve, and subsequently the OMC curve. This alignment pointed towards the highest void ratio occurring at the dry side of optimum, followed by the wet side, and then the OMC.

6.3 Conclusions from permeability characteristics of statically and dynamically compacted soil samples:

- i. Observations on the dry side of the optimum reveal a slightly higher static permeability value compared to the dynamic one. However, the permeabilities of both are approximately within the same order or range.
- ii. When considering the optimum moisture content, slight variations in permeability characteristics were noticed when comparing statically compacted soil with dynamically compacted soil. However, the permeabilities for both methods were generally within the same range.
- iii. Analysis of the wet side of the optimum indicates minor differences in permeability characteristics between statically and dynamically compacted soil. However, the permeabilities of both typically fall within a similar order or range.
- iv. Superimposed permeability curves obtained solely from dynamic compaction at the dry side, optimum moisture content (OMC), and wet side of optimum revealed distinct variations in void ratio. In certain samples, the lines representing dry, wet, and OMC conditions were neatly stacked in that order, while in others, the differences were less noticeable. Nevertheless, the permeability values corresponding to dry, OMC, and wet conditions exhibited slight variations but closely aligned on semi-logarithmic graphs.
- v. Similarly, overlaying permeability curves obtained solely from static compaction at the dry side, OMC, and wet side of optimum exhibited noticeable fluctuations in void ratio. The lines representing dry, wet, and OMC conditions were arranged in sequence, with slight differences in some samples. Nonetheless, the permeability values for the dry, OMC, and wet conditions demonstrated marginal variations while closely aligning on semi-logarithmic graphs.
- vi. The permeability-molding water content relationship for dynamic compaction revealed that the permeability values followed a sequence, with higher values on the dry side, decreasing at OMC, and reaching their lowest on the wet side of the optimum moisture

content. Some samples showed slightly higher permeability values on the wet side compared to OMC, while dry side values remained the highest.

vii. Similarly, the permeability-molding water content relationship for static compaction highlighted a sequence, with higher values on the dry side, decreasing at OMC, and reaching their lowest on the wet side of the optimum spectrum. Notably, some samples displayed slightly elevated permeability values on the wet side compared to OMC, while dry side values-maintained superiority.

6.4. Scope for further study:

To enhance the understanding of the compressibility and permeability properties of soils that have undergone static and dynamic compaction, the following points should be taken into account:

- i. Consolidation tests should be performed beyond $\pm 3\%$ of optimum moisture content for both statically and dynamically compacted soil.
- ii. An examination is required to understand alterations in soil structure and fabric resulting from static and dynamic compaction methods.
- iii. An assessment of the mineralogy of soil samples undergoing consolidation through static and dynamic compaction methods.
- iv. Investigation into the alterations in compaction characteristics during static compaction at varying rates of loading.

REFERENCES

1. Ahmed, S., Lovell Jr, C. W., & Diamond, S. (1974). Pore sizes and strength of compacted clay. *Journal of the Geotechnical Engineering Division*, 100(4), 407-425.
2. Bernhard, R. K., & Krynine, D. P. (1952). Static and dynamic soil compaction. In *Highway Research Board Proceedings* (Vol. 31).
3. Crispim, F. A., Lima, D. C., Schaefer, C. E. G. R., Silva, C. H. C., Carvalho, C. A. B., Barbosa, P. S. A., & Brandão, E. H. (2011). The influence of laboratory compaction methods on soil structure: Mechanical and micromorphological analyses. *Soils and Rocks*, 34(1), 91-98.
4. Delage, P., Audiguier, M., Cui, Y. J., & Howat, M. D. (1996). Microstructure of a compacted silt. *Canadian Geotechnical Journal*, 33(1), 150-158.
5. Diamond, S. (1971). Microstructure and pore structure of impact-compacted clays. *Clays and Clay minerals*, 19, 239-249.
6. Diamond, S. (1970). Pore Size Distributions in Clays. *Clays Clay Miner.* **18**, 7–23.
7. Hafez, M. A., Asmani, M. D., & Nurbaya, S. (2010). Comparison between static and dynamic laboratory compaction methods. *Electronic Journal of Geotechnical Engineering*, 15(1), 1641-1650.
8. Hogentogler, C.A., (1937). *Engineering Properties of Soil*, McGraw-Hill Book Company, Inc., New York.
9. IS 2720-15, (1986). *Methods of Test for Soils: Determination of Consolidation Properties*, Bureau of Indian Standards, New Delhi, India.
10. IS 2720-5, (1985). *Methods of Test for Soils: Determination of Liquid Limit and Plastic Limit*, Bureau of Indian Standards, New Delhi, India.
11. IS 2720-3, (1980). *Methods of Test for Soils: Determination of Specific Gravity*, Bureau of Indian Standards, New Delhi, India.
12. IS 2720-3, (1980). *Methods of Test for Soils: Determination of Water Content Dry Density Relation Using Light Compaction*, Bureau of Indian Standards, New Delhi, India.
13. Kenai, S., Bahar, R., & Benazzoug, M. (2006). Experimental analysis of the effect of some compaction methods on mechanical properties and durability of cement stabilized soil. *Journal of Materials Science*, 41, 6956-6964.

14. Lee, K. L., & Haley, S. C. (1968). Strength of compacted clay at high pressure. *Journal of the Soil Mechanics and Foundations Division*, 94(6), 1303-1332.
15. Mitchell, J. K., Hooper, D. R., & Campenella, R. G. (1965). Permeability of compacted clay. *Journal of the Soil Mechanics and Foundations Division*, 91(4), 41-65.
16. Oliver, M. and Mesbah, A. (1999). Clayey soil behavior under static compaction test, *Materials and structures*, Volume 32; pp: 687-694.
17. Punmia, B.C., Jain, A.K., and Jain, A.K., (2005). *Soil mechanics and foundations*. Sixteenth Edition, Laxmi Publications (P) LTD.
18. Rajan, G., and Rao, A.S.R., (2016). *Basic and applied soil mechanics*. Third Edition, New Age International (P) LTD.
19. Reddy, B. V., & Jagadish, K. S. (1993). The static compaction of soils. *Geotechnique*, 43(2), 337-341.
20. Sharma, B., Deka, A. (2016). Static compaction test and determination of equivalent static pressure. In: *Proceedings of I.G.C., IIT Madras, Chennai, India*, pp. 1-4
21. Sharma, B., Sridharan, A., & Talukdar, P. (2016). Static method to determine compaction characteristics of fine-grained soils. *Geotechnical Testing Journal*, 39(6), 1048-1055.
22. Talukdar, P., Sharma, B., & Sridharan, A. (2014). Determination of compaction characteristics of soil by static compaction method. In *Proceedings of IGC* (pp. 18-20).

Appendix I

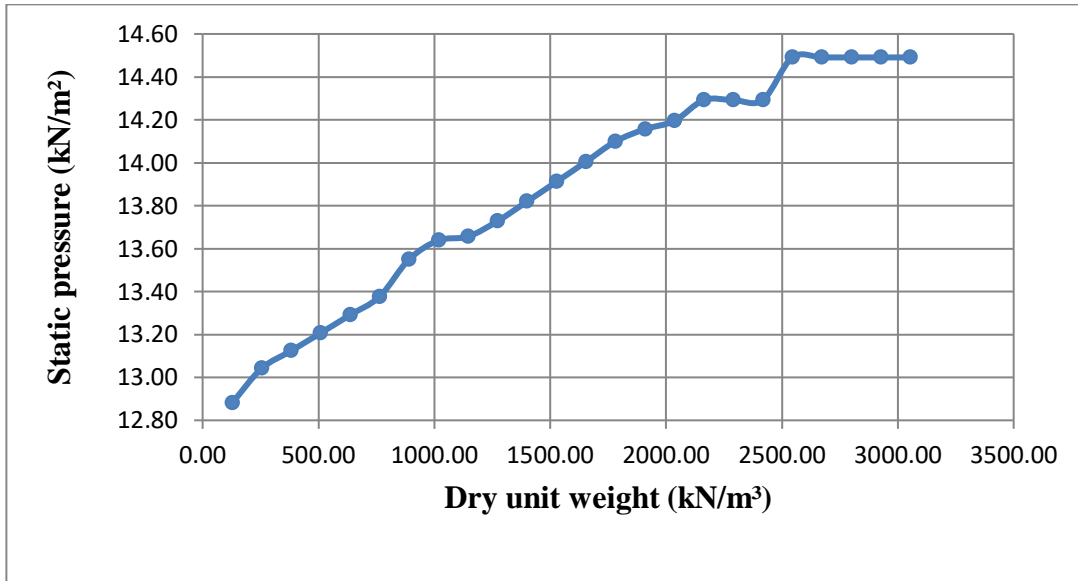


Figure 3.29: Dry unit weight vs Static Pressure curve for sample 3 at 19.64% water content

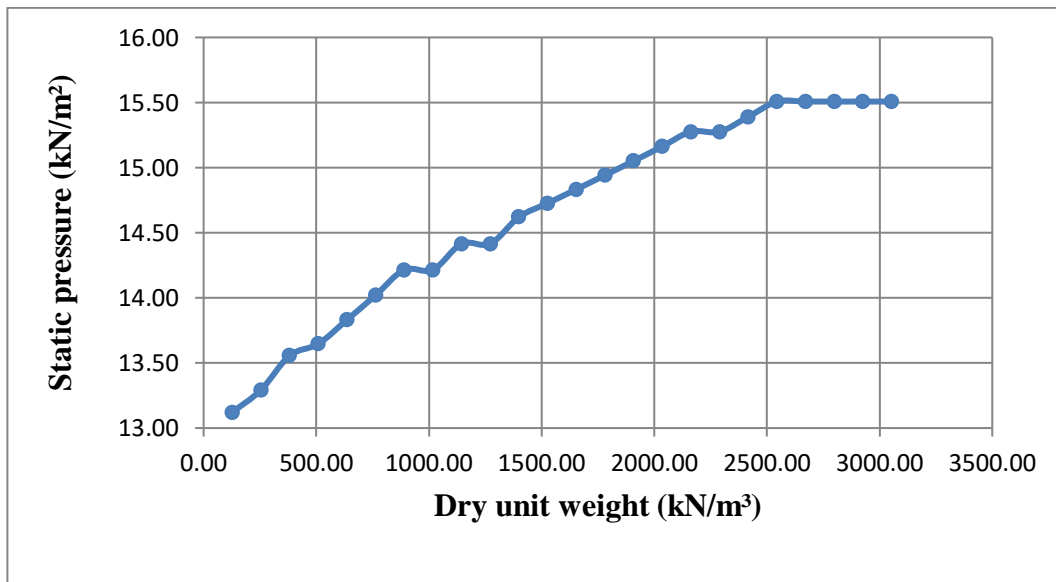


Figure 3.30: Dry unit weight vs Static Pressure curve for sample 3 at 21.95% water content

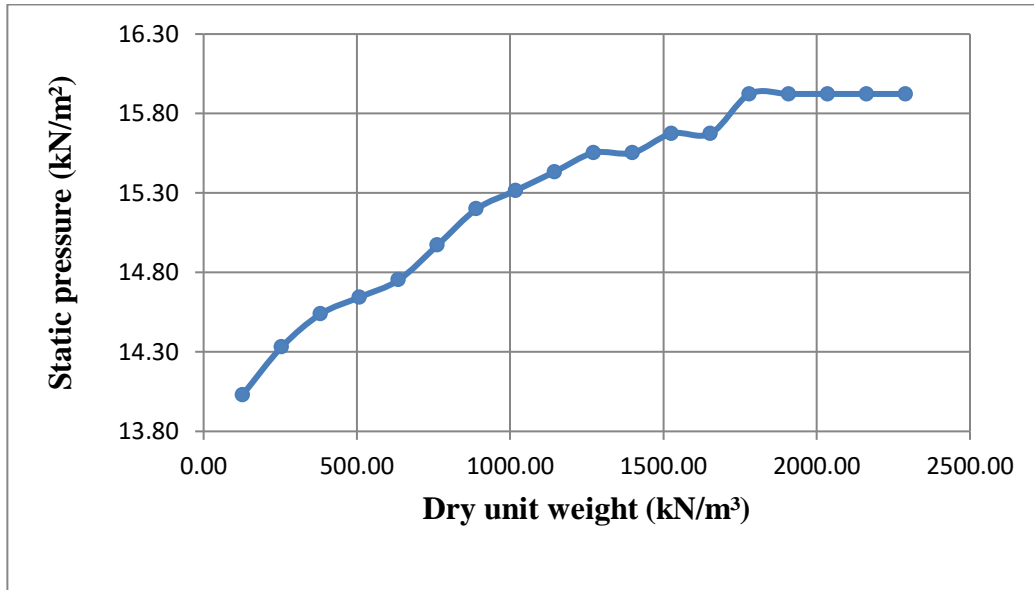


Figure 3.31: Dry unit weight vs Static Pressure curve for sample 3 at 24.43% water content

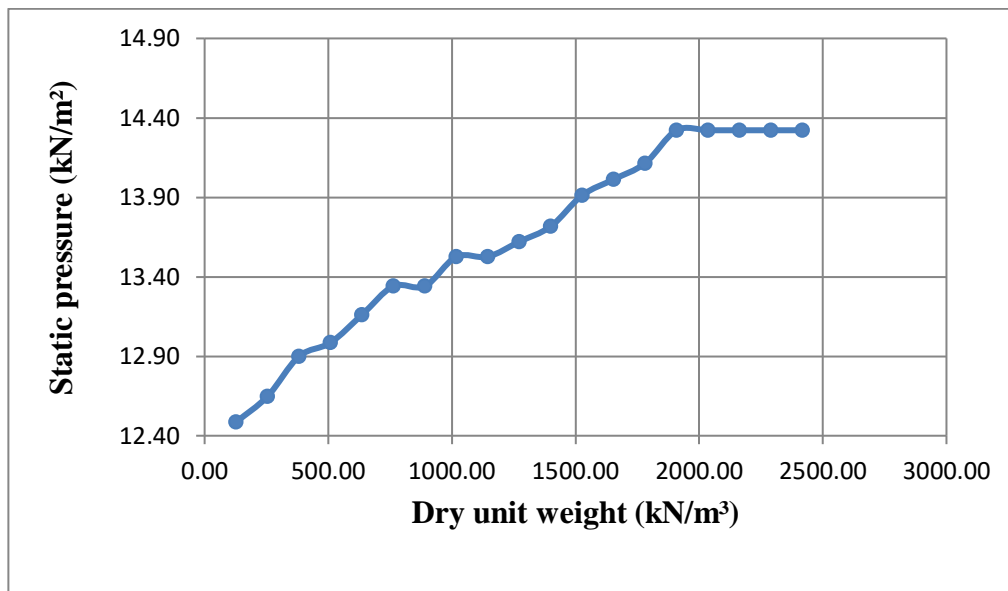


Figure 3.32: Dry unit weight vs Static Pressure curve for sample 3 at 28.16% water content

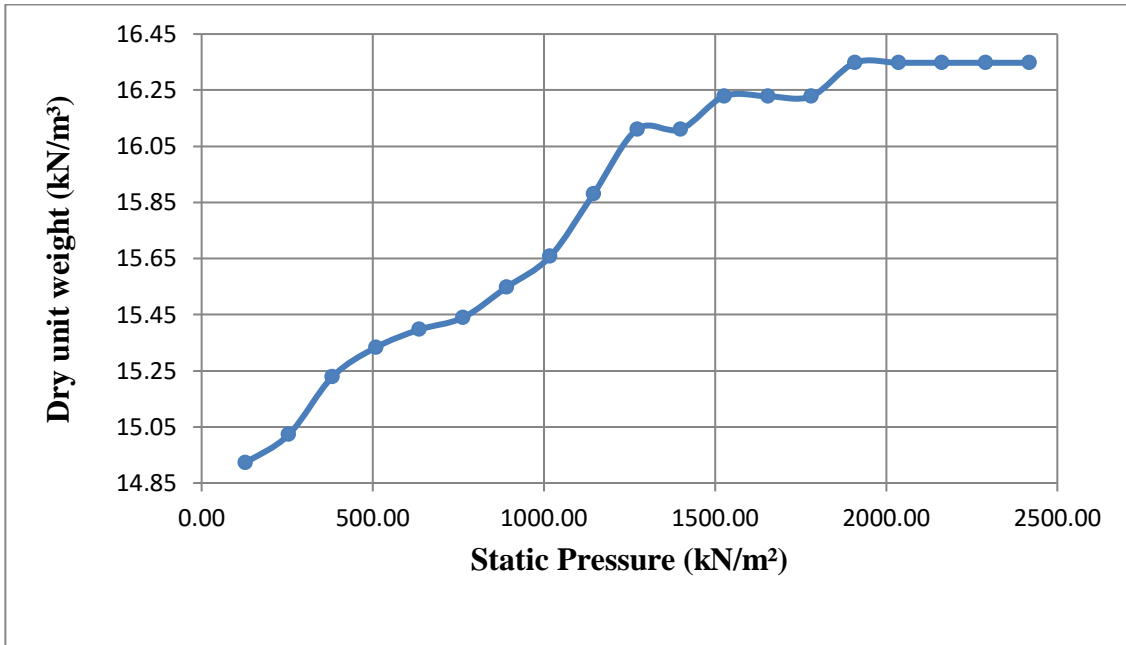


Figure 3.33: Dry unit weight vs Static Pressure curve for sample 4 at 12.28% water content

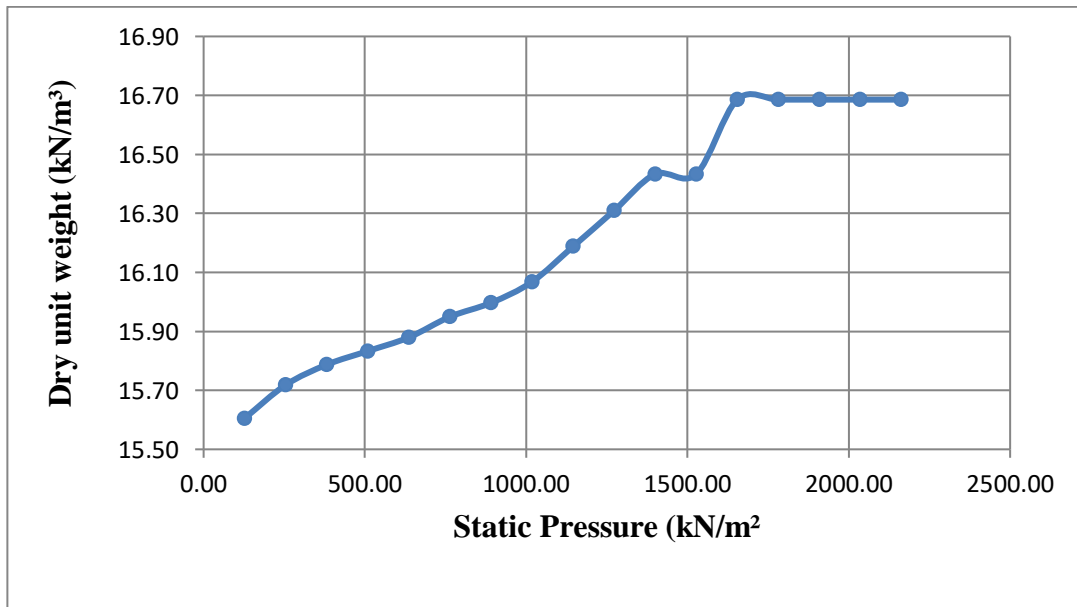


Figure 3.34: Dry unit weight vs Static Pressure curve for sample 4 at 15.09% water content

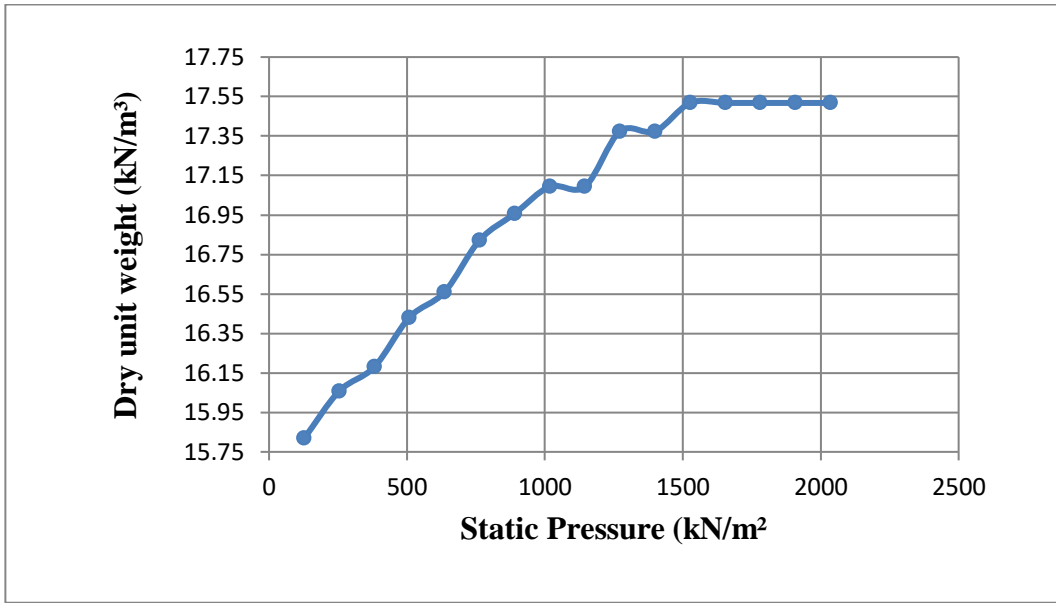


Figure 3.35: Dry unit weight vs Static Pressure curve for sample 4 at 17.77% water content

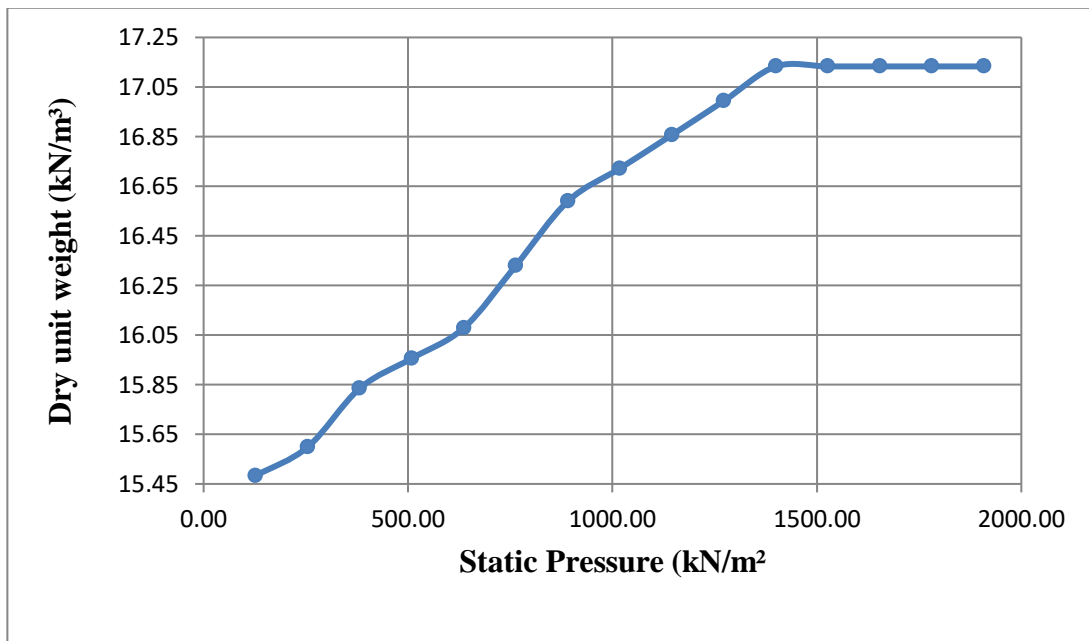


Figure 3.36: Dry unit weight vs Static Pressure curve for sample 4 at 19.43% water content

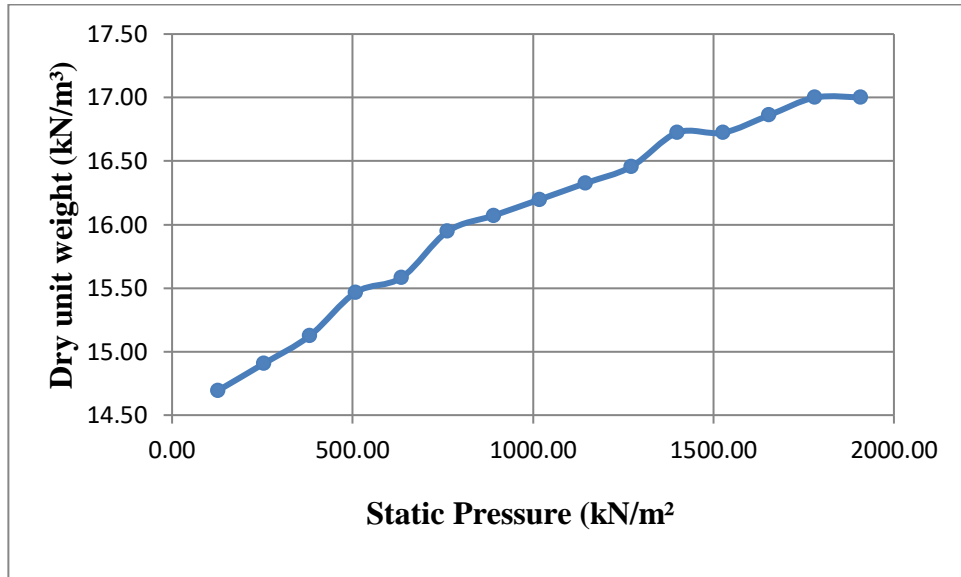


Figure 3.37: Dry unit weight vs Static Pressure curve for sample 4 at 21.36% water content

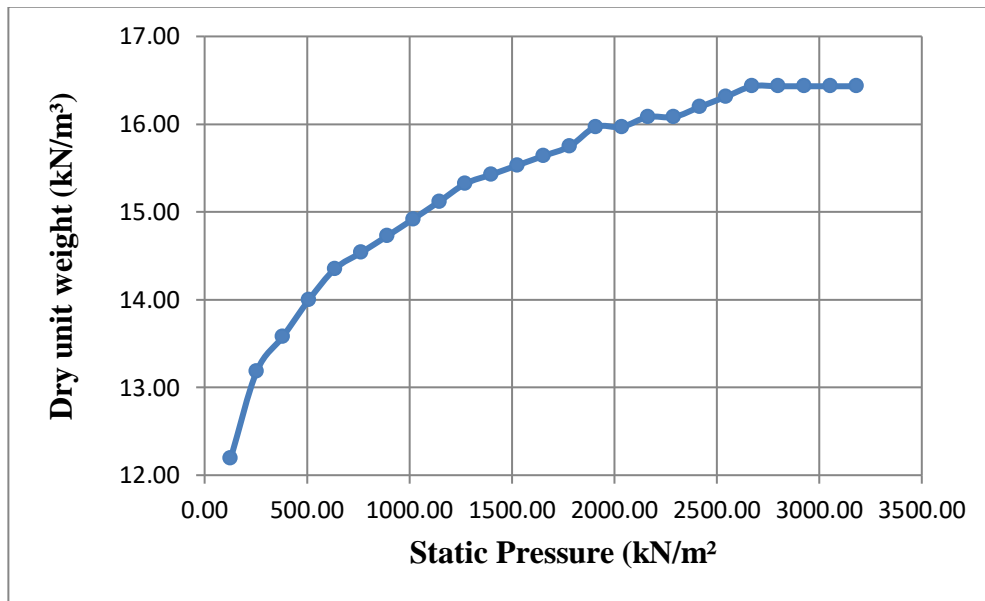


Figure 3.38: Dry unit weight vs Static Pressure curve for sample 5 at 10.09% water content

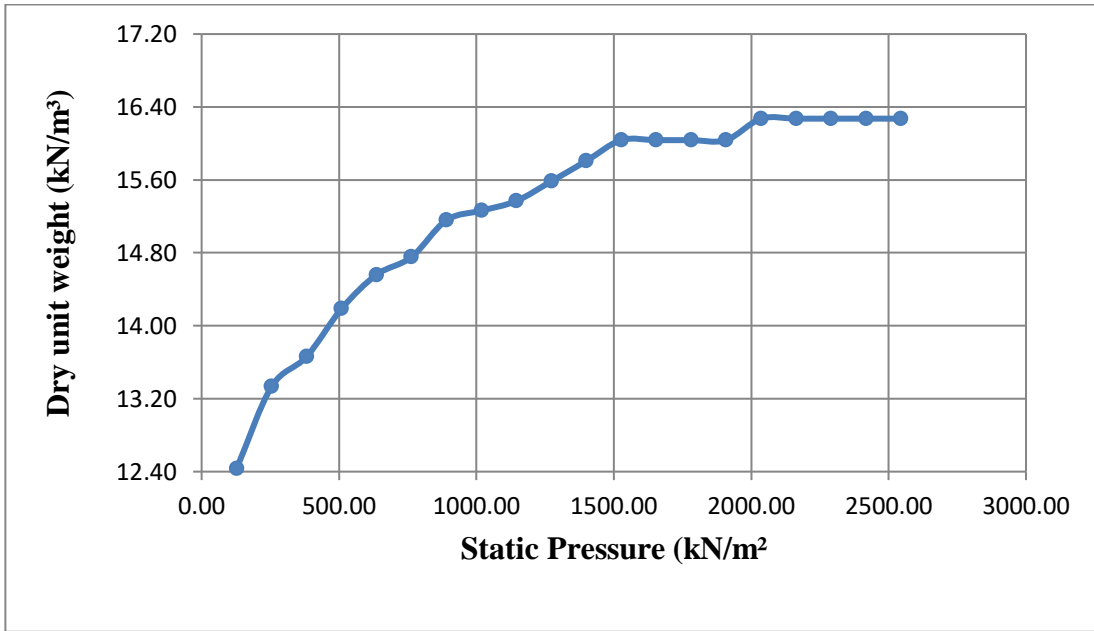


Figure 3.39: Dry unit weight vs Static Pressure curve for sample 5 at 12.80% water content

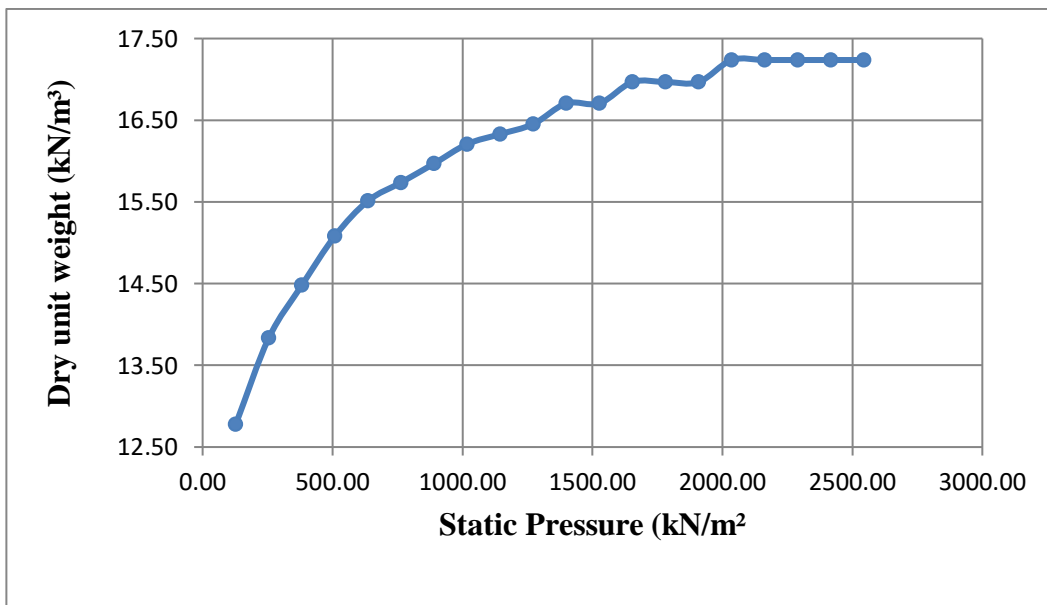


Figure 3.40: Dry unit weight vs Static Pressure curve for sample 5 at 14.94% water content

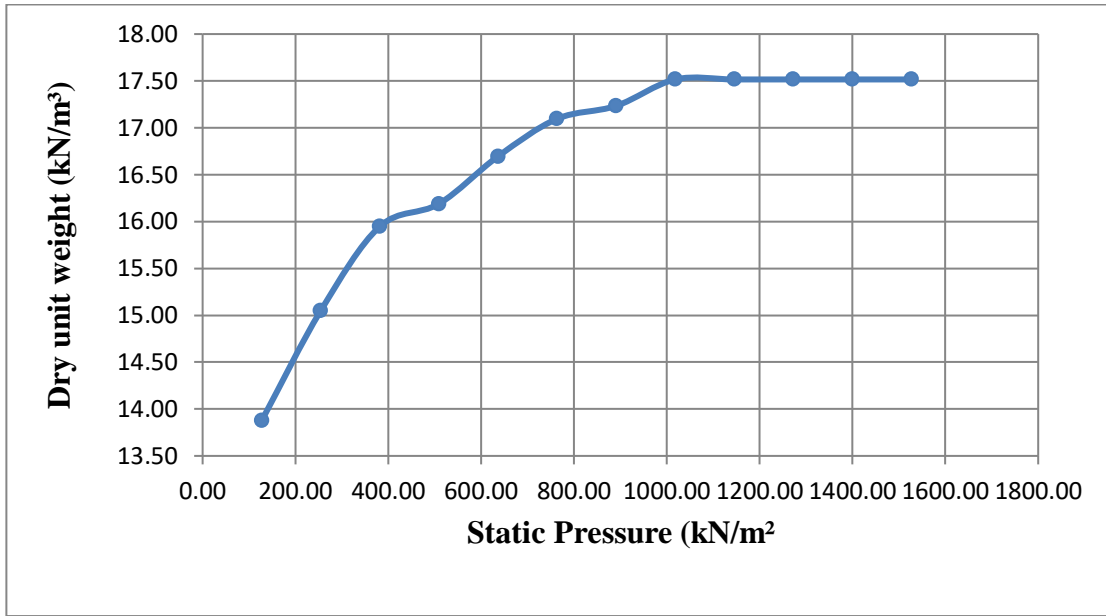


Figure 3.41: Dry unit weight vs Static Pressure curve for sample 5 at 16.82% water content

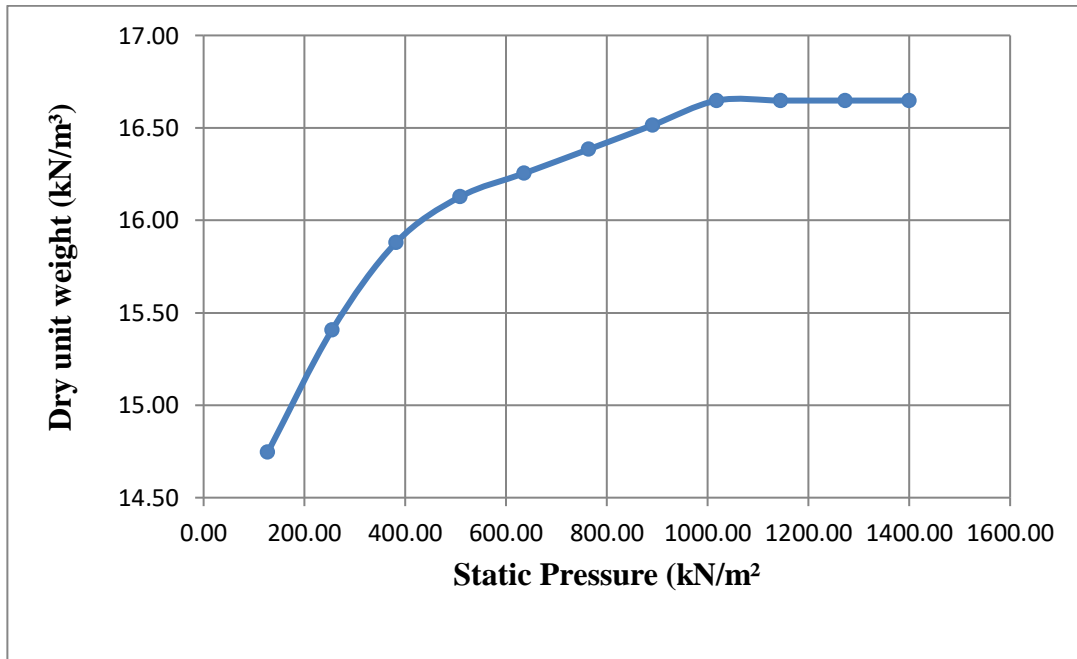


Figure 3.42: Dry unit weight vs Static Pressure curve for sample 5 at 20.93% water content

Appendix II

Table 3.5. Specimen height and void ratio calculation for sample 1 (dynamic at dry of optimum)

| Applied Pressure (kN/m ²) | Final Dial Reading (mm) | No. of division (a) | Dial change, $\Delta H = a \times L.C.$ (mm) | Specimen height, $H = H_1 - \Delta H$ (mm) | Height of voids, $H - H_s$ (mm) | Void ratio, $e = (H - H_s)/H_s$ |
|---------------------------------------|-------------------------|---------------------|--|--|---------------------------------|---------------------------------|
| 5 | 310 | | | 20 | 8.433 | 0.729 |
| 10 | 304 | 6 | 0.06 | 19.94 | 8.373 | 0.724 |
| 20 | 291 | 13 | 0.13 | 19.81 | 8.243 | 0.713 |
| 40 | 284.5 | 6.5 | 0.065 | 19.745 | 8.178 | 0.707 |
| 80 | 272.5 | 12 | 0.12 | 19.625 | 8.058 | 0.697 |
| 160 | 252 | 20.5 | 0.205 | 19.42 | 7.853 | 0.679 |
| 320 | 228 | 24 | 0.24 | 19.18 | 7.613 | 0.658 |
| 640 | 198.5 | 29.5 | 0.295 | 18.885 | 7.318 | 0.633 |

Table 3.6. Specimen height and void ratio calculation for sample 1 (dynamic at optimum moisture content)

| Applied Pressure (kN/m ²) | Final Dial Reading (mm) | No. of division (a) | Dial change, $\Delta H = a \times L.C.$ (mm) | Specimen height, $H = H_1 - \Delta H$ (mm) | Height of voids, $H - H_s$ (mm) | Void ratio, $e = (H - H_s)/H_s$ |
|---------------------------------------|-------------------------|---------------------|--|--|---------------------------------|---------------------------------|
| 5 | 383.9 | | | 20 | 7.398 | 0.587 |
| 10 | 365.4 | 18.5 | 0.185 | 19.815 | 7.213 | 0.572 |
| 20 | 349.7 | 15.7 | 0.157 | 19.658 | 7.056 | 0.560 |
| 40 | 323.9 | 25.8 | 0.258 | 19.4 | 6.798 | 0.539 |
| 80 | 290.1 | 33.8 | 0.338 | 19.062 | 6.460 | 0.513 |
| 160 | 257.2 | 32.9 | 0.329 | 18.733 | 6.131 | 0.486 |
| 320 | 212.3 | 44.9 | 0.449 | 18.284 | 5.682 | 0.451 |
| 640 | 168.5 | 43.8 | 0.438 | 17.846 | 5.244 | 0.416 |

Table 3.7. Specimen height and void ratio calculation for sample 1 (dynamic at wet of optimum)

| Applied Pressure (kN/m ²) | Final Dial Reading (mm) | No. of division (a) | Dial change, $\Delta H = a \times L.C.$ (mm) | Specimen height, $H = H_1 - \Delta H$ (mm) | Height of voids, $H - H_s$ (mm) | Void ratio, $e = (H - H_s)/H_s$ |
|---------------------------------------|-------------------------|---------------------|--|--|---------------------------------|---------------------------------|
| 5 | 383.9 | | | 20 | 8.010 | 0.668 |
| 10 | 365.4 | 18.5 | 0.185 | 19.815 | 7.825 | 0.653 |
| 20 | 349.7 | 15.7 | 0.157 | 19.658 | 7.668 | 0.639 |
| 40 | 323.9 | 25.8 | 0.258 | 19.4 | 7.410 | 0.618 |
| 80 | 290.1 | 33.8 | 0.338 | 19.062 | 7.072 | 0.590 |
| 160 | 257.2 | 32.9 | 0.329 | 18.733 | 6.743 | 0.562 |
| 320 | 212.3 | 44.9 | 0.449 | 18.284 | 6.294 | 0.525 |
| 640 | 161.5 | 50.8 | 0.508 | 17.776 | 5.786 | 0.483 |

Table 3.8. Specimen height and void ratio calculation for sample 1 (static at dry of optimum)

| Applied Pressure (kN/m ²) | Final Dial Reading (mm) | No. of division (a) | Dial change, $\Delta H = a \times L.C.$ (mm) | Specimen height, $H = H_1 - \Delta H$ (mm) | Height of voids, $H - H_s$ (mm) | Void ratio, $e = (H - H_s) / H_s$ |
|---------------------------------------|-------------------------|---------------------|--|--|---------------------------------|-----------------------------------|
| 5 | 358 | | | 20 | 8.433 | 0.729 |
| 10 | 335 | 23 | 0.23 | 19.77 | 8.203 | 0.709 |
| 20 | 318.5 | 16.5 | 0.165 | 19.605 | 8.038 | 0.695 |
| 40 | 309 | 9.5 | 0.095 | 19.51 | 7.943 | 0.687 |
| 80 | 285.5 | 23.5 | 0.235 | 19.275 | 7.708 | 0.666 |
| 160 | 251 | 34.5 | 0.345 | 18.93 | 7.363 | 0.637 |
| 320 | 220.5 | 30.5 | 0.305 | 18.625 | 7.058 | 0.610 |
| 640 | 186.5 | 34 | 0.34 | 18.285 | 6.718 | 0.581 |

Table 3.9. Specimen height and void ratio calculation for sample 1 (static at optimum moisture content)

| Applied Pressure (kN/m ²) | Final Dial Reading (mm) | No. of division (a) | Dial change, $\Delta H = a \times L.C.$ (mm) | Specimen height, $H = H_1 - \Delta H$ (mm) | Height of voids, $H - H_s$ (mm) | Void ratio, $e = (H - H_s) / H_s$ |
|---------------------------------------|-------------------------|---------------------|--|--|---------------------------------|-----------------------------------|
| 5 | 387 | | | 20 | 7.398 | 0.587 |
| 10 | 367.2 | 19.8 | 0.198 | 19.802 | 7.200 | 0.571 |
| 20 | 355.1 | 12.1 | 0.121 | 19.681 | 7.079 | 0.562 |
| 40 | 335.6 | 19.5 | 0.195 | 19.486 | 6.884 | 0.546 |
| 80 | 310.9 | 24.7 | 0.247 | 19.239 | 6.637 | 0.527 |
| 160 | 288.1 | 22.8 | 0.228 | 19.011 | 6.409 | 0.509 |
| 320 | 257.4 | 30.7 | 0.307 | 18.704 | 6.102 | 0.484 |
| 640 | 219.3 | 38.1 | 0.381 | 18.323 | 5.721 | 0.454 |

Table 3.10. Specimen height and void ratio calculation for sample 1 (static at wet of optimum)

| Applied Pressure (kN/m ²) | Final Dial Reading (mm) | No. of division (a) | Dial change, $\Delta H = a \times L.C.$ (mm) | Specimen height, $H = H_1 - \Delta H$ (mm) | Height of voids, $H - H_s$ (mm) | Void ratio, $e = (H - H_s) / H_s$ |
|---------------------------------------|-------------------------|---------------------|--|--|---------------------------------|-----------------------------------|
| 5 | 387 | | | 20 | 8.010 | 0.668 |
| 10 | 367.2 | 19.8 | 0.198 | 19.802 | 7.812 | 0.651 |
| 20 | 355.1 | 12.1 | 0.121 | 19.681 | 7.691 | 0.641 |
| 40 | 335.6 | 19.5 | 0.195 | 19.486 | 7.496 | 0.625 |
| 80 | 310.9 | 24.7 | 0.247 | 19.239 | 7.249 | 0.605 |
| 160 | 288.1 | 22.8 | 0.228 | 19.011 | 7.021 | 0.586 |
| 320 | 257.4 | 30.7 | 0.307 | 18.704 | 6.714 | 0.560 |
| 640 | 219.3 | 38.1 | 0.381 | 18.323 | 6.333 | 0.528 |

Table 3.11. Specimen height and void ratio calculation for sample 2 (dynamic at dry of optimum)

| Applied Pressure (kN/m ²) | Final Dial Reading (mm) | No. of division (a) | Dial change, $\Delta H = a \times L.C.$ (mm) | Specimen height, $H = H_1 - \Delta H$ (mm) | Height of voids, $H - H_s$ (mm) | Void ratio, $e = (H - H_s) / H_s$ |
|---------------------------------------|-------------------------|---------------------|--|--|---------------------------------|-----------------------------------|
| 5 | 393 | | | 20 | 9.071 | 0.830 |
| 10 | 380 | 13 | 0.13 | 19.87 | 8.941 | 0.818 |
| 20 | 368 | 12 | 0.12 | 19.75 | 8.821 | 0.807 |
| 40 | 350 | 18 | 0.18 | 19.57 | 8.641 | 0.791 |
| 80 | 330 | 20 | 0.2 | 19.37 | 8.441 | 0.772 |
| 160 | 307 | 23 | 0.23 | 19.14 | 8.211 | 0.751 |
| 320 | 278 | 29 | 0.29 | 18.85 | 7.921 | 0.725 |
| 640 | 248 | 30 | 0.3 | 18.55 | 7.621 | 0.697 |

Table 3.12. Specimen height and void ratio calculation for sample 2 (dynamic at optimum moisture content)

| Applied Pressure (kN/m ²) | Final Dial Reading (mm) | No. of division (a) | Dial change, $\Delta H = a \times L.C.$ (mm) | Specimen height, $H = H_1 - \Delta H$ (mm) | Height of voids, $H - H_s$ (mm) | Void ratio, $e = (H - H_s) / H_s$ |
|---------------------------------------|-------------------------|---------------------|--|--|---------------------------------|-----------------------------------|
| 5 | 391 | | | 20 | 8.808 | 0.787 |
| 10 | 382.1 | 8.9 | 0.089 | 19.911 | 8.719 | 0.779 |
| 20 | 374.8 | 7.3 | 0.073 | 19.838 | 8.646 | 0.773 |
| 40 | 355.9 | 18.9 | 0.189 | 19.649 | 8.457 | 0.756 |
| 80 | 324.2 | 31.7 | 0.317 | 19.332 | 8.140 | 0.727 |
| 160 | 275.5 | 48.7 | 0.487 | 18.845 | 7.653 | 0.684 |
| 320 | 206 | 69.5 | 0.695 | 18.150 | 6.958 | 0.622 |
| 640 | 121.7 | 84.3 | 0.843 | 17.307 | 6.115 | 0.546 |

Table 3.13. Specimen height and void ratio calculation for sample 2 (dynamic at wet of optimum)

| Applied Pressure (kN/m ²) | Final Dial Reading (mm) | No. of division (a) | Dial change, $\Delta H = a \times L.C.$ (mm) | Specimen height, $H = H_1 - \Delta H$ (mm) | Height of voids, $H - H_s$ (mm) | Void ratio, $e = (H - H_s) / H_s$ |
|---------------------------------------|-------------------------|---------------------|--|--|---------------------------------|-----------------------------------|
| 5 | 390.8 | | | 20 | 8.981 | 0.815 |
| 10 | 381 | 9.8 | 0.098 | 19.902 | 8.883 | 0.806 |
| 20 | 362.4 | 18.6 | 0.186 | 19.716 | 8.697 | 0.789 |
| 40 | 335.5 | 26.9 | 0.269 | 19.447 | 8.428 | 0.765 |
| 80 | 303.2 | 32.3 | 0.323 | 19.124 | 8.105 | 0.736 |
| 160 | 269 | 34.2 | 0.342 | 18.782 | 7.763 | 0.705 |
| 320 | 222.3 | 46.7 | 0.467 | 18.315 | 7.296 | 0.662 |
| 640 | 165 | 57.3 | 0.573 | 17.742 | 6.723 | 0.610 |

Table 3.14. Specimen height and void ratio calculation for sample 2 (static at dry of optimum)

| Applied Pressure (kN/m ²) | Final Dial Reading (mm) | No. of division (a) | Dial change, $\Delta H = a \times L.C.$ (mm) | Specimen height, $H = H_1 - \Delta H$ (mm) | Height of voids, $H - H_s$ (mm) | Void ratio, $e = (H - H_s)/H_s$ |
|---------------------------------------|-------------------------|---------------------|--|--|---------------------------------|---------------------------------|
| 5 | 387 | | | 20 | 9.071 | 0.830 |
| 10 | 370 | 17 | 0.17 | 19.83 | 8.901 | 0.814 |
| 20 | 350 | 20 | 0.2 | 19.63 | 8.701 | 0.796 |
| 40 | 330 | 20 | 0.2 | 19.43 | 8.501 | 0.778 |
| 80 | 305 | 25 | 0.25 | 19.18 | 8.251 | 0.755 |
| 160 | 276 | 29 | 0.29 | 18.89 | 7.961 | 0.728 |
| 320 | 240 | 36 | 0.36 | 18.53 | 7.601 | 0.695 |
| 640 | 205.5 | 34.5 | 0.345 | 18.185 | 7.256 | 0.664 |

Table 3.15. Specimen height and void ratio calculation for sample 2 (static at optimum moisture content)

| Applied Pressure (kN/m ²) | Final Dial Reading (mm) | No. of division (a) | Dial change, $\Delta H = a \times L.C.$ (mm) | Specimen height, $H = H_1 - \Delta H$ (mm) | Height of voids, $H - H_s$ (mm) | Void ratio, $e = (H - H_s)/H_s$ |
|---------------------------------------|-------------------------|---------------------|--|--|---------------------------------|---------------------------------|
| 5 | 397 | | | 20 | 8.808 | 0.787 |
| 10 | 390 | 7 | 0.070 | 19.930 | 8.738 | 0.781 |
| 20 | 384 | 6 | 0.060 | 19.870 | 8.678 | 0.775 |
| 40 | 369 | 15 | 0.150 | 19.72 | 8.528 | 0.762 |
| 80 | 349 | 20 | 0.200 | 19.52 | 8.328 | 0.744 |
| 160 | 308.7 | 40.3 | 0.403 | 19.117 | 7.925 | 0.708 |
| 320 | 265.6 | 43.1 | 0.431 | 18.686 | 7.494 | 0.670 |
| 640 | 221.6 | 44 | 0.440 | 18.246 | 7.054 | 0.630 |

Table 3.16. Specimen height and void ratio calculation for sample 2 (static at wet of optimum)

| Applied Pressure (kN/m ²) | Final Dial Reading (mm) | No. of division (a) | Dial change, $\Delta H = a \times L.C.$ (mm) | Specimen height, $H = H_1 - \Delta H$ (mm) | Height of voids, $H - H_s$ (mm) | Void ratio, $e = (H - H_s)/H_s$ |
|---------------------------------------|-------------------------|---------------------|--|--|---------------------------------|---------------------------------|
| 5 | 392.9 | | | 20 | 8.981 | 0.815 |
| 10 | 383.9 | 9 | 0.090 | 19.91 | 8.891 | 0.807 |
| 20 | 369.8 | 14.1 | 0.141 | 19.769 | 8.750 | 0.794 |
| 40 | 348.9 | 20.9 | 0.209 | 19.56 | 8.541 | 0.775 |
| 80 | 320 | 28.9 | 0.289 | 19.271 | 8.252 | 0.749 |
| 160 | 288 | 32 | 0.320 | 18.951 | 7.932 | 0.720 |
| 320 | 255.5 | 32.5 | 0.325 | 18.626 | 7.607 | 0.690 |
| 640 | 207.3 | 48.2 | 0.482 | 18.144 | 7.125 | 0.647 |

Table 3.17. Specimen height and void ratio calculation for sample 3 (dynamic at dry of optimum)

| Applied Pressure (kN/m ²) | Final Dial Reading (mm) | No. of division (a) | Dial change, $\Delta H = a \times \text{L.C. (mm)}$ | Specimen height, $H = H_1 - \Delta H$ (mm) | Height of voids, $H - H_s$ (mm) | Void ratio, $e = (H - H_s)/H_s$ |
|---------------------------------------|-------------------------|---------------------|---|--|---------------------------------|---------------------------------|
| 5 | 387 | | | 20 | 9.832 | 0.967 |
| 10 | 371 | 16 | 0.16 | 19.84 | 9.672 | 0.951 |
| 20 | 349 | 22 | 0.22 | 19.62 | 9.452 | 0.930 |
| 40 | 319.5 | 29.5 | 0.295 | 19.325 | 9.157 | 0.901 |
| 80 | 285 | 34.5 | 0.345 | 18.98 | 8.812 | 0.867 |
| 160 | 250.5 | 34.5 | 0.345 | 18.635 | 8.467 | 0.833 |
| 320 | 210 | 40.5 | 0.405 | 18.23 | 8.062 | 0.793 |
| 640 | 172 | 38 | 0.38 | 17.85 | 7.682 | 0.756 |

Table 3.18. Specimen height and void ratio calculation for sample 3 (dynamic at optimum moisture content)

| Applied Pressure (kN/m ²) | Final Dial Reading (mm) | No. of division (a) | Dial change, $\Delta H = a \times \text{L.C. (mm)}$ | Specimen height, $H = H_1 - \Delta H$ (mm) | Height of voids, $H - H_s$ (mm) | Void ratio, $e = (H - H_s)/H_s$ |
|---------------------------------------|-------------------------|---------------------|---|--|---------------------------------|---------------------------------|
| 5 | 392.9 | | | 20 | 9.101 | 0.835 |
| 10 | 379.8 | 13.1 | 0.131 | 19.869 | 8.970 | 0.823 |
| 20 | 370.4 | 9.4 | 0.094 | 19.775 | 8.876 | 0.814 |
| 40 | 348.7 | 21.7 | 0.217 | 19.558 | 8.659 | 0.784 |
| 80 | 312 | 36.7 | 0.367 | 19.191 | 8.292 | 0.722 |
| 160 | 247.9 | 64.1 | 0.641 | 18.55 | 7.651 | 0.638 |
| 320 | 158.7 | 89.2 | 0.892 | 17.658 | 6.759 | 0.559 |
| 640 | 72 | 86.7 | 0.867 | 16.791 | 5.892 | 0.471 |

Table 3.19. Specimen height and void ratio calculation for sample 3 (dynamic at wet of optimum)

| Applied Pressure (kN/m ²) | Final Dial Reading (mm) | No. of division (a) | Dial change, $\Delta H = a \times \text{L.C. (mm)}$ | Specimen height, $H = H_1 - \Delta H$ (mm) | Height of voids, $H - H_s$ (mm) | Void ratio, $e = (H - H_s)/H_s$ |
|---------------------------------------|-------------------------|---------------------|---|--|---------------------------------|---------------------------------|
| 5 | 490 | | | 20 | 9.339 | 0.876 |
| 10 | 475.1 | 14.9 | 0.149 | 19.851 | 9.190 | 0.862 |
| 20 | 460.1 | 15 | 0.15 | 19.701 | 9.040 | 0.848 |
| 40 | 429 | 31.1 | 0.311 | 19.39 | 8.729 | 0.819 |
| 80 | 365.1 | 63.9 | 0.639 | 18.751 | 8.090 | 0.759 |
| 160 | 262 | 103.1 | 1.031 | 17.72 | 7.059 | 0.662 |
| 320 | 171.1 | 90.9 | 0.909 | 16.811 | 6.150 | 0.577 |
| 640 | 88 | 83.1 | 0.831 | 15.98 | 5.319 | 0.499 |

Table 3.20. Specimen height and void ratio calculation for sample 3 (static at dry of optimum)

| Applied Pressure (kN/m ²) | Final Dial Reading (mm) | No. of division (a) | Dial change, $\Delta H = a \times \text{L.C. (mm)}$ | Specimen height, $H = H_1 - \Delta H$ (mm) | Height of voids, $H - H_s$ (mm) | Void ratio, $e = (H - H_s) / H_s$ |
|---------------------------------------|-------------------------|---------------------|---|--|---------------------------------|-----------------------------------|
| 5 | 587 | | | 20 | 9.832 | 0.967 |
| 10 | 561 | 26 | 0.260 | 19.740 | 9.572 | 0.941 |
| 20 | 531.5 | 29.5 | 0.295 | 19.445 | 9.277 | 0.912 |
| 40 | 492 | 39.5 | 0.395 | 19.050 | 8.882 | 0.874 |
| 80 | 450 | 42 | 0.420 | 18.630 | 8.462 | 0.832 |
| 160 | 409.5 | 40.5 | 0.405 | 18.225 | 8.057 | 0.792 |
| 320 | 365 | 44.5 | 0.445 | 17.780 | 7.612 | 0.749 |
| 640 | 323.4 | 41.6 | 0.416 | 17.364 | 7.196 | 0.708 |

Table 3.21. Specimen height and void ratio calculation for sample 3 (static at optimum moisture content)

| Applied Pressure (kN/m ²) | Final Dial Reading (mm) | No. of division (a) | Dial change, $\Delta H = a \times \text{L.C. (mm)}$ | Specimen height, $H = H_1 - \Delta H$ (mm) | Height of voids, $H - H_s$ (mm) | Void ratio, $e = (H - H_s) / H_s$ |
|---------------------------------------|-------------------------|---------------------|---|--|---------------------------------|-----------------------------------|
| 5 | 305 | | | 20 | 9.101 | 0.835 |
| 10 | 301 | 4 | 0.04 | 19.96 | 9.061 | 0.831 |
| 20 | 293.5 | 7.5 | 0.075 | 19.885 | 8.986 | 0.824 |
| 40 | 275 | 18.5 | 0.185 | 19.7 | 8.801 | 0.807 |
| 80 | 247 | 28 | 0.28 | 19.42 | 8.521 | 0.772 |
| 160 | 213.6 | 33.4 | 0.334 | 19.086 | 8.187 | 0.731 |
| 320 | 171.8 | 41.8 | 0.418 | 18.668 | 7.769 | 0.693 |
| 640 | 125.7 | 46.1 | 0.461 | 18.207 | 7.308 | 0.650 |

Table 3.22. Specimen height and void ratio calculation for sample 3 (static at wet of optimum)

| Applied Pressure (kN/m ²) | Final Dial Reading (mm) | No. of division (a) | Dial change, $\Delta H = a \times \text{L.C. (mm)}$ | Specimen height, $H = H_1 - \Delta H$ (mm) | Height of voids, $H - H_s$ (mm) | Void ratio, $e = (H - H_s) / H_s$ |
|---------------------------------------|-------------------------|---------------------|---|--|---------------------------------|-----------------------------------|
| 5 | 410.1 | | | 20 | 9.339 | 0.876 |
| 10 | 405.2 | 4.9 | 0.049 | 19.951 | 9.290 | 0.871 |
| 20 | 395 | 10.2 | 0.102 | 19.849 | 9.188 | 0.862 |
| 40 | 370 | 25 | 0.25 | 19.599 | 8.938 | 0.838 |
| 80 | 330.2 | 39.8 | 0.398 | 19.201 | 8.540 | 0.801 |
| 160 | 295.3 | 34.9 | 0.349 | 18.852 | 8.191 | 0.768 |
| 320 | 250.4 | 44.9 | 0.449 | 18.403 | 7.742 | 0.726 |
| 640 | 200.3 | 50.1 | 0.501 | 17.902 | 7.241 | 0.679 |

Table 3.23. Specimen height and void ratio calculation for sample 4 (dynamic at dry of optimum)

| Applied Pressure (kN/m ²) | Final Dial Reading (mm) | No. of division (a) | Dial change, $\Delta H = a \times L.C.$ (mm) | Specimen height, $H=H_1-\Delta H$ (mm) | Height of voids, $H-H_s$ (mm) | Void ratio, $e= (H-H_s)/H_s$ |
|---------------------------------------|-------------------------|---------------------|--|--|-------------------------------|------------------------------|
| 5 | 334 | | | 20 | 7.539 | 0.605 |
| 10 | 328 | 6 | 0.060 | 19.940 | 7.479 | 0.600 |
| 20 | 321.5 | 6.5 | 0.065 | 19.875 | 7.414 | 0.595 |
| 40 | 309 | 12.5 | 0.125 | 19.750 | 7.289 | 0.585 |
| 80 | 289 | 20 | 0.200 | 19.550 | 7.089 | 0.569 |
| 160 | 255.5 | 33.5 | 0.335 | 19.215 | 6.754 | 0.542 |
| 320 | 216 | 39.5 | 0.395 | 18.820 | 6.359 | 0.510 |
| 640 | 173.5 | 42.5 | 0.425 | 18.395 | 5.934 | 0.476 |

Table 3.24. Specimen height and void ratio calculation for sample 4 (dynamic at optimum moisture content)

| Applied Pressure (kN/m ²) | Final Dial Reading (mm) | No. of division (a) | Dial change, $\Delta H = a \times L.C.$ (mm) | Specimen height, $H=H_1-\Delta H$ (mm) | Height of voids, $H-H_s$ (mm) | Void ratio, $e= (H-H_s)/H_s$ |
|---------------------------------------|-------------------------|---------------------|--|--|-------------------------------|------------------------------|
| 5 | 395.7 | | | 20 | 7.105 | 0.551 |
| 10 | 388.7 | 7 | 0.07 | 19.93 | 7.035 | 0.546 |
| 20 | 382.2 | 6.5 | 0.065 | 19.865 | 6.970 | 0.541 |
| 40 | 368.9 | 13.3 | 0.133 | 19.732 | 6.837 | 0.530 |
| 80 | 360.7 | 8.2 | 0.082 | 19.65 | 6.755 | 0.510 |
| 160 | 334.8 | 25.9 | 0.259 | 19.391 | 6.496 | 0.480 |
| 320 | 308.6 | 26.2 | 0.262 | 19.129 | 6.234 | 0.441 |
| 640 | 264.4 | 44.2 | 0.442 | 18.687 | 5.792 | 0.399 |

Table 3.25. Specimen height and void ratio calculation for sample 4 (dynamic at wet of optimum)

| Applied Pressure (kN/m ²) | Final Dial Reading (mm) | No. of division (a) | Dial change, $\Delta H = a \times L.C.$ (mm) | Specimen height, $H=H_1-\Delta H$ (mm) | Height of voids, $H-H_s$ (mm) | Void ratio, $e= (H-H_s)/H_s$ |
|---------------------------------------|-------------------------|---------------------|--|--|-------------------------------|------------------------------|
| 5 | 387.5 | | | 20 | 7.406 | 0.588 |
| 10 | 358.5 | 29 | 0.29 | 19.71 | 7.116 | 0.565 |
| 20 | 343 | 15.5 | 0.155 | 19.555 | 6.961 | 0.553 |
| 40 | 320.2 | 22.8 | 0.228 | 19.327 | 6.733 | 0.535 |
| 80 | 292.7 | 27.5 | 0.275 | 19.052 | 6.458 | 0.513 |
| 160 | 258 | 34.7 | 0.347 | 18.705 | 6.111 | 0.485 |
| 320 | 215.8 | 42.2 | 0.422 | 18.283 | 5.689 | 0.452 |
| 640 | 160.2 | 55.6 | 0.556 | 17.727 | 5.133 | 0.408 |

Table 3.26. Specimen height and void ratio calculation for sample 4 (static at dry of optimum)

| Applied Pressure (kN/m ²) | Final Dial Reading (mm) | No. of division (a) | Dial change, $\Delta H = a \times \text{L.C.}$ (mm) | Specimen height, $H = H_1 - \Delta H$ (mm) | Height of voids, $H - H_s$ (mm) | Void ratio, $e = (H - H_s) / H_s$ |
|---------------------------------------|-------------------------|---------------------|---|--|---------------------------------|-----------------------------------|
| 5 | 380 | | | 20 | 7.539 | 0.605 |
| 10 | 356 | 24 | 0.240 | 19.76 | 7.299 | 0.586 |
| 20 | 340 | 16 | 0.160 | 19.6 | 7.139 | 0.573 |
| 40 | 318.5 | 21.5 | 0.215 | 19.385 | 6.924 | 0.556 |
| 80 | 295 | 23.5 | 0.235 | 19.15 | 6.689 | 0.537 |
| 160 | 260 | 35 | 0.350 | 18.8 | 6.339 | 0.509 |
| 320 | 221 | 39 | 0.390 | 18.41 | 5.949 | 0.477 |
| 640 | 175 | 46 | 0.460 | 17.95 | 5.489 | 0.440 |

Table 3.27. Specimen height and void ratio calculation for sample 4 (static at optimum moisture content)

| Applied Pressure (kN/m ²) | Final Dial Reading (mm) | No. of division (a) | Dial change, $\Delta H = a \times \text{L.C.}$ (mm) | Specimen height, $H = H_1 - \Delta H$ (mm) | Height of voids, $H - H_s$ (mm) | Void ratio, $e = (H - H_s) / H_s$ |
|---------------------------------------|-------------------------|---------------------|---|--|---------------------------------|-----------------------------------|
| 5 | 398.8 | | | 20 | 7.105 | 0.551 |
| 10 | 393.8 | 5 | 0.05 | 19.95 | 7.055 | 0.547 |
| 20 | 389.3 | 4.5 | 0.045 | 19.905 | 7.010 | 0.544 |
| 40 | 379.6 | 9.7 | 0.097 | 19.808 | 6.913 | 0.536 |
| 80 | 373 | 6.6 | 0.066 | 19.742 | 6.847 | 0.518 |
| 160 | 349.6 | 23.4 | 0.234 | 19.508 | 6.613 | 0.493 |
| 320 | 323.8 | 25.8 | 0.258 | 19.25 | 6.355 | 0.452 |
| 640 | 288.4 | 35.4 | 0.354 | 18.896 | 6.001 | 0.415 |

Table 3.28. Specimen height and void ratio calculation for sample 4 (static at wet of optimum)

| Applied Pressure (kN/m ²) | Final Dial Reading (mm) | No. of division (a) | Dial change, $\Delta H = a \times \text{L.C.}$ (mm) | Specimen height, $H = H_1 - \Delta H$ (mm) | Height of voids, $H - H_s$ (mm) | Void ratio, $e = (H - H_s) / H_s$ |
|---------------------------------------|-------------------------|---------------------|---|--|---------------------------------|-----------------------------------|
| 5 | 393.9 | | | 20 | 7.406 | 0.588 |
| 10 | 375 | 18.9 | 0.189 | 19.811 | 7.217 | 0.573 |
| 20 | 360.1 | 14.9 | 0.149 | 19.662 | 7.068 | 0.561 |
| 40 | 338.5 | 21.6 | 0.216 | 19.446 | 6.852 | 0.544 |
| 80 | 318.3 | 20.2 | 0.202 | 19.244 | 6.650 | 0.528 |
| 160 | 287.6 | 30.7 | 0.307 | 18.937 | 6.343 | 0.504 |
| 320 | 249.6 | 38 | 0.38 | 18.557 | 5.963 | 0.473 |
| 640 | 201.5 | 48.1 | 0.481 | 18.076 | 5.482 | 0.435 |

Table 3.29. Specimen height and void ratio calculation for sample 5 (dynamic at dry of optimum)

| Applied Pressure (kN/m ²) | Final Dial Reading (mm) | No. of division (a) | Dial change, $\Delta H = a \times \text{L.C. (mm)}$ | Specimen height, $H = H_1 - \Delta H$ (mm) | Height of voids, $H - H_s$ (mm) | Void ratio, $e = (H - H_s) / H_s$ |
|---------------------------------------|-------------------------|---------------------|---|--|---------------------------------|-----------------------------------|
| 5 | 363.5 | | | 20 | 8.532 | 0.744 |
| 10 | 338.5 | 25 | 0.25 | 19.75 | 8.282 | 0.722 |
| 20 | 319 | 19.5 | 0.195 | 19.555 | 8.087 | 0.705 |
| 40 | 290.5 | 28.5 | 0.285 | 19.27 | 7.802 | 0.680 |
| 80 | 261.6 | 28.9 | 0.289 | 18.981 | 7.513 | 0.655 |
| 160 | 230.5 | 31.1 | 0.311 | 18.67 | 7.202 | 0.628 |
| 320 | 197 | 33.5 | 0.335 | 18.335 | 6.867 | 0.599 |
| 640 | 158.2 | 38.8 | 0.388 | 17.947 | 6.479 | 0.565 |

Table 3.30. Specimen height and void ratio calculation for sample 5 (dynamic at optimum moisture content)

| Applied Pressure (kN/m ²) | Final Dial Reading (mm) | No. of division (a) | Dial change, $\Delta H = a \times \text{L.C. (mm)}$ | Specimen height, $H = H_1 - \Delta H$ (mm) | Height of voids, $H - H_s$ (mm) | Void ratio, $e = (H - H_s) / H_s$ |
|---------------------------------------|-------------------------|---------------------|---|--|---------------------------------|-----------------------------------|
| 5 | 371 | | | 20 | 7.358 | 0.582 |
| 10 | 362.7 | 8.3 | 0.083 | 19.917 | 7.275 | 0.575 |
| 20 | 350.8 | 11.9 | 0.119 | 19.798 | 7.156 | 0.566 |
| 40 | 324.9 | 25.9 | 0.259 | 19.539 | 6.897 | 0.546 |
| 80 | 294 | 30.9 | 0.309 | 19.23 | 6.588 | 0.521 |
| 160 | 258.2 | 35.8 | 0.358 | 18.872 | 6.230 | 0.493 |
| 320 | 223.8 | 34.4 | 0.344 | 18.528 | 5.886 | 0.466 |
| 640 | 180 | 43.8 | 0.438 | 18.09 | 5.448 | 0.431 |

Table 3.31. Specimen height and void ratio calculation for sample 5 (dynamic at wet of optimum)

| Applied Pressure (kN/m ²) | Final Dial Reading (mm) | No. of division (a) | Dial change, $\Delta H = a \times \text{L.C. (mm)}$ | Specimen height, $H = H_1 - \Delta H$ (mm) | Height of voids, $H - H_s$ (mm) | Void ratio, $e = (H - H_s) / H_s$ |
|---------------------------------------|-------------------------|---------------------|---|--|---------------------------------|-----------------------------------|
| 5 | 384.1 | | | 20 | 8.263 | 0.704 |
| 10 | 356.1 | 28 | 0.28 | 19.72 | 7.983 | 0.680 |
| 20 | 332.6 | 23.5 | 0.235 | 19.485 | 7.748 | 0.660 |
| 40 | 307.2 | 25.4 | 0.254 | 19.231 | 7.494 | 0.638 |
| 80 | 274.7 | 32.5 | 0.325 | 18.906 | 7.169 | 0.611 |
| 160 | 242.2 | 32.5 | 0.325 | 18.581 | 6.844 | 0.583 |
| 320 | 202 | 40.2 | 0.402 | 18.179 | 6.442 | 0.549 |
| 640 | 147.5 | 54.5 | 0.545 | 17.634 | 5.897 | 0.502 |

Table 3.32. Specimen height and void ratio calculation for sample 5 (static at dry of optimum)

| Applied Pressure (kN/m ²) | Final Dial Reading (mm) | No. of division (a) | Dial change, $\Delta H = a \times \text{L.C. (mm)}$ | Specimen height, $H = H_1 - \Delta H$ (mm) | Height of voids, $H - H_s$ (mm) | Void ratio, $e = (H - H_s)/H_s$ |
|---------------------------------------|-------------------------|---------------------|---|--|---------------------------------|---------------------------------|
| 5 | 387 | | | 20 | 8.532 | 0.744 |
| 10 | 360 | 27 | 0.27 | 19.73 | 8.262 | 0.720 |
| 20 | 337 | 23 | 0.23 | 19.5 | 8.032 | 0.700 |
| 40 | 305 | 32 | 0.32 | 19.18 | 7.712 | 0.673 |
| 80 | 275 | 30 | 0.3 | 18.88 | 7.412 | 0.646 |
| 160 | 237 | 38 | 0.38 | 18.5 | 7.032 | 0.613 |
| 320 | 192 | 45 | 0.45 | 18.05 | 6.582 | 0.574 |
| 640 | 150 | 42 | 0.42 | 17.63 | 6.162 | 0.537 |

Table 3.33. Specimen height and void ratio calculation for sample 5 (static at optimum moisture content)

| Applied Pressure (kN/m ²) | Final Dial Reading (mm) | No. of division (a) | Dial change, $\Delta H = a \times \text{L.C. (mm)}$ | Specimen height, $H = H_1 - \Delta H$ (mm) | Height of voids, $H - H_s$ (mm) | Void ratio, $e = (H - H_s)/H_s$ |
|---------------------------------------|-------------------------|---------------------|---|--|---------------------------------|---------------------------------|
| 5 | 371.2 | | | 20 | 7.358 | 0.582 |
| 10 | 359.3 | 11.9 | 0.119 | 19.881 | 7.239 | 0.573 |
| 20 | 352.7 | 6.6 | 0.066 | 19.815 | 7.173 | 0.567 |
| 40 | 340.2 | 12.5 | 0.125 | 19.69 | 7.048 | 0.557 |
| 80 | 323.3 | 16.9 | 0.169 | 19.521 | 6.879 | 0.544 |
| 160 | 299.2 | 24.1 | 0.241 | 19.28 | 6.638 | 0.525 |
| 320 | 266.3 | 32.9 | 0.329 | 18.951 | 6.309 | 0.499 |
| 640 | 227.4 | 38.9 | 0.389 | 18.562 | 5.920 | 0.468 |

Table 3.34. Specimen height and void ratio calculation for sample 5 (static at wet of optimum)

| Applied Pressure (kN/m ²) | Final Dial Reading (mm) | No. of division (a) | Dial change, $\Delta H = a \times \text{L.C. (mm)}$ | Specimen height, $H = H_1 - \Delta H$ (mm) | Height of voids, $H - H_s$ (mm) | Void ratio, $e = (H - H_s)/H_s$ |
|---------------------------------------|-------------------------|---------------------|---|--|---------------------------------|---------------------------------|
| 5 | 379.9 | | | 20 | 8.263 | 0.704 |
| 10 | 351.5 | 28.4 | 0.284 | 19.716 | 7.979 | 0.680 |
| 20 | 331.8 | 19.7 | 0.197 | 19.519 | 7.782 | 0.663 |
| 40 | 312.4 | 19.4 | 0.194 | 19.325 | 7.588 | 0.646 |
| 80 | 280.4 | 32 | 0.32 | 19.005 | 7.268 | 0.619 |
| 160 | 250 | 30.4 | 0.304 | 18.701 | 6.964 | 0.593 |
| 320 | 213.2 | 36.8 | 0.368 | 18.333 | 6.596 | 0.562 |
| 640 | 160.1 | 53.1 | 0.531 | 17.802 | 6.065 | 0.517 |

Appendix III

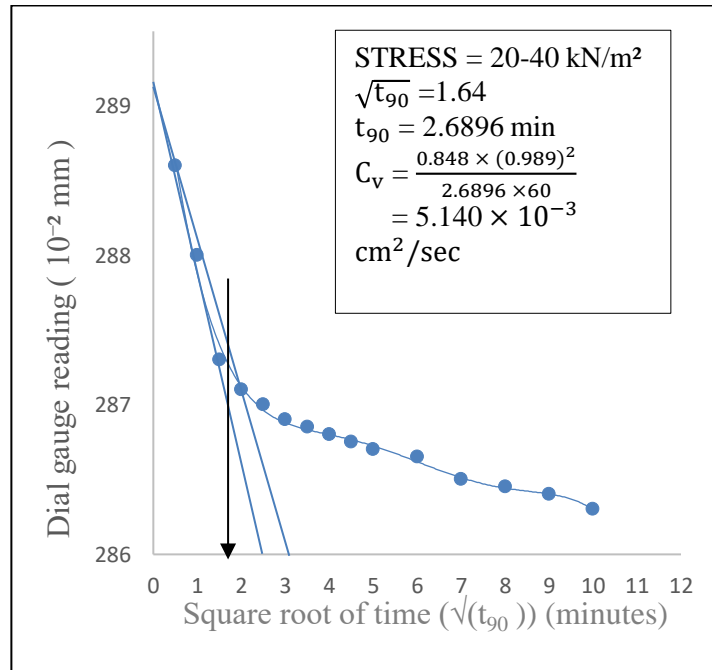


Figure 3.95: Time-consolidation curve of sample 1 (dynamic at dry of optimum) at 20-40kPa

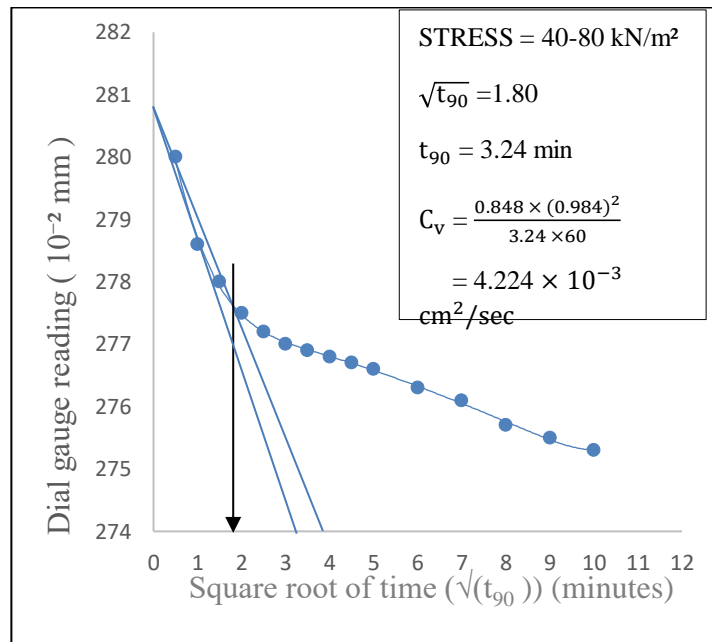


Figure 3.96: Time-consolidation curve of sample 1 (dynamic at dry of optimum) at 40-80kPa

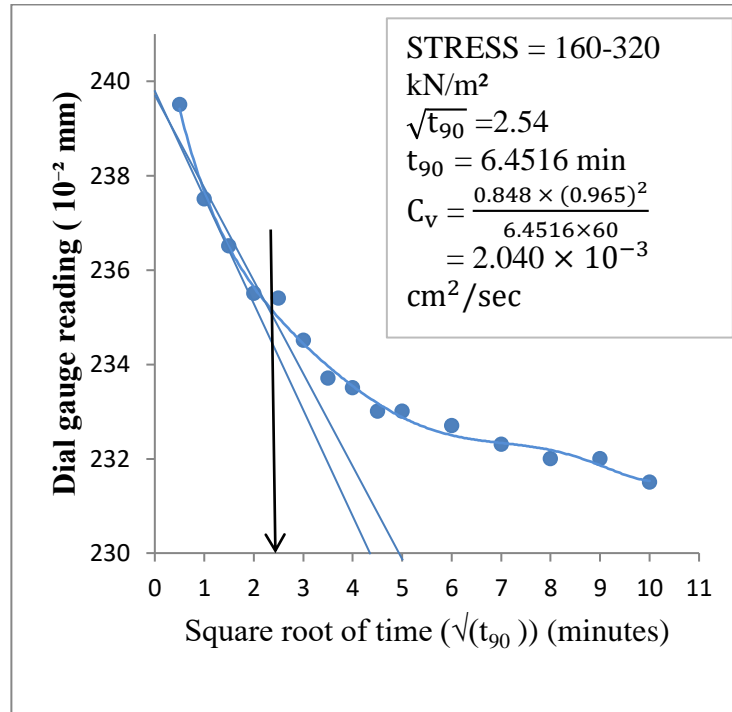


Figure 3.97: Time-consolidation curve of sample 1 (dynamic at dry of optimum) at 160-320kPa

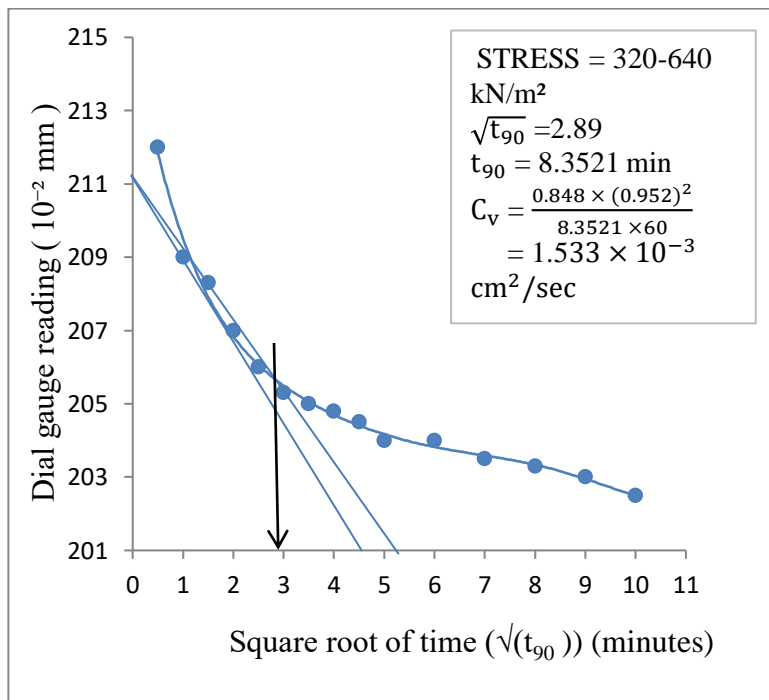


Figure 3.98: Time-consolidation curve of sample 1 (dynamic at dry of optimum) at 320-640kPa

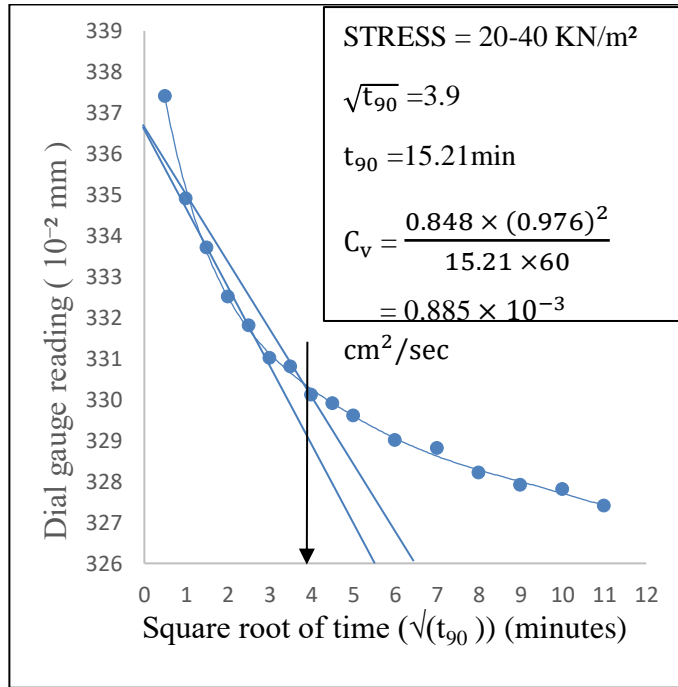


Figure 3.99: Time-consolidation curve of sample 1 (dynamic at optimum moisture content) at 20-40kPa

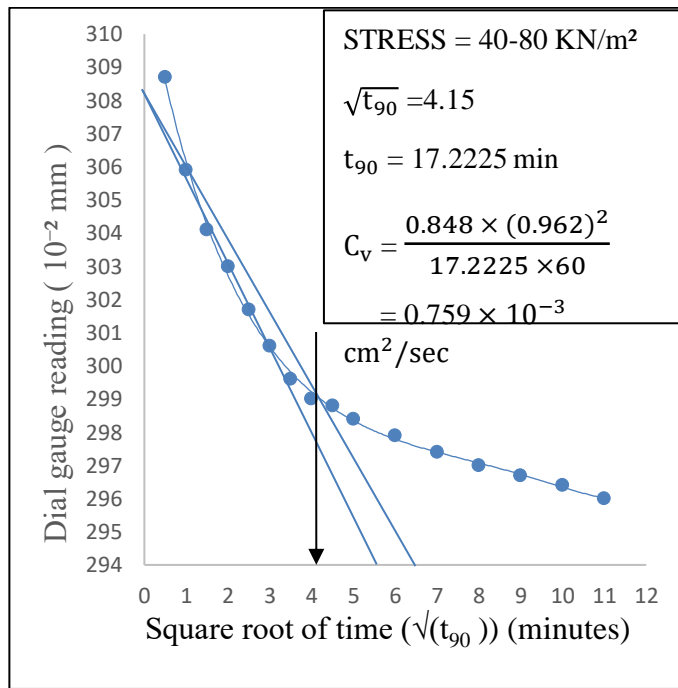


Figure 3.100: Time-consolidation curve of sample 1 (dynamic at optimum moisture content) at 40-80kPa

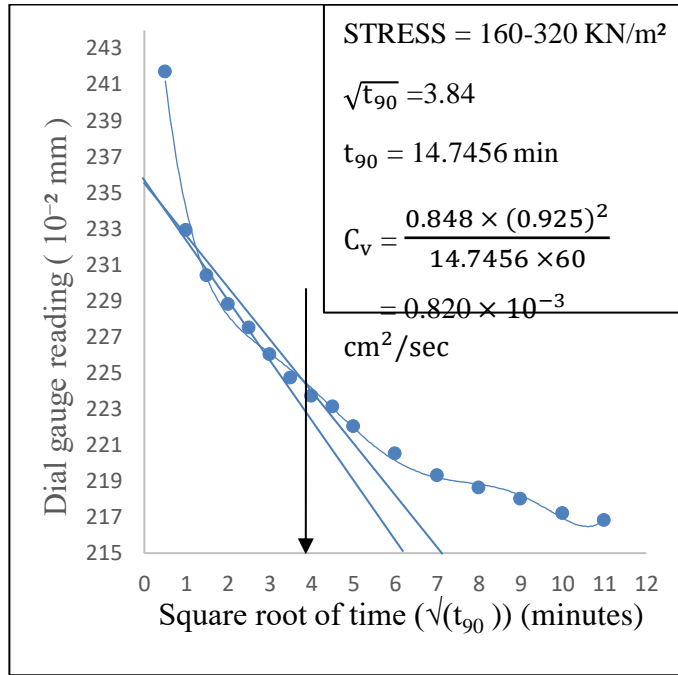


Figure 3.101: Time-consolidation curve of sample 1 (dynamic at optimum moisture content) at 160-320kPa

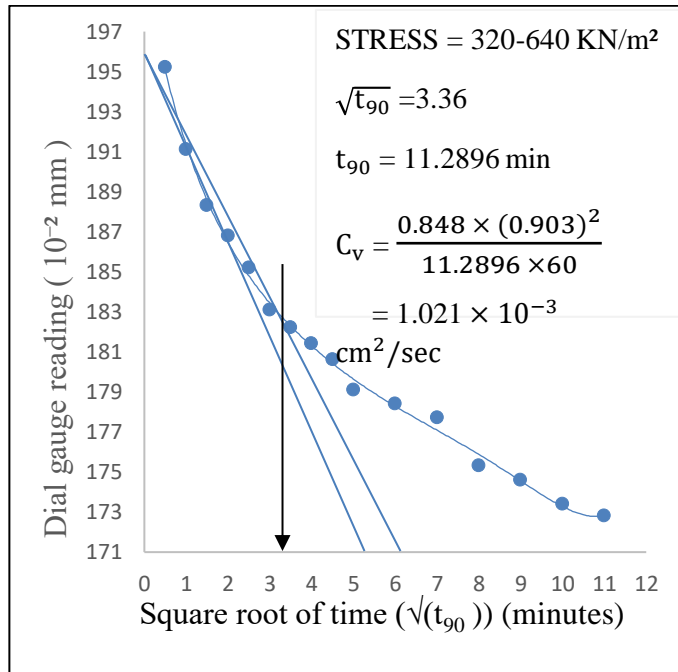


Figure 3.102: Time-consolidation curve of sample 1 (dynamic at optimum moisture content) at 320-640kPa

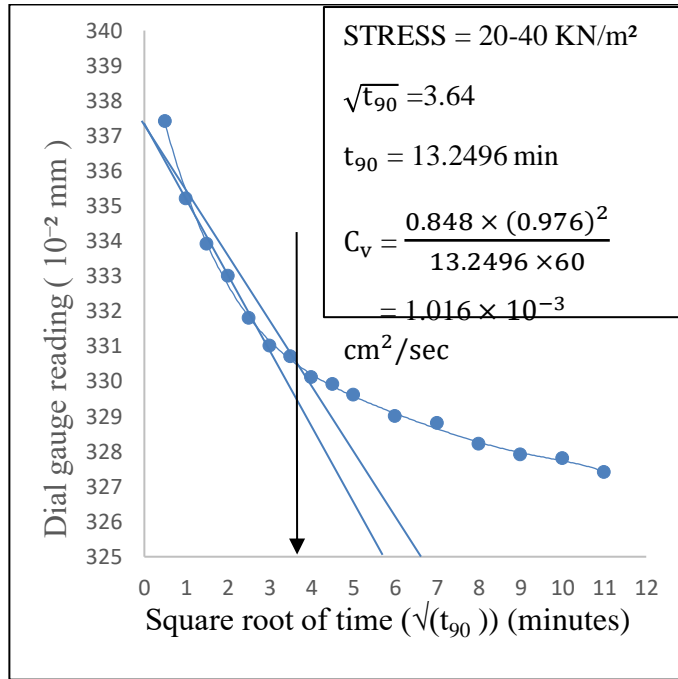


Figure 3.103: Time-consolidation curve of sample 1 (dynamic at wet of optimum) at 20-40kPa

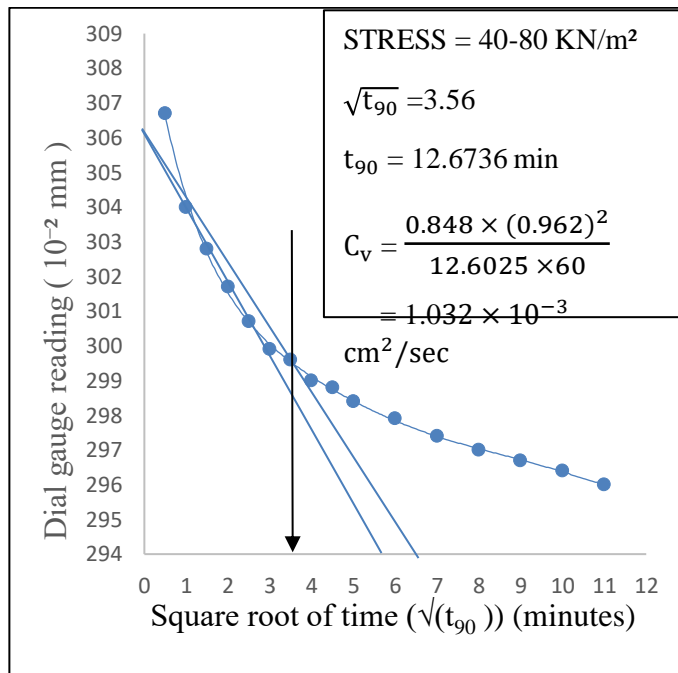


Figure 3.104: Time-consolidation curve of sample 1 (dynamic at wet of optimum) at 40-80kPa

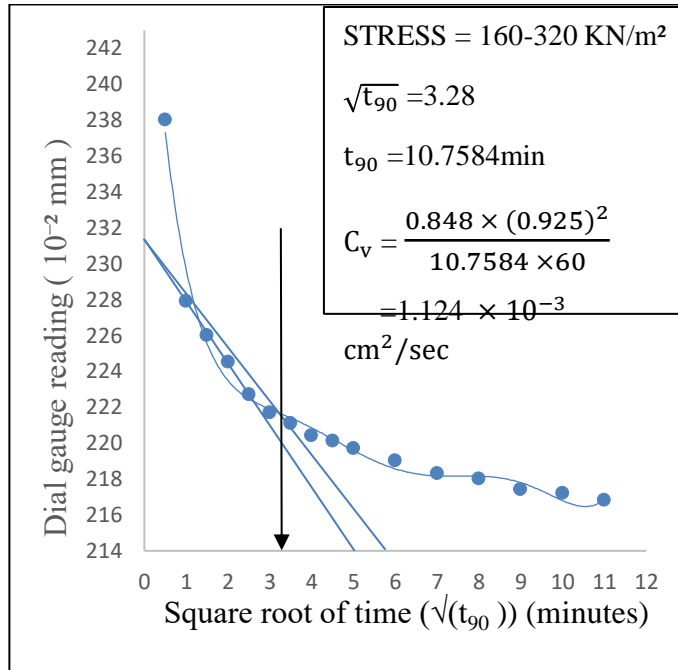


Figure 3.105: Time-consolidation curve of sample 1 (dynamic at wet of optimum) at 160-320kPa

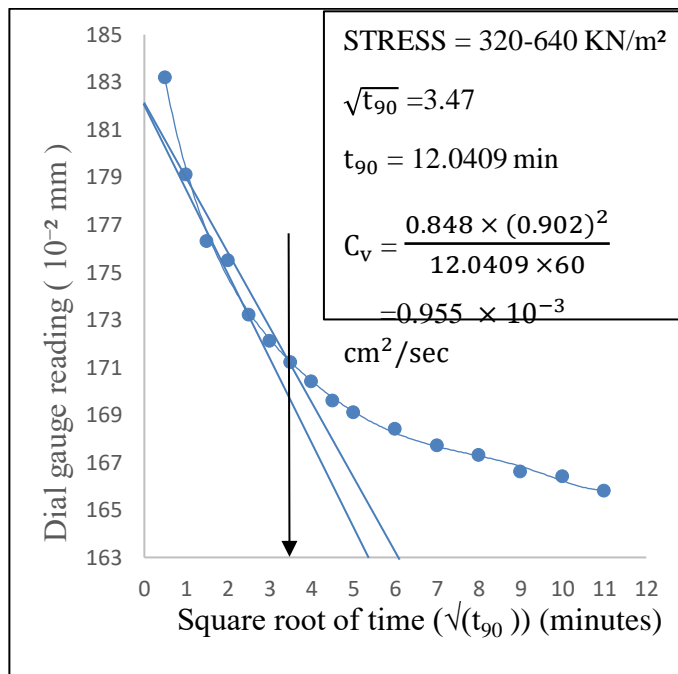


Figure 3.106: Time-consolidation curve of sample 1 (dynamic at wet of optimum) at 320-640kPa

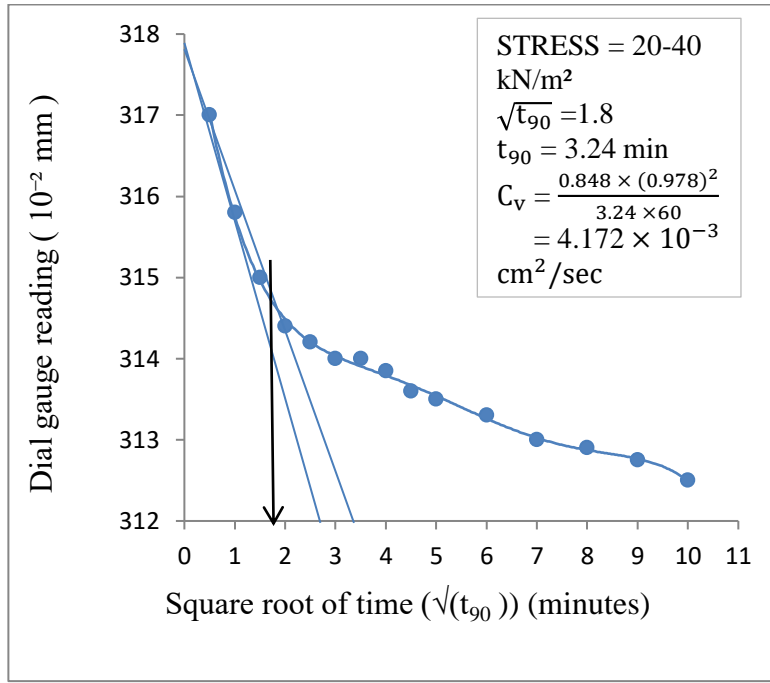


Figure 3.107: Time-consolidation curve of sample 1 (static at dry of optimum) at 20-40kPa

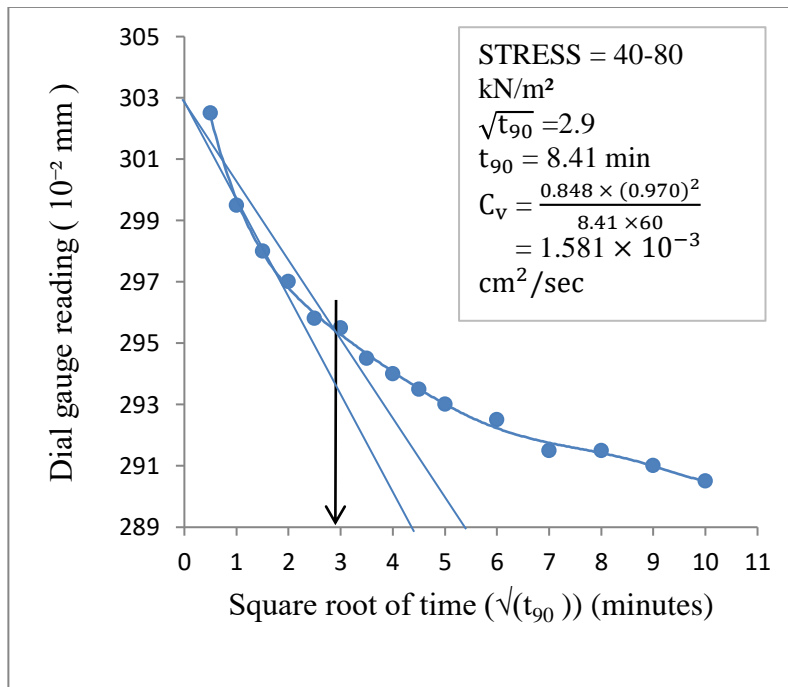


Figure 3.108: Time-consolidation curve of sample 1 (static at dry of optimum) at 40-80kPa

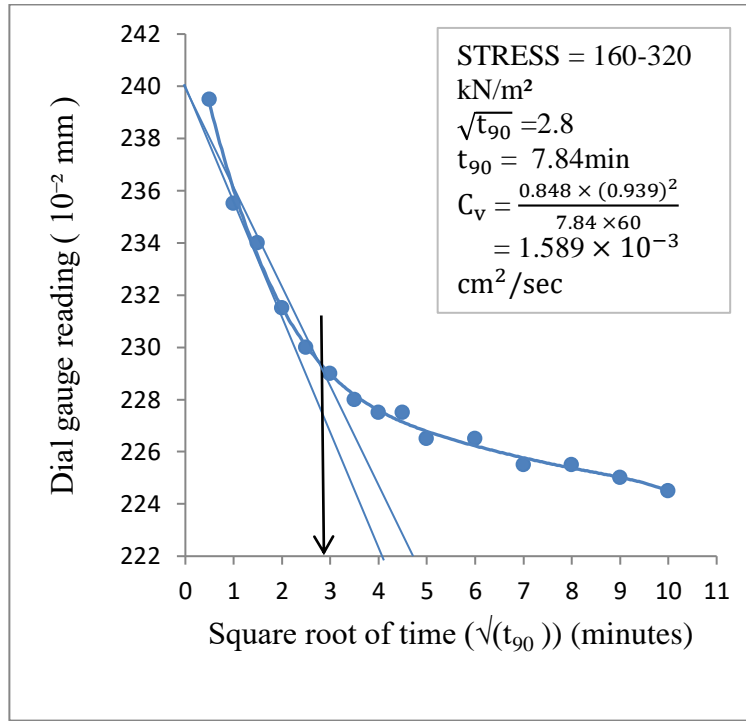


Figure 3.109: Time-consolidation curve of sample 1 (static at dry of optimum) at 160-320kPa

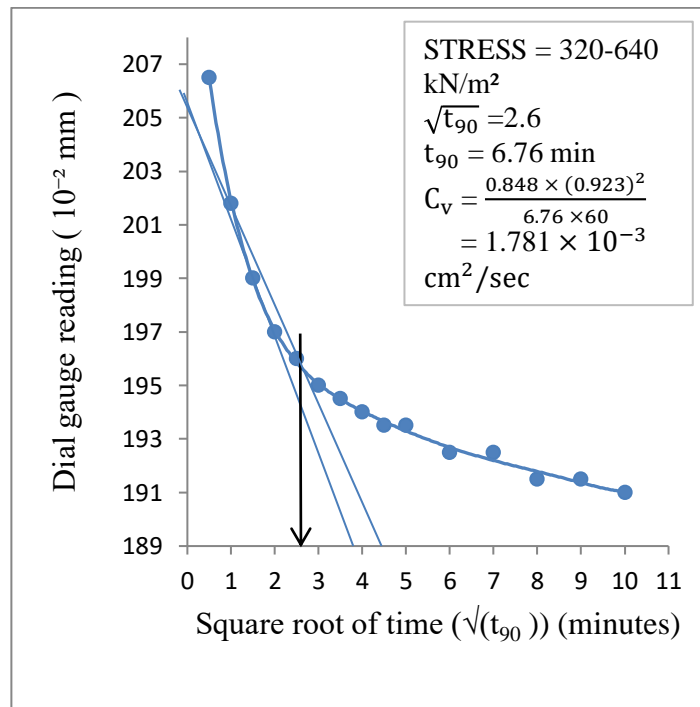


Figure 3.110: Time-consolidation curve of sample 1 (static at dry of optimum) at 320-640kPa

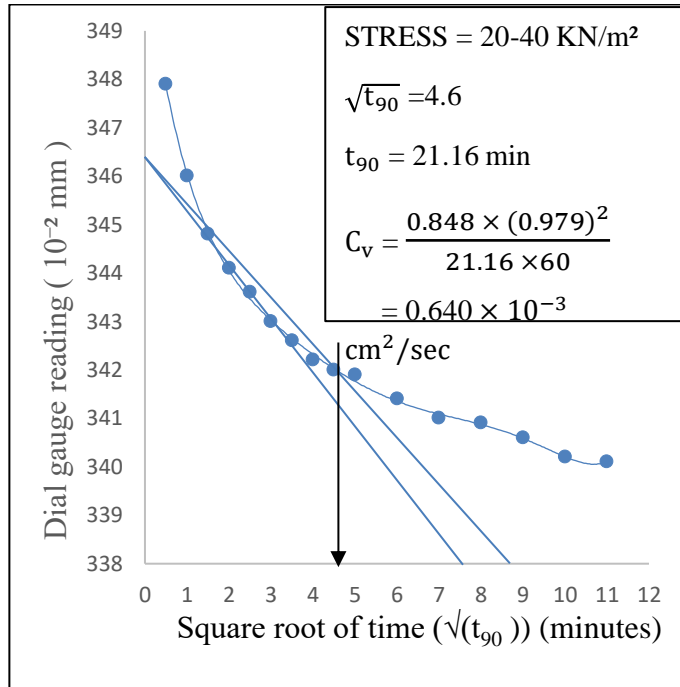


Figure 3.111: Time-consolidation curve of sample 1 (static at optimum moisture content) at 20-40kPa

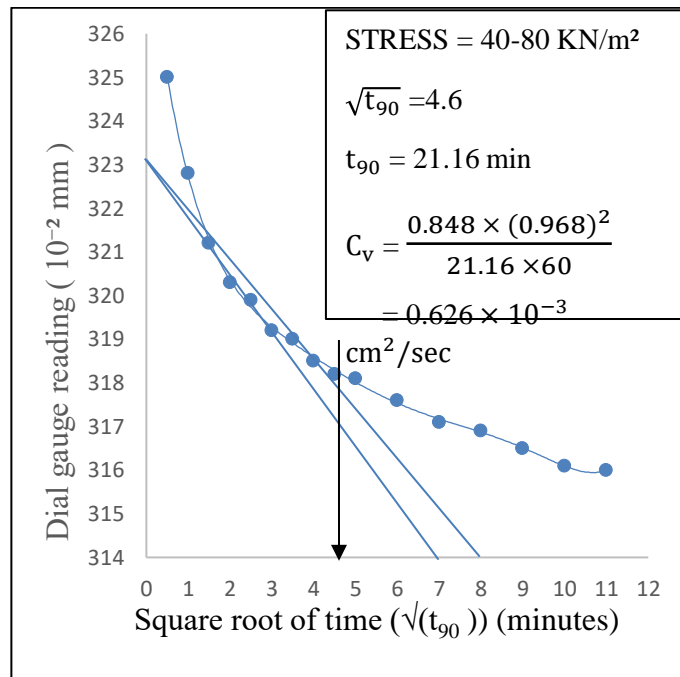


Figure 3.112: Time-consolidation curve of sample 1 (static at optimum moisture content) at 40-80kPa

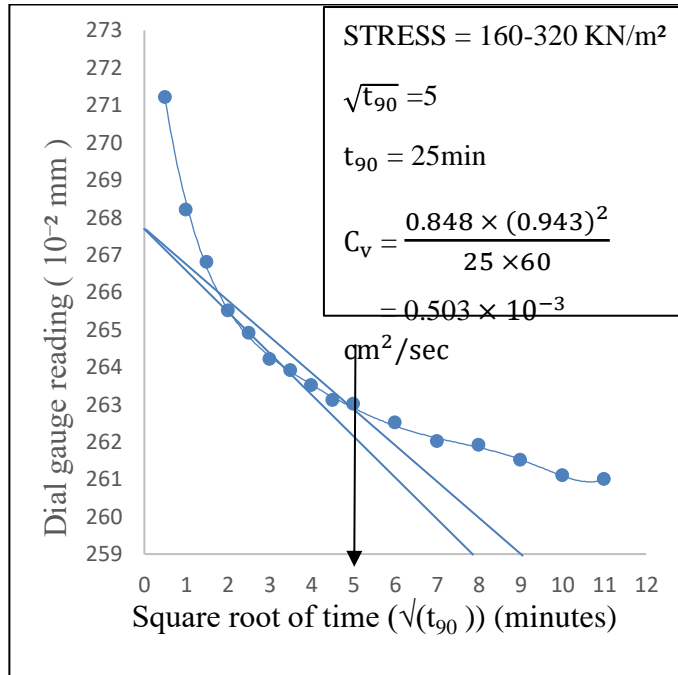


Figure 3.113: Time-consolidation curve of sample 1 (static at optimum moisture content) at 160-320kPa

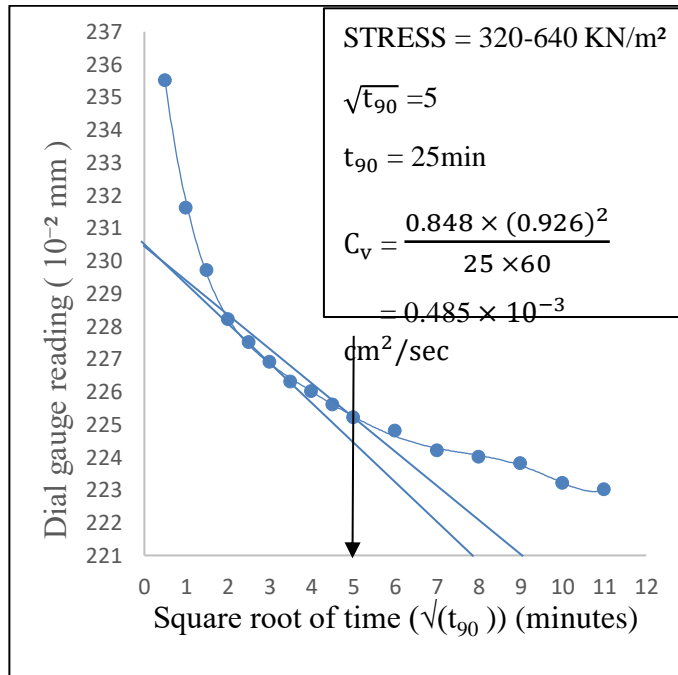


Figure 3.114: Time-consolidation curve of sample 1 (static at optimum moisture content) at 320-640kPa

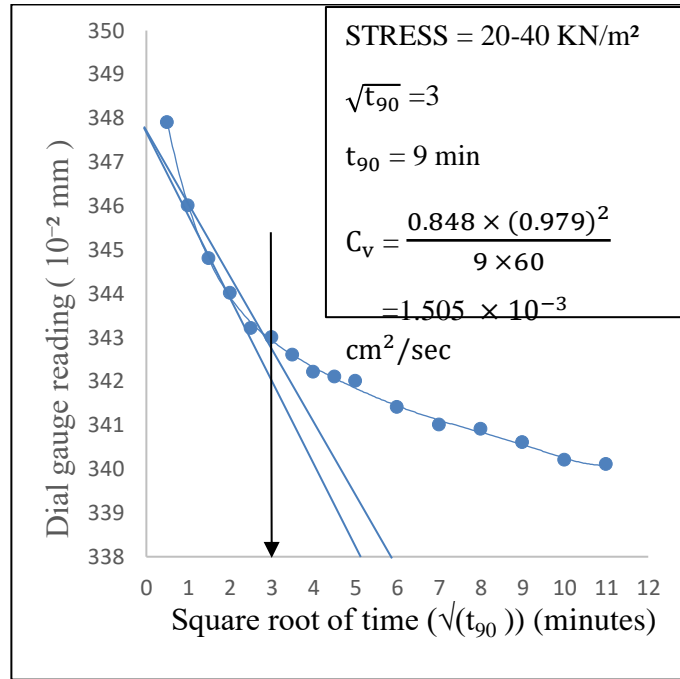


Figure 3.115: Time-consolidation curve of sample 1 (static at wet of optimum) at 20-40kPa

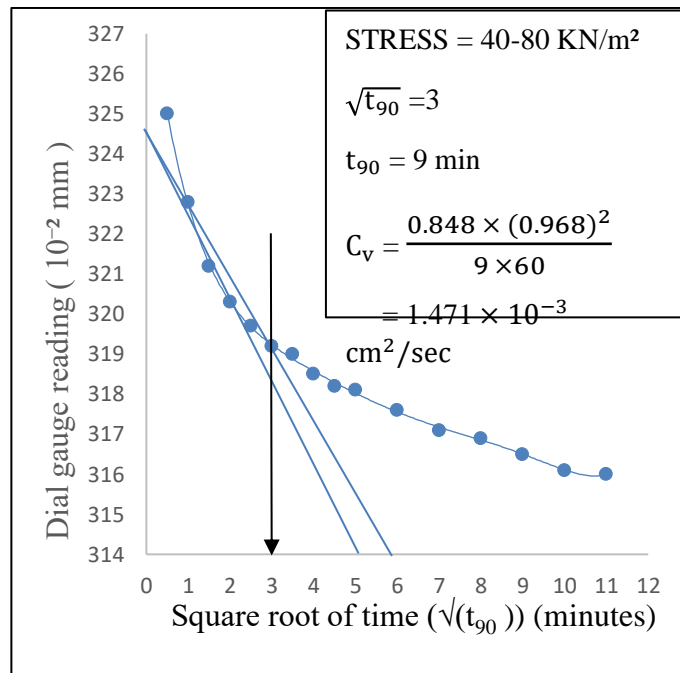


Figure 3.116: Time-consolidation curve of sample 1 (static at wet of optimum) at 40-80kPa

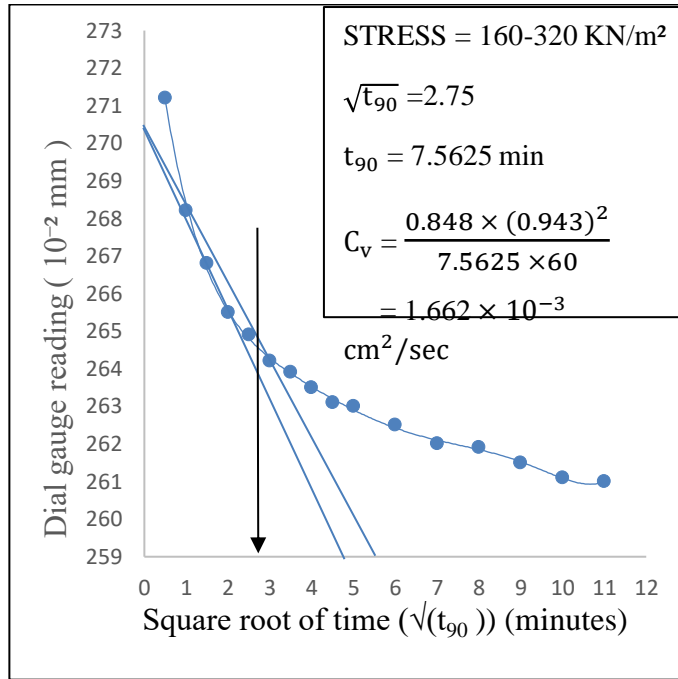


Figure 3.117: Time-consolidation curve of sample 1 (static at wet of optimum) at 160-320kPa

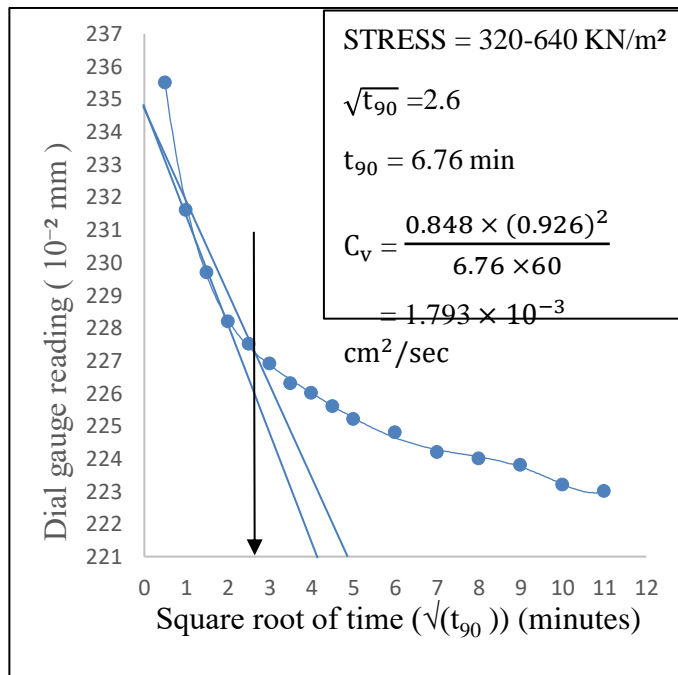


Figure 3.118: Time-consolidation curve of sample 1 (static at wet of optimum) at 320-640kPa

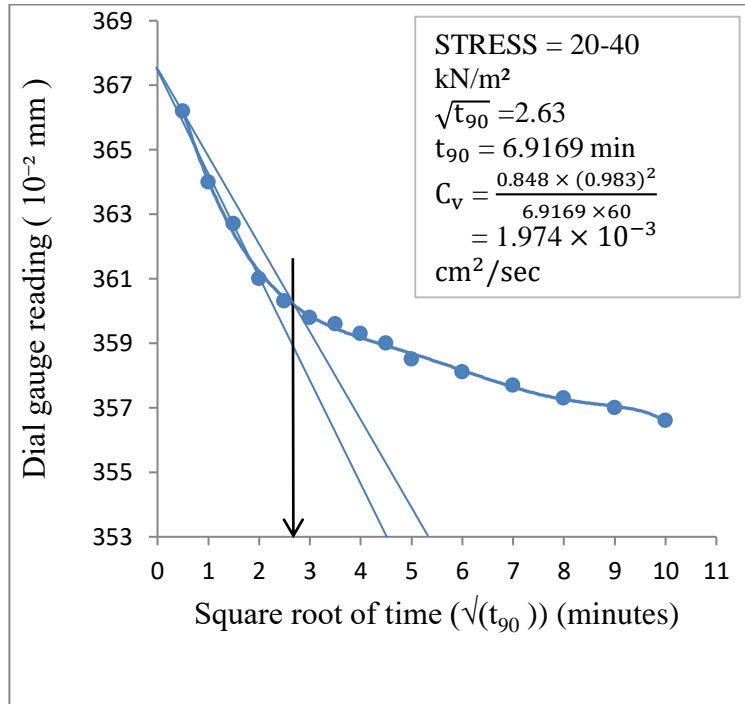


Figure 3.119: Time-consolidation curve of sample 2 (dynamic at dry of optimum) at 20-40kPa

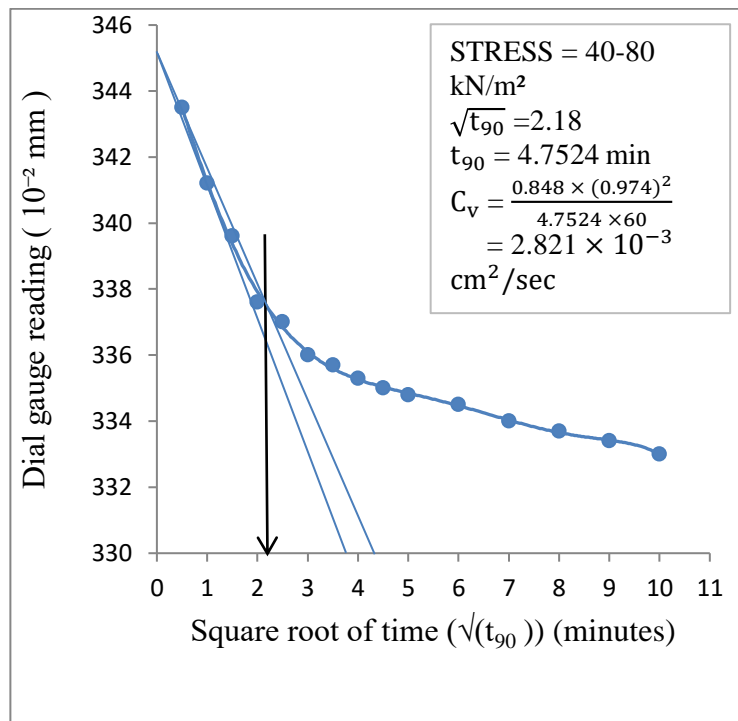


Figure 3.120: Time-consolidation curve of sample 2 (dynamic at dry of optimum) at 40-80kPa

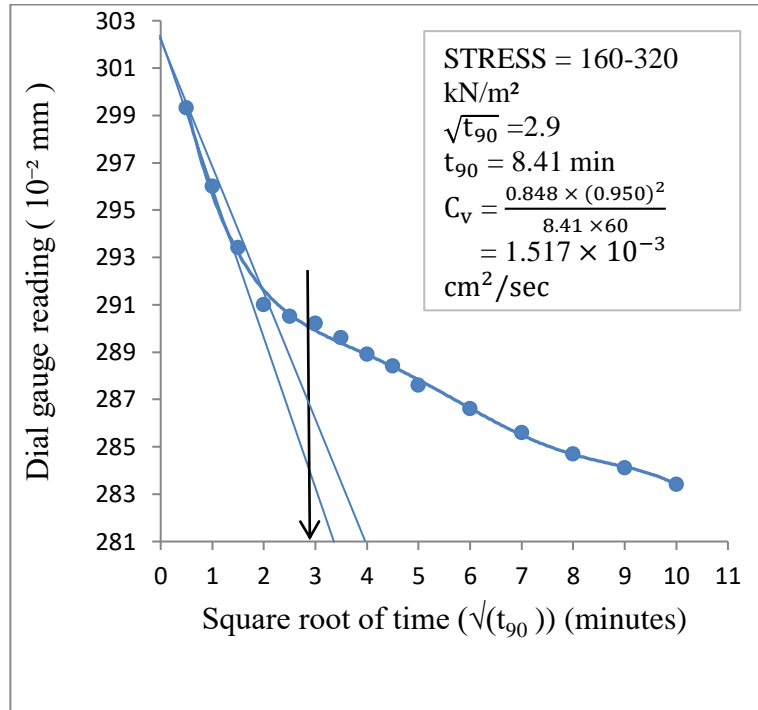


Figure 3.121: Time-consolidation curve of sample 2 (dynamic at dry of optimum) at 160-320kPa

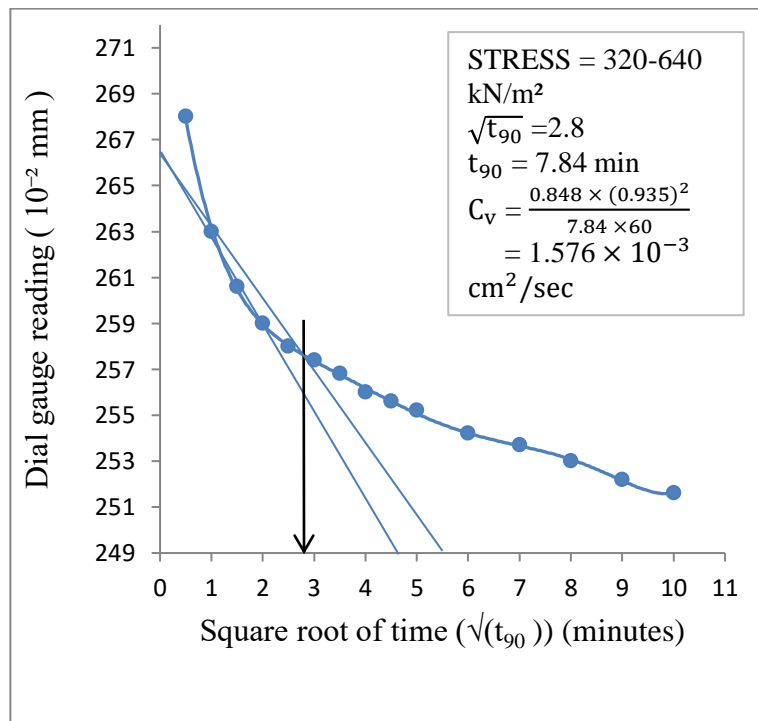


Figure 3.122: Time-consolidation curve of sample 2 (dynamic at dry of optimum) at 320-640kPa

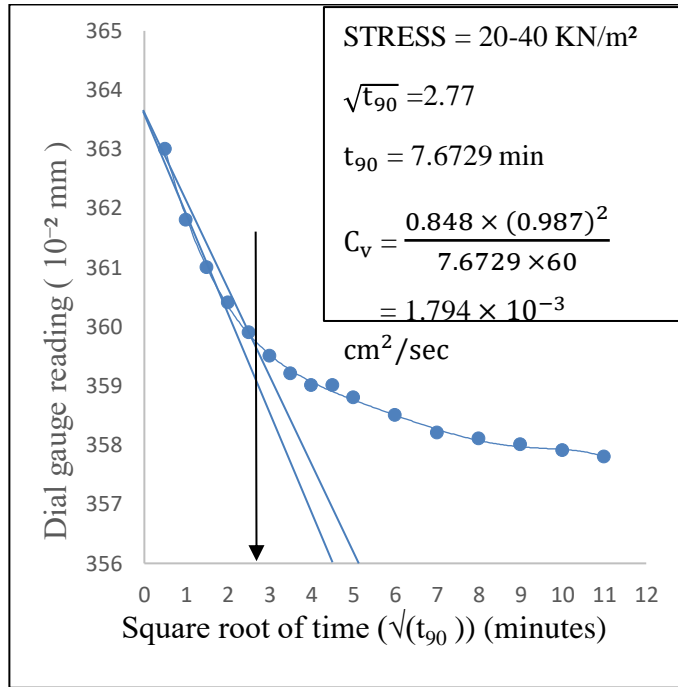


Figure 3.123: Time-consolidation curve of sample 2 (dynamic at optimum moisture content) at 20-40kPa

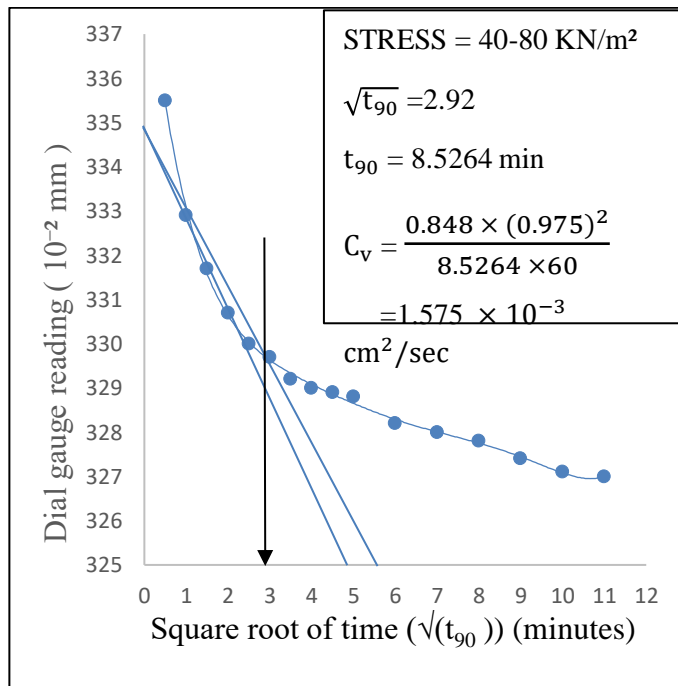


Figure 3.124: Time-consolidation curve of sample 2 (dynamic at optimum moisture content) at 40-80kPa

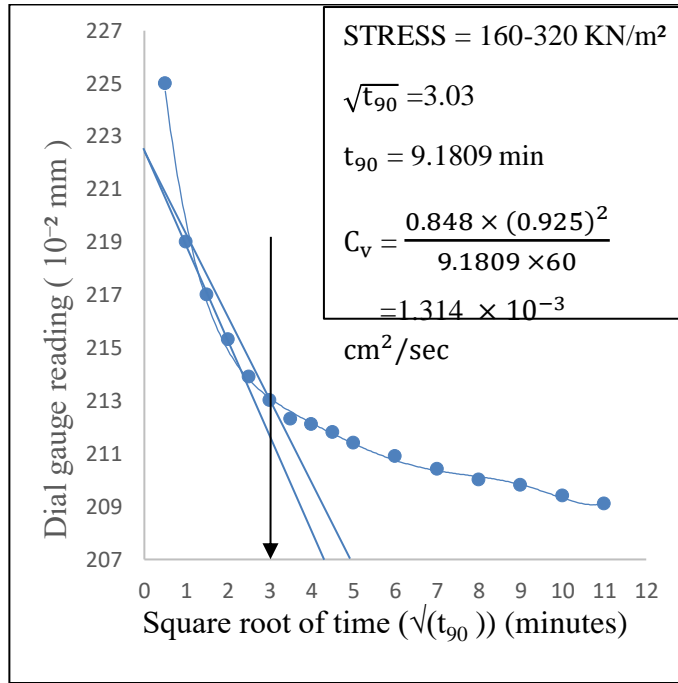


Figure 3.125: Time-consolidation curve of sample 2 (dynamic at optimum moisture content) at 160-320kPa

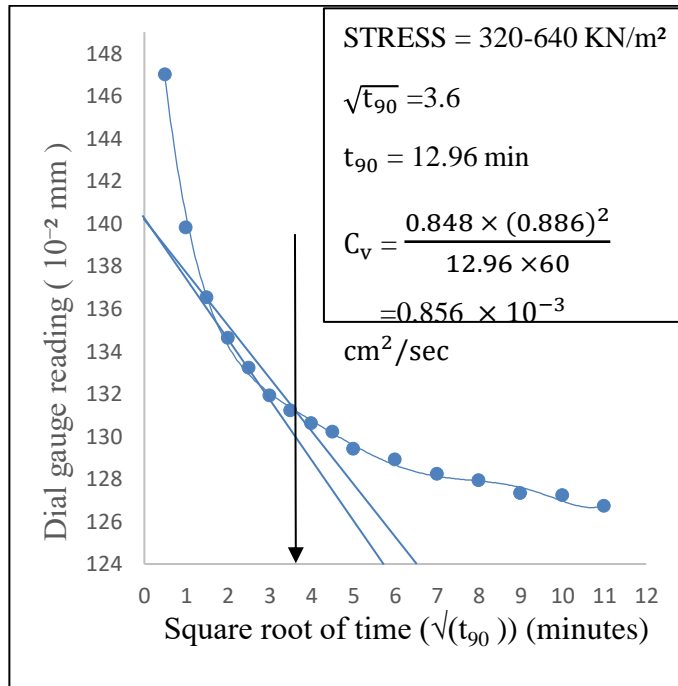


Figure 3.126: Time-consolidation curve of sample 2 (dynamic at optimum moisture content) at 320-640kPa

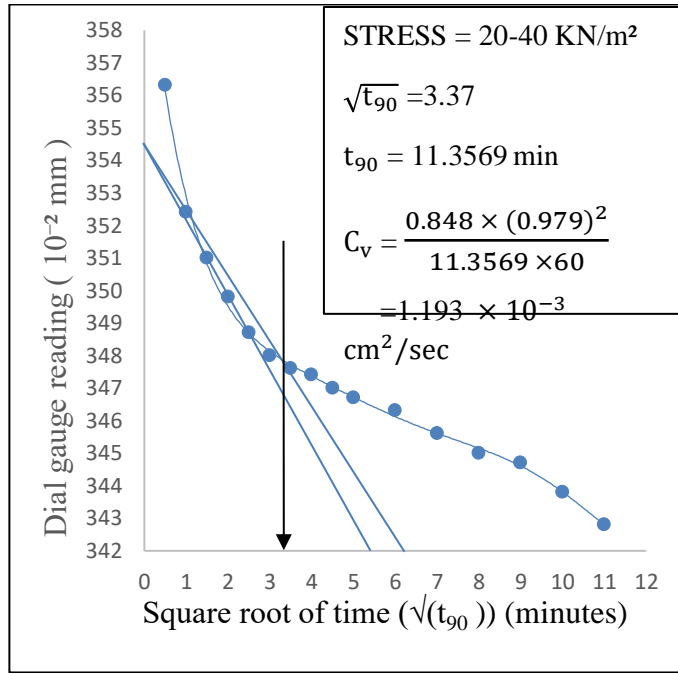


Figure 3.127: Time-consolidation curve of sample 2 (dynamic at wet of optimum) at 20-40kPa

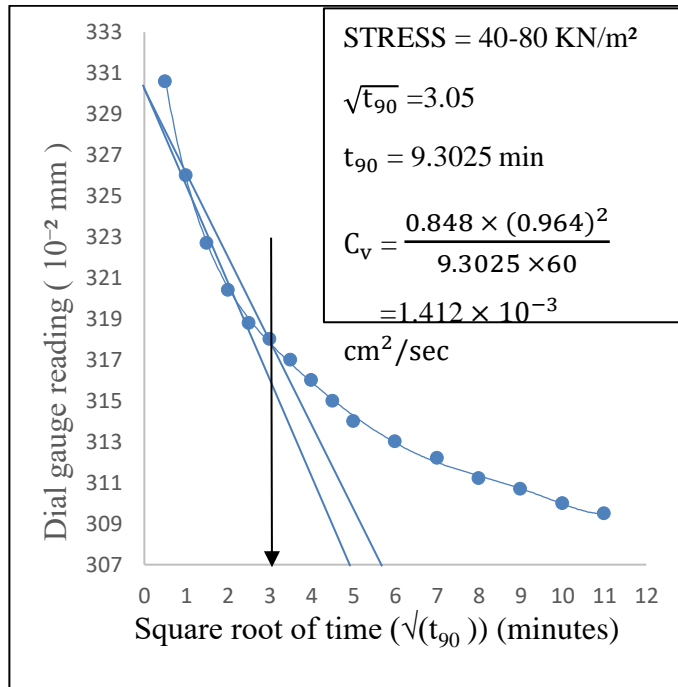


Figure 3.128: Time-consolidation curve of sample 2 (dynamic at wet of optimum) at 40-80kPa

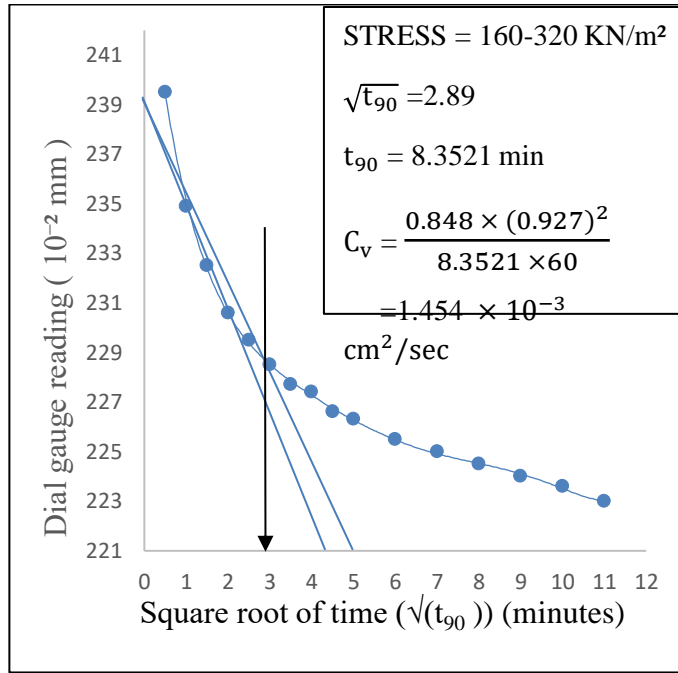


Figure 3.129: Time-consolidation curve of sample 2 (dynamic at wet of optimum) at 160-320kPa

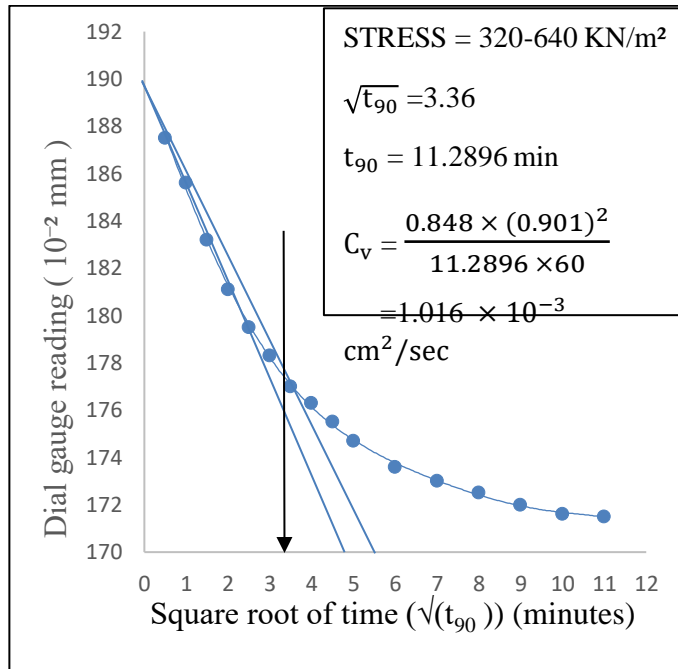


Figure 3.130: Time-consolidation curve of sample 2 (dynamic at wet of optimum) at 320-640kPa

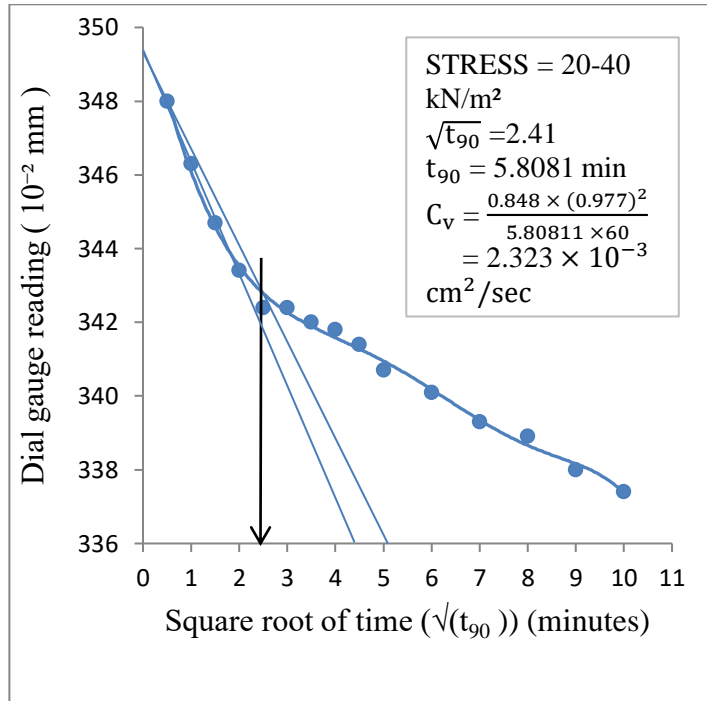


Figure 3.131: Time-consolidation curve of sample 2(static at dry of optimum) at 20-40kPa

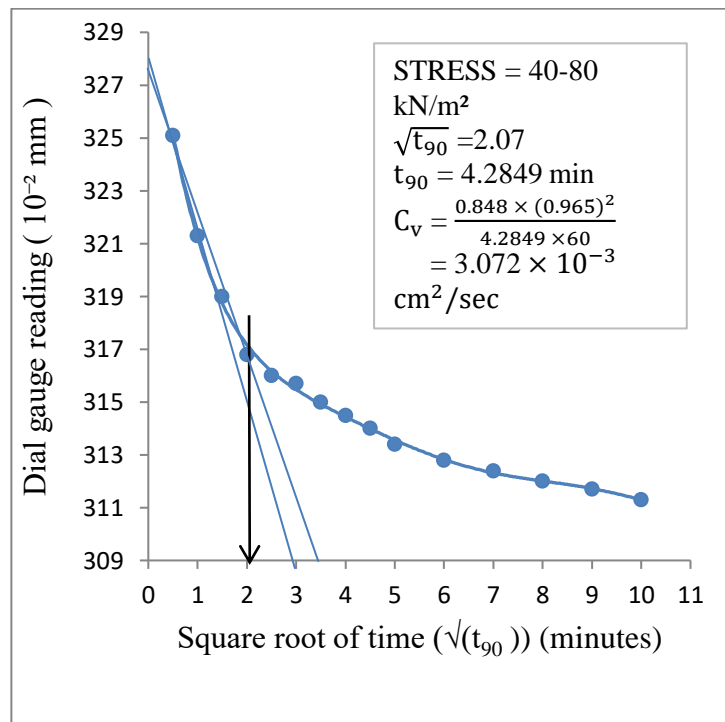


Figure 3.132: Time-consolidation curve of sample 2(static at dry of optimum) at 40-80kPa

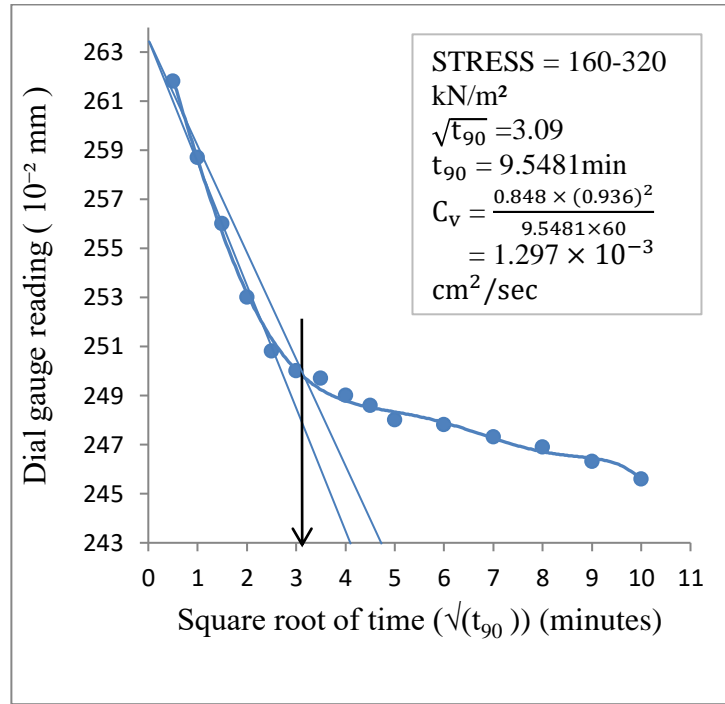


Figure 3.133: Time-consolidation curve of sample 2(static at dry of optimum) at 160-320kPa

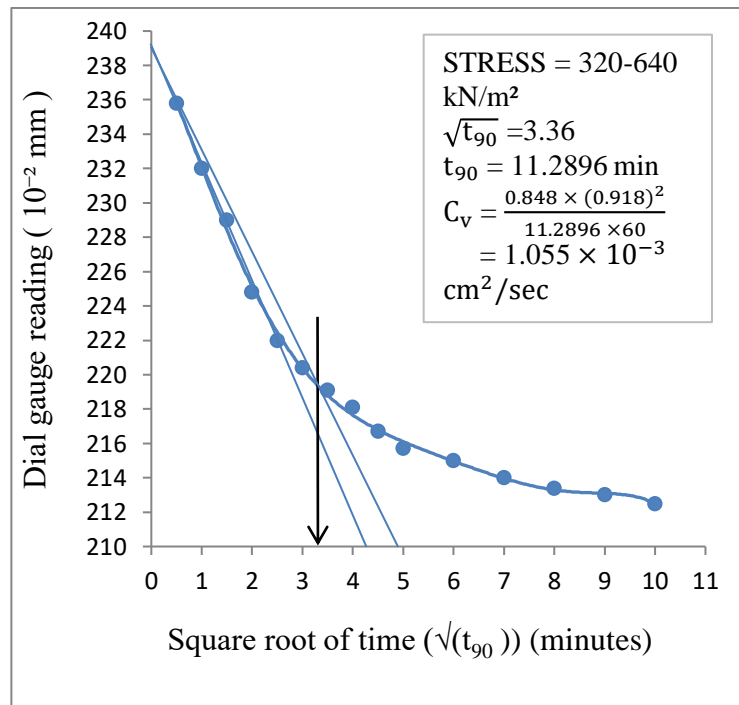


Figure 3.134: Time-consolidation curve of sample 2(static at dry of optimum) at 320-640kPa

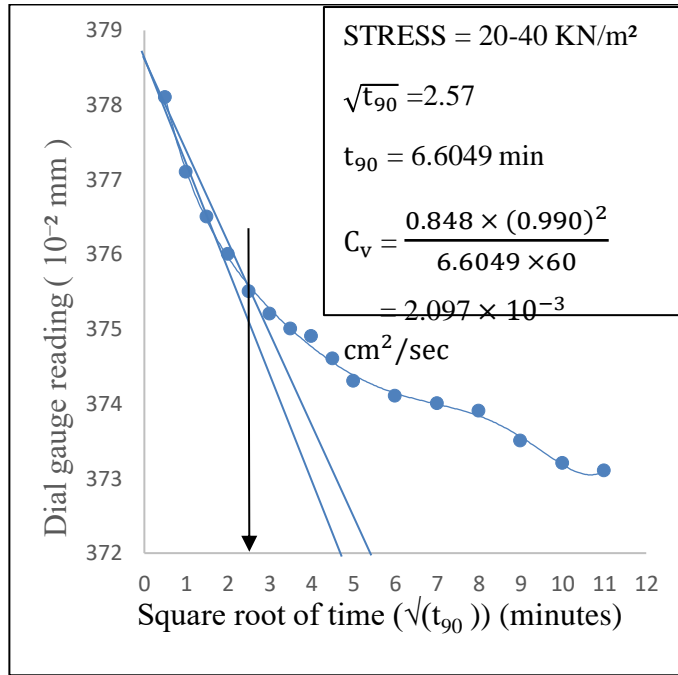


Figure 3.135: Time-consolidation curve of sample 2(static at optimum moisture content) at 20-40kPa

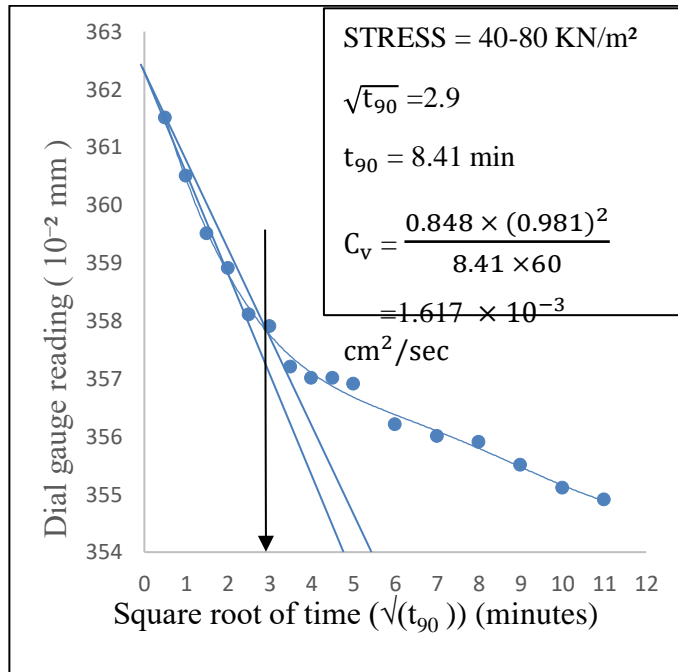


Figure 3.136: Time-consolidation curve of sample 2(static at optimum moisture content) at 40-80kPa

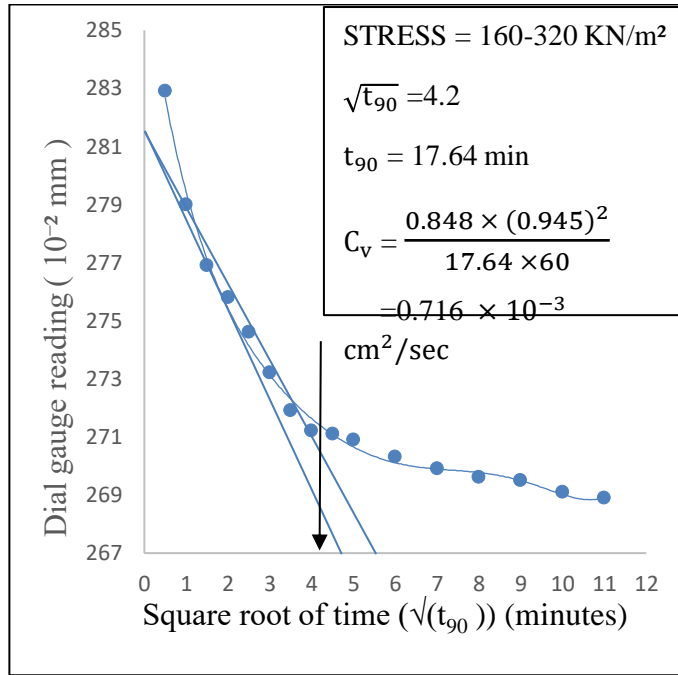


Figure 3.137: Time-consolidation curve of sample 2(static at optimum moisture content) at 160-320kPa

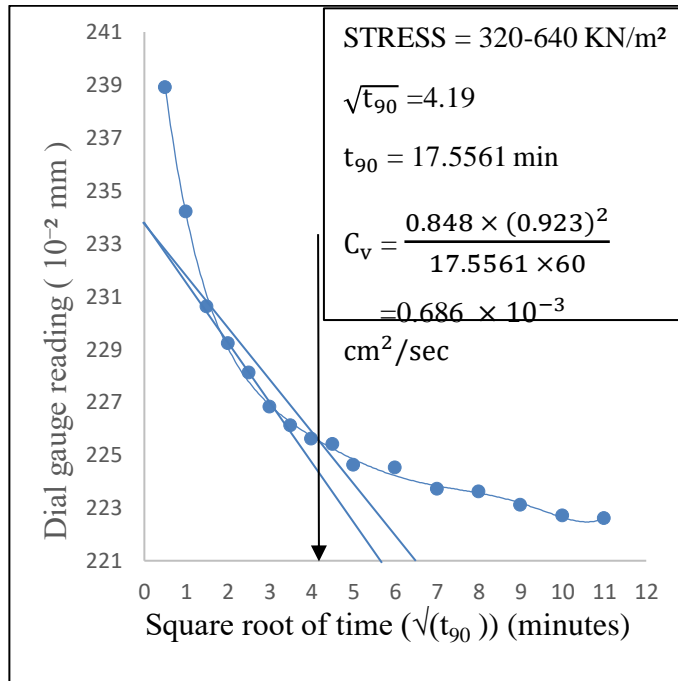


Figure 3.138: Time-consolidation curve of sample 2(static at optimum moisture content) at 320-640kPa

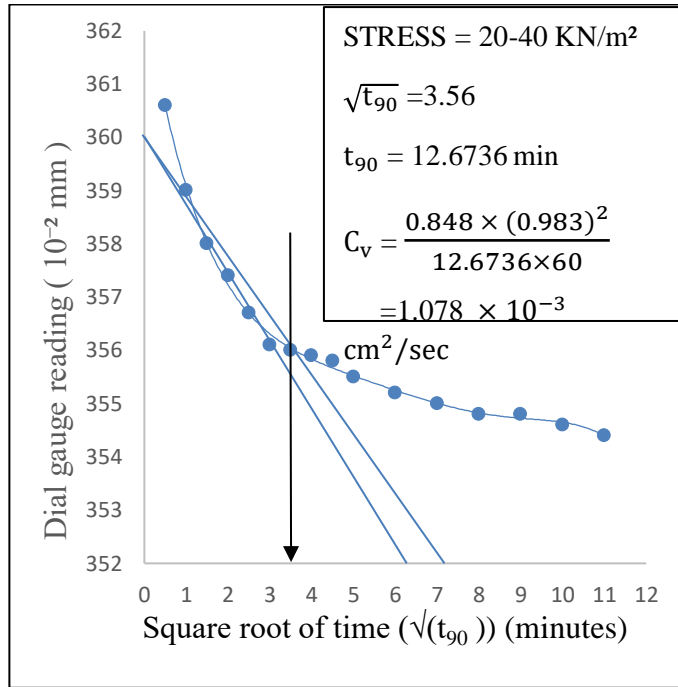


Figure 3.139: Time-consolidation curve of sample 2(static at wet of optimum) at 20-40kPa

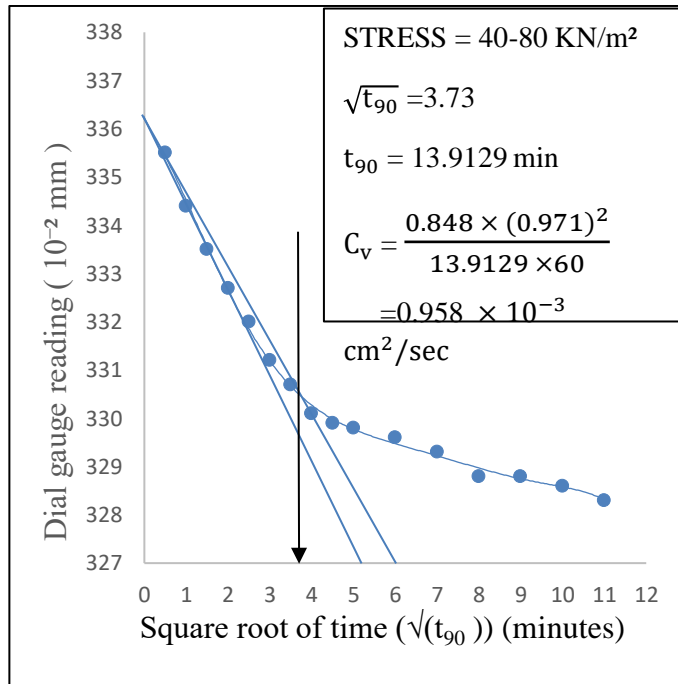


Figure 3.140: Time-consolidation curve of sample 2(static at wet of optimum) at 40-80kPa

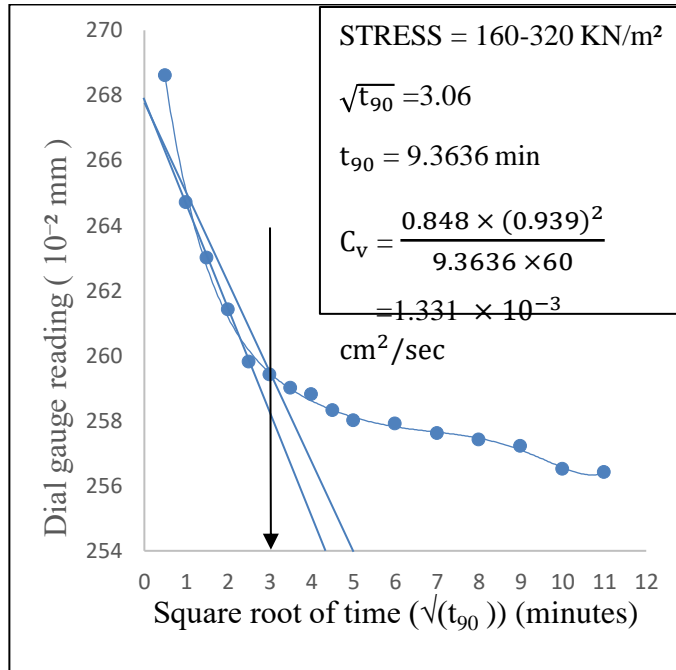


Figure 3.141: Time-consolidation curve of sample 2(static at wet of optimum) at 160-320kPa

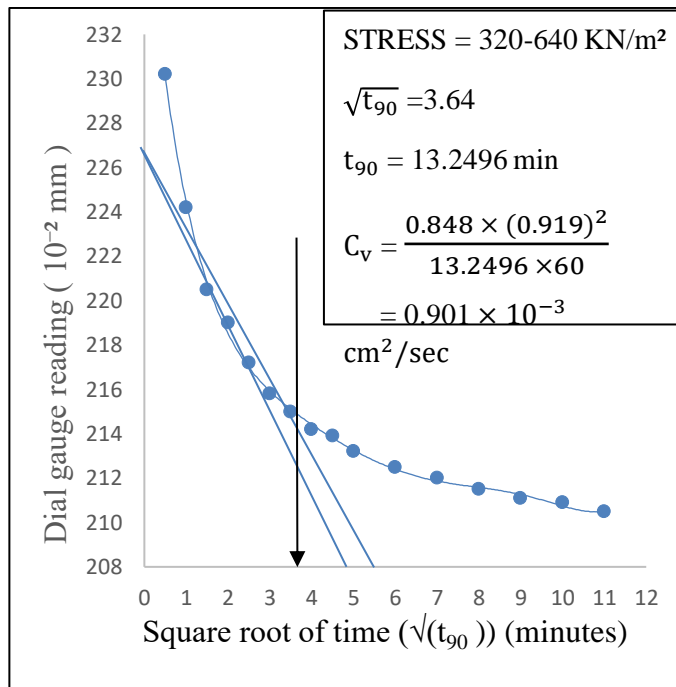


Figure 3.142: Time-consolidation curve of sample 2(static at wet of optimum) at 320-640kPa

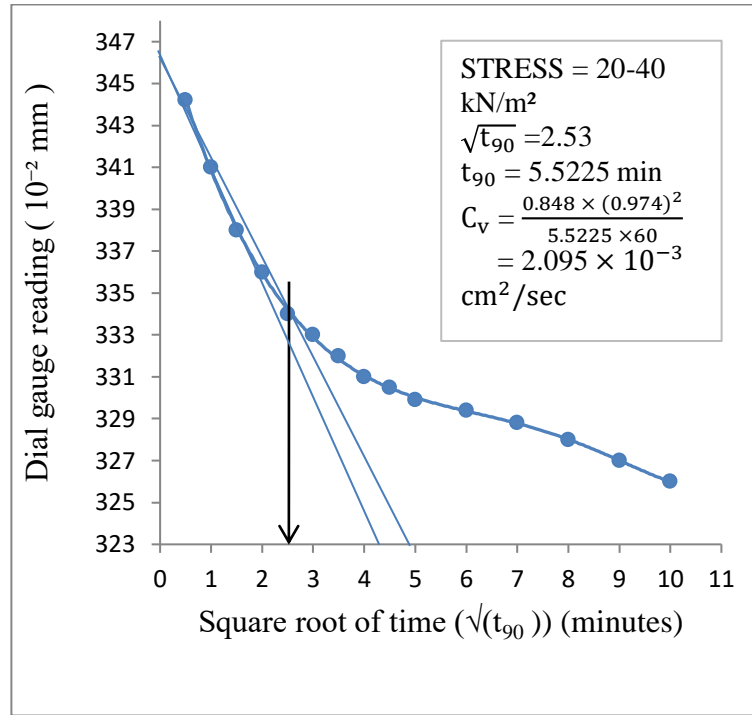


Figure 3.143: Time-consolidation curve of sample 3(dynamic at dry of optimum) at 20-40kPa

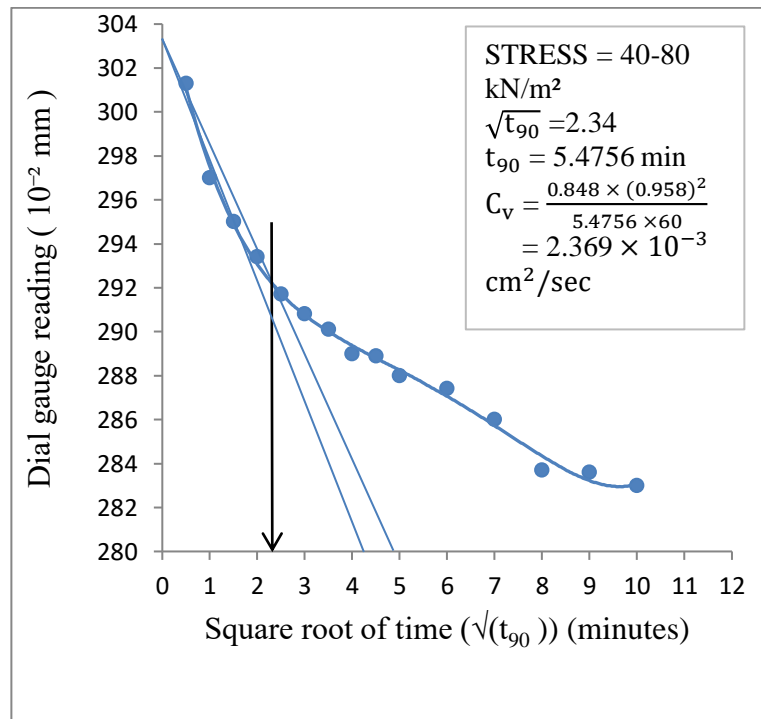


Figure 3.144: Time-consolidation curve of sample 3(dynamic at dry of optimum) at 40-80kPa

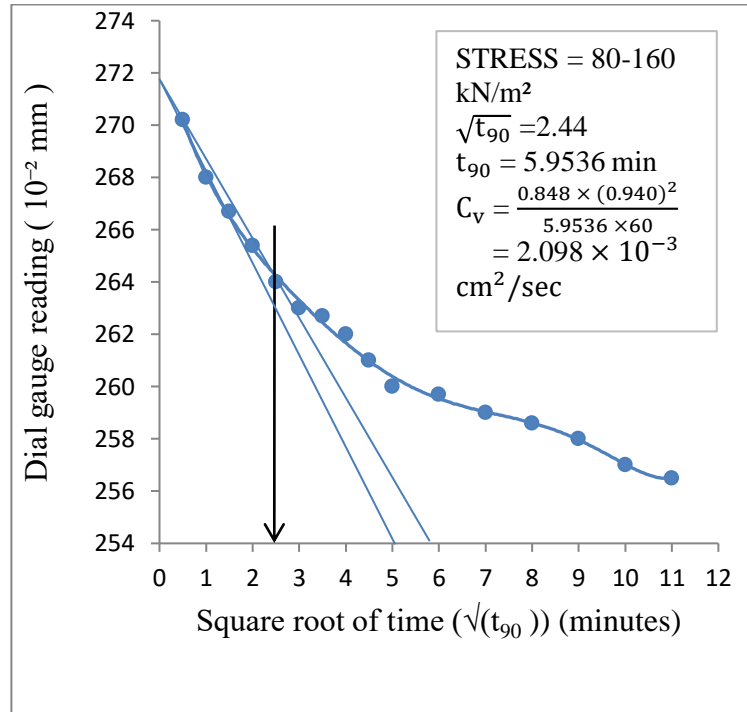


Figure 3.145: Time-consolidation curve of sample 3(dynamic at dry of optimum) at 80-160kPa

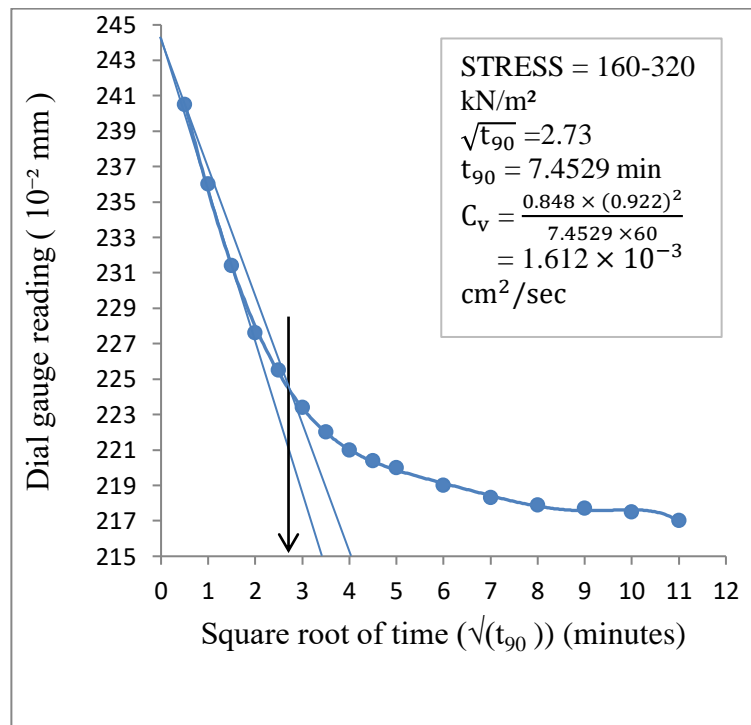


Figure 3.146: Time-consolidation curve of sample 3(dynamic at dry of optimum) at 160-320kPa

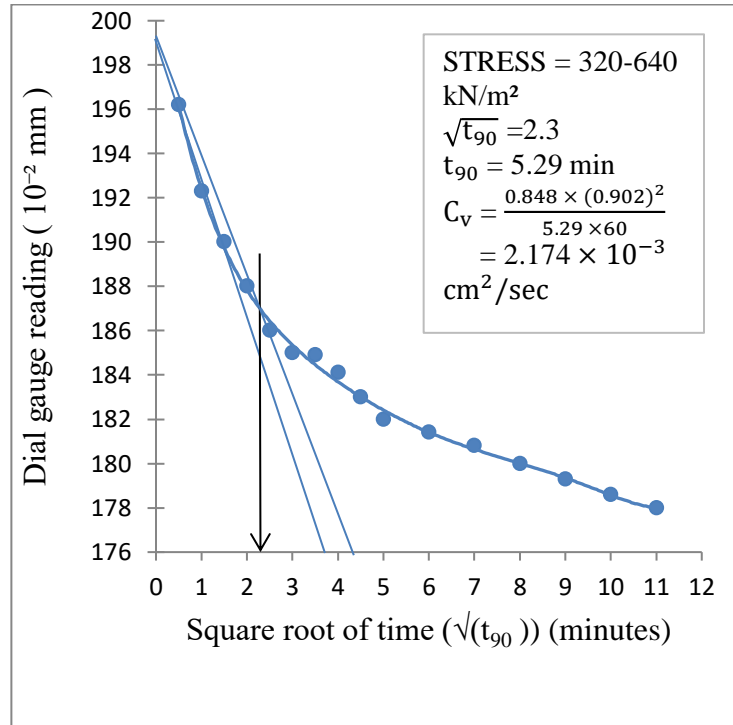


Figure 3.147: Time-consolidation curve of sample 3(dynamic at dry of optimum) at 320-640kPa

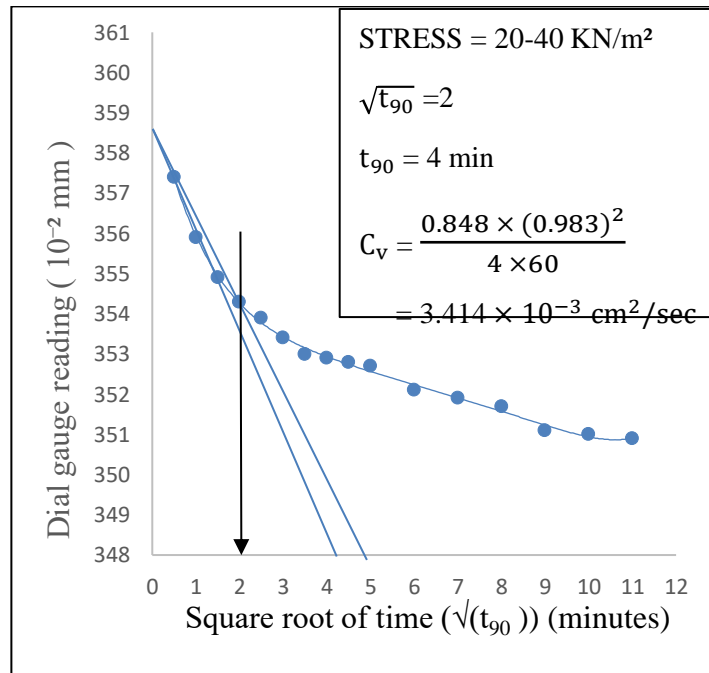


Figure 3.148: Time-consolidation curve of sample 3(dynamic at optimum moisture content) at 20-40kPa

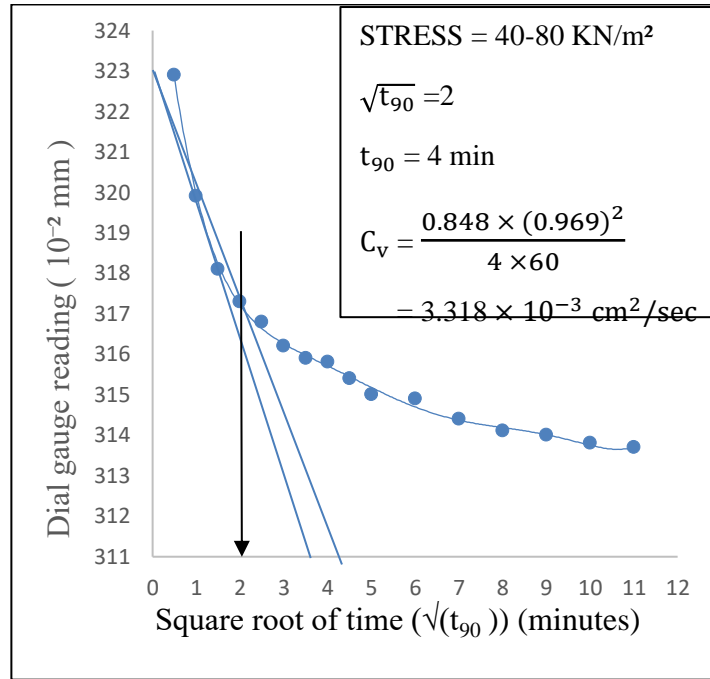


Figure 3.149: Time-consolidation curve of sample 3(dynamic at optimum moisture content) at 40-80kPa

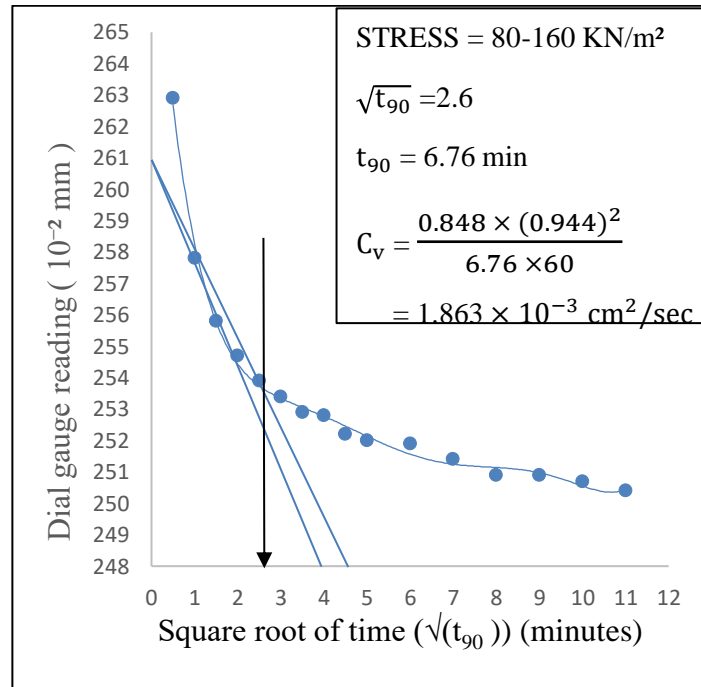


Figure 3.150: Time-consolidation curve of sample 3(dynamic at optimum moisture content) at 80-160kPa

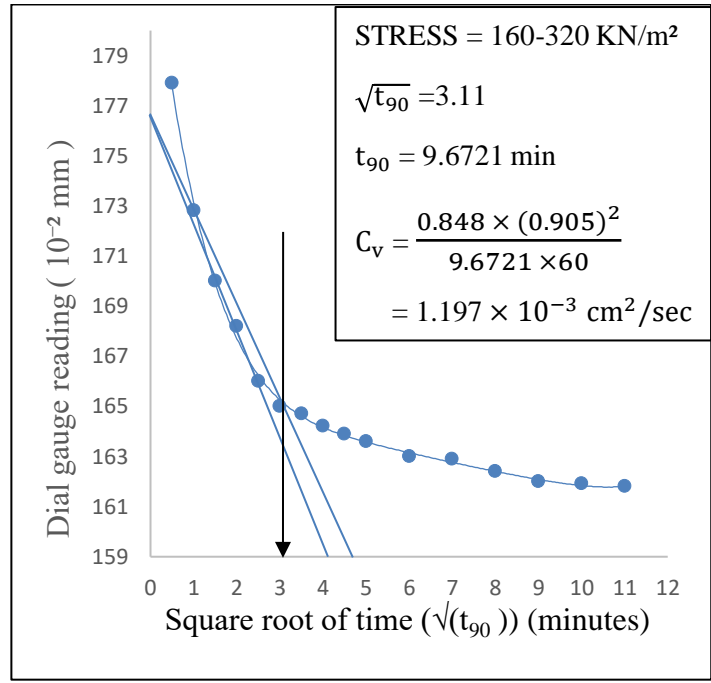


Figure 3.151: Time-consolidation curve of sample 3(dynamic at optimum moisture content) at 160-320kPa

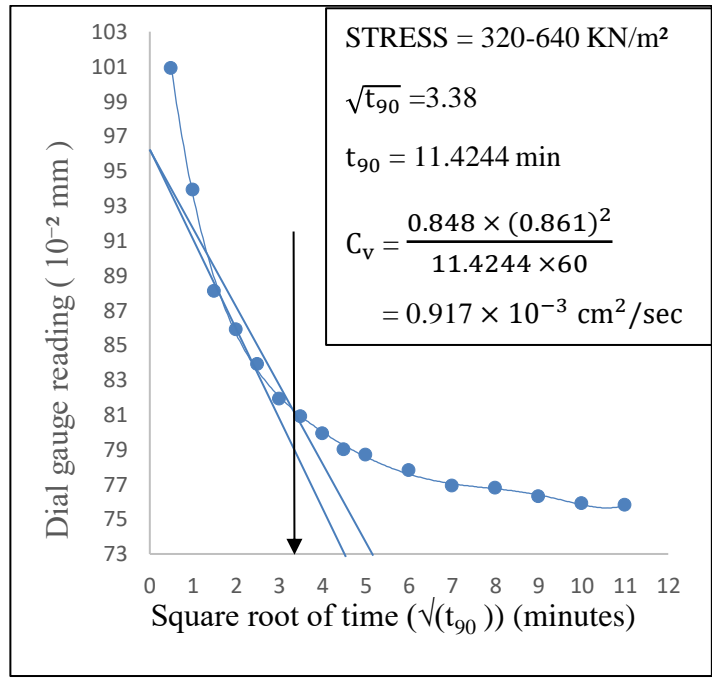


Figure 3.152: Time-consolidation curve of sample 3(dynamic at optimum moisture content) at 320-640kPa

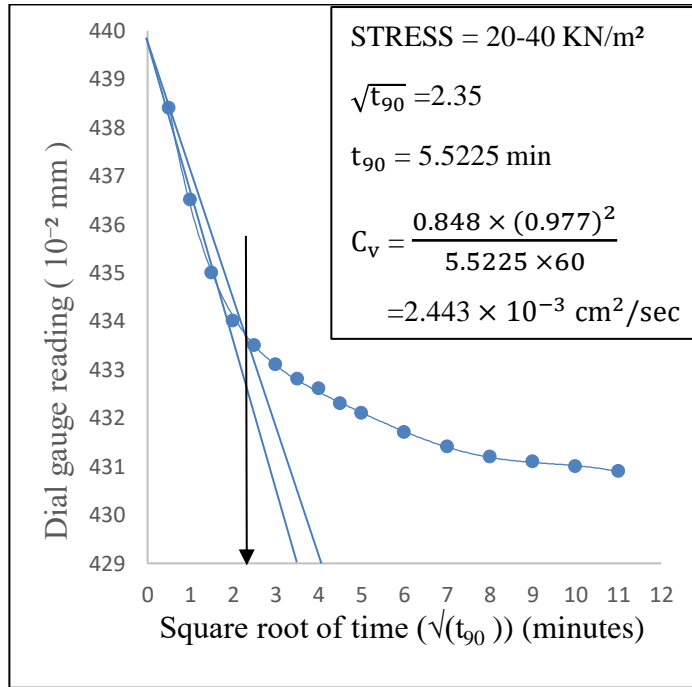


Figure 3.153: Time-consolidation curve of sample 3(dynamic at wet of optimum) at 20-40kPa

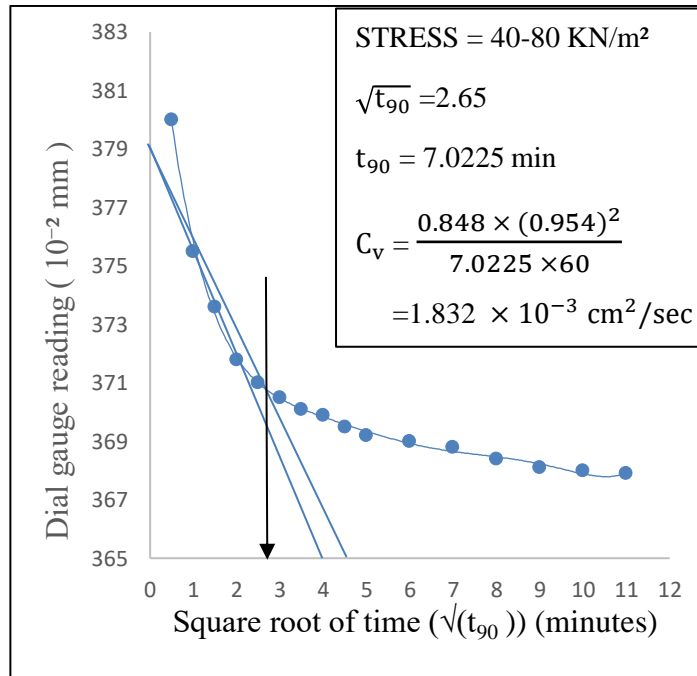


Figure 3.154: Time-consolidation curve of sample 3(dynamic at wet of optimum) at 40-80kPa

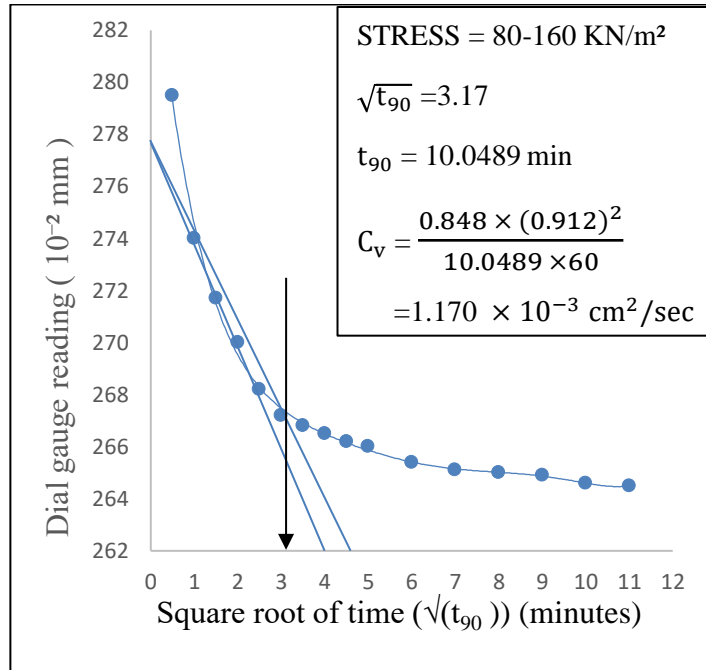


Figure 3.155: Time-consolidation curve of sample 3(dynamic at wet of optimum) at 80-160kPa

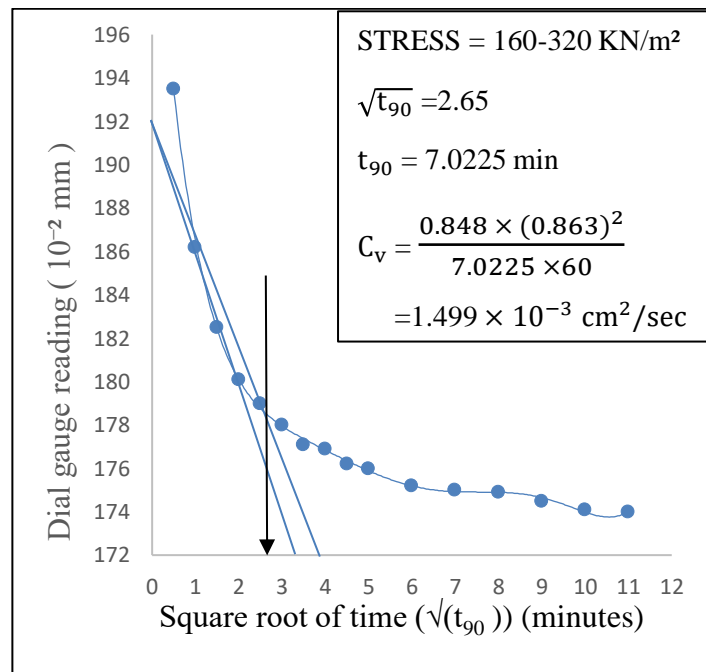


Figure 3.156: Time-consolidation curve of sample 3(dynamic at wet of optimum) at 160-320kPa

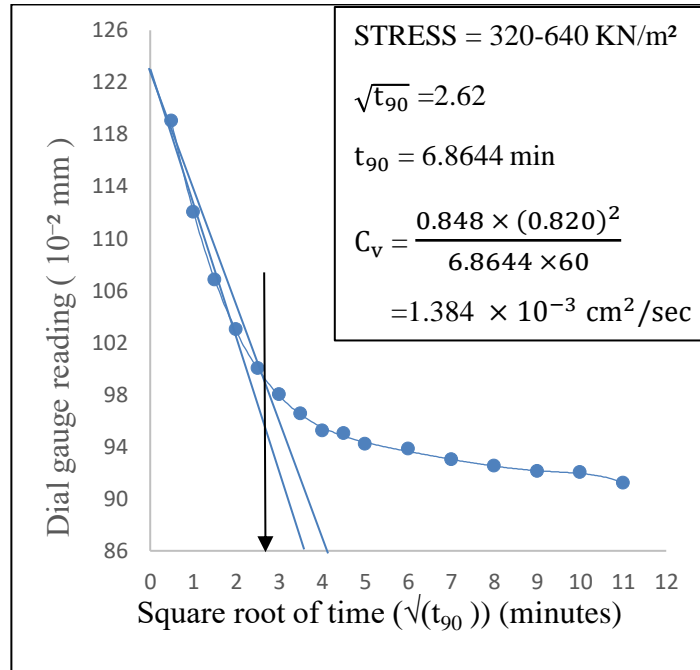


Figure 3.157: Time-consolidation curve of sample 3(dynamic at wet of optimum) at 320-640kPa

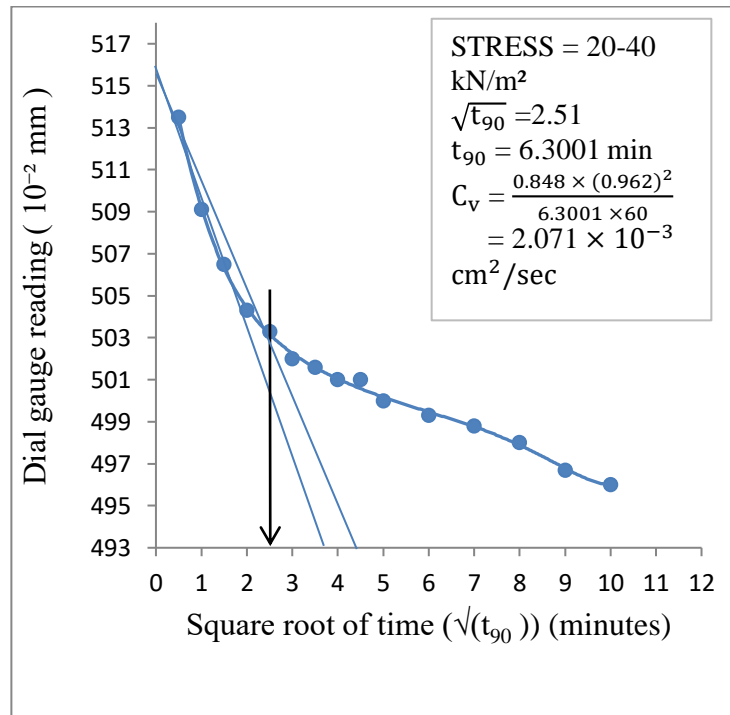


Figure 3.158: Time-consolidation curve of sample 3(static at dry of optimum) at 20-40kPa

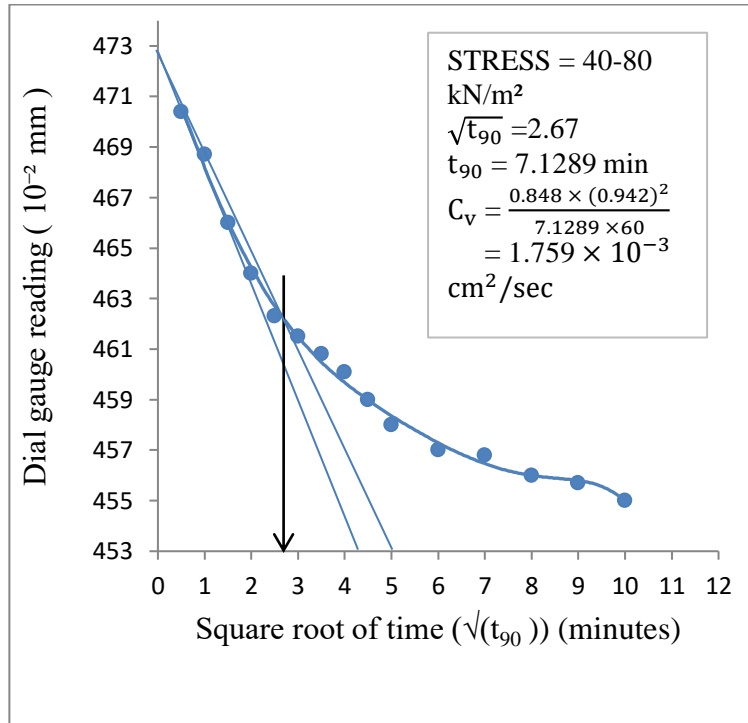


Figure 3.159: Time-consolidation curve of sample 3(static at dry of optimum) at 40-80kPa

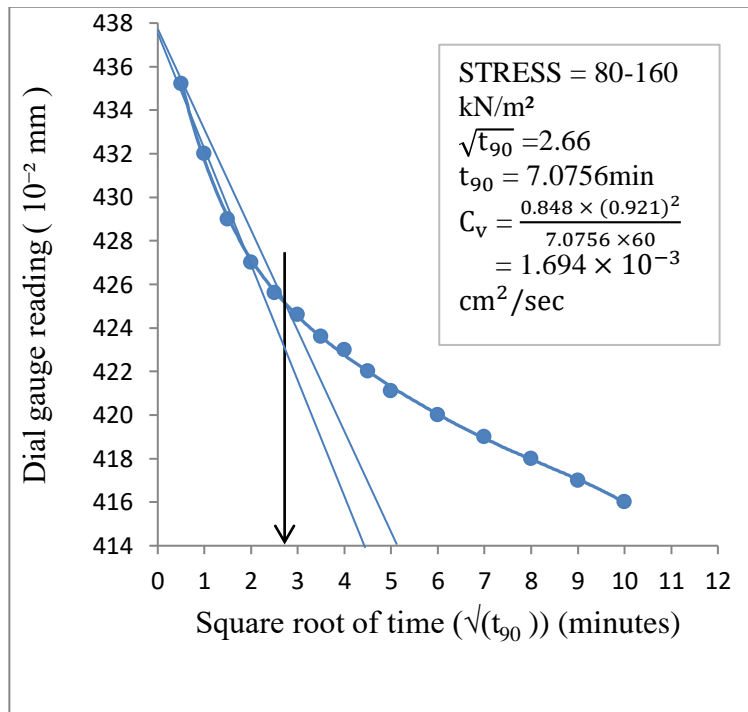


Figure 3.160: Time-consolidation curve of sample 3(static at dry of optimum) at 80-160kPa

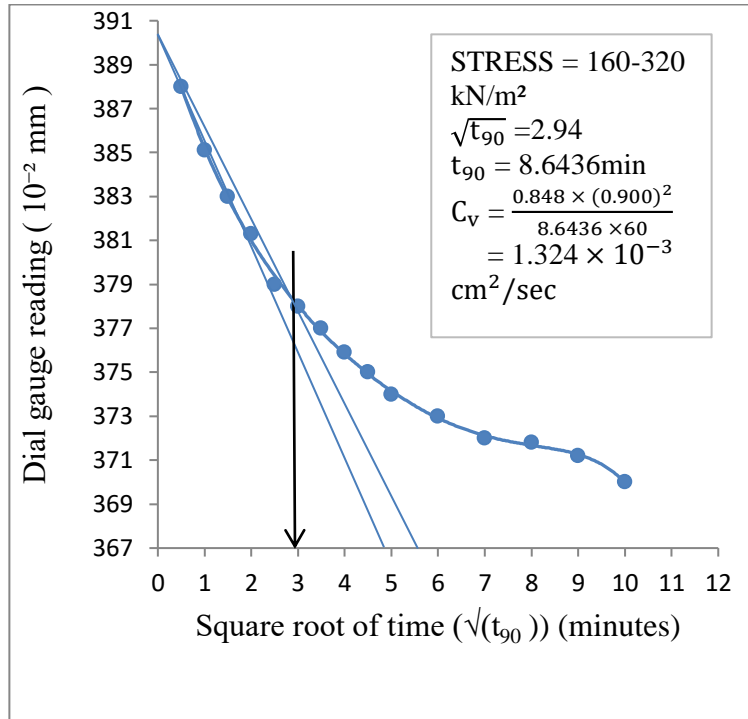


Figure 3.161: Time-consolidation curve of sample 3 (static at dry of optimum) at 160-320kPa

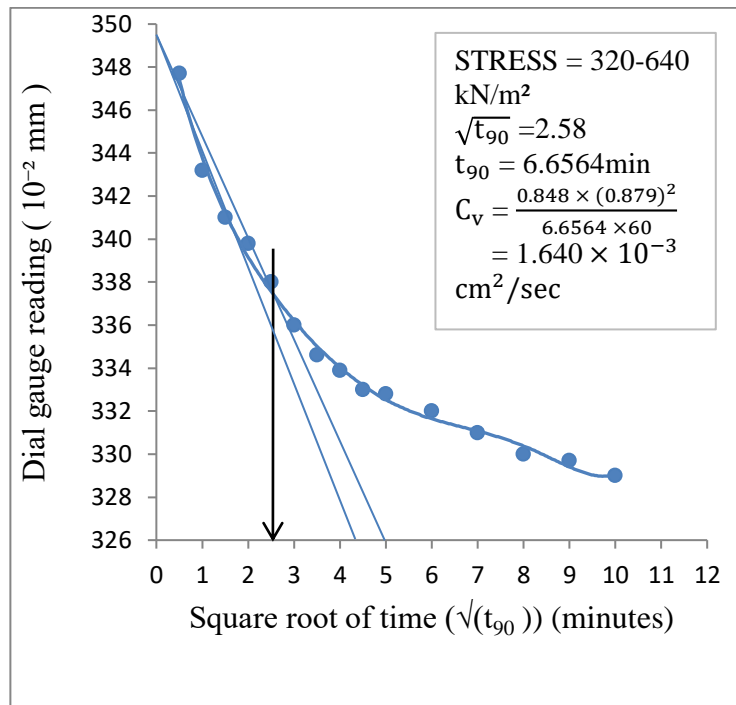


Figure 3.162: Time-consolidation curve of sample 3 (static at dry of optimum) at 320-640kPa

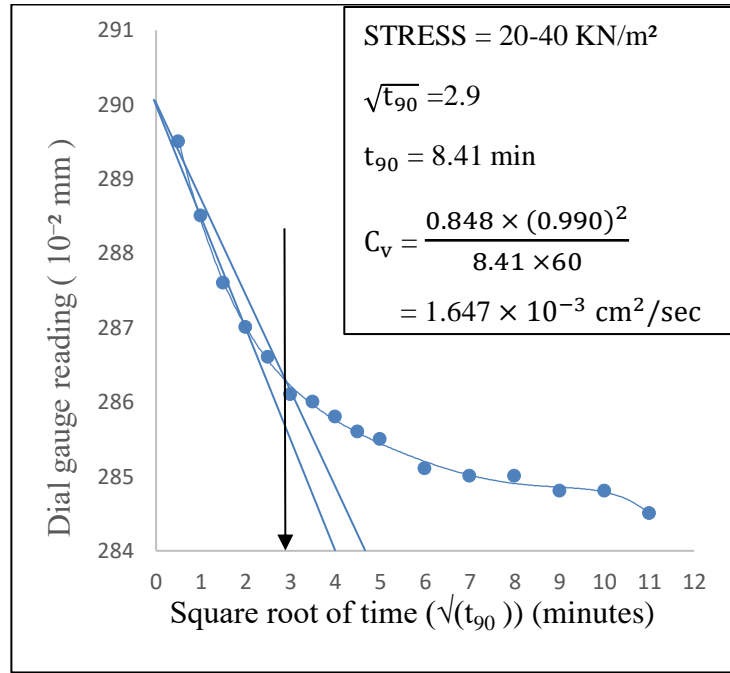


Figure 3.163: Time-consolidation curve of sample 3(static at optimum moisture content) at 20-40kPa

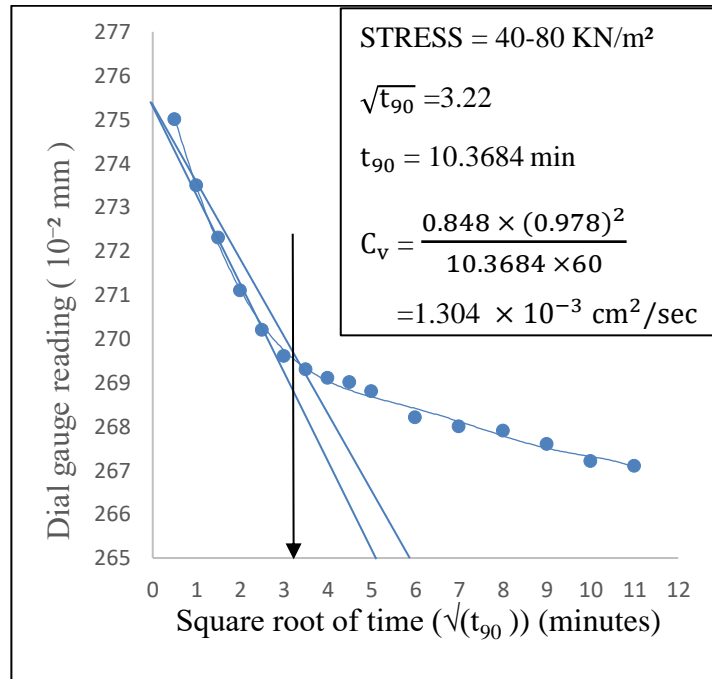


Figure 3.164: Time-consolidation curve of sample 3(static at optimum moisture content) at 40-80kPa

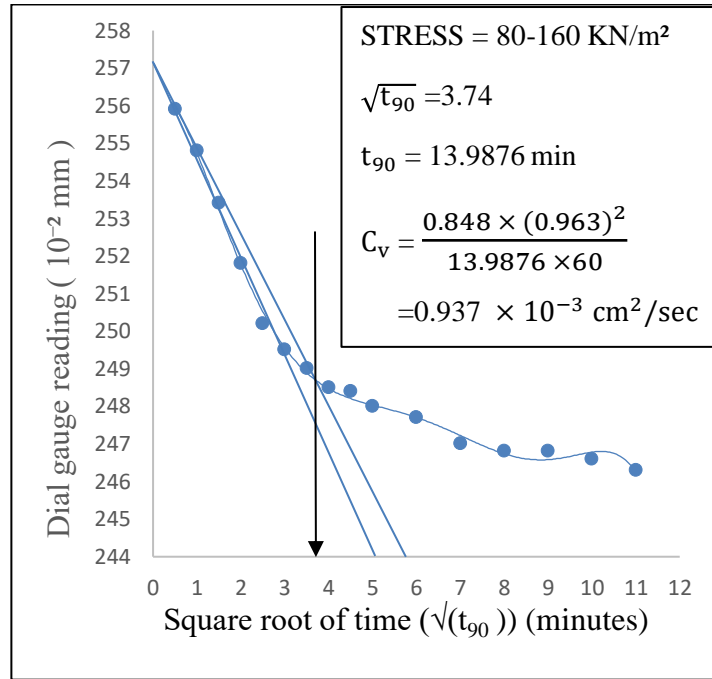


Figure 3.165: Time-consolidation curve of sample 3(static at optimum moisture content) at 80-160kPa

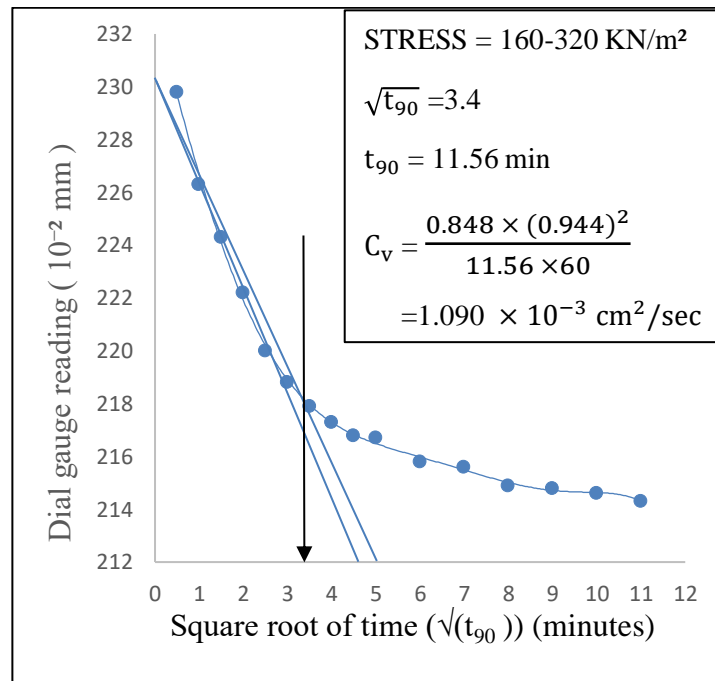


Figure 3.166: Time-consolidation curve of sample 3(static at optimum moisture content) at 160-320kPa

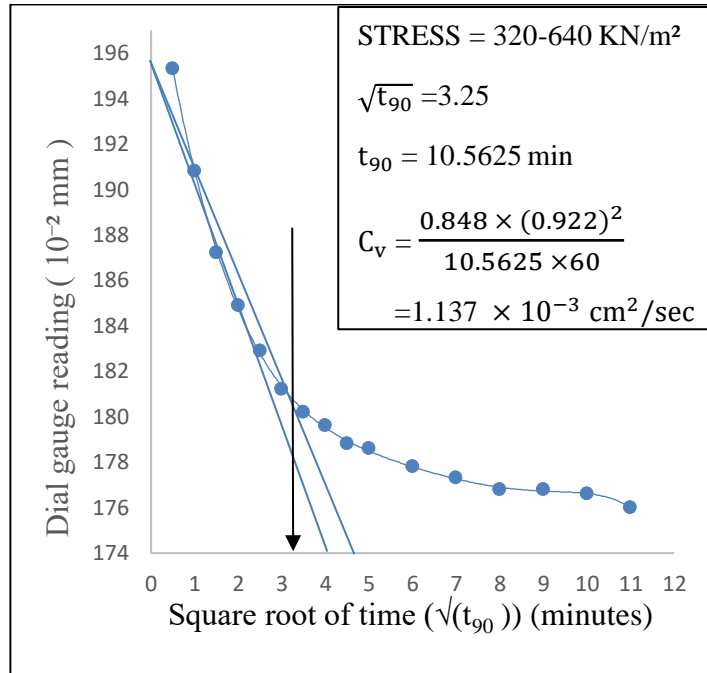


Figure 3.167: Time-consolidation curve of sample 3(static at optimum moisture content) at 320-640kPa

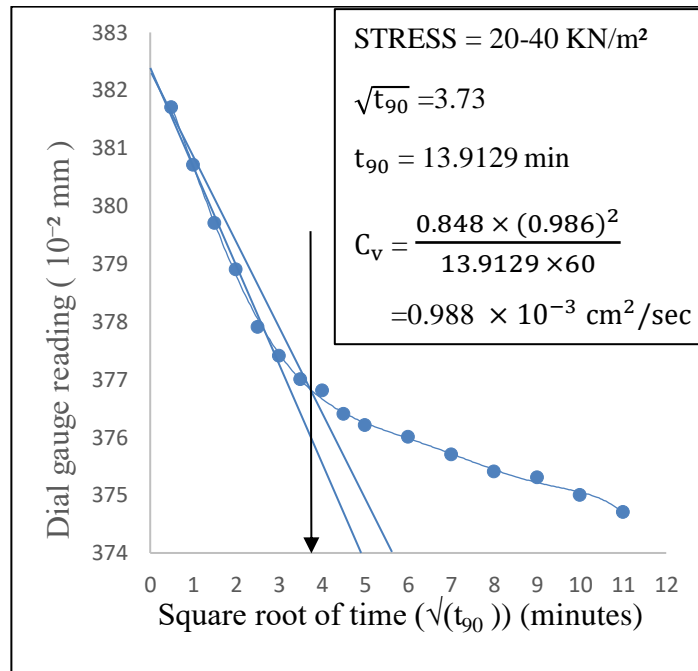


Figure 3.168: Time-consolidation curve of sample 3(static at wet of optimum) at 20-40kPa

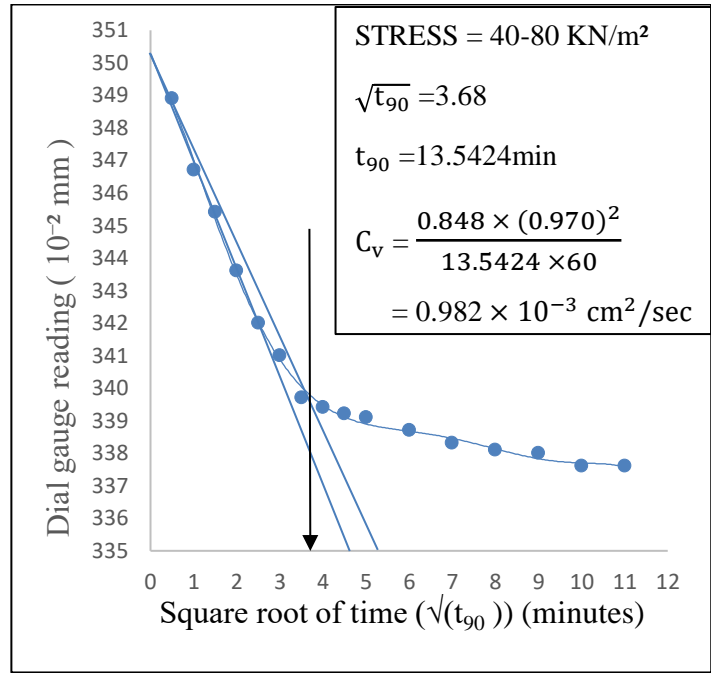


Figure 3.169: Time-consolidation curve of sample 3(static at wet of optimum) at 40-80kPa

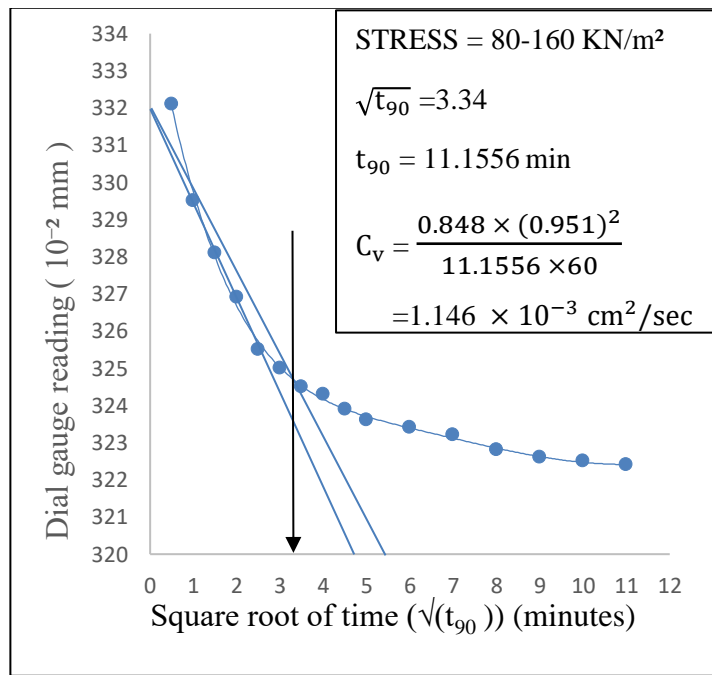


Figure 3.170: Time-consolidation curve of sample 3(static at wet of optimum) at 80-160kPa

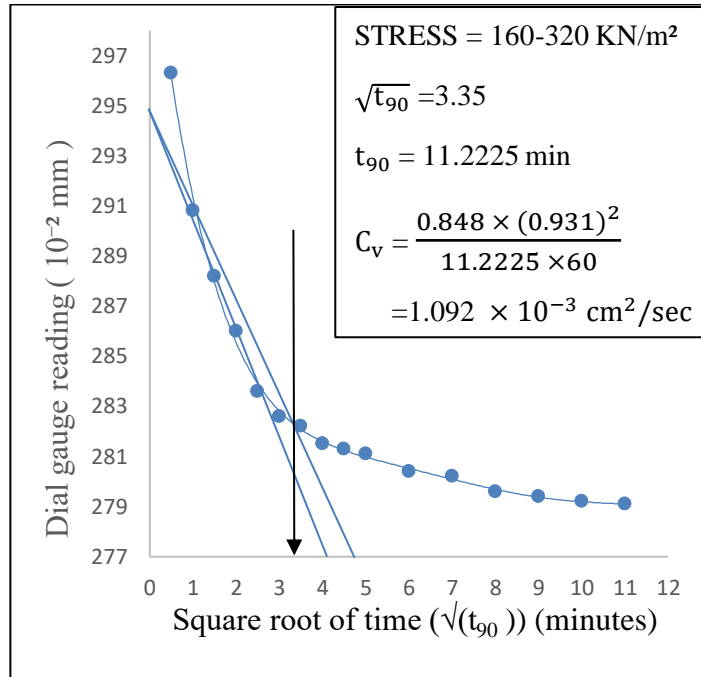


Figure 3.171: Time-consolidation curve of sample 3(static at wet of optimum) at 160-320kPa

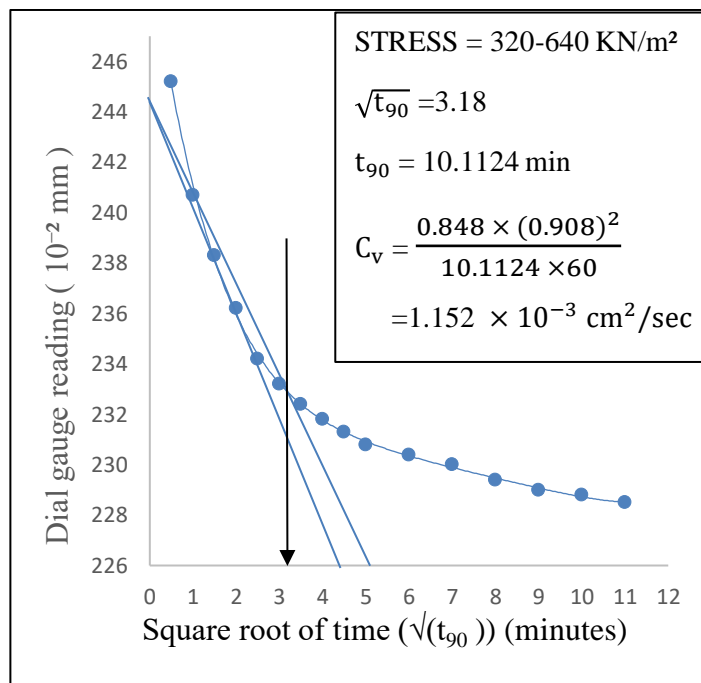


Figure 3.172: Time-consolidation curve of sample 3(static at wet of optimum) at 320-640kPa

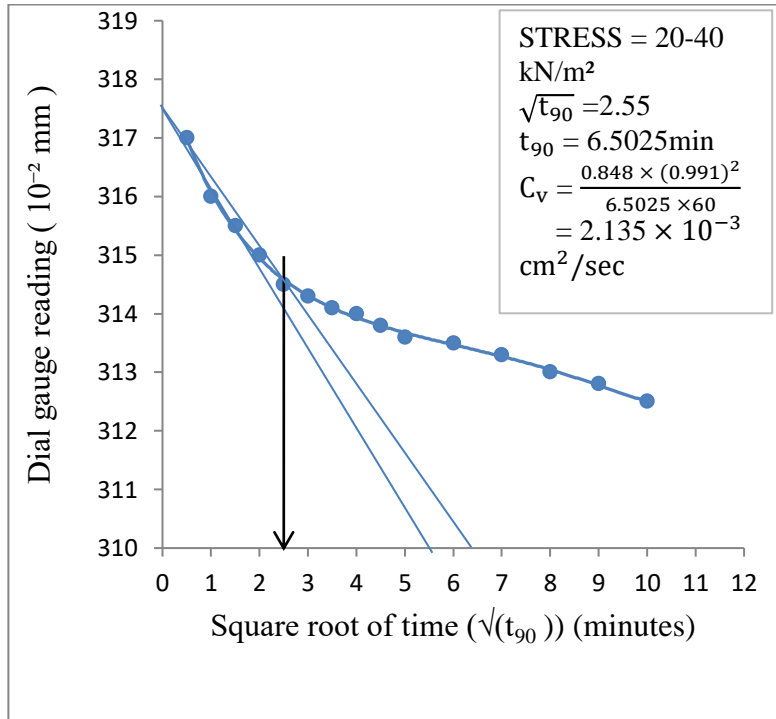


Figure 3.173: Time-consolidation curve of sample 4(dynamic at dry of optimum) at 20-40kPa

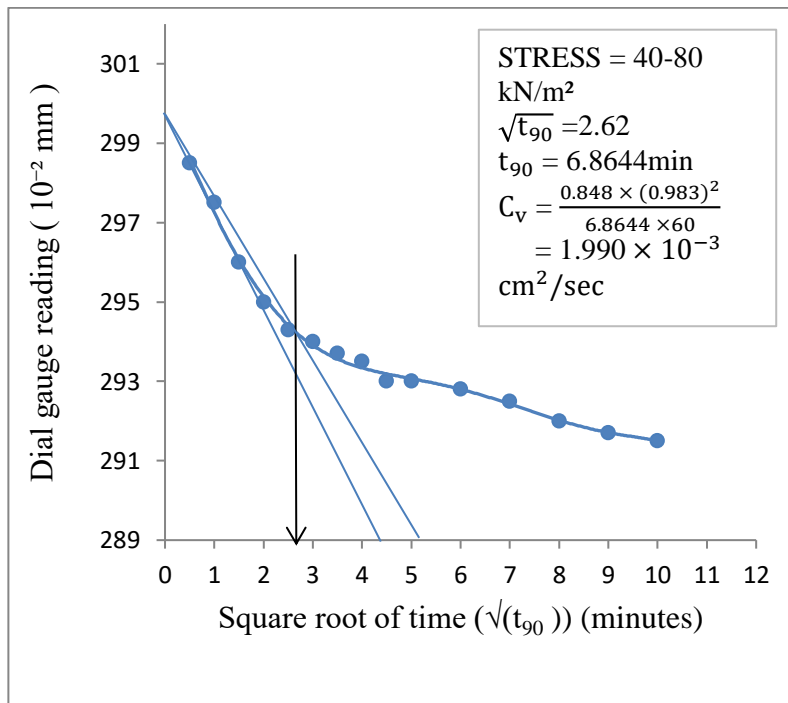


Figure 3.174: Time-consolidation curve of sample 4(dynamic at dry of optimum) at 40-80kPa

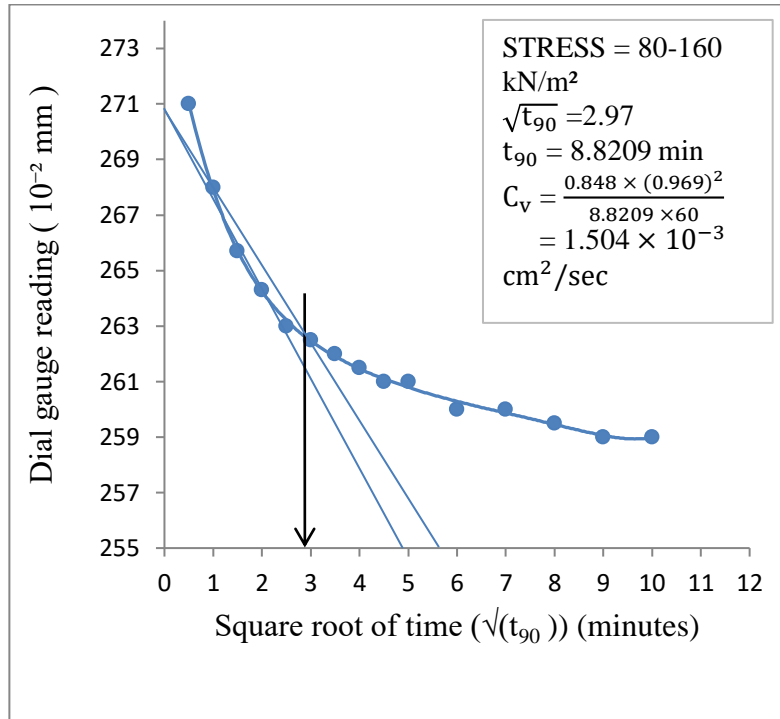


Figure 3.175: Time-consolidation curve of sample 4(dynamic at dry of optimum) at 80-160kPa

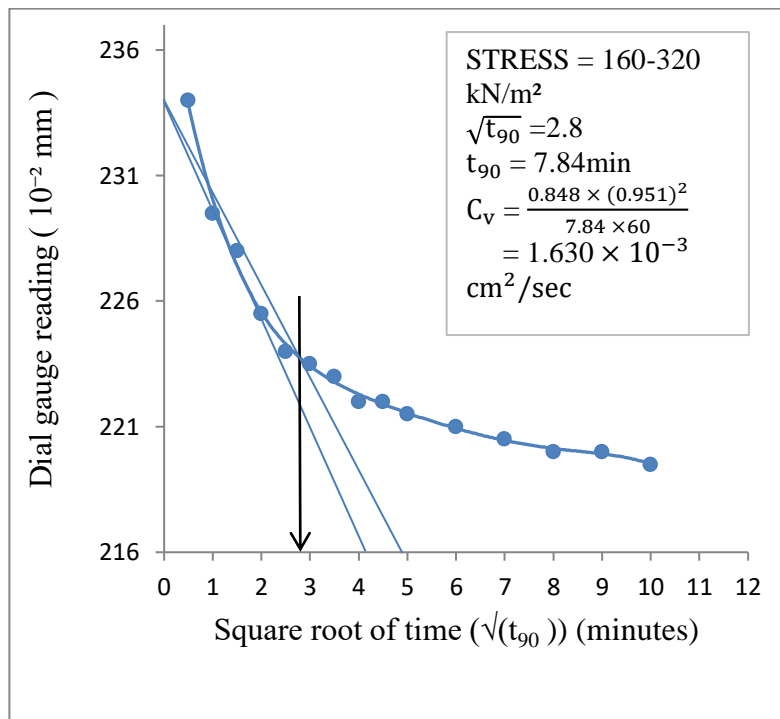


Figure 3.176: Time-consolidation curve of sample 4(dynamic at dry of optimum) at 160-320kPa

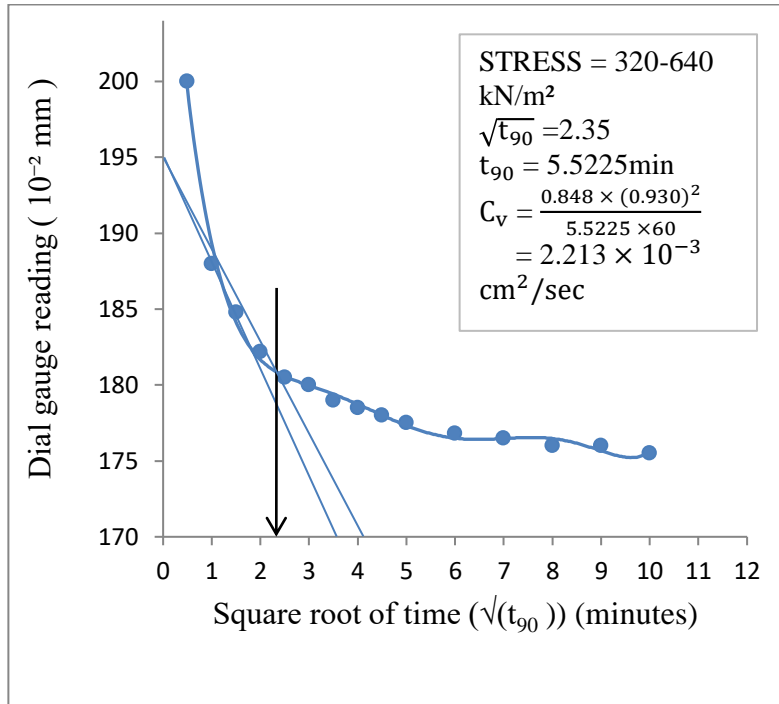


Figure 3.177: Time-consolidation curve of sample 4 (dynamic at dry of optimum) at 320-640 kPa

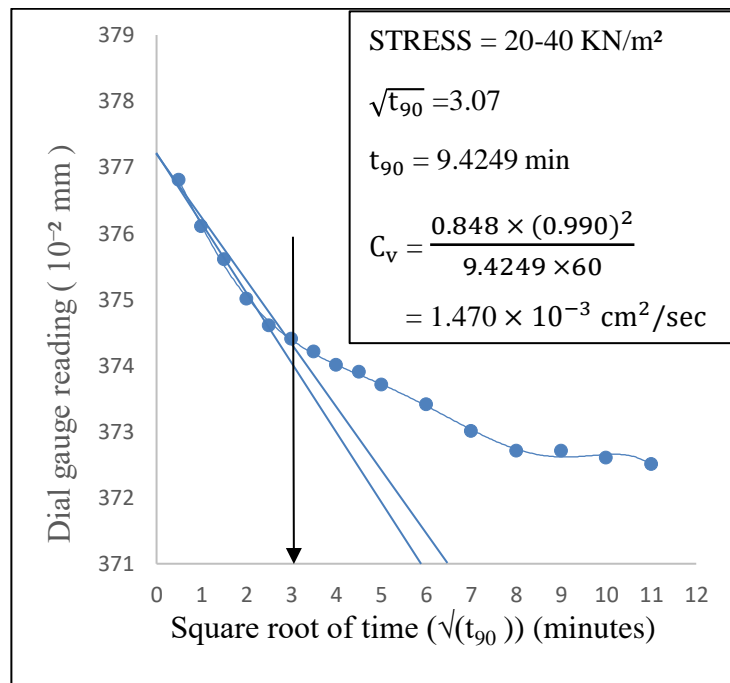


Figure 3.178: Time-consolidation curve of sample 4 (dynamic at optimum moisture content) at 20-40 kPa

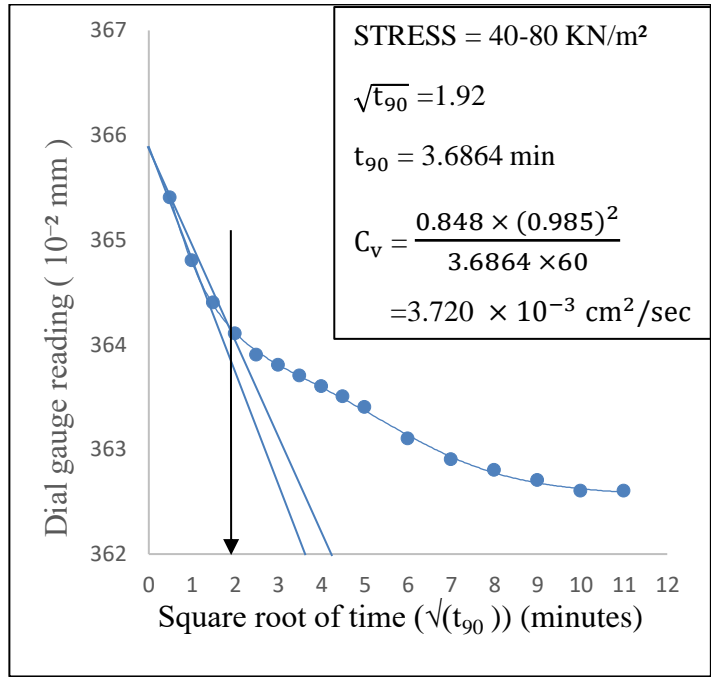


Figure 3.179: Time-consolidation curve of sample 4(dynamic at optimum moisture content) at 40-80kPa

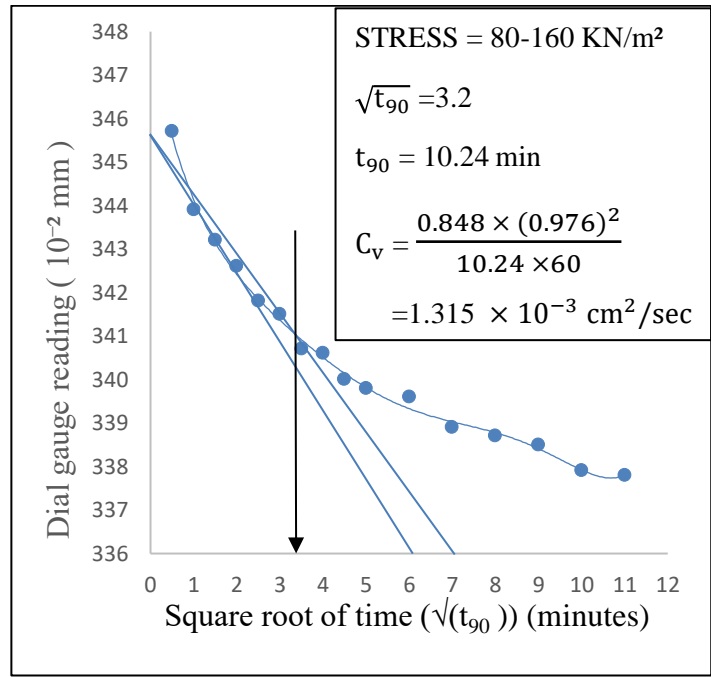


Figure 3.180: Time-consolidation curve of sample 4(dynamic at optimum moisture content) at 80-160kPa

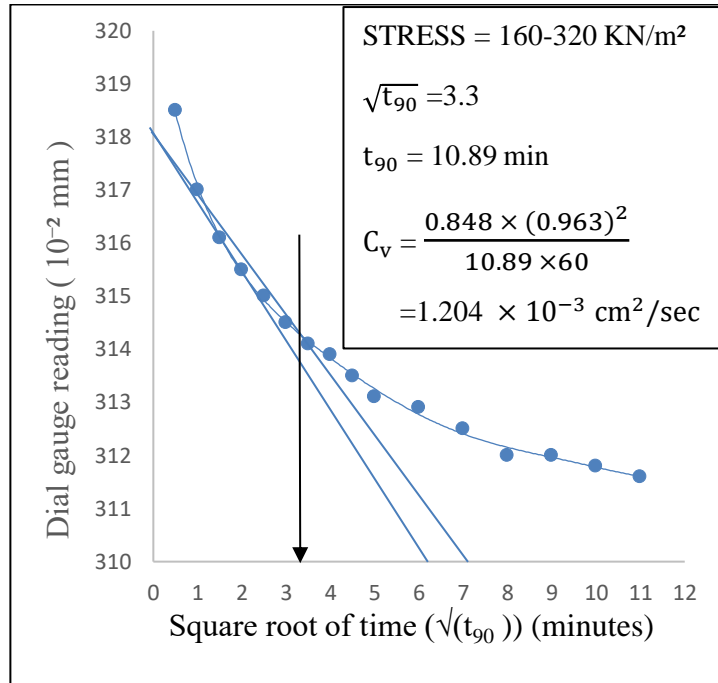


Figure 3.181: Time-consolidation curve of sample 4(dynamic at optimum moisture content) at 160-320kPa

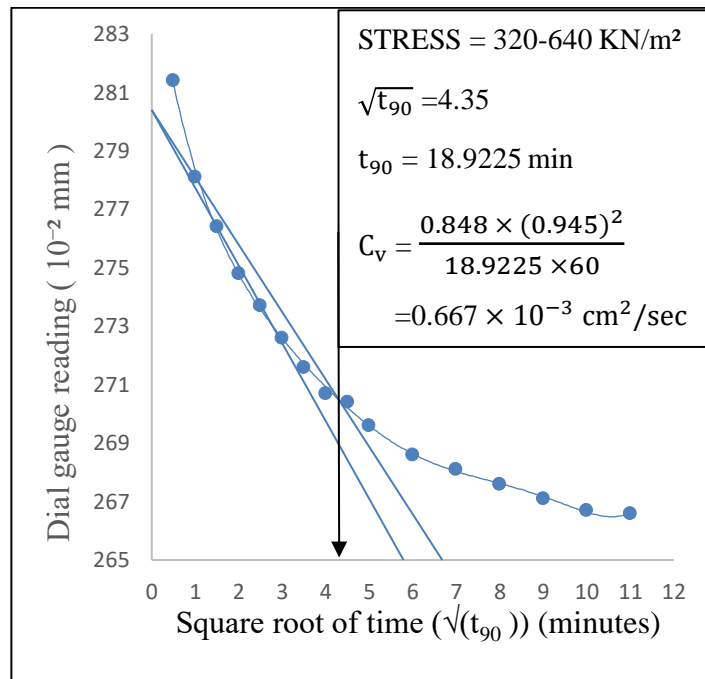


Figure 3.182: Time-consolidation curve of sample 4(dynamic at optimum moisture content) at 320-640kPa

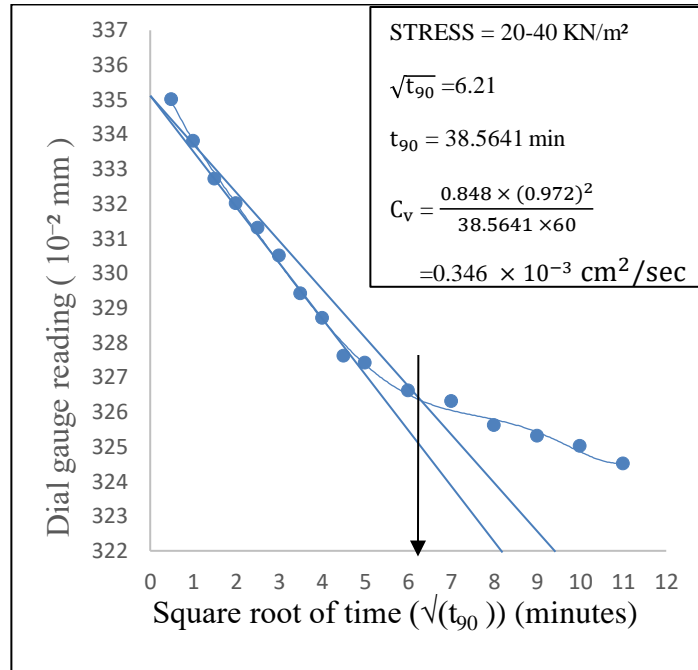


Figure 3.183: Time-consolidation curve of sample 4(dynamic at wet of optimum) at 20-40kPa

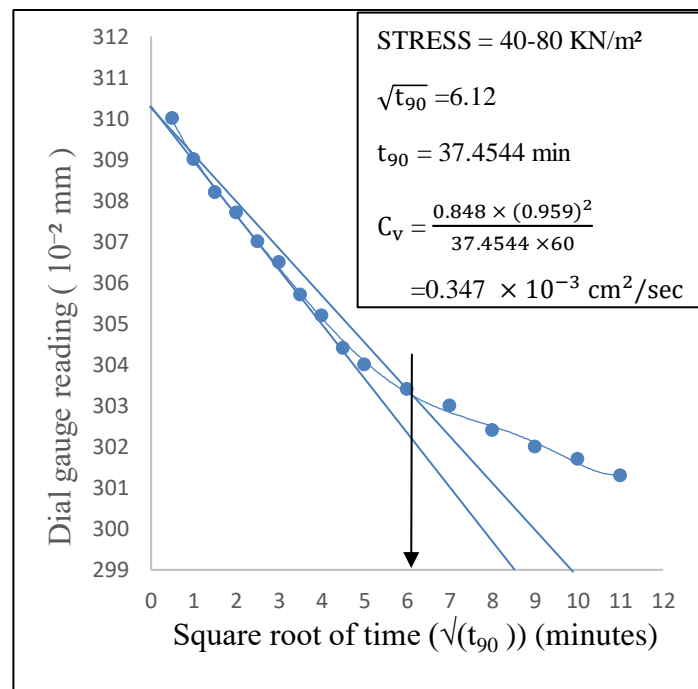


Figure 3.184: Time-consolidation curve of sample 4(dynamic at wet of optimum) at 40-80kPa

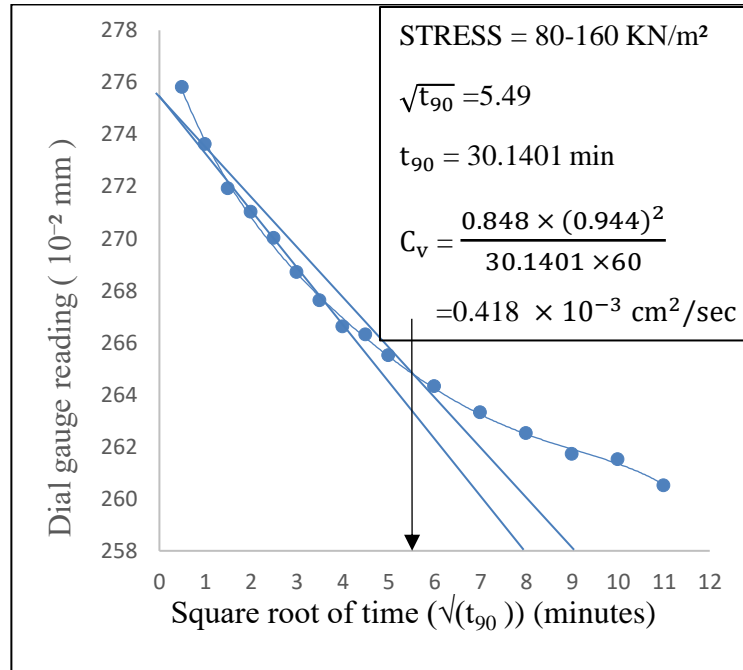


Figure 3.185: Time-consolidation curve of sample 4(dynamic at wet of optimum) at 80-160kPa

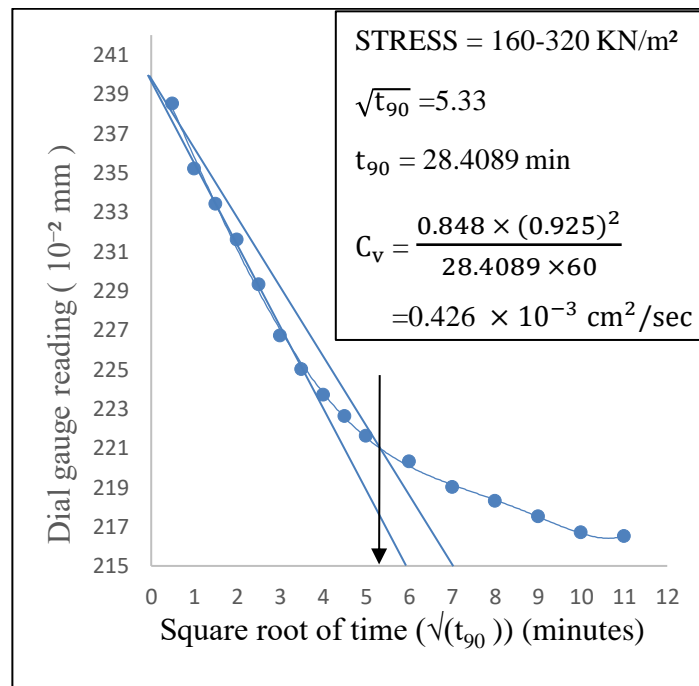


Figure 3.186: Time-consolidation curve of sample 4(dynamic at wet of optimum) at 160-320kPa

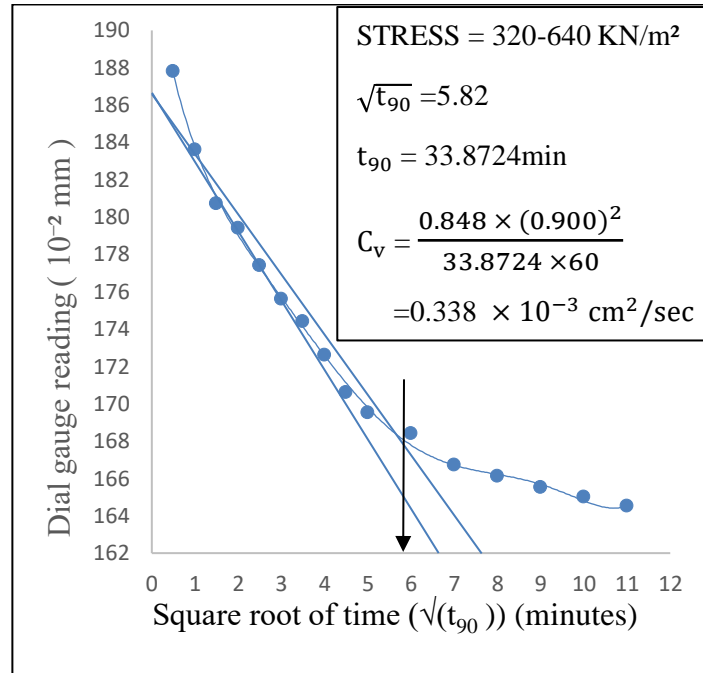


Figure 3.187: Time-consolidation curve of sample 4(dynamic at wet of optimum) at 320-640kPa

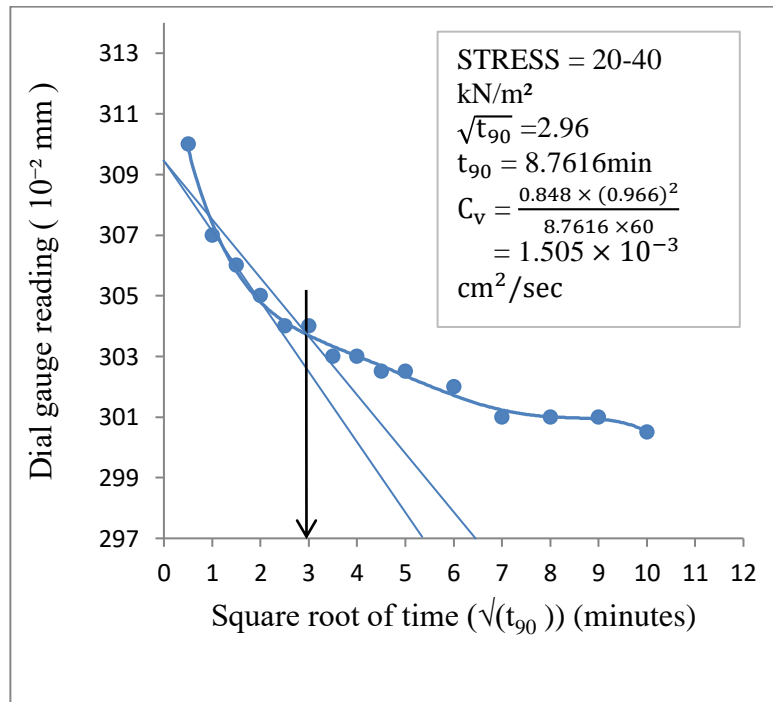


Figure 3.188: Time-consolidation curve of sample 4(static at dry of optimum) at 20-40kPa

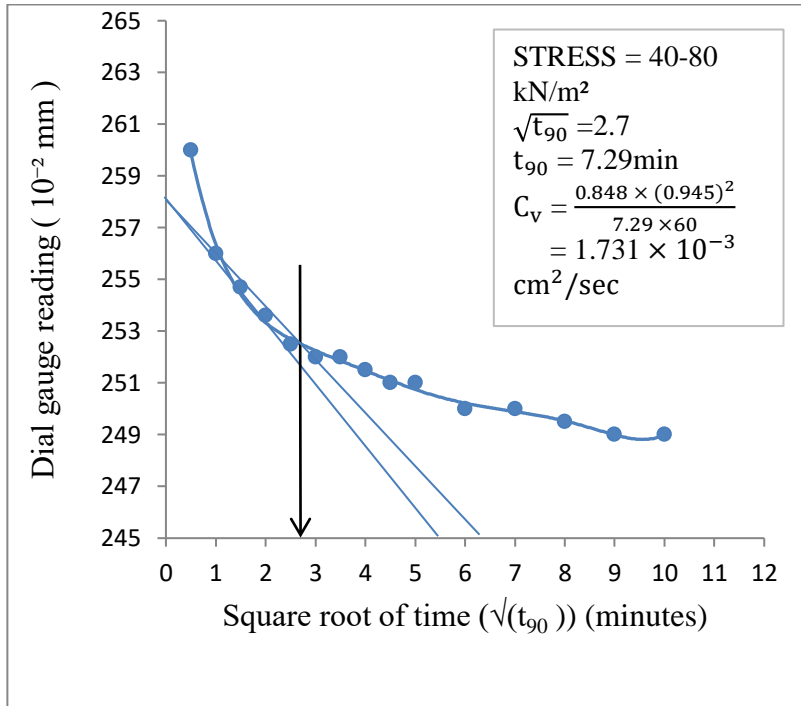


Figure 3.189: Time-consolidation curve of sample 4(static at dry of optimum) at 40-80kPa

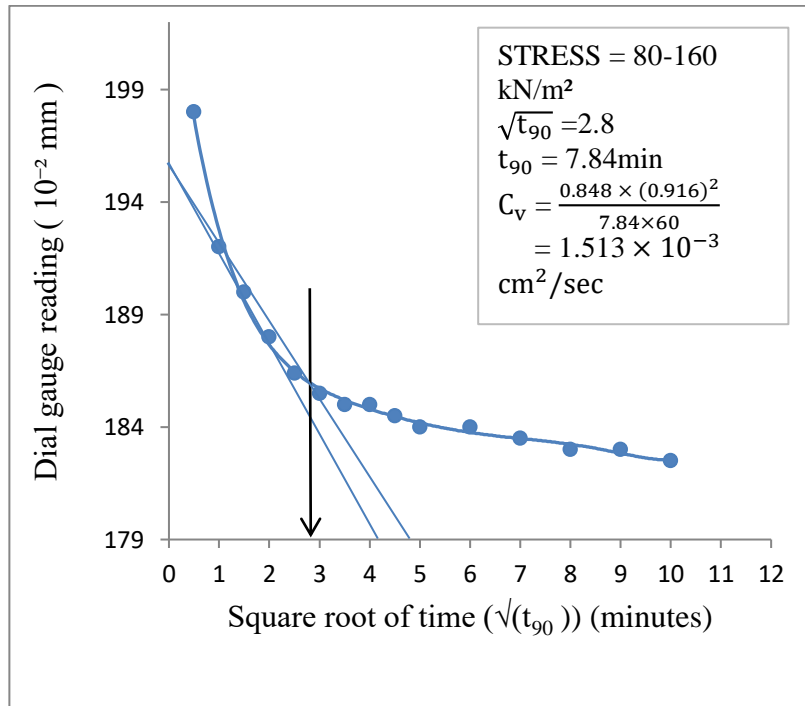


Figure 3.190: Time-consolidation curve of sample 4(static at dry of optimum) at 80-160kPa

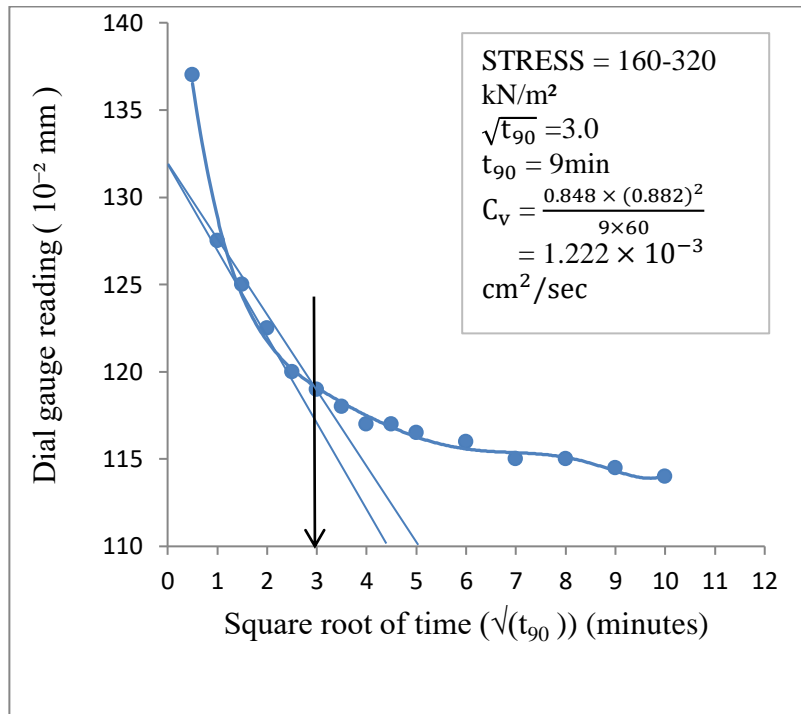


Figure 3.191: Time-consolidation curve of sample 4(static at dry of optimum) at 160-320kPa

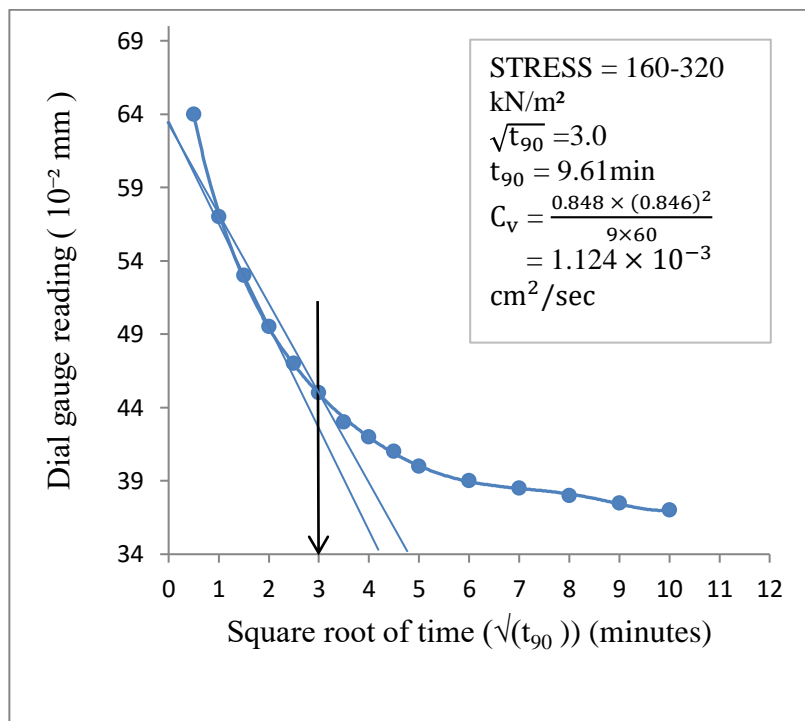


Figure 3.192: Time-consolidation curve of sample 4(static at dry of optimum) at 320-640kPa

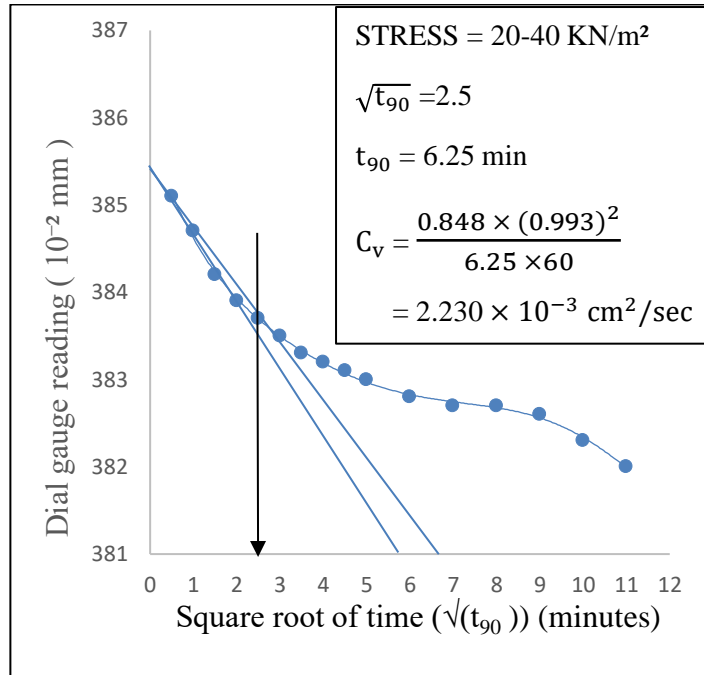


Figure 3.193: Time-consolidation curve of sample 4(static at optimum moisture content) at 20-40kPa

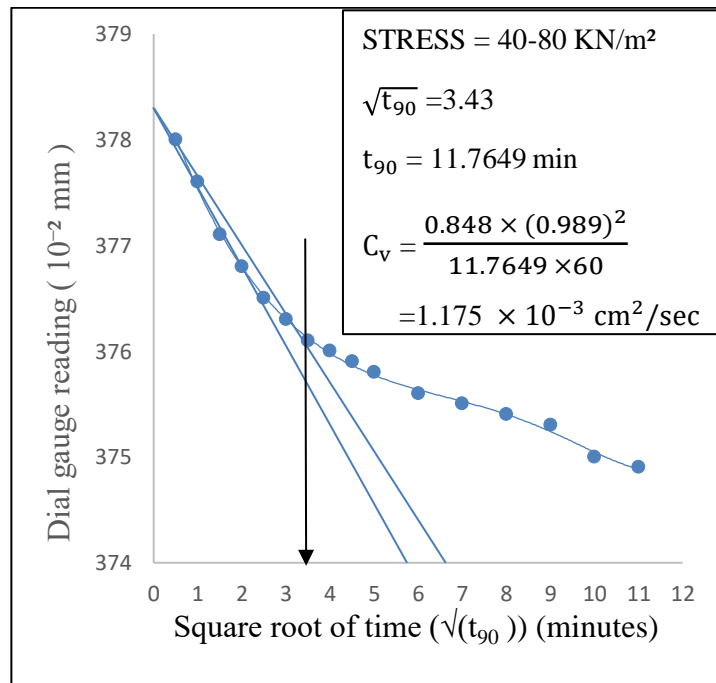


Figure 3.194: Time-consolidation curve of sample 4(static at optimum moisture content) at 40-80kPa

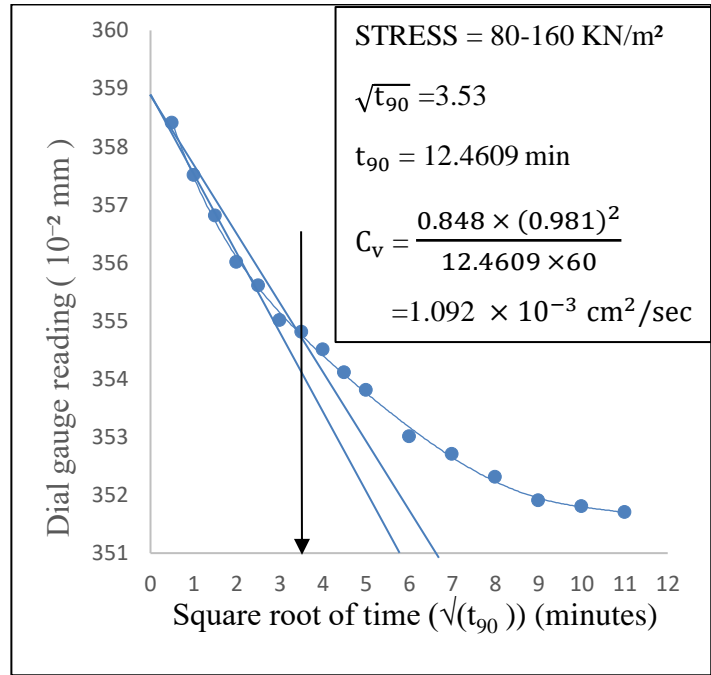


Figure 3.195: Time-consolidation curve of sample 4 (static at optimum moisture content) at 80-160kPa

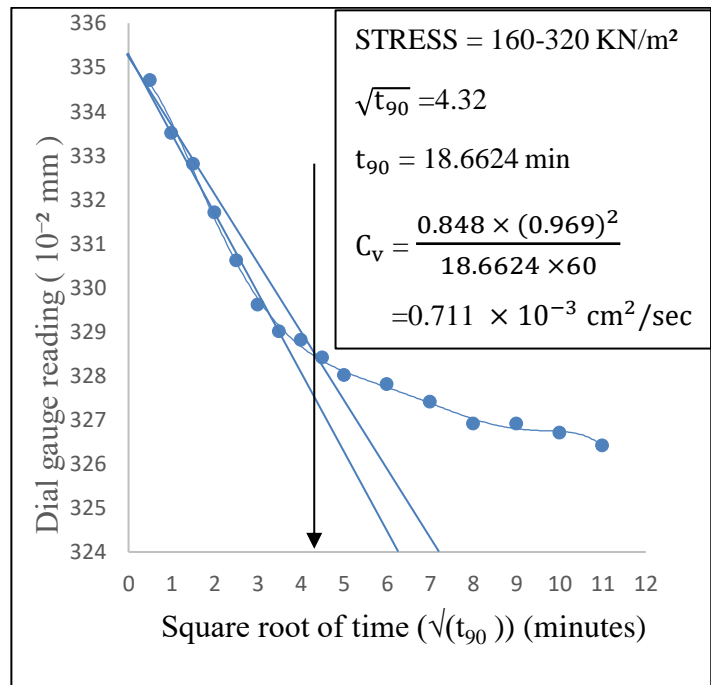


Figure 3.196: Time-consolidation curve of sample 4 (static at optimum moisture content) at 160-320kPa

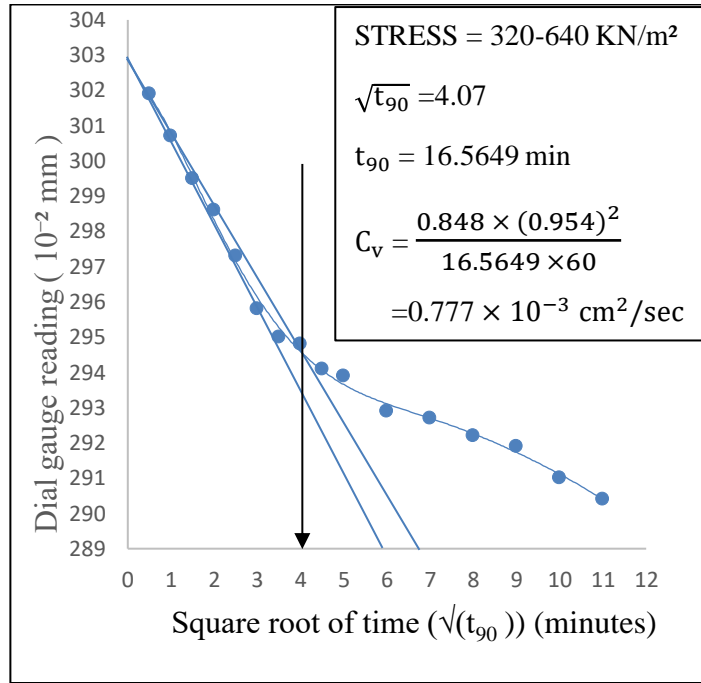


Figure 3.197: Time-consolidation curve of sample 4(static at optimum moisture content) at 320-640kPa

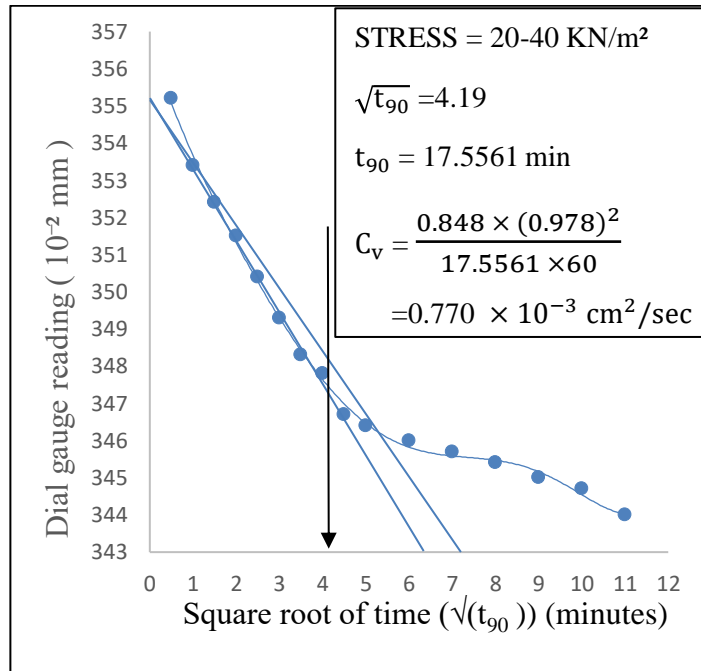


Figure 3.198: Time-consolidation curve of sample 4(static at wet of optimum) at 20-40kPa

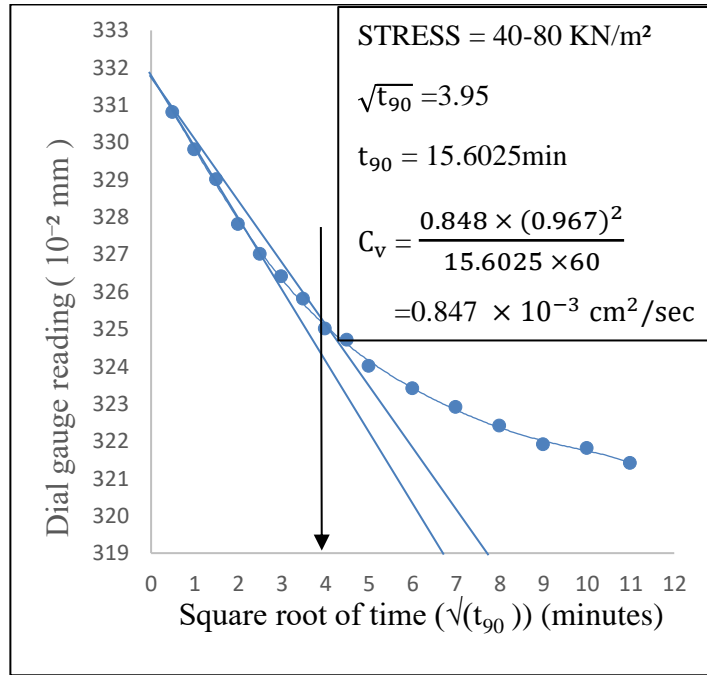


Figure 3.199: Time-consolidation curve of sample 4(static at wet of optimum) at 40-80kPa

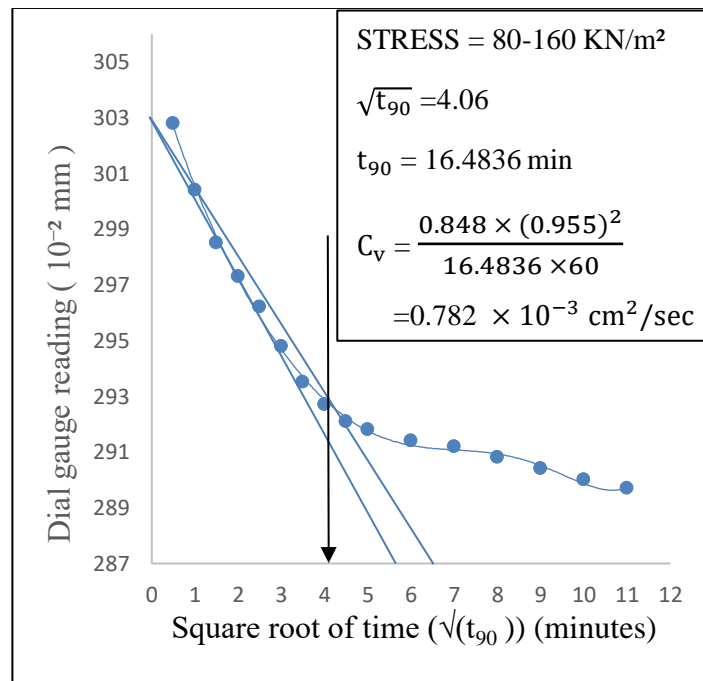


Figure 3.200: Time-consolidation curve of sample 4(static at wet of optimum) at 80-160kPa

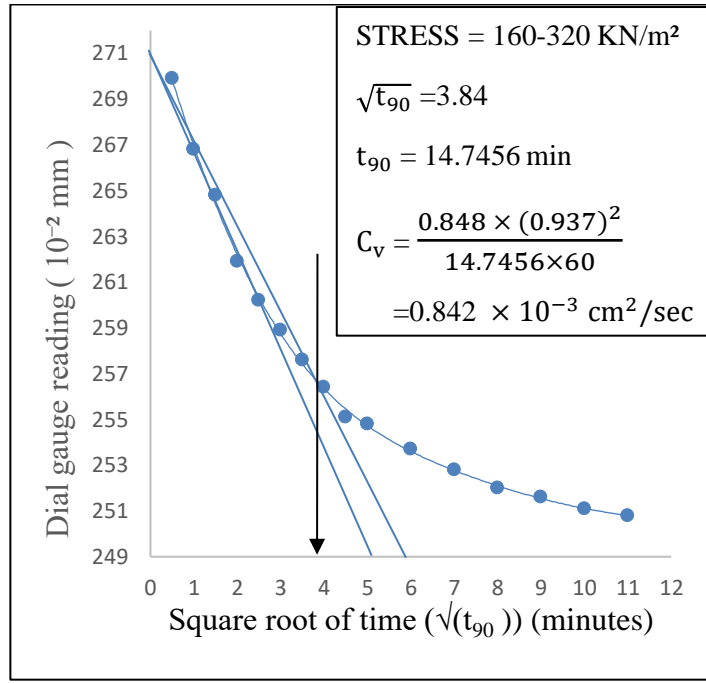


Figure 3.201: Time-consolidation curve of sample 4(static at wet of optimum) at 160-320kPa

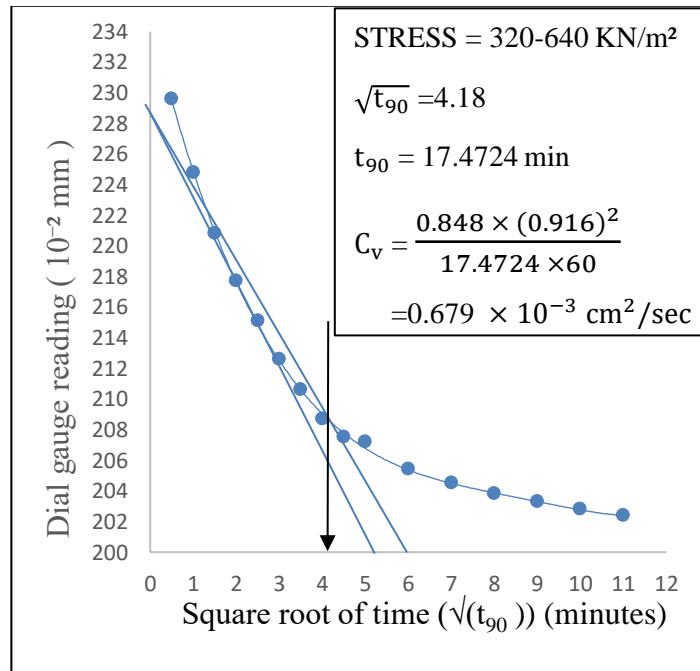


Figure 3.202: Time-consolidation curve of sample 4(static at wet of optimum) at 320-640kPa

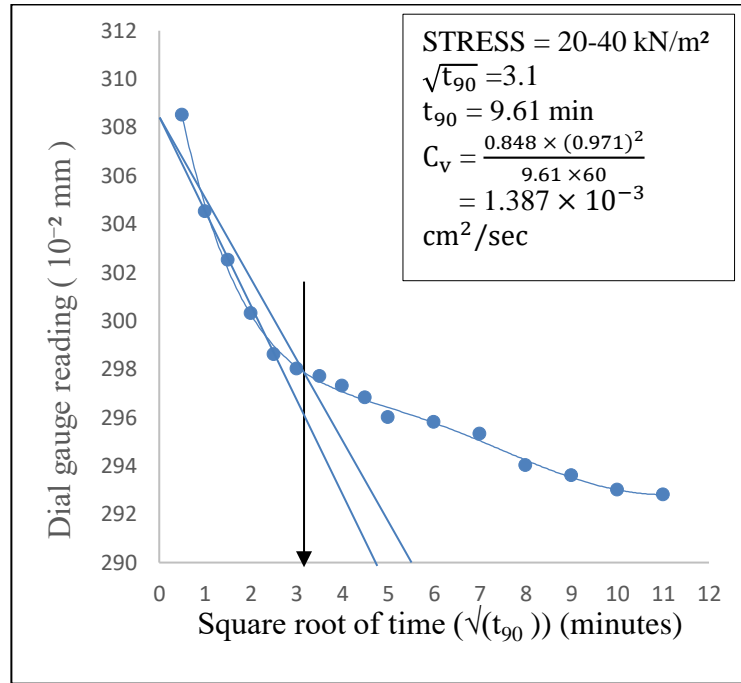


Figure 3.203: Time-consolidation curve of sample 5(dynamic at dry of optimum) at 20-40kPa

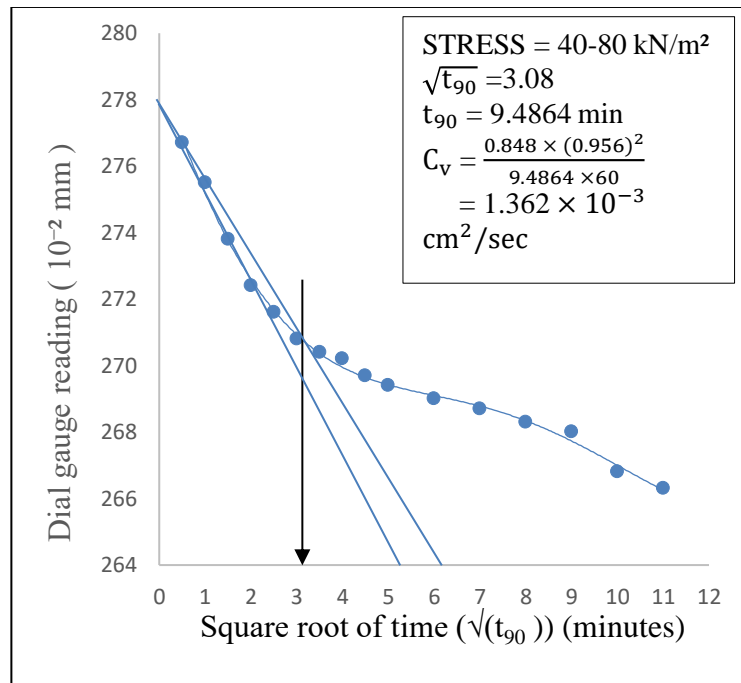


Figure 3.204: Time-consolidation curve of sample 5(dynamic at dry of optimum) at 40-80kPa

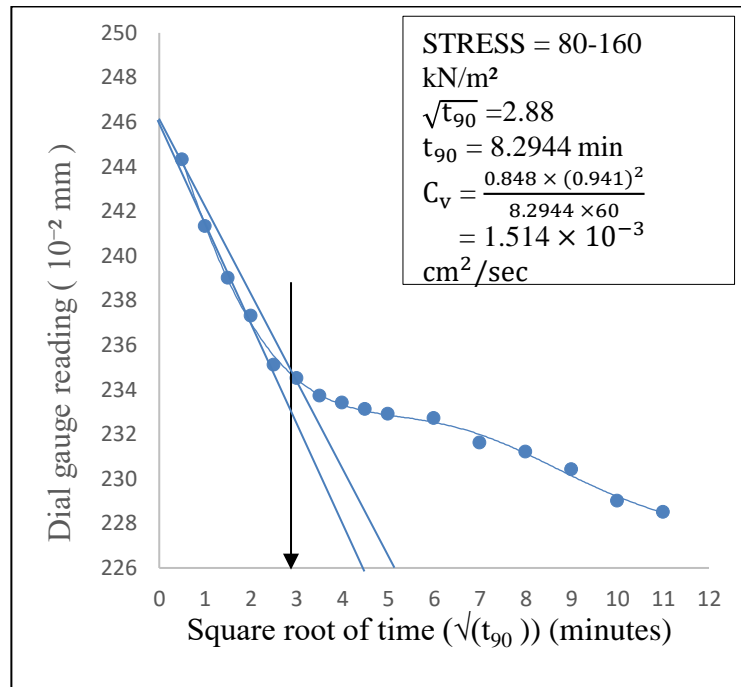


Figure 3.205: Time-consolidation curve of sample 5(dynamic at dry of optimum) at 80-160kPa

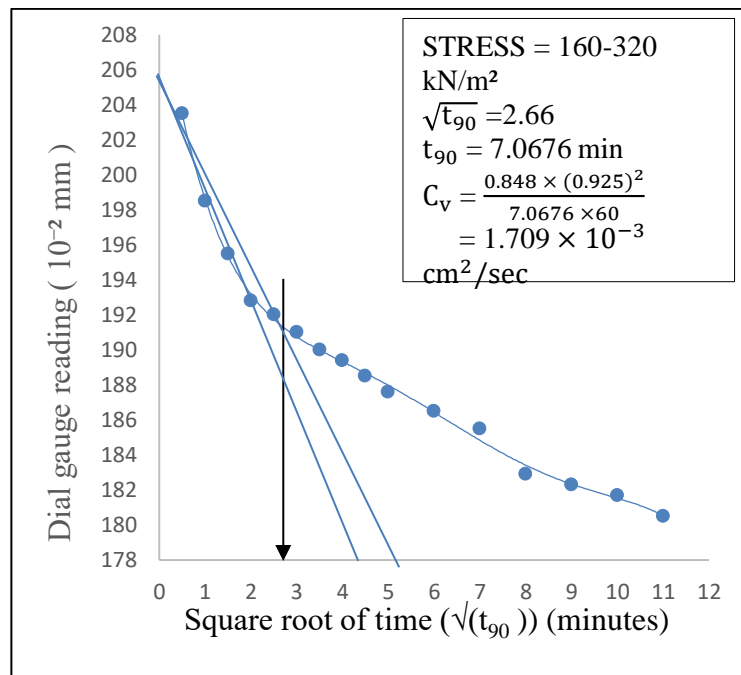


Figure 3.206: Time-consolidation curve of sample 5(dynamic at dry of optimum) at 160-320kPa

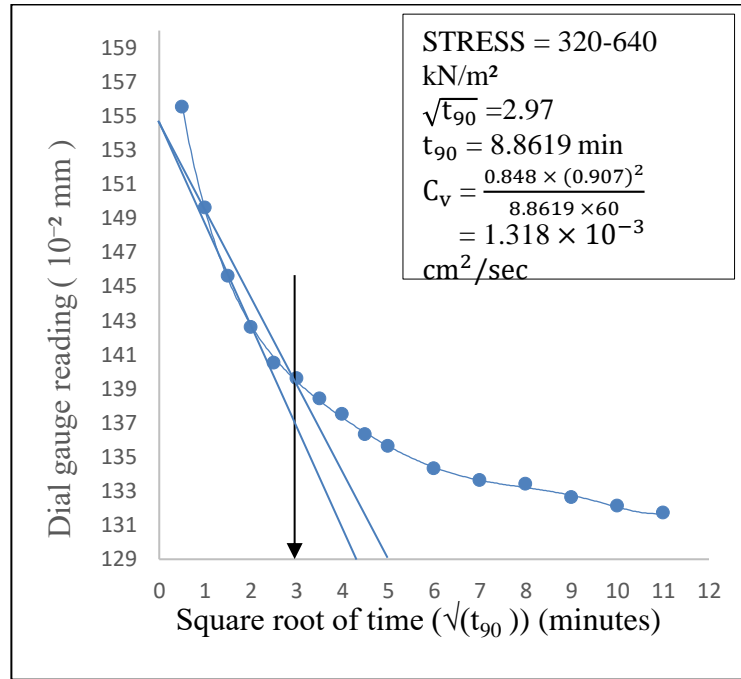


Figure 3.207: Time-consolidation curve of sample 5(dynamic at dry of optimum) at 320-640kPa

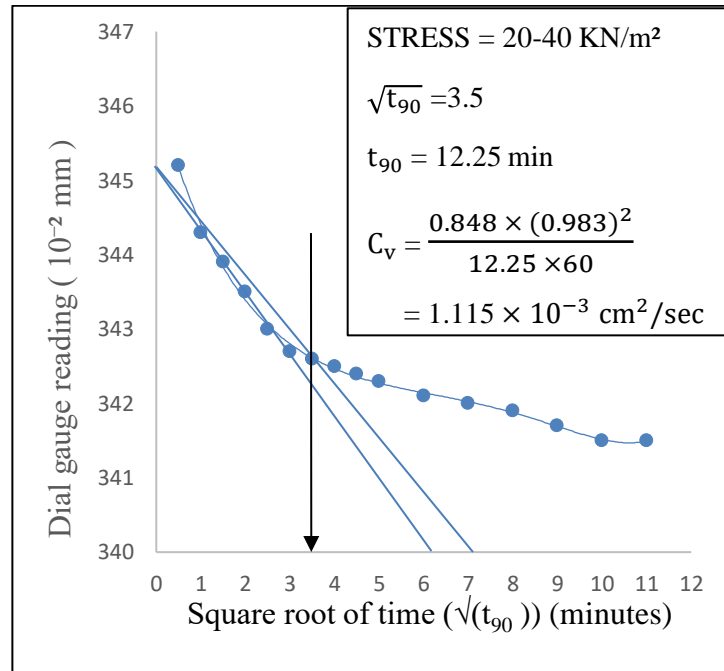


Figure 3.208: Time-consolidation curve of sample 5(dynamic at optimum moisture content) at 20-40kPa

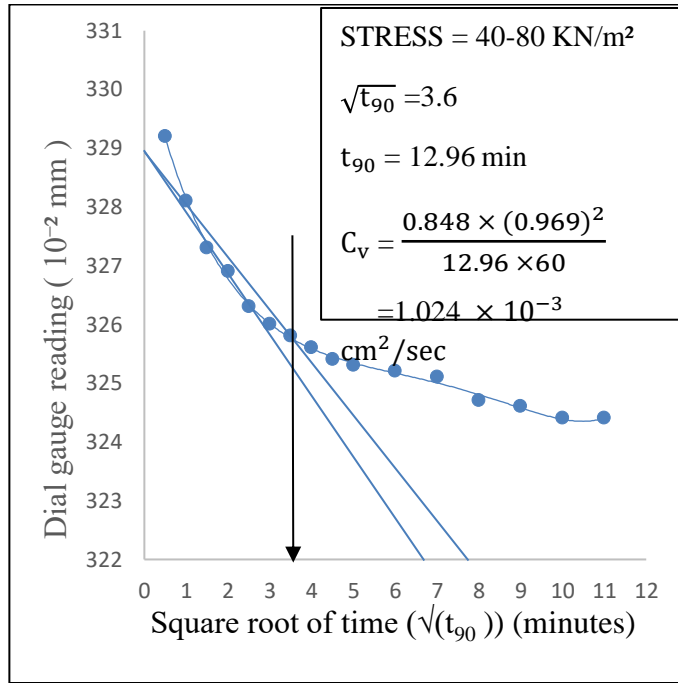


Figure 3.209: Time-consolidation curve of sample 5(dynamic at optimum moisture content) at 40-80kPa

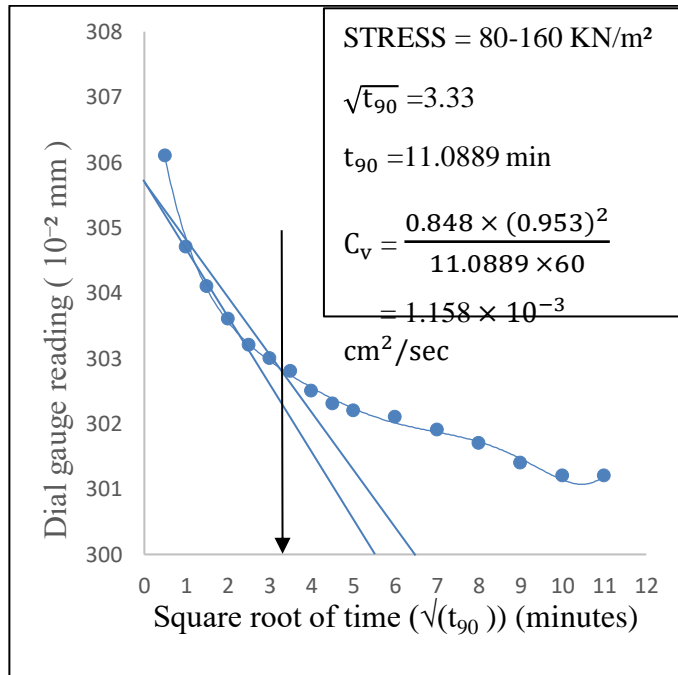


Figure 3.210: Time-consolidation curve of sample 5(dynamic at optimum moisture content) at 80-160kPa

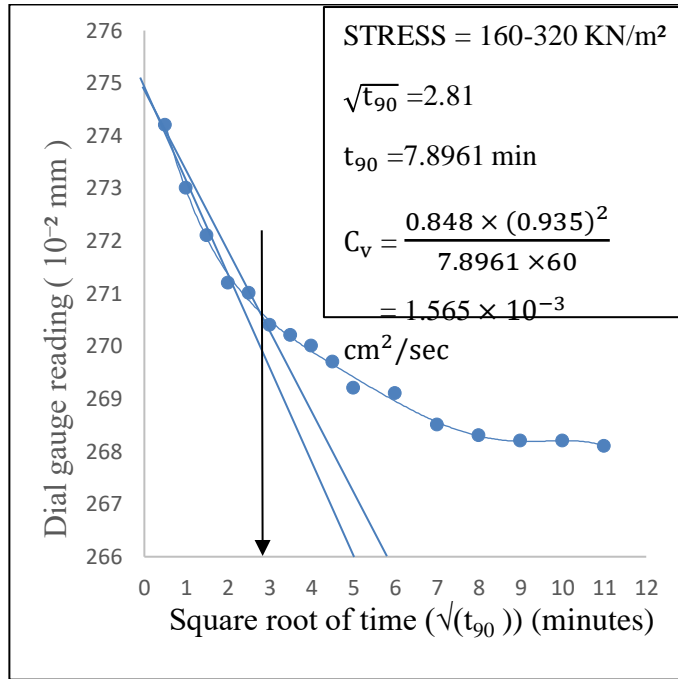


Figure 3.211: Time-consolidation curve of sample 5(dynamic at optimum moisture content) at 160-320kPa

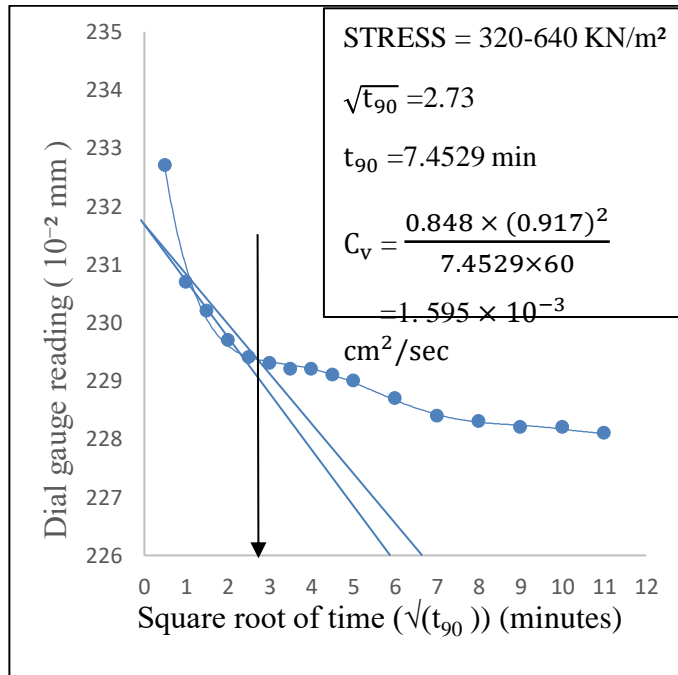


Figure 3.212: Time-consolidation curve of sample 5(dynamic at optimum moisture content) at 320-640kPa

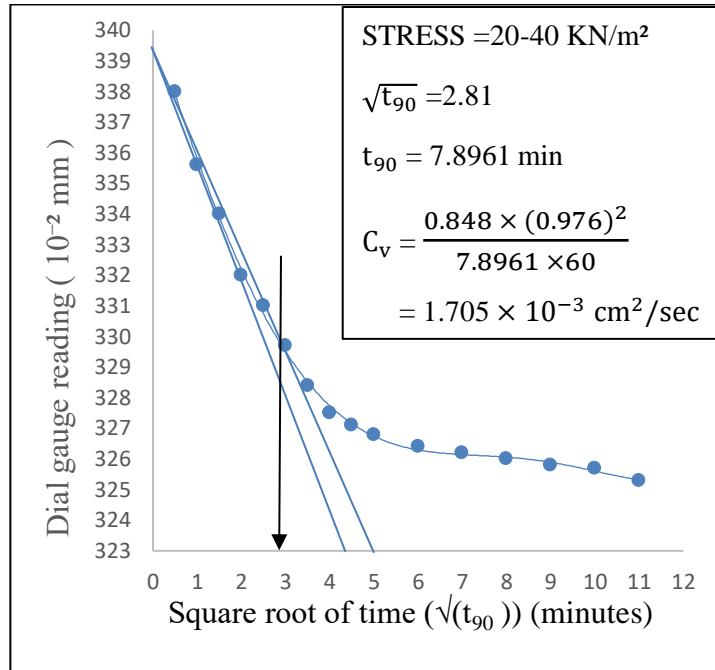


Figure 3.213: Time-consolidation curve of sample 5(dynamic at wet of optimum) at 20-40kPa

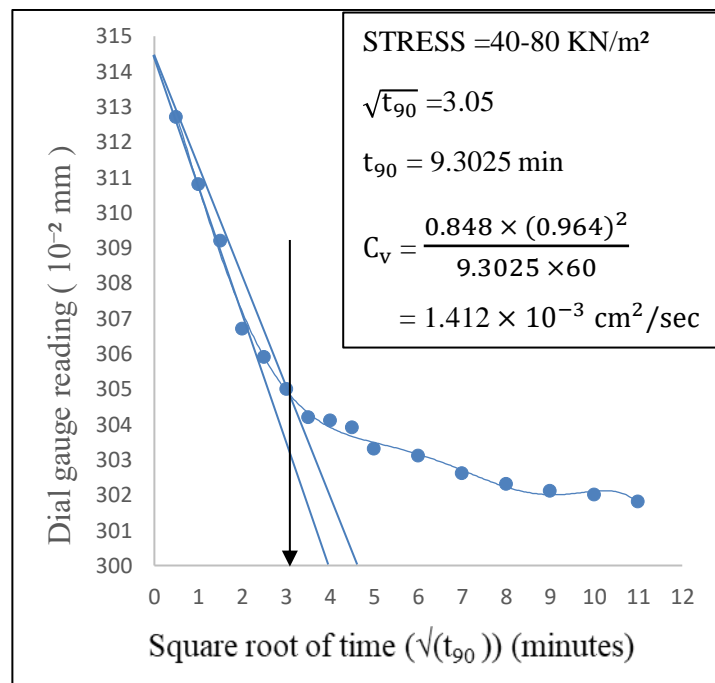


Figure 3.214: Time-consolidation curve of sample 5(dynamic at wet of optimum) at 40-80kPa

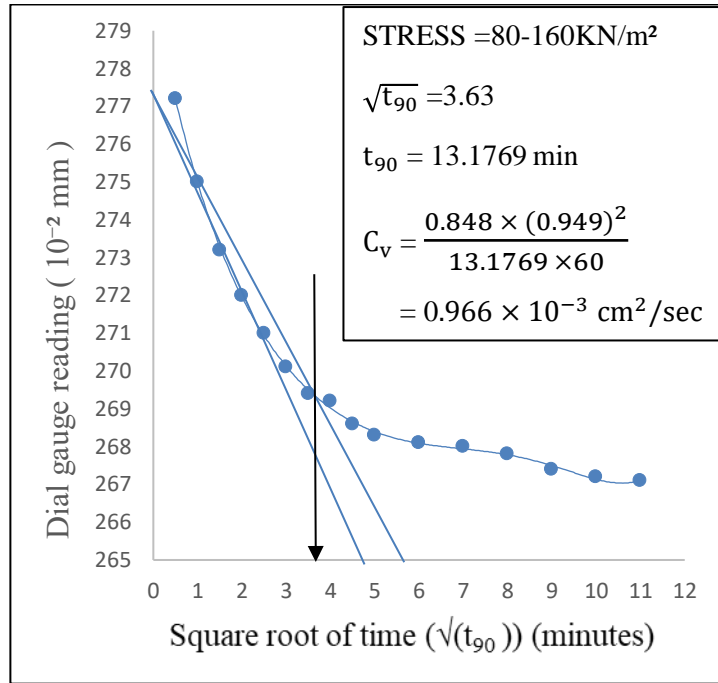


Figure 3.215: Time-consolidation curve of sample 5(dynamic at wet of optimum) at 80-160kPa

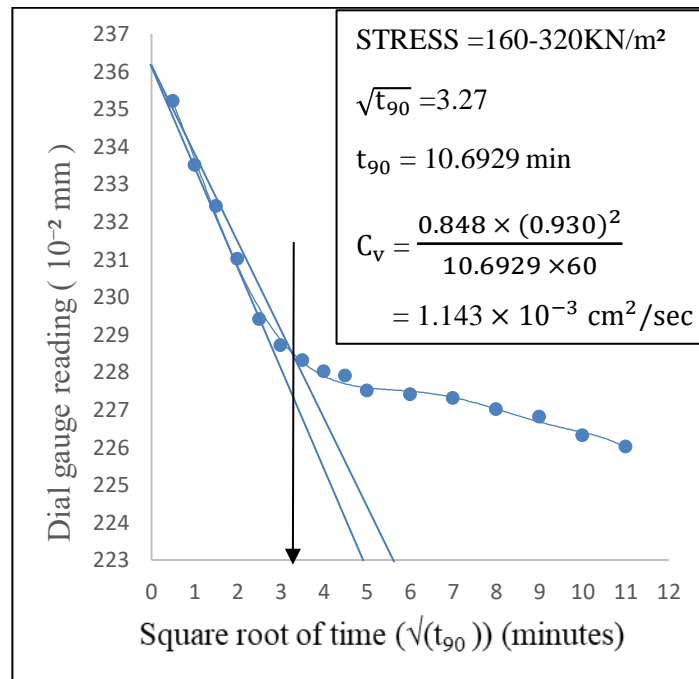


Figure 3.216: Time-consolidation curve of sample 5(dynamic at wet of optimum) at 160-320kPa

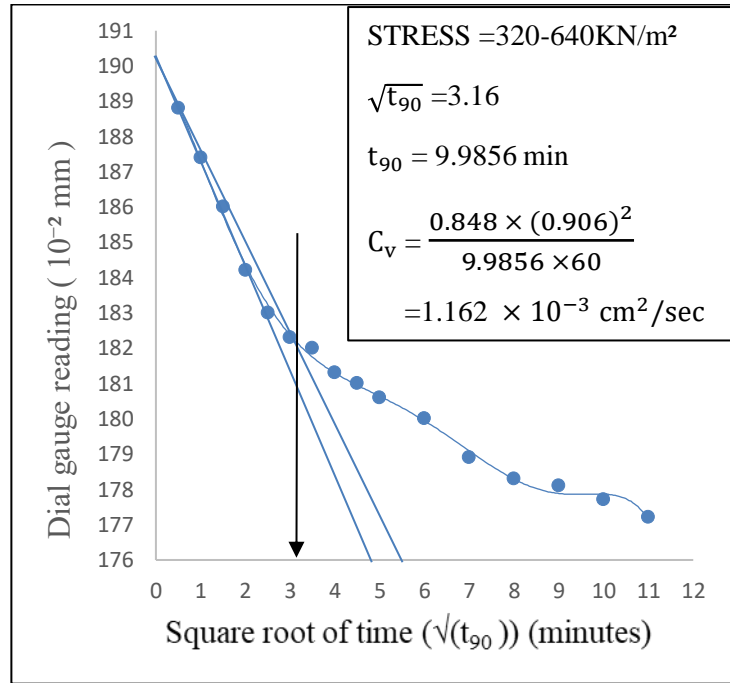


Figure 3.217: Time-consolidation curve of sample 5(dynamic at wet of optimum) at 320-640kPa

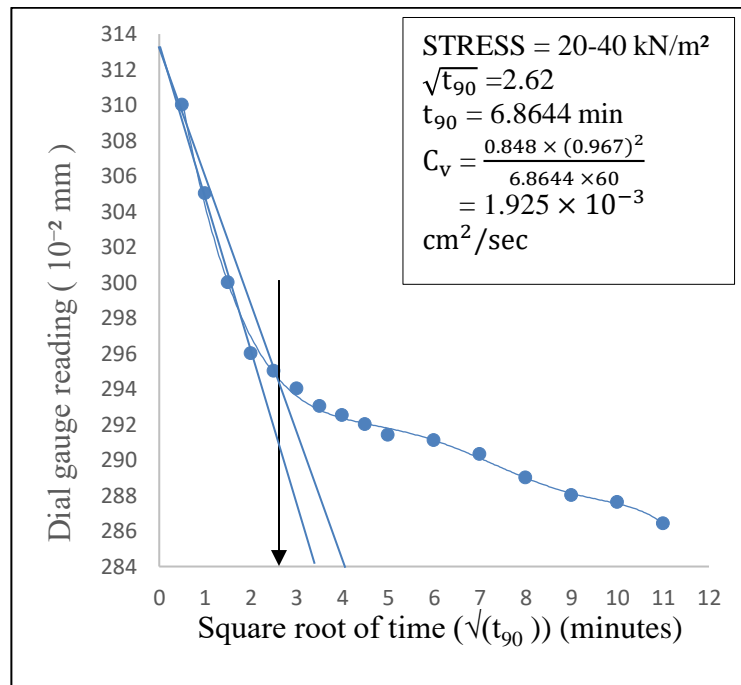


Figure 3.218: Time-consolidation curve of sample 5(static at dry of optimum) at 20-40kPa

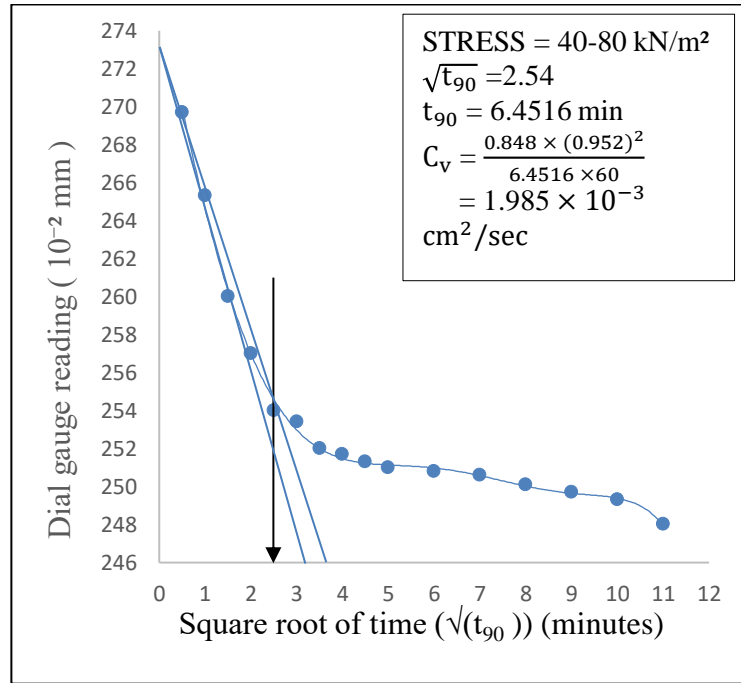


Figure 3.219: Time-consolidation curve of sample 5(static at dry of optimum) at 40-80kPa

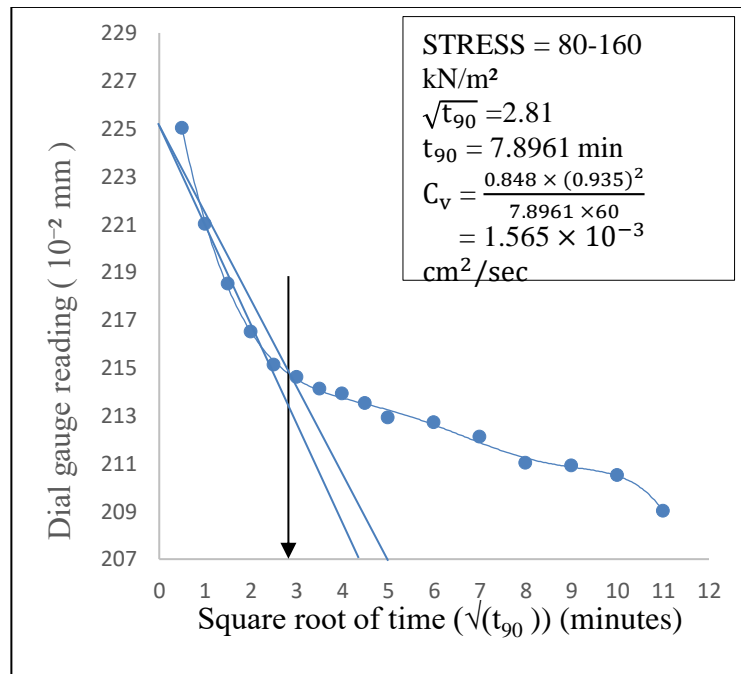


Figure 3.220: Time-consolidation curve of sample 5(static at dry of optimum) at 80-160kPa

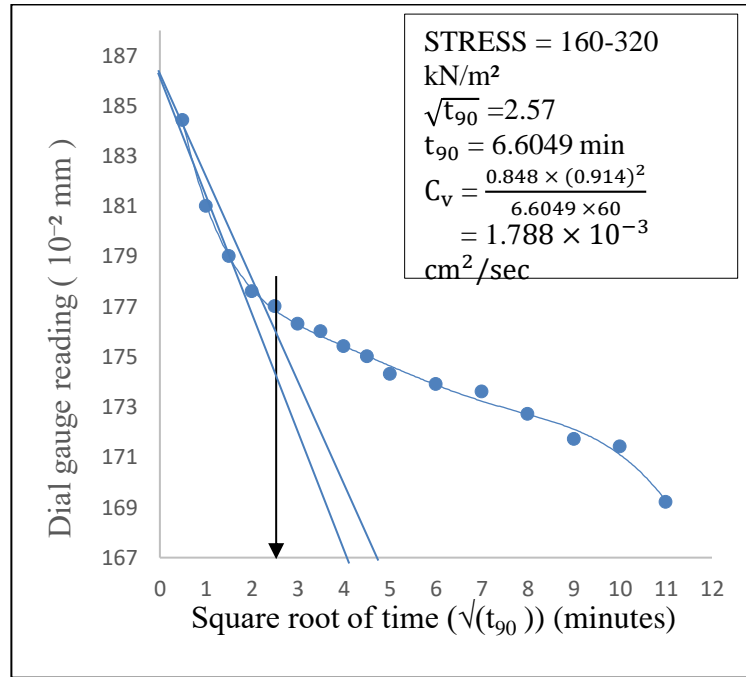


Figure 3.221: Time-consolidation curve of sample 5(static at dry of optimum) at 160-320kPa

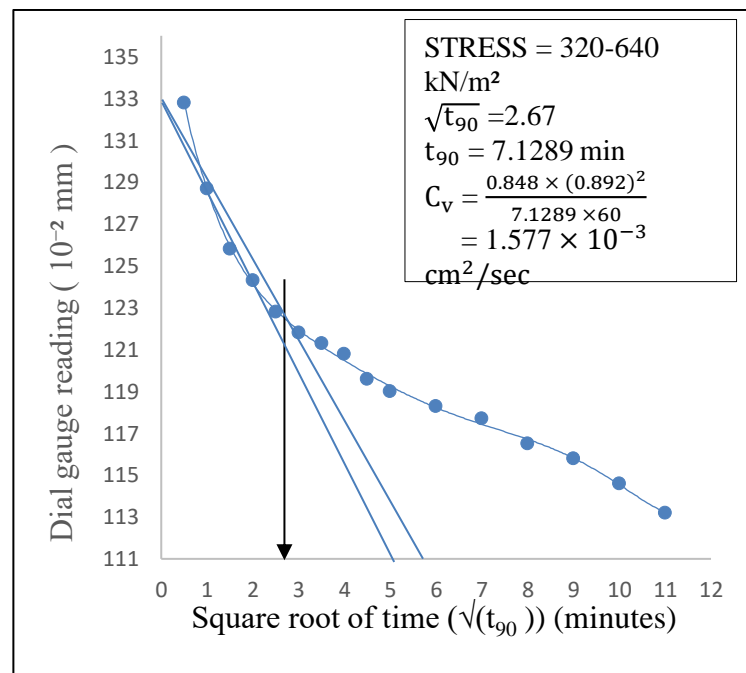


Figure 3.222: Time-consolidation curve of sample 5(static at dry of optimum) at 320-640kPa

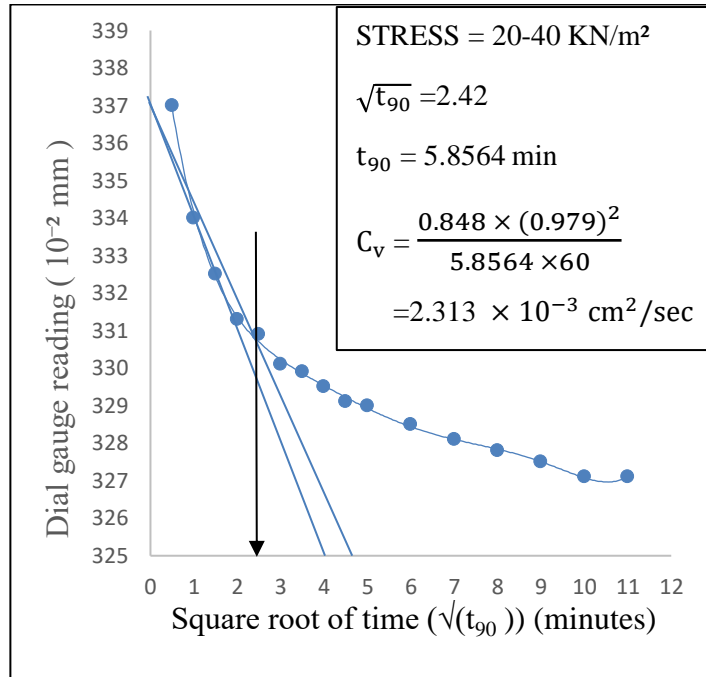


Figure 3.223: Time-consolidation curve of sample 5(static at optimum moisture content) at 20-40kPa

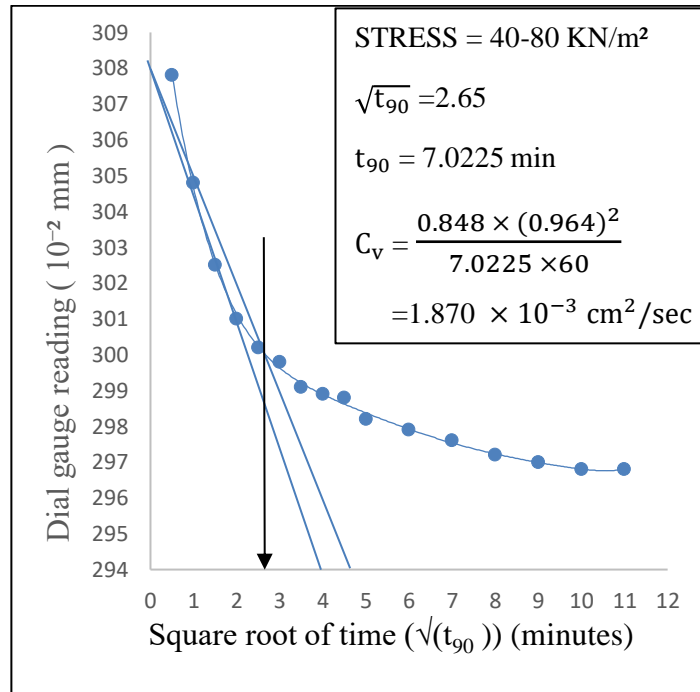


Figure 3.224: Time-consolidation curve of sample 5(static at optimum moisture content) at 40-80kPa

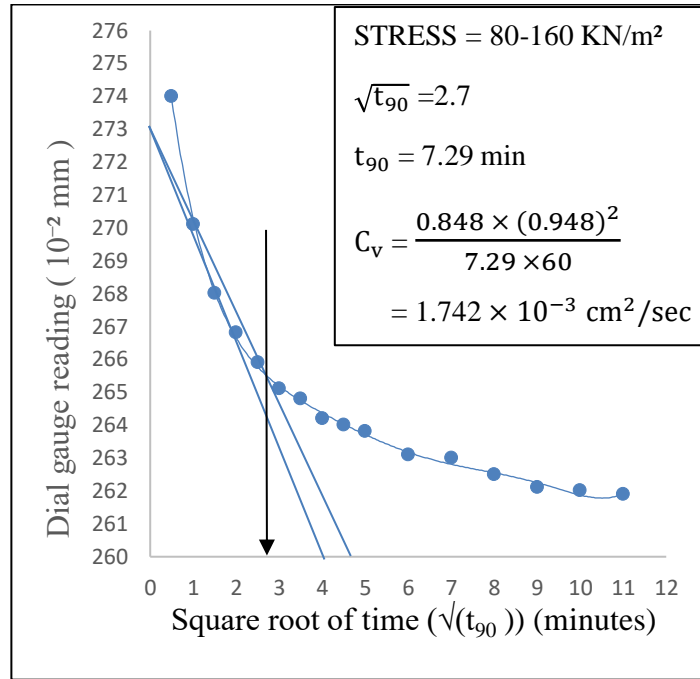


Figure 3.225: Time-consolidation curve of sample 5(static at optimum moisture content) at 80-160kPa

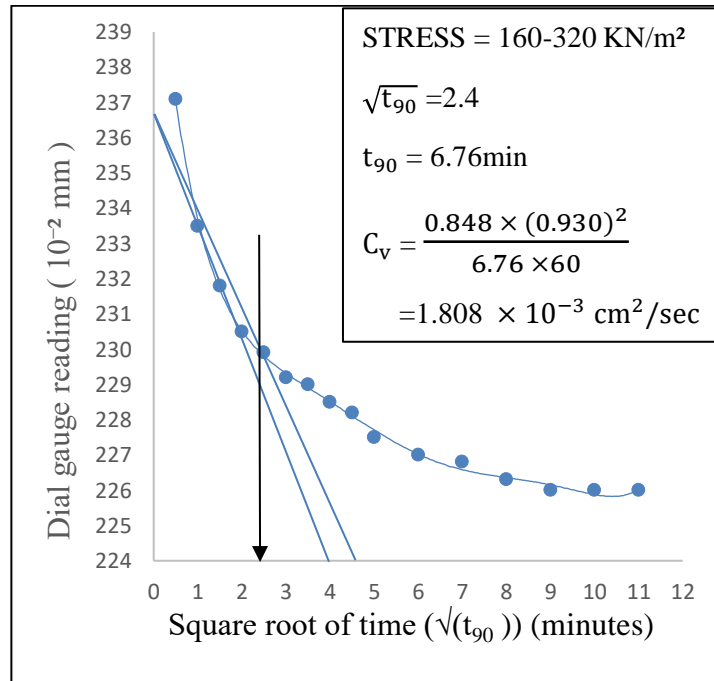


Figure 3.226: Time-consolidation curve of sample 5(static at optimum moisture content) at 160-320kPa

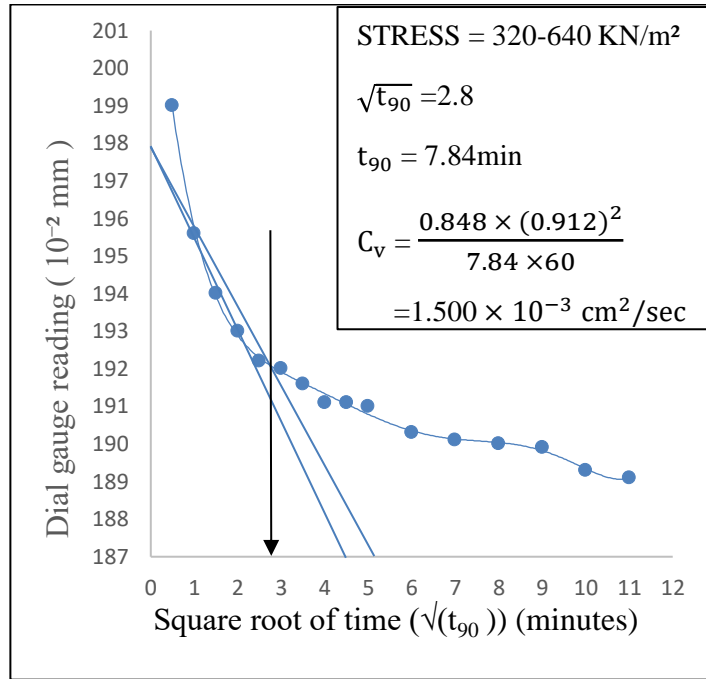


Figure 3.227: Time-consolidation curve of sample 5(static at optimum moisture content) at 320-640kPa

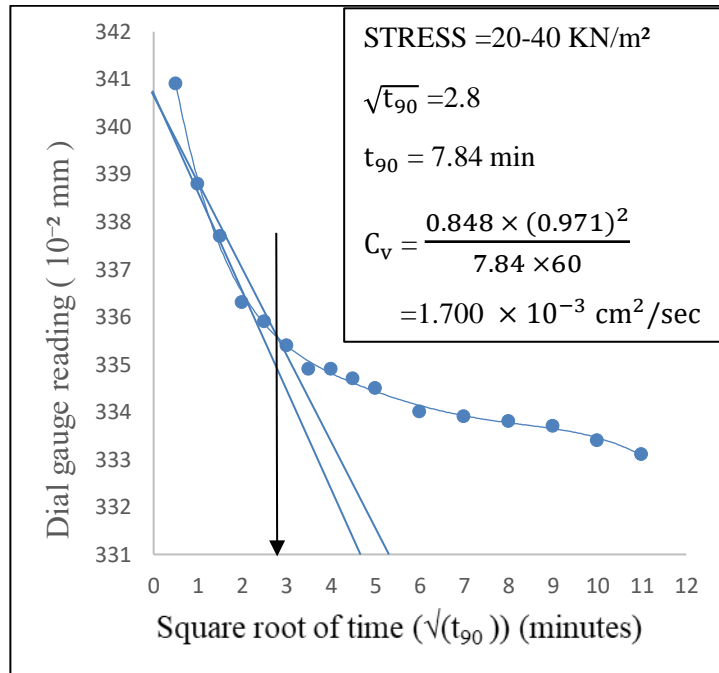


Figure 3.228: Time-consolidation curve of sample 5(static at wet of optimum) at 20-40kPa

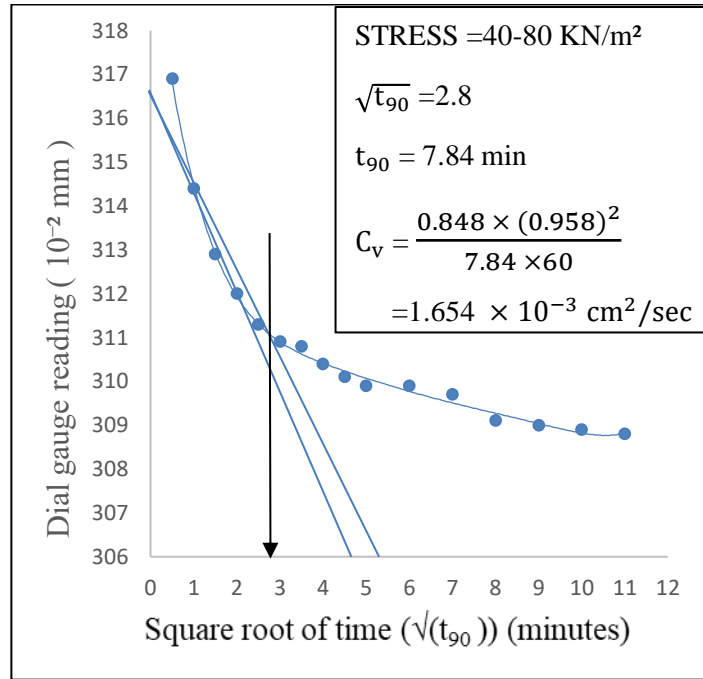


Figure 3.229: Time-consolidation curve of sample 5(static at wet of optimum) at 40-80kPa

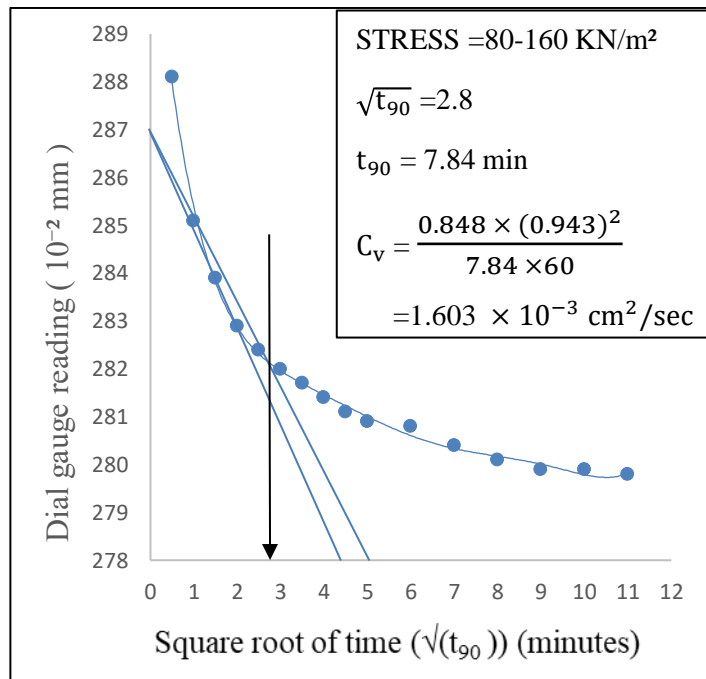


Figure 3.230: Time-consolidation curve of sample 5(static at wet of optimum) at 80-160kPa

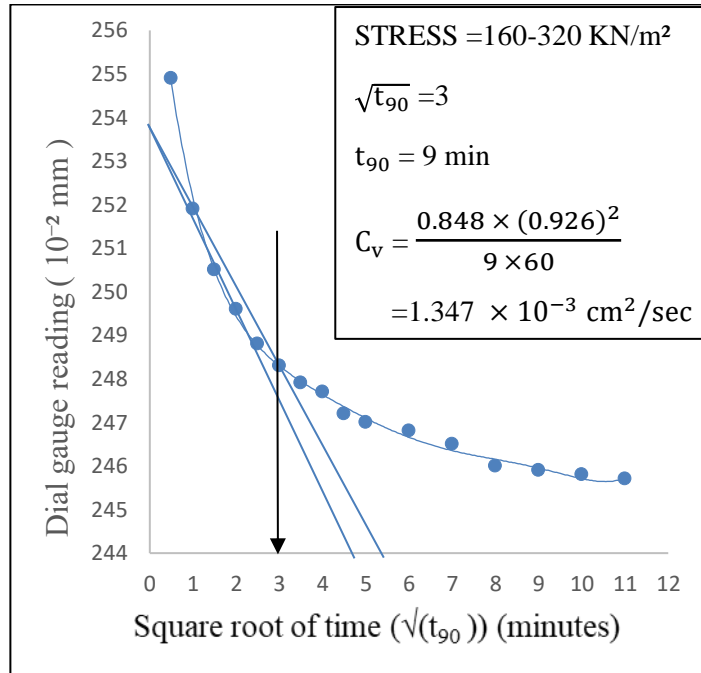


Figure 3.231: Time-consolidation curve of sample 5 (static at wet of optimum) at 160-320kPa

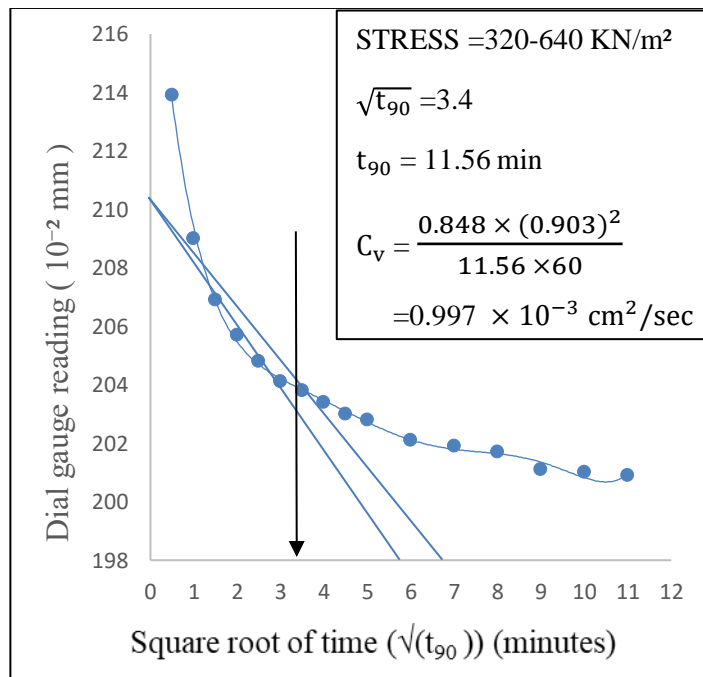


Figure 3.232: Time-consolidation curve of sample 5 (static at wet of optimum) at 320-640kPa

Appendix IV

Table 3.41. Consolidation and permeability properties of sample 2(dynamic at dry of optimum)

| Applied Pressure | Void ratio | Coefficient of compressibility, a_v (m ² /kN) | Coefficient of volume compressibility, m_v (m ² /kN) | Coefficient of consolidation, C_v (cm ² /sec) | Coefficient of permeability, k (cm/sec) |
|-------------------|------------|--|---|--|---|
| kN/m ² | e | | | | |
| 5 | 0.830 | | | | |
| 10 | 0.818 | 2.379×10^{-3} | 1.300×10^{-3} | | |
| 20 | 0.807 | 1.098×10^{-3} | 0.604×10^{-3} | | |
| 40 | 0.791 | 0.824×10^{-3} | 0.456×10^{-3} | 1.974×10^{-3} | 8.825×10^{-8} |
| 80 | 0.772 | 0.458×10^{-3} | 0.255×10^{-3} | 2.821×10^{-3} | 7.071×10^{-8} |
| 160 | 0.751 | 0.263×10^{-3} | 0.148×10^{-3} | 4.329×10^{-3} | 6.103×10^{-8} |
| 320 | 0.725 | 0.166×10^{-3} | 0.095×10^{-3} | 3.798×10^{-3} | 3.528×10^{-8} |
| 640 | 0.697 | 0.086×10^{-3} | 0.050×10^{-3} | 1.576×10^{-3} | 0.989×10^{-8} |

Table 3.42. Consolidation and permeability properties of sample 2(dynamic at optimum moisture content)

| Applied Pressure | Void ratio | Coefficient of compressibility, a_v (m ² /kN) | Coefficient of volume compressibility, m_v (m ² /kN) | Coefficient of consolidation, C_v (cm ² /sec) | Coefficient of permeability, k (cm/sec) |
|-------------------|------------|--|---|--|---|
| kN/m ² | e | | | | |
| 5 | 0.787 | | | | |
| 10 | 0.779 | 1.590×10^{-3} | 0.890×10^{-3} | | |
| 20 | 0.773 | 0.652×10^{-3} | 0.367×10^{-3} | | |
| 40 | 0.756 | 0.844×10^{-3} | 0.476×10^{-3} | 1.754×10^{-3} | 8.197×10^{-8} |
| 80 | 0.727 | 0.708×10^{-3} | 0.403×10^{-3} | 1.575×10^{-3} | 6.232×10^{-8} |
| 160 | 0.684 | 0.544×10^{-3} | 0.315×10^{-3} | 1.500×10^{-3} | 4.634×10^{-8} |
| 320 | 0.622 | 0.388×10^{-3} | 0.230×10^{-3} | 1.137×10^{-3} | 2.571×10^{-8} |
| 640 | 0.546 | 0.235×10^{-3} | 0.145×10^{-3} | 0.620×10^{-3} | 0.883×10^{-8} |

Table 3.43. Consolidation and permeability properties of sample 2(dynamic at wet of optimum)

| Applied Pressure | Void ratio | Coefficient of compressibility, a_v (m ² /kN) | Coefficient of volume compressibility, m_v (m ² /kN) | Coefficient of consolidation, C_v (cm ² /sec) | Coefficient of permeability, k (cm/sec) |
|-------------------|------------|--|---|--|---|
| kN/m ² | e | | | | |
| 5 | 0.815 | | | | |
| 10 | 0.806 | 1.779×10^{-3} | 0.980×10^{-3} | | |
| 20 | 0.789 | 1.688×10^{-3} | 0.935×10^{-3} | | |
| 40 | 0.765 | 1.221×10^{-3} | 0.682×10^{-3} | 1.193×10^{-3} | 7.984×10^{-8} |
| 80 | 0.736 | 0.733×10^{-3} | 0.415×10^{-3} | 1.412×10^{-3} | 5.752×10^{-8} |
| 160 | 0.705 | 0.388×10^{-3} | 0.224×10^{-3} | 1.680×10^{-3} | 3.684×10^{-8} |
| 320 | 0.662 | 0.265×10^{-3} | 0.155×10^{-3} | 1.454×10^{-3} | 2.217×10^{-8} |
| 640 | 0.610 | 0.163×10^{-3} | 0.098×10^{-3} | 1.016×10^{-3} | 0.974×10^{-8} |

Table 3.44. Consolidation and permeability properties of sample 2(static at dry of optimum)

| Applied Pressure | Void ratio | Coefficient of compressibility, a_v (m ² /kN) | Coefficient of volume compressibility, m_v (m ² /kN) | Coefficient of consolidation, C_v (cm ² /sec) | Coefficient of permeability, k (cm/sec) |
|-------------------|------------|--|---|--|---|
| kN/m ² | e | | | | |
| 5 | 0.830 | | | | |
| 10 | 0.814 | 3.111×10^{-3} | 1.700×10^{-3} | | |
| 20 | 0.796 | 1.830×10^{-3} | 1.009×10^{-3} | | |
| 40 | 0.778 | 0.915×10^{-3} | 0.509×10^{-3} | 2.323×10^{-3} | 11.609×10^{-8} |
| 80 | 0.755 | 0.572×10^{-3} | 0.322×10^{-3} | 3.072×10^{-3} | 9.694×10^{-8} |
| 160 | 0.728 | 0.332×10^{-3} | 0.189×10^{-3} | 2.112×10^{-3} | 3.916×10^{-8} |
| 320 | 0.695 | 0.206×10^{-3} | 0.119×10^{-3} | 1.297×10^{-3} | 1.516×10^{-8} |
| 640 | 0.664 | 0.099×10^{-3} | 0.058×10^{-3} | 1.055×10^{-3} | 0.602×10^{-8} |

Table 3.45. Consolidation and permeability properties of sample 2(static at optimum moisture content)

| Applied Pressure | Void ratio | Coefficient of compressibility, a_v (m ² /kN) | Coefficient of volume compressibility, m_v (m ² /kN) | Coefficient of consolidation, C_v (cm ² /sec) | Coefficient of permeability, k (cm/sec) |
|-------------------|------------|--|---|--|---|
| kN/m ² | e | | | | |
| 5 | 0.787 | | | | |
| 10 | 0.781 | 1.251×10^{-3} | 0.700×10^{-3} | | |
| 20 | 0.775 | 0.536×10^{-3} | 0.301×10^{-3} | | |
| 40 | 0.762 | 0.670×10^{-3} | 0.377×10^{-3} | 2.097×10^{-3} | 7.765×10^{-8} |
| 80 | 0.744 | 0.447×10^{-3} | 0.254×10^{-3} | 1.617×10^{-3} | 4.022×10^{-8} |
| 160 | 0.708 | 0.450×10^{-3} | 0.258×10^{-3} | 0.974×10^{-3} | 2.466×10^{-8} |
| 320 | 0.670 | 0.241×10^{-3} | 0.141×10^{-3} | 0.714×10^{-3} | 0.987×10^{-8} |
| 640 | 0.630 | 0.123×10^{-3} | 0.074×10^{-3} | 0.686×10^{-3} | 0.495×10^{-8} |

Table 3.46. Consolidation and permeability properties of sample 2(static at wet of optimum)

| Applied Pressure | Void ratio | Coefficient of compressibility, a_v (m ² /kN) | Coefficient of volume compressibility, m_v (m ² /kN) | Coefficient of consolidation, C_v (cm ² /sec) | Coefficient of permeability, k (cm/sec) |
|-------------------|------------|--|---|--|---|
| kN/m ² | e | | | | |
| 5 | 0.815 | | | | |
| 10 | 0.807 | 1.634×10^{-3} | 0.900×10^{-3} | | |
| 20 | 0.794 | 1.280×10^{-3} | 0.708×10^{-3} | | |
| 40 | 0.775 | 0.948×10^{-3} | 0.529×10^{-3} | 1.078×10^{-3} | 5.590×10^{-8} |
| 80 | 0.749 | 0.656×10^{-3} | 0.369×10^{-3} | 0.958×10^{-3} | 3.471×10^{-8} |
| 160 | 0.720 | 0.363×10^{-3} | 0.208×10^{-3} | 1.238×10^{-3} | 2.521×10^{-8} |
| 320 | 0.690 | 0.184×10^{-3} | 0.107×10^{-3} | 1.331×10^{-3} | 1.400×10^{-8} |
| 640 | 0.647 | 0.137×10^{-3} | 0.081×10^{-3} | 0.901×10^{-3} | 0.715×10^{-8} |

Table 3.47. Consolidation and permeability properties of sample 3(dynamic at dry of optimum)

| Applied Pressure | Void ratio | Coefficient of compressibility, a_v (m ² /kN) | Coefficient of volume compressibility, m_v (m ² /kN) | Coefficient of consolidation, C_v (cm ² /sec) | Coefficient of permeability, k (cm/sec) |
|-------------------|------------|--|---|--|---|
| kN/m ² | e | | | | |
| 5 | 0.967 | | | | |
| 10 | 0.951 | 3.147×10^{-3} | 1.600×10^{-3} | | |
| 20 | 0.930 | 2.164×10^{-3} | 1.109×10^{-3} | | |
| 40 | 0.901 | 1.451×10^{-3} | 0.752×10^{-3} | 2.095×10^{-3} | 15.451×10^{-8} |
| 80 | 0.867 | 0.848×10^{-3} | 0.446×10^{-3} | 2.369×10^{-3} | 10.372×10^{-8} |
| 160 | 0.833 | 0.424×10^{-3} | 0.227×10^{-3} | 2.098×10^{-3} | 4.676×10^{-8} |
| 320 | 0.793 | 0.249×10^{-3} | 0.136×10^{-3} | 1.612×10^{-3} | 2.148×10^{-8} |
| 640 | 0.756 | 0.117×10^{-3} | 0.065×10^{-3} | 2.174×10^{-3} | 1.389×10^{-8} |

Table 3.48. Consolidation and permeability properties of sample 3(dynamic at optimum moisture content)

| Applied Pressure | Void ratio | Coefficient of compressibility, a_v (m ² /kN) | Coefficient of volume compressibility, m_v (m ² /kN) | Coefficient of consolidation, C_v (cm ² /sec) | Coefficient of permeability, k (cm/sec) |
|-------------------|------------|--|---|--|---|
| kN/m ² | e | | | | |
| 5 | 0.835 | | | | |
| 10 | 0.823 | 2.404×10^{-3} | 1.310×10^{-3} | | |
| 20 | 0.814 | 0.862×10^{-3} | 0.473×10^{-3} | | |
| 40 | 0.784 | 1.495×10^{-3} | 0.824×10^{-3} | 2.276×10^{-3} | 1.440×10^{-7} |
| 80 | 0.722 | 1.567×10^{-3} | 0.878×10^{-3} | 1.776×10^{-3} | 9.573×10^{-8} |
| 160 | 0.638 | 1.048×10^{-3} | 0.608×10^{-3} | 1.279×10^{-3} | 3.634×10^{-8} |
| 320 | 0.559 | 0.493×10^{-3} | 0.301×10^{-3} | 1.197×10^{-3} | 1.537×10^{-8} |
| 640 | 0.471 | 0.275×10^{-3} | 0.176×10^{-3} | 0.799×10^{-3} | 1.112×10^{-8} |

Table 3.49. Consolidation and permeability properties of sample 3(dynamic at wet of optimum)

| Applied Pressure | Void ratio | Coefficient of compressibility, a_v (m ² /kN) | Coefficient of volume compressibility, m_v (m ² /kN) | Coefficient of consolidation, C_v (cm ² /sec) | Coefficient of permeability, k (cm/sec) |
|-------------------|------------|--|---|--|---|
| kN/m ² | e | | | | |
| 5 | 0.876 | | | | |
| 10 | 0.862 | 2.795×10^{-3} | 1.490×10^{-3} | | |
| 20 | 0.848 | 1.407×10^{-3} | 0.756×10^{-3} | | |
| 40 | 0.819 | 1.459×10^{-3} | 0.789×10^{-3} | 2.443×10^{-3} | 13.916×10^{-8} |
| 80 | 0.759 | 1.498×10^{-3} | 0.824×10^{-3} | 1.832×10^{-3} | 9.481×10^{-8} |
| 160 | 0.662 | 1.209×10^{-3} | 0.687×10^{-3} | 1.170×10^{-3} | 2.889×10^{-8} |
| 320 | 0.577 | 0.533×10^{-3} | 0.321×10^{-3} | 1.199×10^{-3} | 1.771×10^{-8} |
| 640 | 0.499 | 0.244×10^{-3} | 0.154×10^{-3} | 1.384×10^{-3} | 0.947×10^{-8} |

Table 3.50. Consolidation and permeability properties of sample 3(static at dry of optimum)

| Applied Pressure | Void ratio | Coefficient of compressibility, a_v (m^2/kN) | Coefficient of volume compressibility, m_v (m^2/kN) | Coefficient of consolidation, C_v (cm^2/sec) | Coefficient of permeability, k (cm/sec) |
|------------------|------------|---|---|--|---|
| kN/m^2 | e | | | | |
| 5 | 0.967 | | | | |
| 10 | 0.941 | 5.114×10^{-3} | 2.600×10^{-3} | | |
| 20 | 0.912 | 2.901×10^{-3} | 1.494×10^{-3} | | |
| 40 | 0.874 | 1.942×10^{-3} | 1.016×10^{-3} | 2.071×10^{-3} | 20.635×10^{-8} |
| 80 | 0.832 | 1.033×10^{-3} | 0.551×10^{-3} | 1.759×10^{-3} | 9.511×10^{-8} |
| 160 | 0.792 | 0.498×10^{-3} | 0.272×10^{-3} | 1.694×10^{-3} | 4.516×10^{-8} |
| 320 | 0.749 | 0.274×10^{-3} | 0.153×10^{-3} | 1.324×10^{-3} | 1.982×10^{-8} |
| 640 | 0.708 | 0.128×10^{-3} | 0.073×10^{-3} | 1.64×10^{-3} | 1.176×10^{-8} |

Table 3.51. Consolidation and permeability properties of sample 3(static at optimum moisture content)

| Applied Pressure | Void ratio | Coefficient of compressibility, a_v (m^2/kN) | Coefficient of volume compressibility, m_v (m^2/kN) | Coefficient of consolidation, C_v (cm^2/sec) | Coefficient of permeability, k (cm/sec) |
|------------------|------------|---|---|--|---|
| kN/m^2 | e | | | | |
| 5 | 0.835 | | | | |
| 10 | 0.831 | 0.734×10^{-3} | 0.400×10^{-3} | | |
| 20 | 0.824 | 0.688×10^{-3} | 0.376×10^{-3} | | |
| 40 | 0.807 | 0.849×10^{-3} | 0.465×10^{-3} | 1.646×10^{-3} | 7.511×10^{-8} |
| 80 | 0.772 | 0.887×10^{-3} | 0.491×10^{-3} | 1.304×10^{-3} | 6.277×10^{-8} |
| 160 | 0.731 | 0.513×10^{-3} | 0.289×10^{-3} | 0.937×10^{-3} | 2.659×10^{-8} |
| 320 | 0.693 | 0.238×10^{-3} | 0.137×10^{-3} | 1.090×10^{-3} | 1.467×10^{-8} |
| 640 | 0.650 | 0.134×10^{-3} | 0.079×10^{-3} | 1.137×10^{-3} | 0.885×10^{-8} |

Table 3.52. Consolidation and permeability properties of sample 3(static at wet of optimum)

| Applied Pressure | Void ratio | Coefficient of compressibility, a_v (m^2/kN) | Coefficient of volume compressibility, m_v (m^2/kN) | Coefficient of consolidation, C_v (cm^2/sec) | Coefficient of permeability, k (cm/sec) |
|------------------|------------|---|---|--|---|
| kN/m^2 | e | | | | |
| 5 | 0.876 | | | | |
| 10 | 0.871 | 0.919×10^{-3} | 0.490×10^{-3} | | |
| 20 | 0.862 | 0.957×10^{-3} | 0.511×10^{-3} | | |
| 40 | 0.838 | 1.173×10^{-3} | 0.630×10^{-3} | 0.988×10^{-3} | 6.104×10^{-8} |
| 80 | 0.801 | 0.933×10^{-3} | 0.508×10^{-3} | 0.982×10^{-3} | 4.891×10^{-8} |
| 160 | 0.768 | 0.409×10^{-3} | 0.227×10^{-3} | 1.146×10^{-3} | 2.554×10^{-8} |
| 320 | 0.726 | 0.263×10^{-3} | 0.149×10^{-3} | 1.092×10^{-3} | 1.595×10^{-8} |
| 640 | 0.679 | 0.147×10^{-3} | 0.085×10^{-3} | 1.152×10^{-3} | 0.961×10^{-8} |

Table 3.53. Consolidation and permeability properties of sample 4(dynamic at dry of optimum)

| Applied Pressure | Void ratio | Coefficient of compressibility, a_v (m ² /kN) | Coefficient of volume compressibility, m_v (m ² /kN) | Coefficient of consolidation, C_v (cm ² /sec) | Coefficient of permeability, k (cm/sec) |
|-------------------|------------|--|---|--|---|
| kN/m ² | e | | | | |
| 5 | 0.605 | | | | |
| 10 | 0.600 | 0.963×10^{-3} | 0.600×10^{-3} | | |
| 20 | 0.595 | 0.522×10^{-3} | 0.326×10^{-3} | | |
| 40 | 0.585 | 0.502×10^{-3} | 0.314×10^{-3} | 2.135×10^{-3} | 6.586×10^{-8} |
| 80 | 0.569 | 0.401×10^{-3} | 0.253×10^{-3} | 1.990×10^{-3} | 4.942×10^{-8} |
| 160 | 0.542 | 0.336×10^{-3} | 0.214×10^{-3} | 1.504×10^{-3} | 3.160×10^{-8} |
| 320 | 0.510 | 0.198×10^{-3} | 0.128×10^{-3} | 1.630×10^{-3} | 2.054×10^{-8} |
| 640 | 0.475 | 0.109×10^{-3} | 0.072×10^{-3} | 2.213×10^{-3} | 1.568×10^{-8} |

Table 3.54. Consolidation and permeability properties of sample 4(dynamic at optimum moisture content)

| Applied Pressure | Void ratio | Coefficient of compressibility, a_v (m ² /kN) | Coefficient of volume compressibility, m_v (m ² /kN) | Coefficient of consolidation, C_v (cm ² /sec) | Coefficient of permeability, k (cm/sec) |
|-------------------|------------|--|---|--|---|
| kN/m ² | e | | | | |
| 5 | 0.551 | | | | |
| 10 | 0.546 | 1.086×10^{-3} | 0.700×10^{-3} | | |
| 20 | 0.541 | 0.504×10^{-3} | 0.326×10^{-3} | | |
| 40 | 0.530 | 0.516×10^{-3} | 0.335×10^{-3} | 1.470×10^{-3} | 4.327×10^{-8} |
| 80 | 0.510 | 0.505×10^{-3} | 0.330×10^{-3} | 3.720×10^{-3} | 3.205×10^{-8} |
| 160 | 0.480 | 0.375×10^{-3} | 0.248×10^{-3} | 1.305×10^{-3} | 2.104×10^{-8} |
| 320 | 0.441 | 0.244×10^{-3} | 0.165×10^{-3} | 1.204×10^{-3} | 1.145×10^{-8} |
| 640 | 0.399 | 0.131×10^{-3} | 0.091×10^{-3} | 0.667×10^{-3} | 0.596×10^{-8} |

Table 3.55. Consolidation and permeability properties of sample 4(dynamic at wet of optimum)

| Applied Pressure | Void ratio | Coefficient of compressibility, a_v (m ² /kN) | Coefficient of volume compressibility, m_v (m ² /kN) | Coefficient of consolidation, C_v (cm ² /sec) | Coefficient of permeability, k (cm/sec) |
|-------------------|------------|--|---|--|---|
| kN/m ² | e | | | | |
| 5 | 0.588 | | | | |
| 10 | 0.565 | 4.605×10^{-3} | 2.900×10^{-3} | | |
| 20 | 0.553 | 1.231×10^{-3} | 0.786×10^{-3} | | |
| 40 | 0.535 | 0.905×10^{-3} | 0.583×10^{-3} | 0.346×10^{-3} | 2.879×10^{-8} |
| 80 | 0.513 | 0.546×10^{-3} | 0.356×10^{-3} | 0.347×10^{-3} | 1.911×10^{-8} |
| 160 | 0.485 | 0.344×10^{-3} | 0.228×10^{-3} | 0.418×10^{-3} | 0.934×10^{-8} |
| 320 | 0.452 | 0.209×10^{-3} | 0.141×10^{-3} | 0.426×10^{-3} | 0.589×10^{-8} |
| 640 | 0.408 | 0.138×10^{-3} | 0.095×10^{-3} | 0.338×10^{-3} | 0.315×10^{-8} |

Table 3.56. Consolidation and permeability properties of sample 4(static at dry of optimum)

| Applied Pressure | Void ratio | Coefficient of compressibility, a_v (m^2/kN) | Coefficient of volume compressibility, m_v (m^2/kN) | Coefficient of consolidation, C_v (cm^2/sec) | Coefficient of permeability, k (cm/sec) |
|------------------|------------|---|---|--|---|
| kN/m^2 | e | | | | |
| 5 | 0.605 | | | | |
| 10 | 0.586 | 3.852×10^{-3} | 2.400×10^{-3} | | |
| 20 | 0.573 | 1.284×10^{-3} | 0.810×10^{-3} | | |
| 40 | 0.556 | 0.863×10^{-3} | 0.548×10^{-3} | 1.505×10^{-3} | 8.098×10^{-8} |
| 80 | 0.537 | 0.471×10^{-3} | 0.303×10^{-3} | 1.731×10^{-3} | 5.146×10^{-8} |
| 160 | 0.509 | 0.351×10^{-3} | 0.228×10^{-3} | 1.513×10^{-3} | 3.391×10^{-8} |
| 320 | 0.477 | 0.196×10^{-3} | 0.130×10^{-3} | 1.222×10^{-3} | 1.554×10^{-8} |
| 640 | 0.450 | 0.085×10^{-3} | 0.058×10^{-3} | 1.124×10^{-3} | 0.636×10^{-8} |

Table 3.57. Consolidation and permeability properties of sample 4(static at optimum moisture content)

| Applied Pressure | Void ratio | Coefficient of compressibility, a_v (m^2/kN) | Coefficient of volume compressibility, m_v (m^2/kN) | Coefficient of consolidation, C_v (cm^2/sec) | Coefficient of permeability, k (cm/sec) |
|------------------|------------|---|---|--|---|
| kN/m^2 | e | | | | |
| 5 | 0.551 | | | | |
| 10 | 0.547 | 0.775×10^{-3} | 0.500×10^{-3} | | |
| 20 | 0.544 | 0.349×10^{-3} | 0.226×10^{-3} | | |
| 40 | 0.536 | 0.376×10^{-3} | 0.244×10^{-3} | 2.230×10^{-3} | 5.330×10^{-8} |
| 80 | 0.518 | 0.453×10^{-3} | 0.295×10^{-3} | 1.175×10^{-3} | 3.396×10^{-8} |
| 160 | 0.493 | 0.313×10^{-3} | 0.206×10^{-3} | 1.092×10^{-3} | 2.205×10^{-8} |
| 320 | 0.452 | 0.256×10^{-3} | 0.172×10^{-3} | 0.711×10^{-3} | 1.197×10^{-8} |
| 640 | 0.415 | 0.116×10^{-3} | 0.080×10^{-3} | 0.776×10^{-3} | 0.606×10^{-8} |

Table 3.58. Consolidation and permeability properties of sample 4(static at wet of optimum)

| Applied Pressure | Void ratio | Coefficient of compressibility, a_v (m^2/kN) | Coefficient of volume compressibility, m_v (m^2/kN) | Coefficient of consolidation, C_v (cm^2/sec) | Coefficient of permeability, k (cm/sec) |
|------------------|------------|---|---|--|---|
| kN/m^2 | e | | | | |
| 5 | 0.588 | | | | |
| 10 | 0.573 | 3.001×10^{-3} | 1.890×10^{-3} | | |
| 20 | 0.561 | 1.183×10^{-3} | 0.752×10^{-3} | | |
| 40 | 0.544 | 0.858×10^{-3} | 0.549×10^{-3} | 0.770×10^{-3} | 4.149×10^{-8} |
| 80 | 0.528 | 0.401×10^{-3} | 0.260×10^{-3} | 0.847×10^{-3} | 2.158×10^{-8} |
| 160 | 0.504 | 0.305×10^{-3} | 0.199×10^{-3} | 0.782×10^{-3} | 1.530×10^{-8} |
| 320 | 0.473 | 0.189×10^{-3} | 0.125×10^{-3} | 0.842×10^{-3} | 1.036×10^{-8} |
| 640 | 0.435 | 0.119×10^{-3} | 0.081×10^{-3} | 0.679×10^{-3} | 0.540×10^{-8} |

Table 3.59. Consolidation and permeability properties of sample 5 (dynamic at dry of optimum)

| Applied Pressure | Void ratio | Coefficient of compressibility, a_v (m ² /kN) | Coefficient of volume compressibility, m_v (m ² /kN) | Coefficient of consolidation, C_v (cm ² /sec) | Coefficient of permeability, k (cm/sec) |
|-------------------|------------|--|---|--|---|
| kN/m ² | e | | | | |
| 5 | 0.744 | | | | |
| 10 | 0.722 | 4.360×10^{-3} | 2.500×10^{-3} | | |
| 20 | 0.705 | 1.700×10^{-3} | 0.987×10^{-3} | | |
| 40 | 0.680 | 1.243×10^{-3} | 0.729×10^{-3} | 1.387×10^{-3} | 9.915×10^{-8} |
| 80 | 0.655 | 0.630×10^{-3} | 0.382×10^{-3} | 1.362×10^{-3} | 5.104×10^{-8} |
| 160 | 0.628 | 0.339×10^{-3} | 0.205×10^{-3} | 1.514×10^{-3} | 3.042×10^{-8} |
| 320 | 0.599 | 0.183×10^{-3} | 0.112×10^{-3} | 1.709×10^{-3} | 1.880×10^{-8} |
| 640 | 0.565 | 0.106×10^{-3} | 0.066×10^{-3} | 1.318×10^{-3} | 0.855×10^{-8} |

Table 3.60. Consolidation and permeability properties of sample 5 (dynamic at optimum moisture content)

| Applied Pressure | Void ratio | Coefficient of compressibility, a_v (m ² /kN) | Coefficient of volume compressibility, m_v (m ² /kN) | Coefficient of consolidation, C_v (cm ² /sec) | Coefficient of permeability, k (cm/sec) |
|-------------------|------------|--|---|--|---|
| kN/m ² | e | | | | |
| 5 | 0.582 | | | | |
| 10 | 0.575 | 1.313×10^{-3} | 0.830×10^{-3} | | |
| 20 | 0.566 | 0.941×10^{-3} | 0.597×10^{-3} | | |
| 40 | 0.546 | 1.024×10^{-3} | 0.654×10^{-3} | 1.115×10^{-3} | 7.155×10^{-8} |
| 80 | 0.521 | 0.611×10^{-3} | 0.395×10^{-3} | 1.024×10^{-3} | 3.972×10^{-8} |
| 160 | 0.493 | 0.354×10^{-3} | 0.233×10^{-3} | 1.158×10^{-3} | 2.444×10^{-8} |
| 320 | 0.466 | 0.170×10^{-3} | 0.114×10^{-3} | 1.565×10^{-3} | 1.679×10^{-8} |
| 640 | 0.436 | 0.091×10^{-3} | 0.062×10^{-3} | 1.595×10^{-3} | 0.797×10^{-8} |

Table 3.61. Consolidation and permeability properties of sample 5 (dynamic at wet of optimum)

| Applied Pressure | Void ratio | Coefficient of compressibility, a_v (m ² /kN) | Coefficient of volume compressibility, m_v (m ² /kN) | Coefficient of consolidation, C_v (cm ² /sec) | Coefficient of permeability, k (cm/sec) |
|-------------------|------------|--|---|--|---|
| kN/m ² | e | | | | |
| 5 | 0.704 | | | | |
| 10 | 0.680 | 4.771×10^{-3} | 2.800×10^{-3} | | |
| 20 | 0.660 | 2.002×10^{-3} | 1.192×10^{-3} | | |
| 40 | 0.638 | 1.082×10^{-3} | 0.652×10^{-3} | 1.705×10^{-3} | 9.042×10^{-8} |
| 80 | 0.611 | 0.692×10^{-3} | 0.422×10^{-3} | 1.459×10^{-3} | 4.847×10^{-8} |
| 160 | 0.583 | 0.346×10^{-3} | 0.215×10^{-3} | 0.988×10^{-3} | 2.083×10^{-8} |
| 320 | 0.549 | 0.214×10^{-3} | 0.135×10^{-3} | 1.143×10^{-3} | 1.516×10^{-8} |
| 640 | 0.502 | 0.145×10^{-3} | 0.094×10^{-3} | 1.162×10^{-3} | 0.811×10^{-8} |

Table 3.62. Consolidation and permeability properties of sample 5(static at dry of optimum)

| Applied Pressure | Void ratio | Coefficient of compressibility, a_v (m ² /kN) | Coefficient of volume compressibility, m_v (m ² /kN) | Coefficient of consolidation, C_v (cm ² /sec) | Coefficient of permeability, k (cm/sec) |
|-------------------|------------|--|---|--|---|
| kN/m ² | e | | | | |
| 5 | 0.744 | | | | |
| 10 | 0.720 | 4.709×10^{-3} | 2.700×10^{-3} | | |
| 20 | 0.700 | 2.006×10^{-3} | 1.166×10^{-3} | | |
| 40 | 0.673 | 1.395×10^{-3} | 0.821×10^{-3} | 1.925×10^{-3} | 15.495×10^{-8} |
| 80 | 0.646 | 0.654×10^{-3} | 0.391×10^{-3} | 1.985×10^{-3} | 7.615×10^{-8} |
| 160 | 0.613 | 0.414×10^{-3} | 0.252×10^{-3} | 1.565×10^{-3} | 3.863×10^{-8} |
| 320 | 0.574 | 0.245×10^{-3} | 0.152×10^{-3} | 1.788×10^{-3} | 2.667×10^{-8} |
| 640 | 0.537 | 0.114×10^{-3} | 0.073×10^{-3} | 1.577×10^{-3} | 1.125×10^{-8} |

Table 3.63. Consolidation and permeability properties of sample 5(static at optimum moisture content)

| Applied Pressure | Void ratio | Coefficient of compressibility, a_v (m ² /kN) | Coefficient of volume compressibility, m_v (m ² /kN) | Coefficient of consolidation, C_v (cm ² /sec) | Coefficient of permeability, k (cm/sec) |
|-------------------|------------|--|---|--|---|
| kN/m ² | e | | | | |
| 5 | 0.582 | | | | |
| 10 | 0.573 | 1.883×10^{-3} | 1.190×10^{-3} | | |
| 20 | 0.567 | 0.522×10^{-3} | 0.332×10^{-3} | | |
| 40 | 0.557 | 0.494×10^{-3} | 0.315×10^{-3} | 2.313×10^{-3} | 7.157×10^{-8} |
| 80 | 0.544 | 0.334×10^{-3} | 0.215×10^{-3} | 1.870×10^{-3} | 3.936×10^{-8} |
| 160 | 0.525 | 0.238×10^{-3} | 0.154×10^{-3} | 1.742×10^{-3} | 2.637×10^{-8} |
| 320 | 0.499 | 0.163×10^{-3} | 0.107×10^{-3} | 1.808×10^{-3} | 1.892×10^{-8} |
| 640 | 0.467 | 0.099×10^{-3} | 0.066×10^{-3} | 1.500×10^{-3} | 0.968×10^{-8} |

Table 3.64. Consolidation and permeability properties of sample 5(static at wet of optimum)

| Applied Pressure | Void ratio | Coefficient of compressibility, a_v (m ² /kN) | Coefficient of volume compressibility, m_v (m ² /kN) | Coefficient of consolidation, C_v (cm ² /sec) | Coefficient of permeability, k (cm/sec) |
|-------------------|------------|--|---|--|---|
| kN/m ² | e | | | | |
| 5 | 0.704 | | | | |
| 10 | 0.680 | 4.839×10^{-3} | 2.840×10^{-3} | | |
| 20 | 0.663 | 1.678×10^{-3} | 0.999×10^{-3} | | |
| 40 | 0.646 | 0.826×10^{-3} | 0.497×10^{-3} | 1.700×10^{-3} | 8.288×10^{-8} |
| 80 | 0.619 | 0.682×10^{-3} | 0.414×10^{-3} | 1.654×10^{-3} | 6.717×10^{-8} |
| 160 | 0.593 | 0.324×10^{-3} | 0.200×10^{-3} | 1.603×10^{-3} | 3.144×10^{-8} |
| 320 | 0.562 | 0.196×10^{-3} | 0.123×10^{-3} | 1.347×10^{-3} | 1.625×10^{-8} |
| 640 | 0.517 | 0.141×10^{-3} | 0.091×10^{-3} | 0.997×10^{-3} | 0.885×10^{-8} |

Appendix V

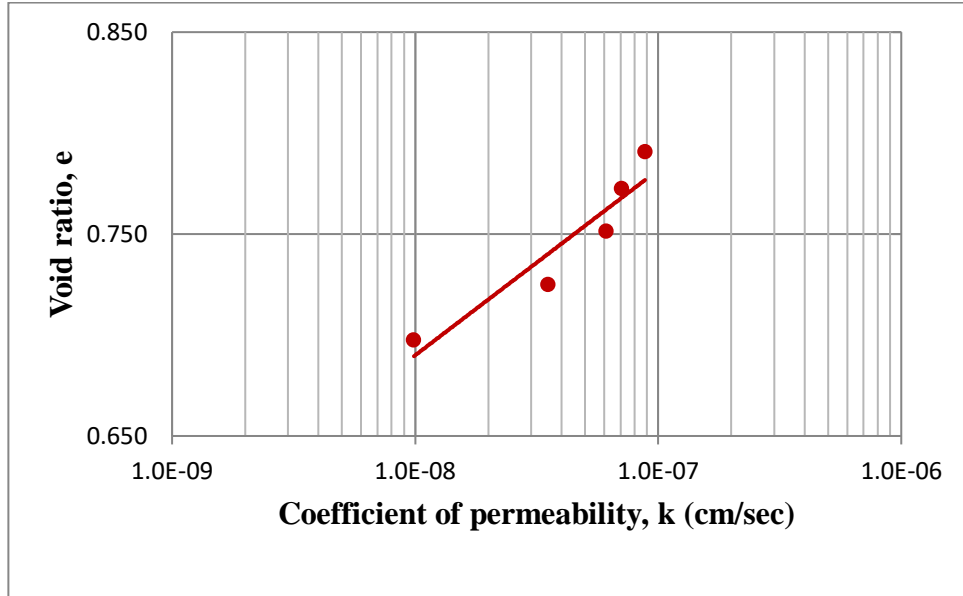


Figure 3.239: Void ratio vs. Coefficient of permeability for sample 2 (dynamic at dry of optimum)

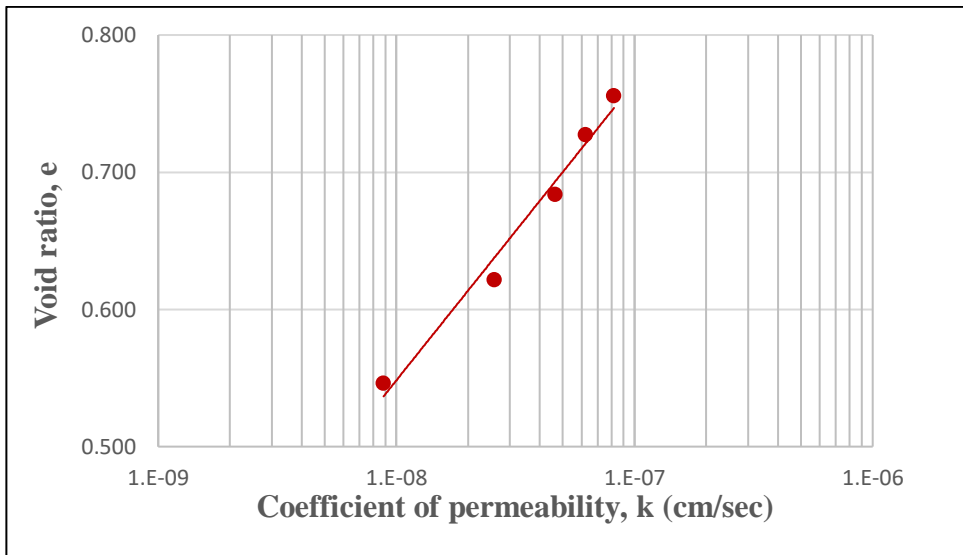


Figure 3.240: Void ratio vs. Coefficient of permeability for sample 2 (dynamic at optimum moisture content)

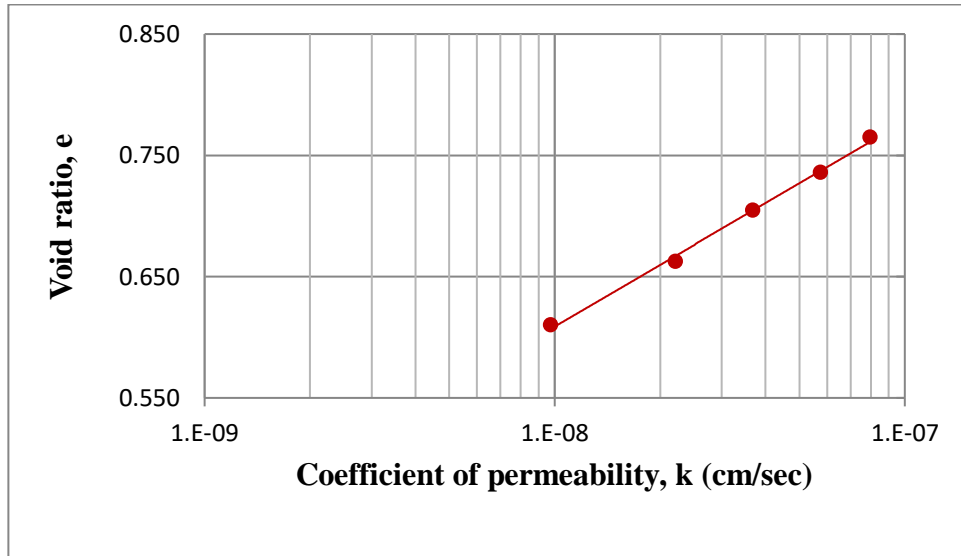


Figure 3.241: Void ratio vs. Coefficient of permeability for sample 2 (dynamic at wet of optimum)

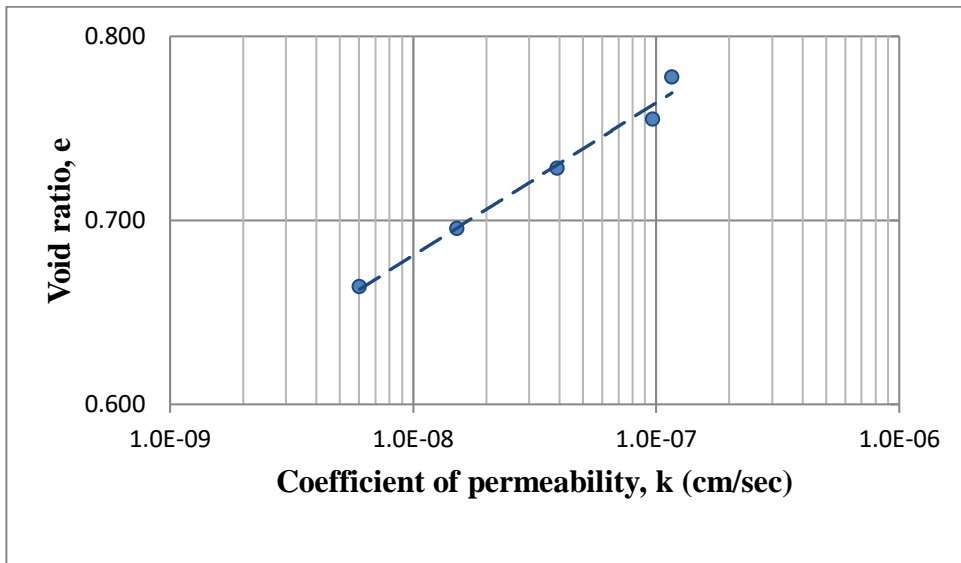


Figure 3.242: Void ratio vs. Coefficient of permeability for sample 2 (static at dry of optimum)

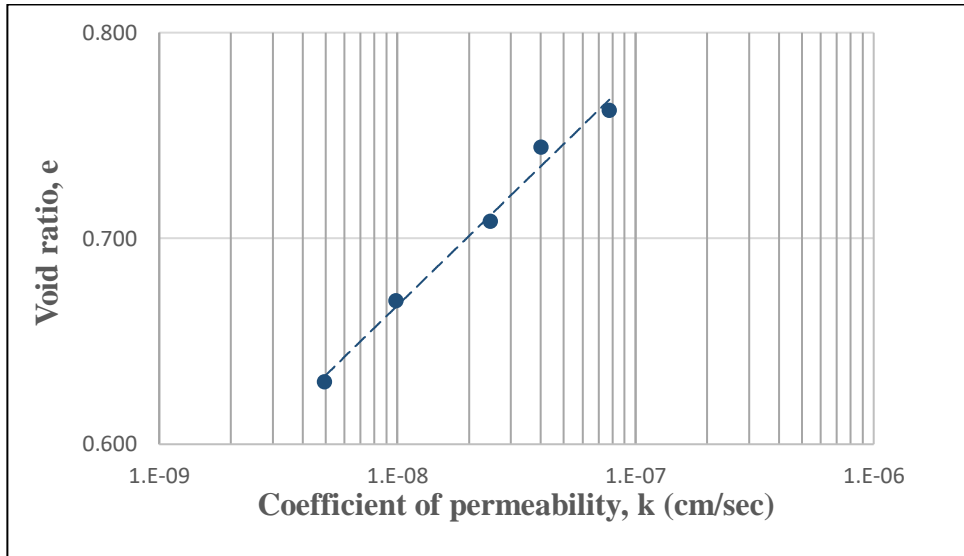


Figure 3.243: Void ratio vs. Coefficient of permeability for sample 2 (static at optimum moisture content)

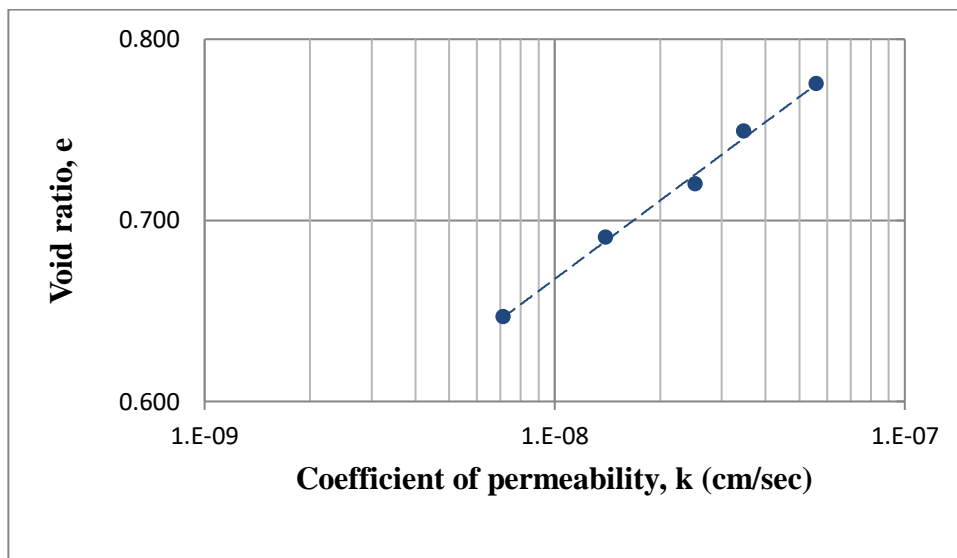


Figure 3.244: Void ratio vs. Coefficient of permeability for sample 2 (static at wet of optimum)

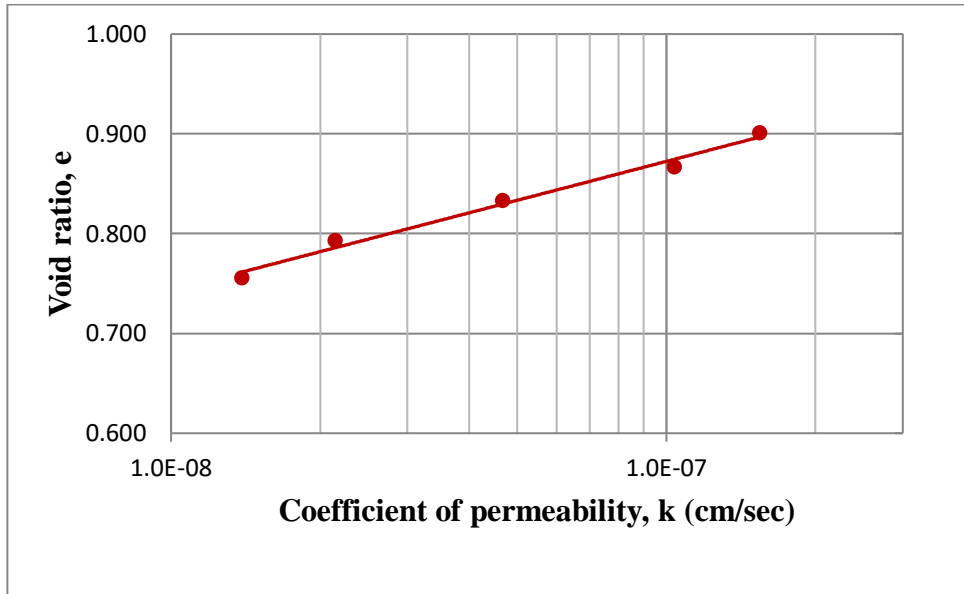


Figure 3.245: Void ratio vs. Coefficient of permeability for sample 3 (dynamic at dry of optimum)

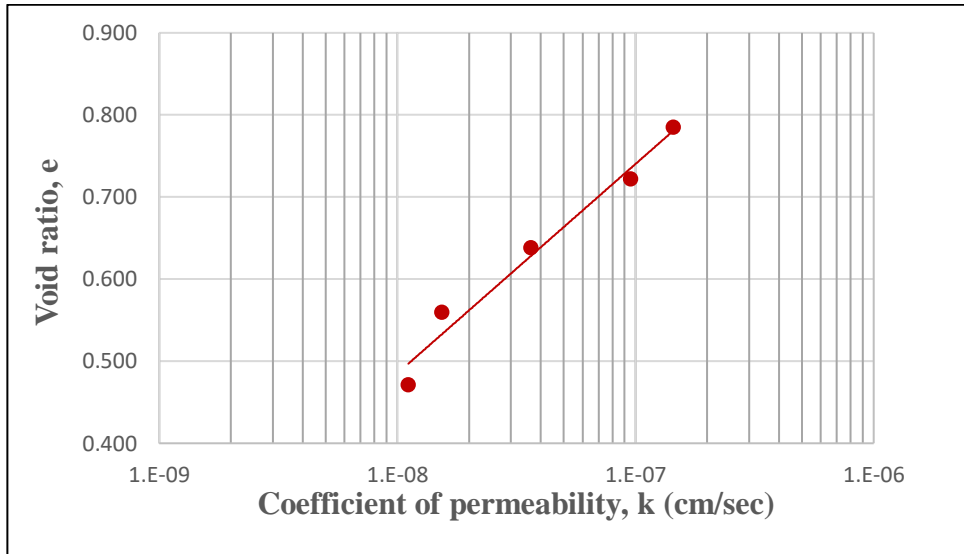


Figure 3.246: Void ratio vs. Coefficient of permeability for sample 3 (dynamic at optimum moisture content)

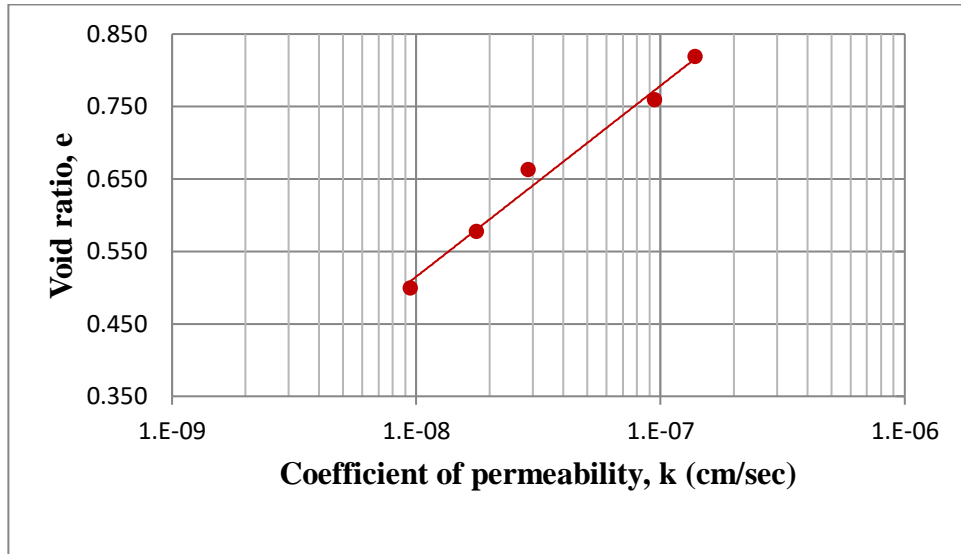


Figure 3.247: Void ratio vs. Coefficient of permeability for sample 3 (dynamic at wet of optimum)

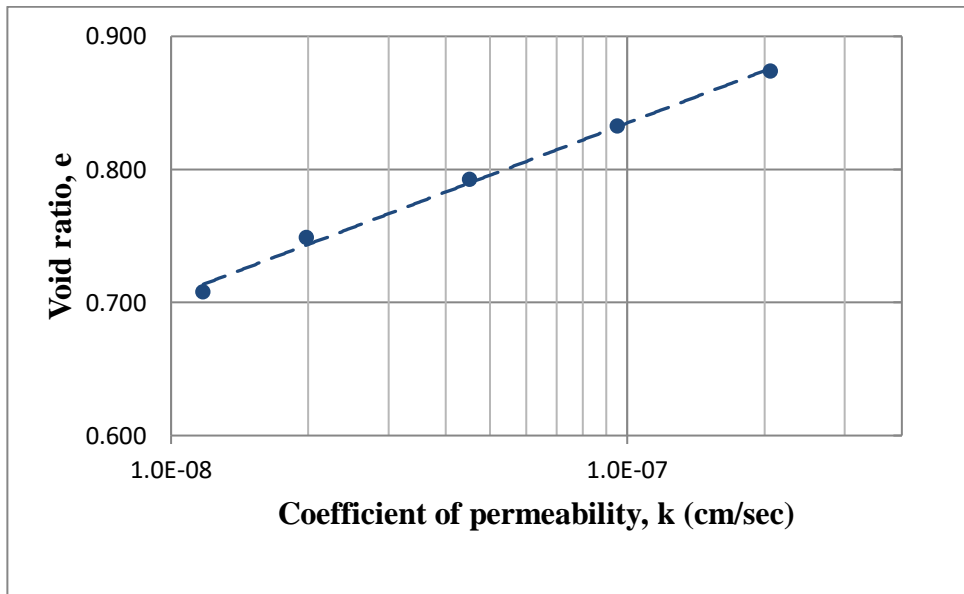


Figure 3.248: Void ratio vs. Coefficient of permeability for sample 3 (static at dry of optimum)

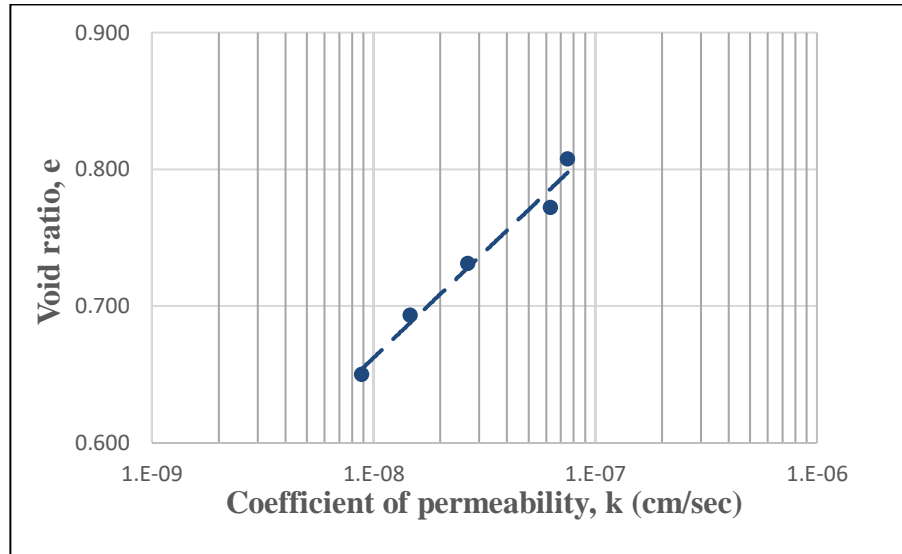


Figure 3.249: Void ratio vs. Coefficient of permeability for sample 3 (static at optimum moisture content)

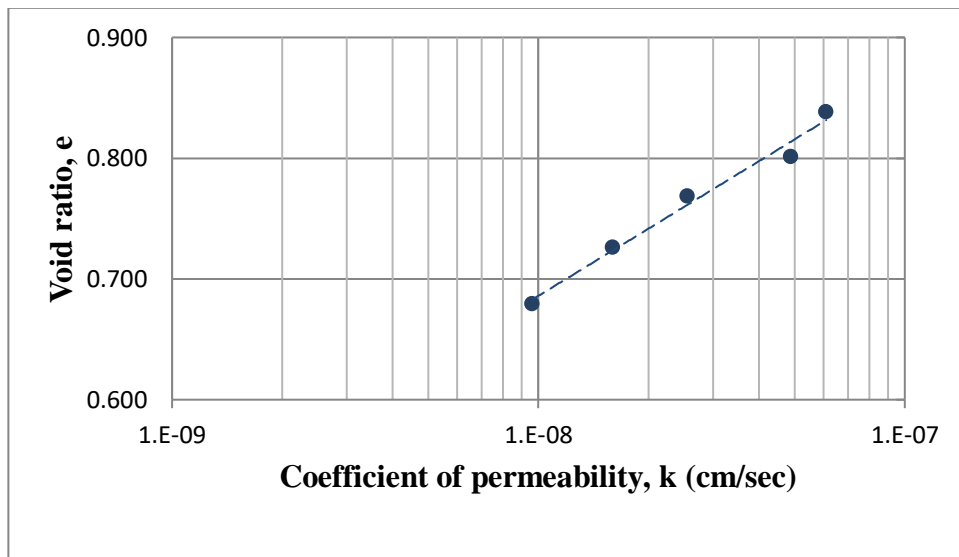


Figure 3.250: Void ratio vs. Coefficient of permeability for sample 3 (static at wet of optimum)

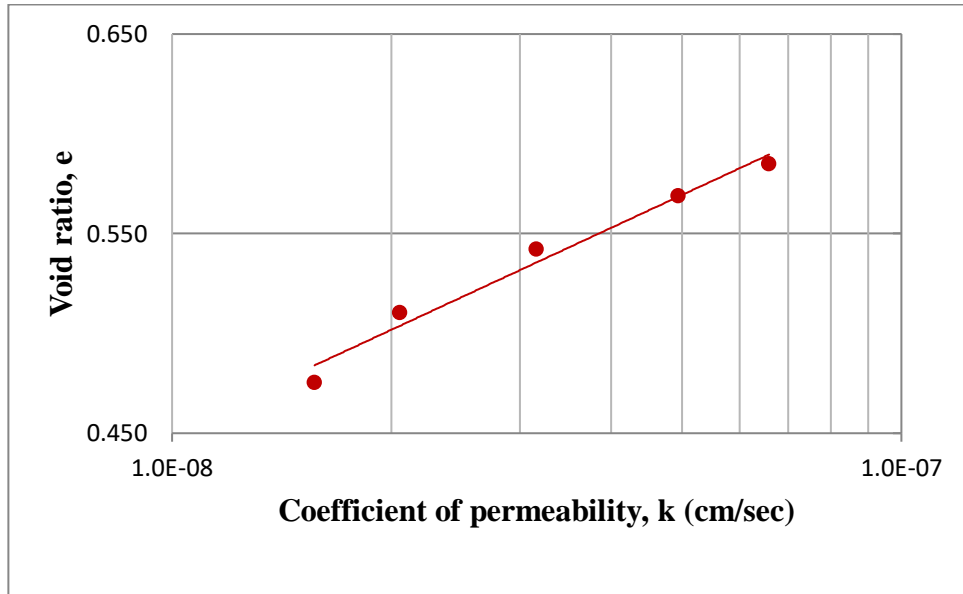


Figure 3.251: Void ratio vs. Coefficient of permeability for sample 4 (dynamic at dry of optimum)

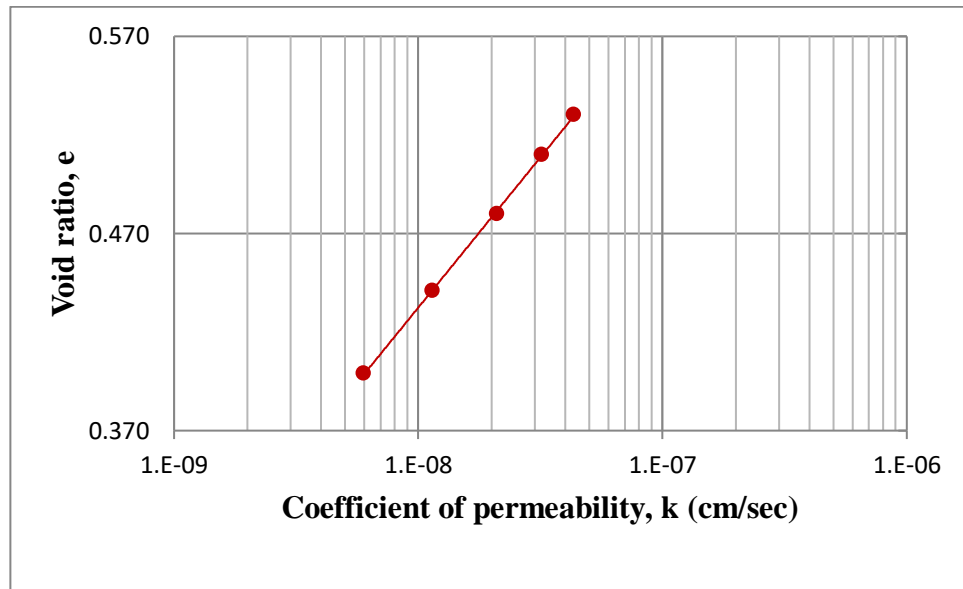


Figure 3.252: Void ratio vs. Coefficient of permeability for sample 4 (dynamic at optimum moisture content)

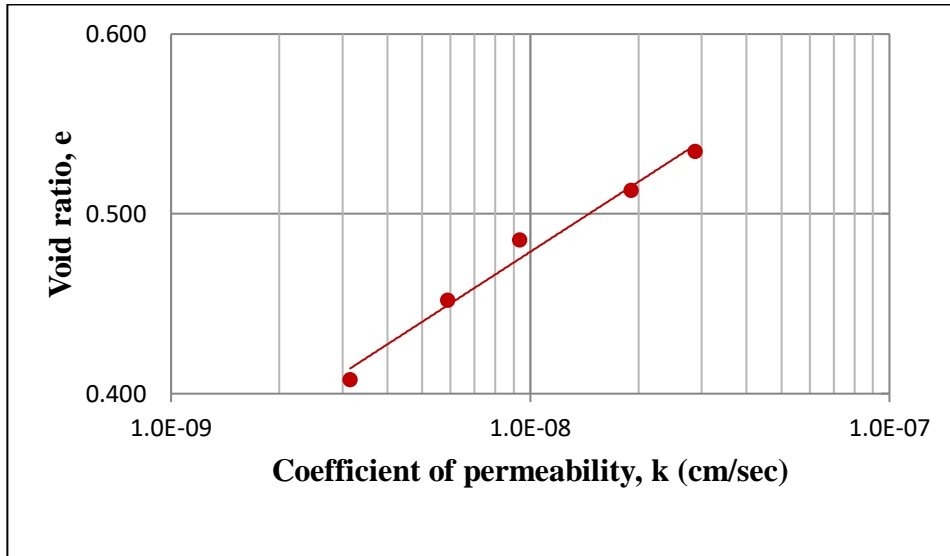


Figure 3.253: Void ratio vs. Coefficient of permeability for sample 4 (dynamic at wet of optimum)

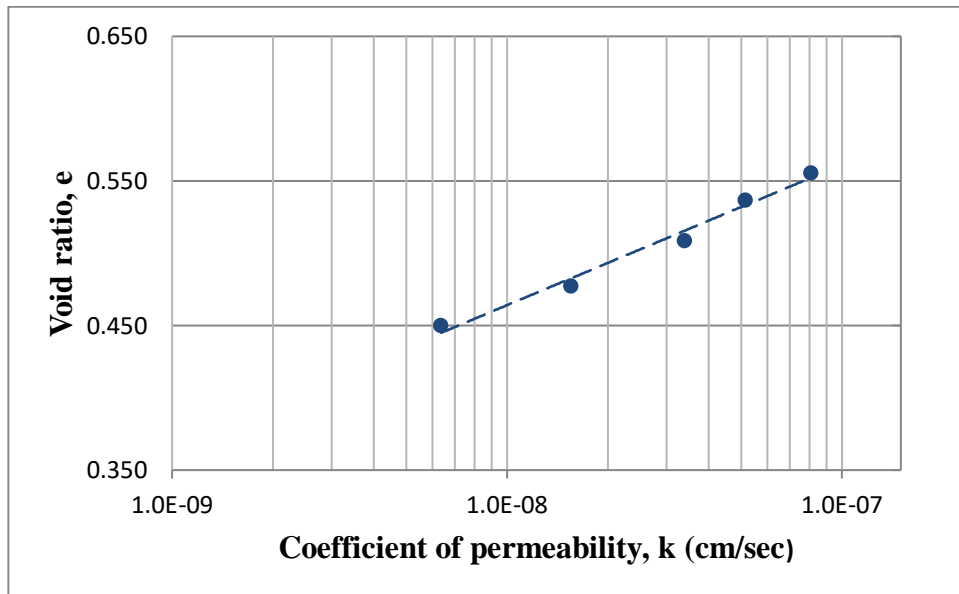


Figure 3.254: Void ratio vs. Coefficient of permeability for sample 4 (static at dry of optimum)

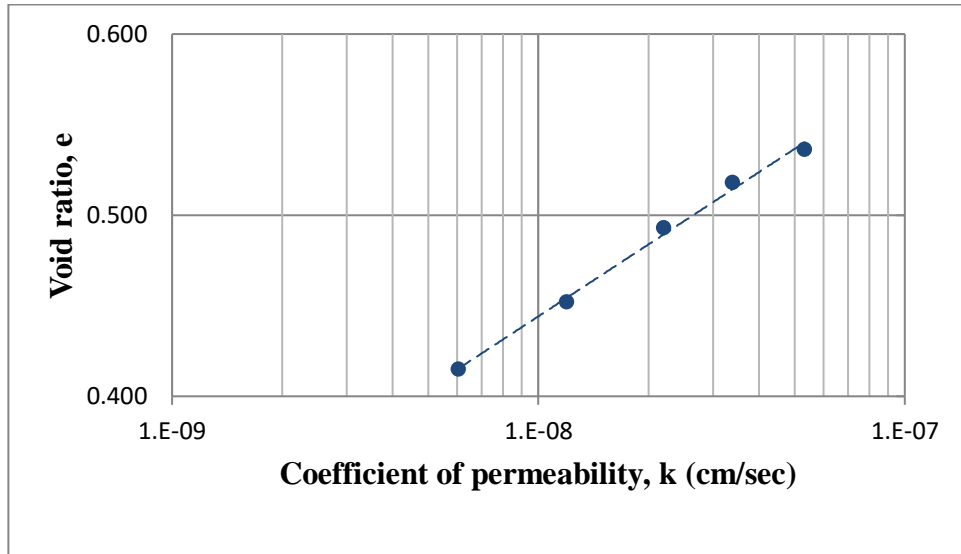


Figure 3.255: Void ratio vs. Coefficient of permeability for sample 4 (static at optimum moisture content)

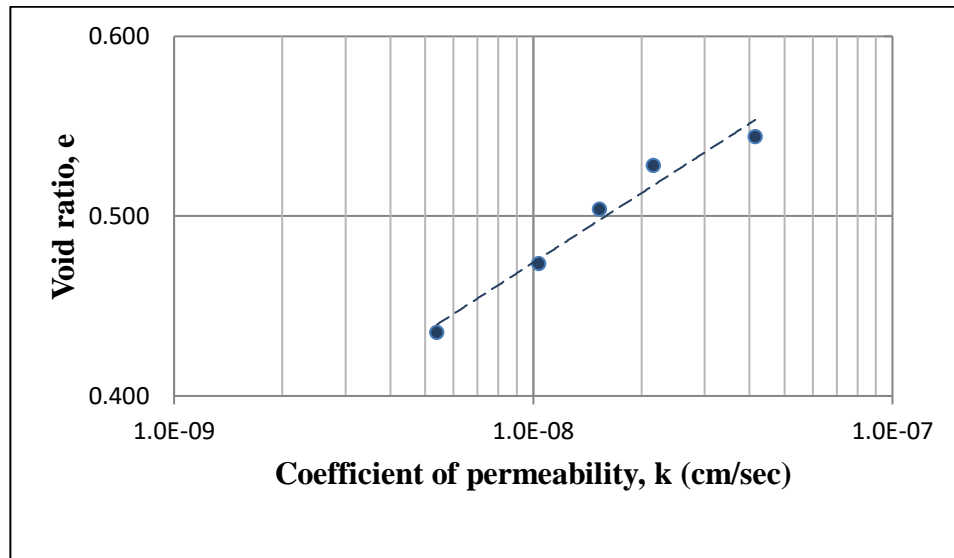


Figure 3.256: Void ratio vs. Coefficient of permeability for sample 4 (static at wet of optimum)

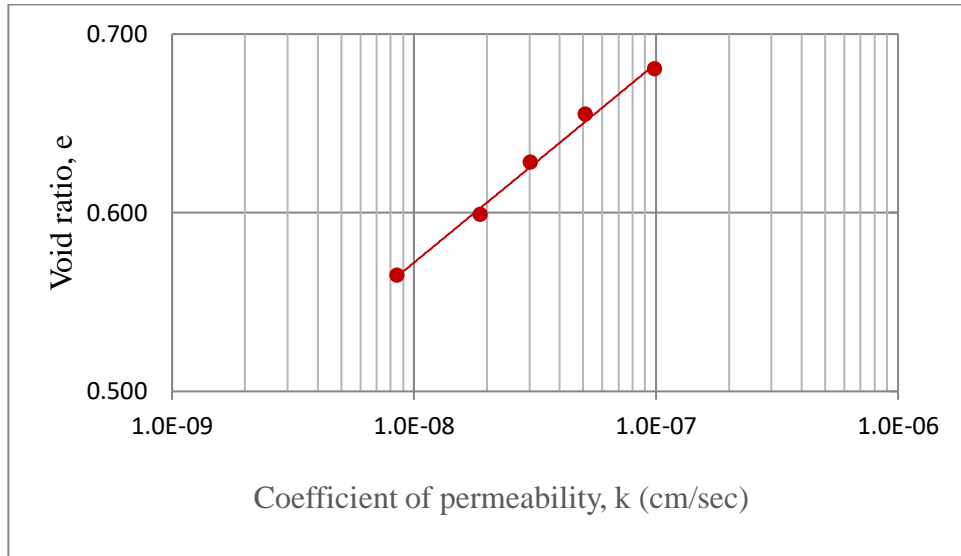


Figure 3.257: Void ratio vs. Coefficient of permeability for sample 5 (dynamic at dry of optimum)

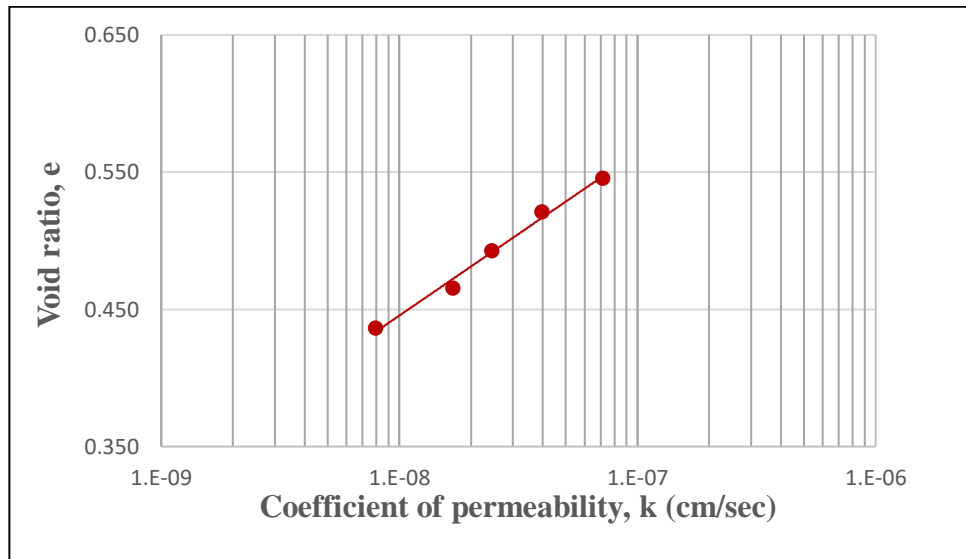


Figure 3.258: Void ratio vs. Coefficient of permeability for sample 5 (dynamic at optimum moisture content)

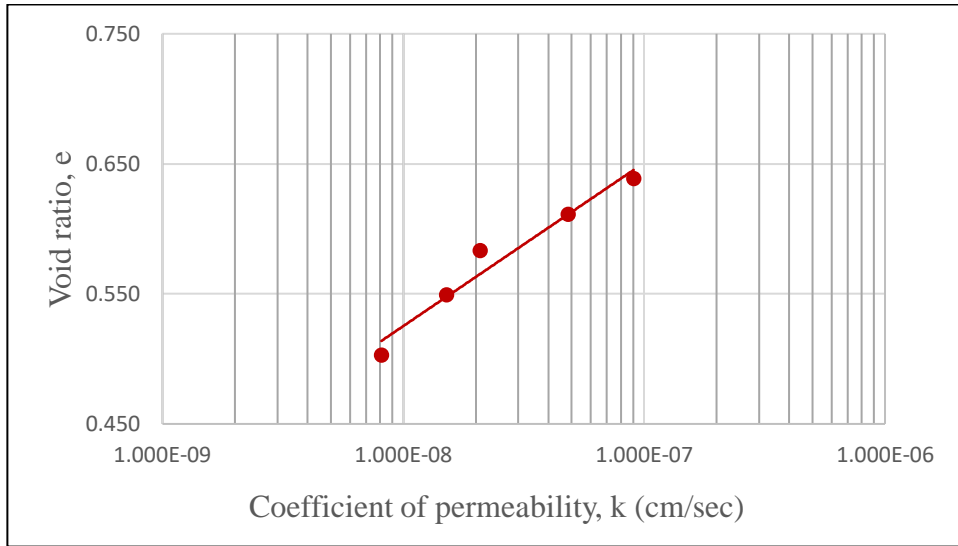


Figure 3.259: Void ratio vs. Coefficient of permeability for sample 5 (dynamic at wet of optimum)

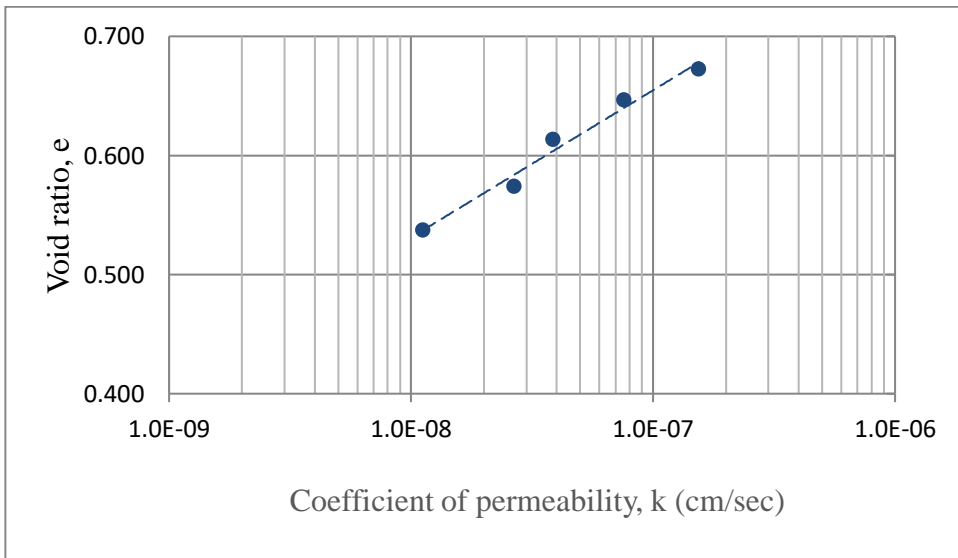


Figure 3.260: Void ratio vs. Coefficient of permeability for sample 5 (static at dry of optimum)

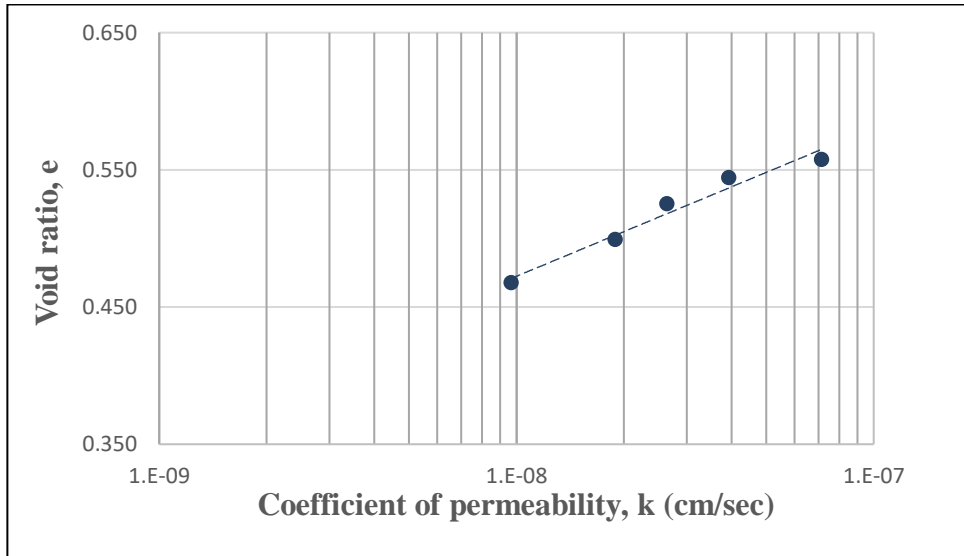


Figure 3.261: Void ratio vs. Coefficient of permeability for sample 5 (static at optimum moisture content)

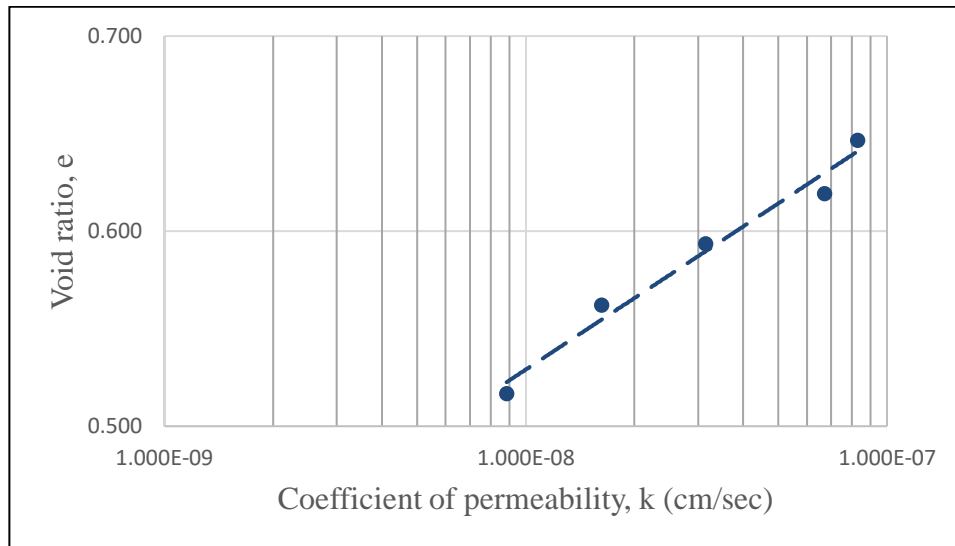


Figure 3.262: Void ratio vs. Coefficient of permeability for sample 5 (static at wet of optimum)